Seismic Evaluation of Bolted Connections in Non-Seismic Concentrically Braced Frames

Molly Mae Johnson

A thesis

submitted in partial fulfillment of the

requirements for the degree of

Master of Science in Civil Engineering

University of Washington

2014

Committee:

Charles Roeder

Dawn Lehman

Jeffrey Berman

Program Authorized to Offer Degree:

Civil and Environmental Engineering

University of Washington

Abstract

Seismic Evaluation of Bolted Connections in

Non-Seismic Concentrically Braced Frames

Molly Mae Johnson

Chair of Supervisory Committee:

Dr. Charles W. Roeder

Department of Civil and Environmental Engineering

Steel concentrically braced frames (CBFs) resist lateral load through braces that concentrically frame into the centerline of the beam-to-column joint or into an opposing brace, typically with gusset plate connections. Current design specifications for special concentrically braced frames (SCBFs) require a number of special ductile detailing requirements to encourage increased drift capacity and ductility in the system. Often in areas of high seismicity the brace-to-gusset plate connections are welded. Although bolted connections provide an attractive alternative in terms of constructability, few tests have investigated seismic performance of bolted SCBF connections. Prior to the early 1990s, CBFs were not designed to meet ductile detailing and design requirements and engineers more commonly employed bolted brace-to-gusset plate connections. Yet these older systems also have not been widely investigated. An experimental research program was undertaken to study the seismic performance of older bolted CBF connections. The

experimental results were analyzed to draw conclusions on the seismic performance of old CBF bolted connections and to identify deficiencies of systems utilizing older CBF bolted connection details. The data was used to create an initial approach to evaluating and retrofitting CBFs on a subsystem level using ASCE 41.

Acknowledgements

I would like to thank my advisors: Charles Roeder, Dawn Lehman, and Jeffrey Berman for the opportunity of being on this project. This project was all encompassing – from countless hours working in the structures lab building these steel braced frames, to countless hours writing and analyzing data. I learned to be critical during fabrication and then critical during analysis. My advisors challenged me to dig deeper, try harder, and push beyond what I thought possible.

I would like to thank my best friend Anna Cecilia Hernandez – I could not have done this work without her relentless support and encouragement. She was a constant beacon of light for me who, even while in Texas, still checked to make sure I was eating and sleeping enough. She was someone strong I could lean on while she continuously reminded me to look at the big picture of what I had accomplished. Her friendship and caring knows no geographic limits and for that I am eternally grateful.

I would like to thank my family who believed in me even when I didn't believe in myself. My two amazing parents would do anything to help me achieve my dreams – they would drop everything the second I needed help. My mom knows me better than I know myself and knew what I needed even before I said it. I can't count the number of hours she lost sleep over my late night phone calls – because even if it were midnight in Seattle and 3am her time she would always listen to me. Without my family I wouldn't be where I am today.

I'd like to thank my research team: Dan Sloat, Andy Sen, and Ryan Ballard. I couldn't have asked for a better colleague to have than Dan. He was a great research partner despite our

Patriots/Seahawks rivalry. And while at first I think he thought I only needed him around to do the heavy lifting (literally), I grew to see him as an invaluable friend. I learned a lot from him and am confident he will be a great engineer. Andy was also a wonderful friend; I could always count on him to be in my corner, put things in perspective, and give me words of encouragement and endless kindness (probably southern hospitality). And, while Ryan was relatively new to the project, he also helped encourage me towards my goals. I'd like to thank everyone who worked with me in the structures lab – especially Tony Nyguen, Kelli Slaven, and Jean-Luc Jackson. Getting to know you, work with you and become friends with you was a great experience and I am appreciative beyond words for your help!

I'd like to thank Spencer Livermore for being an incredible friend, understanding me, and making me laugh. Spencer would do anything for a friend and I am lucky to call him one. I'd also like to thank: Bryan Kennedy for his jokes; Travis Thornstead for knowing the ins and outs of the lab and always answering my questions; Max Stephens for listening to and believing in me; Vince for teaching me to navigate the lab; and Doug for his welding and for always being in a good mood while welding. And to everyone in my graduating class – we created amazing memories and I will always value your friendship!

I'd also like to thank my boyfriend Ian Thomas Wells - whose love and support never wavered all the way from Boston.

This thesis is dedicated to everyone following the arduous path to her or his dreams.

TABLE OF CONTENTS

1 INTRODUCTION 18

1.1 OVERVIEW OF CONCENTRICALLY BRACED FRAMES 18

1.2 OVERVIEW OF DESIGN METHODOLOGIES 19

1.3 RESEARCH MOTIVATION 21

1.4 RESEARCH GOALS 22

1.5 OVERVIEW OF REPORT 22

2 LITERATURE REVIEW 23

2.1 INTRODUCTION 23

2.2 PREVIOUS CBF RESEARCH 24

2.2.1 TREMBLAY [2002] 24

2.2.2 SHABACK AND BROWN [2003] 25

2.3 PREVIOUS UW SCBF RESEARCH 27

2.4 IDENTIFICATION AND PRIOR TESTING OF NCBF DEFICIENCIES 37

2.5 SUMMARY 49

3 SPECIMEN DESIGN 50

3.1 INTRODUCTION 50

3.2 BOLTED NCBF CONNECTIONS FROM INFRASTRUCTURE REVIEW 50

3.3 OVERVIEW OF UFM AND LIMIT STATE CALCULATIONS 53

3.3.1 BRACE NET SECTION FRACTURE 60

3.3.2 BLOCK SHEAR 60

3.3.3 WHITMORE GUSSET PLATE YIELDING 61

3.3.4 WHITMORE GUSSET PLATE FRACTURE 62
3.3.5 GUSSET PLATE BUCKLING 63
3.3.6 BASE METAL FRACTURE 63
3.3.7 INTERFACE WELD FRACTURE 64
3.3.8 BOLT SHEAR 65
3.3.9 BOLT BEARING 66

3.4 SPECIMEN DESIGN PARAMETERS 66

3.5 MATERIAL PROPERTIES 74

4 EXPERIMENTAL TEST SETUP 75

4.1 INTRODUCTION 75

4.2 OVERVIEW OF EXPERIMENTAL CONFIGURATION 75

4.3 TEST SETUP COMPONENTS 78

4.3.1 STRONG FLOOR AND STRONG WALL 78
4.3.2 CHANNEL ASSEMBLY 78
4.3.3 OUT-OF-PLANE SUPPORTS 80
4.3.4 GRAVITY LOAD SYSTEM 81
4.3.5 REACTION BLOCK AND ACTUATOR 82
4.3.6 LOAD TRANSFER BEAM 83
4.3.7 ADDITIONAL TEST SPECIMEN DETAILS TO ACCOMMODATE TEST SETUP 84

4.4 INSTRUMENTATION 86

4.4.1 STRAIN GAUGES 87
4.4.2 POTENTIOMETERS 89
4.4.3 NORTHERN DIGITAL, INC. - OPTOTRAK 91
4.4.4 VISUAL OBSERVATIONS 93

4.5 LOAD PROTOCOL 94

4.6 TESTING PREPARATION 96

5 TEST RESULTS & OBSERVATIONS 97

5.1 INTRODUCTION 97

5.2 OVERVIEW OF PERFORMANCE STATES 100

5.2.1 PLATE AND FRAME YIELDING (Y) 104
5.2.2 BUCKLING (B) 107
5.2.3 WELD TEARING AND FRACTURE (W) 109
5.2.4 BOLT DAMAGE STATES (BO) 110

5.3 BOLTED NCBF TEST OBSERVATIONS 113

5.3.1 NHSS-B1 114

5.3.1.1 SPECIMEN OVERVIEW 114
5.3.1.2 MODERATE DAMAGE STATES (DS1 & DS2) 120
5.3.1.3 SEVERE DAMAGE STATES (DS3 & DS4) 123
5.3.1.4 SPECIMEN SUMMARY OF RESULTS 126

5.3.2 NHSS-B2 131

5.3.2.1 SPECIMEN OVERVIEW 131
5.3.2.2 MODERATE DAMAGE STATES (DS1 & DS2) 137
5.3.2.3 SEVERE DAMAGE STATES (DS3 & DS4) 138
5.3.2.4 SPECIMEN SUMMARY OF RESULTS 140

5.3.3 NHSS-B3 144

5.3.3.1 SPECIMEN OVERVIEW 144
5.3.3.2 MODERATE DAMAGE STATES (DS1 & DS2) 150
5.3.3.3 SEVERE DAMAGE STATES (DS3 & DS4) 152
5.3.3.4 SPECIMEN SUMMARY OF RESULTS 159

6 DATA ANALYSIS 166

6.1 INTRODUCTION 166

6.2 BRACED FRAME SYSTEM BEHAVIOR 166

6.2.1 APPLIED STORY SHEAR VERSUS STORY DRIFT RESPONSE 169
6.2.2 STIFFNESS COMPARISONS 171

6.2.3 ENERGY DISSIPATION 174
6.2.4 POST-FAILURE BEHAVIOR 179
6.3 GUSSET PLATE CONNECTION RESPONSE 181
6.4 BOLT DAMAGE 185
6.5 WELD DAMAGE 188
6.6 BRACE RESPONSE 192
6.6.1 EXPERIMENTAL EFFECTIVE LENGTH FACTOR, *K* 195
6.6.2 BRACE AXIAL FORCE VERSUS DRIFT RESPONSE 196
6.6.3 BRACE BUCKLED SHAPE 201
6.6.4 BRACE ELONGATION 204
6.7 NW & SE CONNECTION RESPONSE 207
7 EVALUATION 2
8 SUMMARY & CONCLUSIONS 222
8.1 SUMMARY OF SPECIMEN PERFORMANCE 222
8.2 RESEARCH CONCLUSIONS 223
8.3 RECOMMENDATIONS FOR FUTURE RESEARCH 225
APPENDIX A: DRAWINGS 229
A.1 NHSS-B1 229
A.2 NHSS-B2 234
A.3 NHSS-B3 239
APPENDIX B: LOAD HISTORIES 240
APPENDIX C: CALCULATIONS 244

TABLE OF FIGURES

FIGURE 1.1 - RESPONSE OF SINGLE BRACE VS. OPPOSING BRACES [POWELL, 2010] 18

FIGURE 1.2 - POTENTIAL YIELD MECHANISMS AND FAILURE MODES FOR SCBFS [POWELL, 2010] 20

FIGURE 2.1 - GEOMETRY OF BRACE SPECIMENS (TREMBLAY, 2002) 25

FIGURE 2.2 - TEST FRAME ASSEMBLY (SHABACK AND BROWN, 2003) 26

FIGURE 2.3 - NORMALIZED HYSTERETIC CURVE COMPARISON (SHABACK AND BROWN, 2003) 26

FIGURE 2.4 - UW TEST SETUP ORIENTATION 29

FIGURE 2.5 - SPECIMEN HSS-05 FORCE VS. DRIFT RATIO RESPONSE (JOHNSON, 2005) 30

FIGURE 2.6 - SPECIMEN HSS-16 FORCE VS. DRIFT RESPONSE (KOTULKA, 2007) 31

FIGURE 2.7 - CRACKING IN EXTENSION PLATE AT -2.86% DRIFT (MODIFIED FROM KOTULKA, 2007) 32

FIGURE 2.8 - NE COLUMN CONNECTION BASE METAL FRACTURE AT -2.66% DRIFT (MODIFIED FROM KOTULKA, 2007) 33

FIGURE 2.9 - SPECIMEN HSS-19 FORCE VS. DRIFT RESPONSE (POWELL, 2010) 34

FIGURE 2.10 - FRACTURED SPLICE PLATE AT END OF TEST (MODIFIED FROM POWELL, 2010) 35

FIGURE 2.11 - SPECIMEN HSS-20 FORCE VS. DRIFT RESPONSE (POWELL, 2010) 36

FIGURE 2.12 - SPECIMEN HSS-21 FORCE VS. DRIFT RESPONSE (POWELL, 2010) 37

FIGURE 2.13 - NCBF 32 TEST DETAILS (HSIAO ET AL., 2011) 40

FIGURE 2.14 - PILOT NCBF 32 BEHAVIOR (HSIAO ET AL., 2011) 41

FIGURE 2.15 - BOLT BEARING DEFORMATION 42

FIGURE 2.16 – BOLT DEFORMATION 44

FIGURE 2.17 – PHOTOS OF BOLT SHEAR FAILURE FROM NHSS-B3 45

FIGURE 2.18 - BOLT TEAR OUT FAILURE [2] 46

FIGURE 2.19 - BOLTED NET SECTION FRACTURE [4] 46

FIGURE 2.20 - BLOCK SHEAR FAILURE [MODIFIED FROM 1] 47

FIGURE 2.21 - SCHEMATIC DRAWING OF BOLT PRYING [5] 48

FIGURE 3.1 – EXISTING BOLTED NCBF CONNECTION NHSS-REF-B1 51

FIGURE 3.2 - EXISTING BOLTED NCBF CONNECTION NHSS-REF-B2 52

FIGURE 3.3 - FORCE TRANSFER BY THE UFM [CIVES REF.] 54

FIGURE 3.4 - WHITMORE WIDTH ILLUSTRATION [MODIFIED FROM ROEDER ET AL., 2011] 61

FIGURE 3.5 - PHOTO OF TENSION RUPTURE AT WHITMORE SECTION [2] 62

FIGURE 3.6 – GUSSET PLATE BUCKLING LENGTH DETERMINATION [2] 63

FIGURE 3.7 - SCHEMATIC DRAWING OF VARIABLES A, B, N FOR ECCENTRICITY CALCULATION 66
FIGURE 3.8 - SPECIMEN CONNECTION DRAWINGS 70

FIGURE 4.1 - CAD DRAWING OF THE UW TEST SETUP 76
FIGURE 4.2 - UW TEST SETUP IN THE SRL 77
FIGURE 4.3 - CROSS SECTION OF CHANNEL ASSEMBLY AND STRONG WALL [POWELL, 2010] 79
FIGURE 4.4 - PLAN VIEW OF CHANNEL ASSEMBLY AND SOUTH BASE CONNECTION [POWELL, 2010] 79
FIGURE 4.5 - CHANNEL ASSEMBLY IN SW CORNER AT WEST COLUMN BASE 80
FIGURE 4.6 - OOP RESTRAINT SYSTEM 81
FIGURE 4.7 - GRAVITY LOAD SYSTEM LAYOUT IN THE WEST COLUMN [POWELL, 2010] 82
FIGURE 4.8 - ACTUATOR AND REACTION BLOCK COMPONENTS [POWELL, 2010] 83
FIGURE 4.9 - ACTUATOR AND REACTION BLOCK COMPONENTS [POWELL, 2010] 83
FIGURE 4.10 - LOAD TRANSFER BEAM LAYOUT [POWELL, 2010] 84
FIGURE 4.11 - DIAGRAM OF WEB DOUBLER PLATE IN NW CORNER OF THE BRACED FRAME 85
FIGURE 4.12 - COLUMN STIFFENER DETAIL 86
FIGURE 4.13 - TYPICAL STRAIN GAUGE LAYOUT 88
FIGURE 4.14 - TYPICAL POTENTIOMETER LAYOUT 90
FIGURE 4.15 - TYPICAL OPTOTRAK LED LAYOUT 92
FIGURE 4.16 - SAMPLE LED LAYOUT FROM SHSS-B2 93
FIGURE 4.17 - GENERAL TESTING LOAD PROTOCOL 95

FIGURE 5.1 - FRAME ORIENTATION 97
FIGURE 5.2 - SPECIMEN DRIFT RANGES 100
FIGURE 5.3 - TYPICAL YIELD PROGRESSION ON GUSSET PLATE (FROM SPECIMEN SHSS-B2) 105
FIGURE 5.4 - TYPICAL YIELD PROGRESSION IN COLUMNS (FROM SPECIMEN SHSS-B1) 106
FIGURE 5.5 - TYPICAL BRACE FRACTURE PROGRESSION: A. B1, B. B2, C. B3, D. B3-HINGE, E. BT, F. BF 108
FIGURE 5.6 - TYPICAL LOCAL BUCKLING PROGRESSION IN BEAM (FROM SPECIMEN SHSS-B1) 109
FIGURE 5.7 - PROGRESSION OF WELD FRACTURE (FROM SPECIMEN SHSS-B2) 110
FIGURE 5.8 - BOLT PERFORMANCE STATE (FROM SPECIMEN NHSS-B3) 111
FIGURE 5.9 - BOLT DAMAGE FROM SPECIMEN NHSS-B3, LEFT TO RIGHT: BOLT DAMAGE, SHEAR TAB DAMAGE, BEAM WEB & GUSSET PLATE DAMAGE 112
FIGURE 5.10 - NHSS-B1 CONNECTION DRAWING 115
FIGURE 5.11 - SPECIMEN NHSS-B1 APPLIED STORY SHEAR VS. STORY DRIFT HYSTERETIC BEHAVIOR 116

FIGURE 5.12 - YIELDING IN NE GUSSET PLATE AND SHEAR TAB AT +0.2% DRIFT 120
FIGURE 5.13 - NE CORNER LOCAL FLANGE BUCKLING (B1) AT -1.0% DRIFT 121
FIGURE 5.14 - ROTATION OF NORTH FLANGE OF SOUTH BEAM IN SW CORNER 121
FIGURE 5.15 - ILLUSTRATION OF THE SW CORNER BEAM AND COLUMN ROTATIONS WITH BRACE IN COMPRESSION 122
FIGURE 5.16 - GAP BETWEEN SHEAR PLATE AND GUSSET PLATE IN NE CORNER 122
FIGURE 5.17 - ROTATION OF THE EAST FLANGE OF THE WEST COLUMN AT +1.1% DRIFT 123
FIGURE 5.18 - BRACE LOCAL DEFORMATION (B3-CUPPING) AT MIDSPAN AT -2.7% DRIFT 124
FIGURE 5.19 - BRACE TEARING (BT) AT MIDSPAN AT +1.9% DRIFT 125
FIGURE 5.20 - DAMAGE IN WEST COLUMN IN SW CORNER AT -2.8% DRIFT 125
FIGURE 5.21 - BRACE FRACTURE (BF) AT +2.2% DRIFT 125
FIGURE 5.22 - PROGRESSION OF WELD CRACKING IN NE BEAM TO GUSSET PLATE CONNECTION 127
FIGURE 5.23 - SE CORNER BOLT DAMAGE 128
FIGURE 5.24 - NE CORNER BOLT DAMAGE 129
FIGURE 5.25 - SW CORNER BOLT DAMAGE 130
FIGURE 5.26 - NW CORNER BOLT DAMAGE 130
FIGURE 5.27 - SPECIMEN NHSS-B2 CONNECTION DRAWING 132
FIGURE 5.28 - SPECIMEN NHSS-B2 APPLIED STORY SHEAR VS. STORY DRIFT HYSTERETIC BEHAVIOR 133
FIGURE 5.29 - PRE-TEST YIELDING IN NE CORNER ON EAST COLUMN 137
FIGURE 5.30 - INITIAL YIELDING (Y1) ON SW GUSSET PLATE 137
FIGURE 5.31 - INCREASED DAMAGE IN THE NE CORNER AT -1.1% DRIFT 139
FIGURE 5.32 - NE CONNECTION FAILURE IN FINAL TENSILE CYCLE 140
FIGURE 5.33 - SE CORNER BOLT DAMAGE 141
FIGURE 5.34 - NE CORNER BOLT DAMAGE 142
FIGURE 5.35 - PHOTO EVIDENCE OF BOLT DAMAGE IN NE CORNER 142
FIGURE 5.36 - SW CORNER BOLT DAMAGE 143
FIGURE 5.37 - NW CORNER BOLT DAMAGE 143
FIGURE 5.38 - SPECIMEN NHSS-B3 CONNECTION DRAWING 145
FIGURE 5.39 - SPECIMEN NHSS-B3 APPLIED STORY SHEAR VS. STORY DRIFT HYSTERETIC BEHAVIOR 146
FIGURE 5.40 - INITIAL YIELDING (Y1) IN NE CORNER 150
FIGURE 5.41 - GUSSET PLATE BENDING IN NE CORNER AT -0.92% DRIFT 151
FIGURE 5.42 - YIELDING (Y1) IN THE NW CORNER 151
FIGURE 5.43 - GUSSET PLATE ROTATION AT -1.3% DRIFT 152

FIGURE 5.44 - MODERATE YIELDING (Y2) ON THE WEST FLANGE OF THE WEST COLUMN AT -1.6% DRIFT.....153
FIGURE 5.45 - 1 IN. GAP BETWEEN NE GUSSET PLATE AND BEAM AT +0.88% DRIFT.....154
FIGURE 5.46 - BOLT HOLE ELONGATION IN THE GUSSET PLATE IN THE NE CORNER.....154
FIGURE 5.47 - BRACE "S" SHAPE AT +1.0% DRIFT.....155
FIGURE 5.48 - LOCAL BUCKLING (B1) IN THE NW CORNER OF THE FRAME AT -2.8% DRIFT.....156
FIGURE 5.49 - IN-PLANE BRACE BUCKLING AT -3.1% DRIFT.....156
FIGURE 5.50 - LOCAL BUCKLING (B1) OF THE WEST FLANGE OF THE WEST COLUMN.....157
FIGURE 5.51 - VISIBLE GAP IN GUSSET PLATE TO BEAM AT +2.3% DRIFT.....157
FIGURE 5.52 - FINAL TEST PHOTOS AT -3.7% DRIFT.....158
FIGURE 5.53 - PROGRESSION OF NE BEAM TO GUSSET PLATE WELD FRACTURE.....161
FIGURE 5.54 - PROGRESSION OF SW BEAM TO GUSSET PLATE WELD FRACTURE.....162
FIGURE 5.55 - SE CORNER BOLT DAMAGE.....162
FIGURE 5.56 - NE CORNER BOLT DAMAGE.....163
FIGURE 5.57 - BOLT HOLE ELONGATION IN NE GUSSET PLATE.....164
FIGURE 5.58 - BOLT DAMAGE IN NE GUSSET PLATE.....164
FIGURE 5.59 - SW CORNER BOLT DAMAGE.....165
FIGURE 5.60 - NW CORNER BOLT DAMAGE.....165

FIGURE 6.1 - APPLIED STORY SHEAR VS. STORY DRIFT HYSTERETIC RESPONSE.....170
FIGURE 6.2 – SAMPLE STIFFNESS CALCULATION FOR SPECIMEN NHSS-B1.....172
FIGURE 6.3 - BACKBONE CURVES FOR NCBF BOLTED SPECIMENS.....173
FIGURE 6.4 - ENERGY DISSIPATION CALCULATION (KOTULKA, 2007).....175
FIGURE 6.5 - CUMULATIVE BRACED FRAME SYSTEM ENERGY DISSIPATED FOR NCBF SPECIMENS.....176
FIGURE 6.6 - POST-FRACTURE APPLIED LATERAL LOAD VS. DISPLACEMENT RESPONSE.....181
FIGURE 6.7 - DIAGRAM OF OOP GUSSET PLATE ROTATION.....182
FIGURE 6.8 - LEDS USED TO PLOT GUSSET PLATE OOP DISPLACED SHAPE (FROM SPECIMEN NHSS-B1).....182
FIGURE 6.9 - HYSTERETIC RESPONSE FOR MAXIMUM GUSSET PLATE OOP ROTATION.....183
FIGURE 6.10 - GUSSET PLATE OOP DISPLACEMENT ALONG GUSSET PLATE LENGTH.....184
FIGURE 6.11 - BOLT/HOLE NUMBERING FOR NCBF SPECIMENS.....186
FIGURE 6.12 - NORMALIZED WELD CRACK LENGTH FOR EACH SPECIMEN COMPARED TO HSS-05.....189
FIGURE 6.13 - IDEALIZED INELASTIC BRACE BEHAVIOR UNDER CYCLIC LOADING [MODIFIED FROM POWELL, 2010].....192
FIGURE 6.14 - CROSS SECTION OF BRACE SHOWING STRAIN GAUGE LAYOUT.....197

FIGURE 6.15 - COLUMN SHEAR CALCULATIONS FROM STRAIN GAUGES 198
FIGURE 6.16 – NORMALIZED BRACE AXIAL FORCE (P/PY) VS. STORY DRIFT (%) FOR EACH TEST SPECIMEN 199
FIGURE 6.17 - BRACE OUT-OF-PLANE BUCKLED SHAPE FOR EACH SPECIMEN 202
FIGURE 6.18 - COMPARISON OF NCBF BRACE BUCKLED SHAPES AT B2 AND NHSS-B1 MAX OOP DISPLACEMENT 204
FIGURE 6.19 - BRACE ELONGATION VS. TOTAL DRIFT RANGE FOR NCBF SPECIMENS 206
FIGURE 6.20 - SHEAR TAB ROTATION CALCULATION [POWELL, 2010] 207
FIGURE 6.21 - NW SHEAR TAB ROTATIONS FOR NCBF SPECIMENS 208
FIGURE 6.22 - SE SHEAR TAB ROTATIONS FOR NCBF SPECIMENS 209

FIGURE 7.1 - EVALUATION PROCESS [ASCE 41/13] 211
FIGURE 7.2 - RETROFIT PROCESS [ASCE-41/13] 212
FIGURE 7.3 - GENERALIZED FORCE-DEFORMATION RELATION FOR STEEL ELEMENTS OR COMPONENTS [1] 215
FIGURE 7.4 – NCBF FORCE-DEFORMATION PLOTS 218
FIGURE 7.5 - COMBINED FORCE-DEFORMATION CURVES FOR NCBF BOLTED SPECIMENS 220

FIGURE A.1 - NHSS-B1 FULL FRAME DRAWING 229
FIGURE A.2 - NHSS-B1 CONNECTION DRAWING 230
FIGURE A.3 - NHSS-B1 LED OPTOTRAK LAYOUT 231
FIGURE A.4 - NHSS-B1 POTENTIOMETER LAYOUT 232
FIGURE A.5 - NHSS-B1 STRAIN GAUGE LAYOUT 233
FIGURE A.6 - NHSS-B2 FULL FRAME DRAWING 234
FIGURE A.7 - NHSS-B2 CONNECTION DRAWING 235
FIGURE A.8 - NHSS-B2 LED OPTOTRAK LAYOUT 236
FIGURE A.9 - NHSS-B2 POTENTIOMETER LAYOUT 237
FIGURE A.10 - NHSS-B2 STRAIN GAUGE LAYOUT 238
FIGURE A.11 - NHSS-B3 FULL FRAME DRAWING 239
FIGURE A.12 - NHSS-B3 CONNECTION DRAWING 240
FIGURE A.13 - NHSS-B3 LED OPTOTRAK LAYOUT 241
FIGURE A.14 - NHSS-B3 POTENTIOMETER LAYOUT 242
FIGURE A.15 - NHSS-B3 STRAIN GAUGE LAYOUT 243

TABLE OF TABLES

TABLE 2.1 - PREVIOUS UW SCBF TEST SPECIMENS [DRAWINGS: JOHNSON (2005), KOTULKA (2007), POWELL (2010)] 28

TABLE 3.1 - VARIABLES USED IN UFM 55
TABLE 3.2 - AISC LIMIT STATE EQUATIONS 57
TABLE 3.3 - BDP LIMIT STATE EQUATIONS 58
TABLE 3.4 - VARIABLES USED IN LIMIT STATE EQUATIONS 59
TABLE 3.5 - DCR VALUES FOR REFERENCE CONNECTIONS 67
TABLE 3.6 - BOLTED TEST SPECIMEN DESCRIPTIONS 69
TABLE 3.7 - NCBF BOLTED TEST SPECIMEN DCR VALUES FROM AISC EQUATIONS 71
TABLE 3.8 - CHARPY V-NOTCH TEST RESULTS ON WELD MATERIAL 74

TABLE 4.1 - TARGET DISPLACEMENT PER CYCLE FOR APPLIED LOADING PROTOCOL 95

TABLE 5.1 – OVERVIEW OF SPECIMEN TEST MATRIX 99
TABLE 5.2 - PERFORMANCE STATE DESCRIPTIONS 101
TABLE 5.3 - DAMAGE STATE DESCRIPTIONS 103
TABLE 5.4 - DEMAND TO CAPACITY RATIOS WITH AISC EQUATIONS 113
TABLE 5.5 – COMPARISON OF BDP AND AISC DCR VALUES FOR BEAM TO GUSSET PLATE WELD 114
TABLE 5.6 - PROGRESSION OF DAMAGE IN NE CORNER 117
TABLE 5.7 - PROGRESSION OF DAMAGE IN SW CORNER 118
TABLE 5.8 - PROGRESSION OF DAMAGE IN BRACE, NW CORNER, AND SE CORNER 119
TABLE 5.9 - PROGRESSION OF DAMAGE IN NE CORNER 134
TABLE 5.10 - PROGRESSION OF DAMAGE IN SW CORNER 135
TABLE 5.11 - PROGRESSION OF DAMAGE IN NW & SE CORNERS 136
TABLE 5.12 - PROGRESSION OF DAMAGE IN NE CORNER 147
TABLE 5.13 - PROGRESSION OF DAMAGE IN SW CORNER 148
TABLE 5.14 - PROGRESSION OF DAMAGE IN NW & SE CORNER 149

TABLE 6.1 - SUMMARIZED TEST SPECIMEN PERFORMANCE 168
TABLE 6.2 – STIFFNESS COMPARISON OF TEST SPECIMENS 172
TABLE 6.3 - ENERGY DISSIPATION COMPARISON 177

TABLE 6.4 - POST-FAILURE STIFFNESS COMPARISON 180
TABLE 6.5 - BOLT HOLE ELONGATION PER NCBF SPECIMEN 186
TABLE 6.6 - BOLT DEFORMATION OF NCBF SPECIMENS 187
TABLE 6.7 - COMPARISON OF BEAM TO GUSSET PLATE WELD DCR USING DIFFERENT DEMANDS 190
TABLE 6.8 - INITIAL WELD TEARING CORRELATIONS IN NE BEAM TO GUSSET PLATE WELD 190
TABLE 6.9 - WELD PROPAGATION INFORMATION FOR NE BEAM TO GUSSET PLATE WELD 191
TABLE 6.10 - COMPARISON OF BRACE PERFORMANCE STATES 194
TABLE 6.11 - COMPARISON OF EXPERIMENTAL BRACE QUANTITIES 196
TABLE 6.12 - BRACE QUANTITY COMPARISONS 200
TABLE 6.13 – MAXIMUM BRACE ELONGATION VALUES FOR EACH SPECIMEN 205

TABLE 7.1 - DAMAGE CONTROL AND BUILDING PERFORMANCE LEVELS [MODIFIED FROM TABLE C2-2 FROM ASCE 41] 213
TABLE 7.2 - STRUCTURAL PERFORMANCE LEVELS AND ILLUSTRATIVE DAMAGE STATES [MODIFIED FROM TABLE C2-3 FROM ASCE 41] 214
TABLE 7.3 - MODELING PARAMETERS AND ACCEPTANCE CRITERIA FOR NONLINEAR PROCEDURES - STRUCTURAL STEEL COMPONENTS - AXIAL ACTIONS [MODIFIED FROM TABLE 9-7 IN THE STANDARD] 216
TABLE 7.4 – TENSION MODELING PARAMETERS 219
TABLE 7.5 - COMPRESSION MODELING PARAMETERS 219
TABLE 7.6 – COMBINED MODELING PARAMETERS 221

TABLE B.1 - NHSS-B1 LOAD HISTORY 244
TABLE B.2 - NHSS-B2 LOAD HISTORY 245
TABLE B.3 - NHSS-B3 LOAD HISTORY 246

CHAPTER 1: INTRODUCTION

1.1 Overview of Concentrically Braced Frames

During an earthquake, a building must resist large lateral forces from the ground accelerations. Steel concentrically braced frames (CBFs) resist this lateral load through braces that concentrically frame into the centerline of the beam-to-column joint or into an opposing brace, typically with gusset plate connections. Often, engineers use CBFs in pairs of opposing braces to produce comparable responses in both displacement directions, shown in Figure 1.1, rather than a single diagonal brace, which results in an asymmetric hysteretic response (due to brace buckling). Regularly, in areas of high seismicity the gusset plate connections (to column, beam, and brace) are welded, but bolted connections can provide an attractive alternative in terms of constructability. Currently, there is uncertainty surrounding bolted CBF performance because of limited available research. Prior to the early 1990s, CBFs were not designed to meet modern ductile detailing and design requirements and engineers more commonly employed bolted gusset plate connections. The CBF configuration provides significant elastic stiffness through axial stiffness of the braces. Additionally, CBFs dissipate a large amount of energy through the inelastic deformation of the braces and/or connecting elements. This energy dissipation is critical to the system because it dampens the structure's dynamic response to an earthquake.

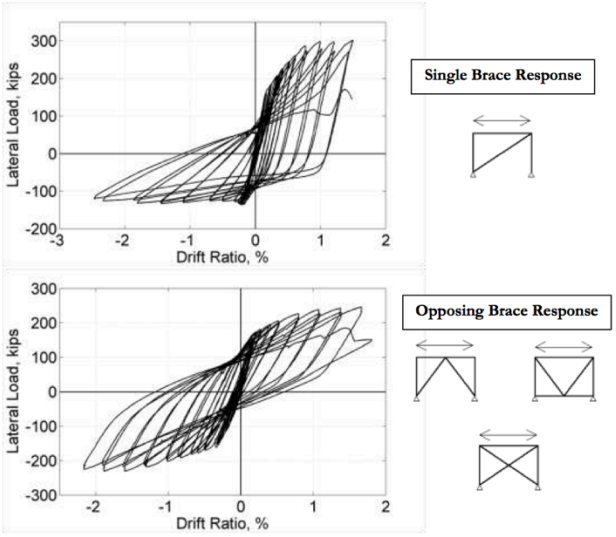

Figure 1.1 - Response of Single Brace vs. Opposing Braces [Powell, 2010]

1.2 Overview of Design Methodologies

A building's response to an earthquake is a function of the building's mass and stiffness, and the particular earthquake's ground motion frequency. Prior to the 1988 Uniform Building Code (UBC), engineers approached CBF design from a force-based perspective, where the braced frame components were designed for the building's base shear. This force-based methodology often is uneconomical as it results in larger structural members in order to provide adequate strength in the system to resist lateral loads. At that time, there was no consideration of overstrength factors, material property variability, or rotational demands on components from brace out-of-plane displacements. These older CBFs are herein referred to as non-seismic concentrically braced frames (NCBFs).

When the building's structure cannot fully resist the seismic forces elastically, there will be yielding within the structural system as shown in Figure 1.2. These older CBFs did not require special detailing to accommodate these yielding mechanisms, out-of-plane brace buckling, or to ensure ductile behavior, making the seismic response of NCBFs uncertain. Without special detailing requirements, NCBF connections are vulnerable to brittle failure modes, such as those listed in Figure 1.2 (excluding brace fracture) that could occur before the brace capacity has fully developed. Connection failures will significantly reduce the frame resistance, drift capacity, and ductility of the CBF system. There are a large number of NCBFs currently in use throughout the United States that pose a significant potential safety risk because their behavior is not well known. Unfortunately, at this time, there has been limited research conducted to quantify this risk posed by NCBF systems.

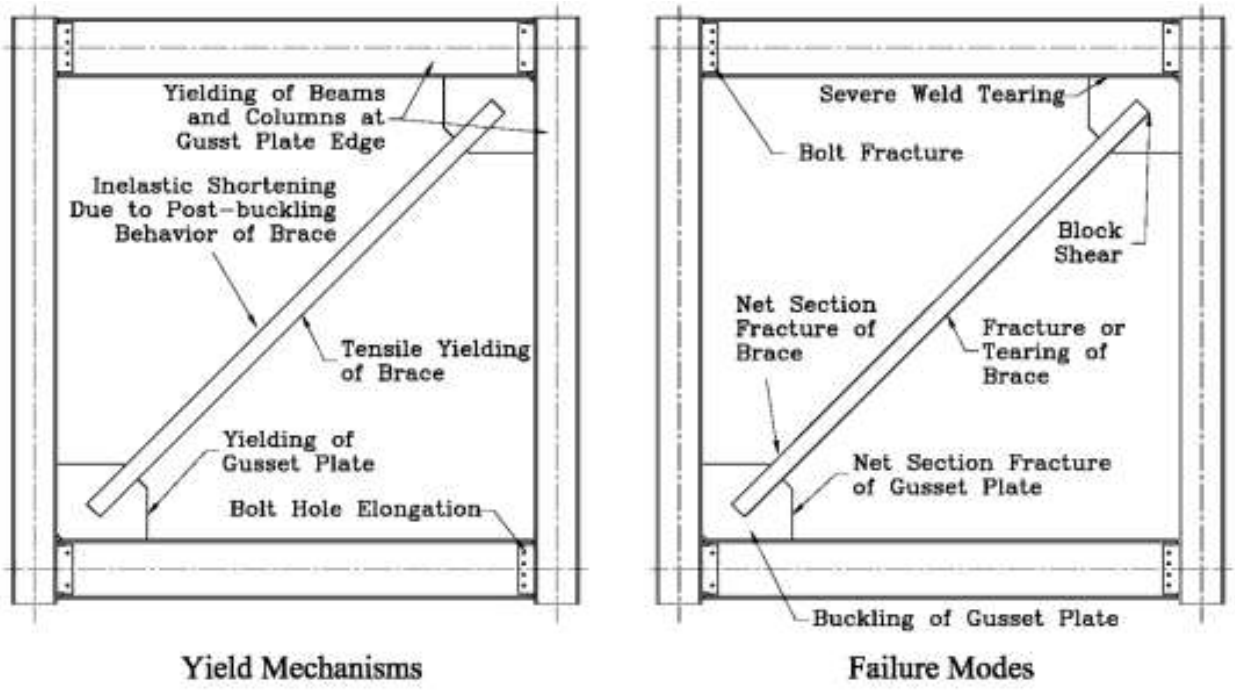

Figure 1.2 - Potential Yield Mechanisms and Failure Modes for SCBFs [Powell, 2010]

The yield mechanisms shown can be beneficial for energy absorption in the system, in particular the brace tensile yielding and compressive buckling. Currently, there are two common design methodologies for ductile design of Special Concentrically Braced Frames (SCBFs), which encourage these yield mechanisms unlike NCBF design. These methodologies were developed to increase drift capacity of the CBFs from the previously used force-based design of CBF specimens.

The first modern design procedure has been developed since the early 1990s and uses the American Institute of Steel Construction (AISC) Specifications and Seismic Provisions. AISC approaches ductile design from a capacity-based procedure by detailing the connections for the expected capacity of the brace. The gusset plate connections must also accommodate the inelastic rotations from brace out-of-plane demands. This approach focuses on inelastic capacity of the brace (as opposed to in the connections and framing elements) to determine the force in the connection. This methodology uses resistance factors to protect against uncertainties in the

calculations. The resistance factors for bolted connection limit states are all low and conservative due to limited research, leading to more conservative bolted connection designs.

The second modern design procedure has been recently developed by research on SCBFs at the University of Washington (UW). This Balanced Design Procedure (BDP, Roeder et al., 2011) aims to add ductility and drift capacity to the system by allowing additional inelastic deformation in the gusset plate and framing elements. A new series of balance factors has been developed to replace the resistance factors from the AISC methodology. These balance factors are less conservative and aim to create a yielding hierarchy of brace buckling, brace tensile yielding, gusset plate yielding, beam and column yielding, and then brace fracture. However, balance factors were not developed for bolted connection limit states due to limited testing data. The majority of prior SCBF research at the UW was on welded gusset plate connections. The intent of both current SCBF methodologies is to ensure adequate connection capacity to develop the brace capacity with an increased drift range and result in a ductile failure mode of brace fracture.

1.3 Research Motivation

The research presented in this thesis was funded by the National Science Foundation (NSF): "NEESR: Collaborative Developments for Seismic Rehabilitation of Vulnerable Braced Frames". For this thesis, I tested three single bay, single story NCBF specimens that were funded by NSF. These NCBF experiments are part of a larger initiative to explore NCBF seismic behavior and identify specific NCBF vulnerabilities. The UW is working alongside the University of California, Berkeley, and the National Center for Research on Earthquake Engineering (NCREE) in Taiwan for this experimental initiative.

As mentioned, in all three design methodologies, there has been limited research conducted on bolted braced frame performance. There is a high level of uncertainty surrounding bolted behavior under seismic loading in CBF systems, in particular for NCBF specimens whose seismic response is not understood as well as modern designed systems. Regarding modern construction, bolted connections can provide an appealing alternative to welding in terms of constructability if they have comparable ductile responses to welded connections.

1.4 Research Goals

The specific goals for the research within this thesis are listed below.

1. Improve the understanding of NCBF seismic performance and identify their critical deficiencies through three NCBF experiments.
2. Specifically, to experimentally and analytically evaluate the seismic performance of bolted beam to column and gusset plate to column shear tab connections in these NCBF specimens.

1.5 Overview of Report

This thesis contains the results, analysis of, and recommendations from three experimental tests completed at the University of Washington's Structural Research Laboratory (UW SRL) between July 29, 2013 and December 19, 2013. Chapter 2 discusses a literature review of previous research relevant to these tests and their implications. It also details yield mechanisms and failure modes characteristic of bolted connections. Chapter 3 describes the design of each specimen with in-depth analysis of a number of limit states. Chapter 3 also highlights the differences between the AISC and BDP's approach to SCBF design and elaborates on identified NCBF deficiencies in the bolted connections studied. Chapter 4 details the experimental test setup and instrumentation layouts. Chapter 5 documents the test observations from each experiment, in particular describing connection behavior and the visible yield mechanisms and failure modes shown in Figure 1.2. Chapter 6 includes an extensive analysis of the data collected from each test. It reports on the overall frame behavior such as the hysteretic envelopes, stiffness values, and energy dissipation capabilities, and the component behavior such as brace out-of-plane displacement, gusset plate rotations, and bolt/weld damage. Chapter 7 provides an evaluation of the specimens based on the experimental findings using the ASCE/SEI Standard 41-13 for the Seismic Evaluation and Retrofit of Existing Buildings. And finally, Chapter 8 summarizes and draws conclusions from the research.

CHAPTER 2: LITERATURE REVIEW

2.1 Introduction

Considerable research has been conducted to improve the design of SCBFs and their performance. While CBFs are considered to be among the most efficient of steel structural systems, they are not considered ductile. In past earthquakes, CBF systems experienced extensive damage that required significant upgrade and repair work (Rai and Goel, 2003). Section 2.2 of this chapter will discuss past research on SCBFs, highlighting the work of Shaback and Brown (2003) and Tremblay (2002). Previous theses from the UW by Johnson (2005), Kotulka (2007), and Powell (2010), discuss other CBF research such as Whitmore (1952), Bjorhovde and Chakrabarti (1985), Jain et al (1978), Aslani and Goel (1989) and more.

The UW has spent substantial time testing various SCBF connections to better understand SCBF performance under increased cyclic loading. Examples of parameters studied include: gusset plate geometry, beam to column connection method, bolted vs. welded connections, and plate thicknesses. Through series of single bay, single story tests in the UW SRL and multi-story tests at the NCREE lab in Taiwan, the behavior of SCBFs has been examined and better detailed from past UW graduate students: Johnson (2005), Herman (2007), Lumpkin (2009), Clark (2009), Kotulka (2010), and Powell (2010). While many tests had a brace fracture failure mode, their total resistance and total drift ranges varied based on the gusset plate and beam to column connections. A number of these tests will be discussed in Section 2.3 to provide background for the two modern designed bolted SCBF specimens, SHSS-B1 and SHSS-B2, tested in this thesis' bolted series of experiments. These previously tested SCBF connections can provide context for how a current bolted SCBF connection compares in performance to a current welded SCBF connection.

The Northridge Earthquake in 1994 illuminated vulnerabilities present in many different lateral load resisting systems. For CBFs, common failure modes were brace fracture and brace connection failures (Rai and Goel, 2003). CBFs designed and constructed prior to the Northridge Earthquake have not been studied in great detail, leaving the behavior of these NCBFs and the

risk they pose to the community largely undefined. NCBF systems are believed to have myriad deficiencies that could lead to sudden and brittle failures in the event of a large earthquake. To further examine and explore perceived vulnerabilities of these older connections, the UW designed and tested a series of braced frame specimens modeled on older building details. Section 2.4 of this chapter will discuss the infrastructure review conducted by Sloat (2014) that identified the most severe deficiencies in the older NCBF connections. Section 2.4 will also discuss the performance of a pilot NCBF specimen tested by Powell (2010). The purpose of these NCBF experiments is to investigate the controlling failure mechanisms for the NCBFs to provide engineers with a better understanding of the components that require retrofit. For this thesis, three deficient bolted NCBF connections, NHSS-B1, NHSS-B2, and NHSS-B3, were tested. Sloat (2014) and Sen (2014) conducted a series of experiments on welded NCBF connection designs and possible retrofit strategies of deficient connections.

2.2 Previous CBF Research

The research discussed in this section is a small portion of the research conducted on CBFs. The two studies discussed below were component-based experiments rather than full-scale system experiments. However, substantial research has been conducted of both kinds and more information can be found in the aforementioned theses.

2.2.1 Tremblay [2002]

For the research from Tremblay (2002), a total of 76 cyclic loading tests of bracing members from 9 test programs were reviewed to inform the seismic design of CBFs. Parameters studied within the programs were: brace section type, brace cross sectional area, brace end conditions, brace effective slenderness, and material properties of the brace. Figure 2.1 shows schematic illustrations of the various geometries for the braces studied. It was found that brace fracture life (i.e. the number of cycles the brace can achieve prior to fracture) and brace ductility relies heavily upon the effective slenderness of the brace, and to a "lesser extent" the width to thickness ratio (Tremblay, 2002). The research showed that local buckling at the brace plastic hinge was more severe in braces with low slenderness values (despite the width to thickness value) because higher compressive strains were induced in the plastic hinges in those specimens. The researchers also concluded that slender braces were able to achieve higher total ductility

(dissipate more total energy) and reach larger drift ranges prior to fracture because the strain demand at the plastic hinge reduces with brace slenderness (Tremblay, 2002).

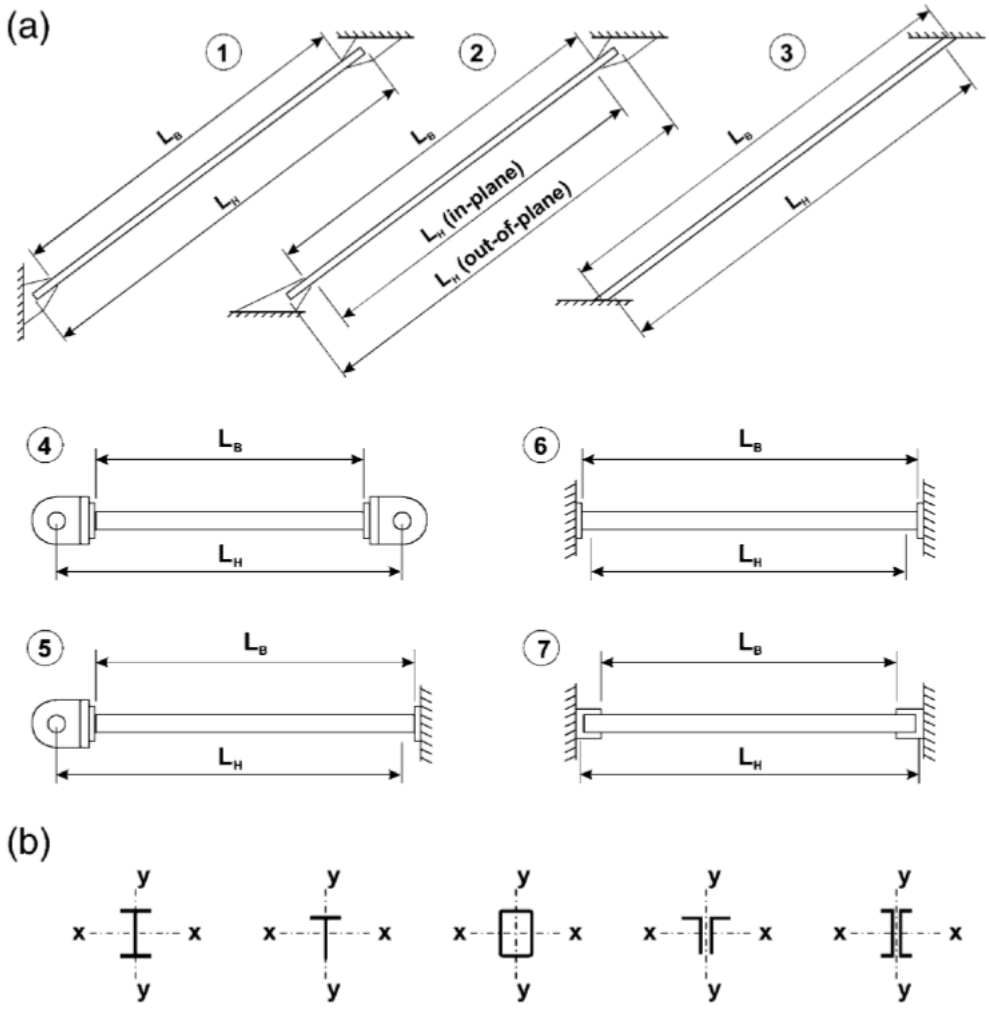

Figure 2.1 - Geometry of Brace Specimens (Tremblay, 2002)

2.2.2 Shaback and Brown [2003]

For this experimental study, nine full-scale HSS shape brace specimens with typical end connections were tested under axial cyclic loading until failure in the test setup shown in Figure 2.2. One disadvantage of SCBFs is early HSS brace fracture due to low-cycle fatigue, which can impact the lateral stiffness and energy dissipation capabilities of the SCBF (Shaback and Brown, 2003). This research found that the effective slenderness ratio and the width to thickness ratio were parameters that highly influenced the fracture life of HSS braces. Previous research (Tang and Goel, 1987) found that more slender specimens experience less severe buckling. To illustrate

the effect of the slenderness ratio on brace hysteretic performance, two specimens with almost identical width to thickness ratios and different slenderness values were compared within Shaback and Brown (2003). The normalized force versus normalized displacement response is presented in Figure 2.3.

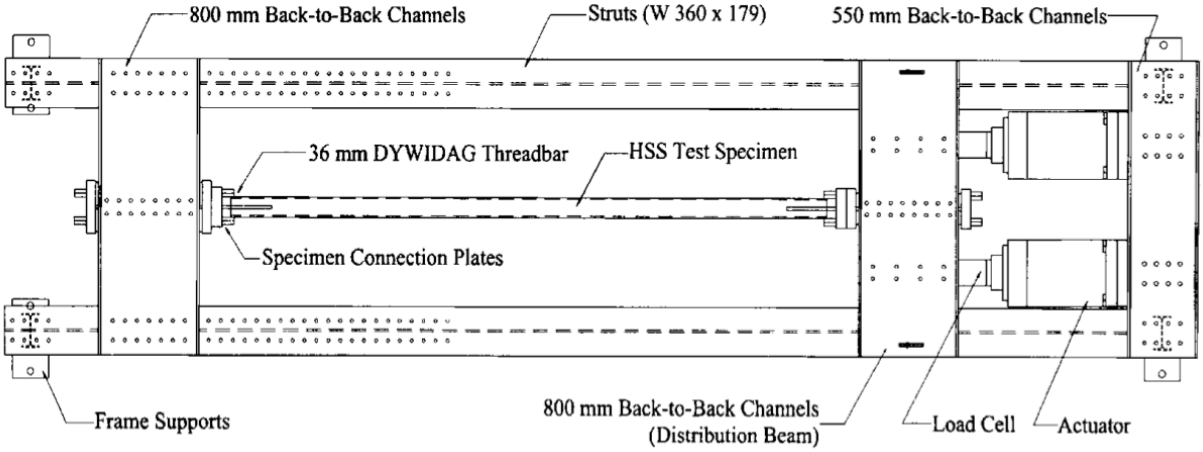

Figure 2.2 - Test Frame Assembly (Shaback and Brown, 2003)

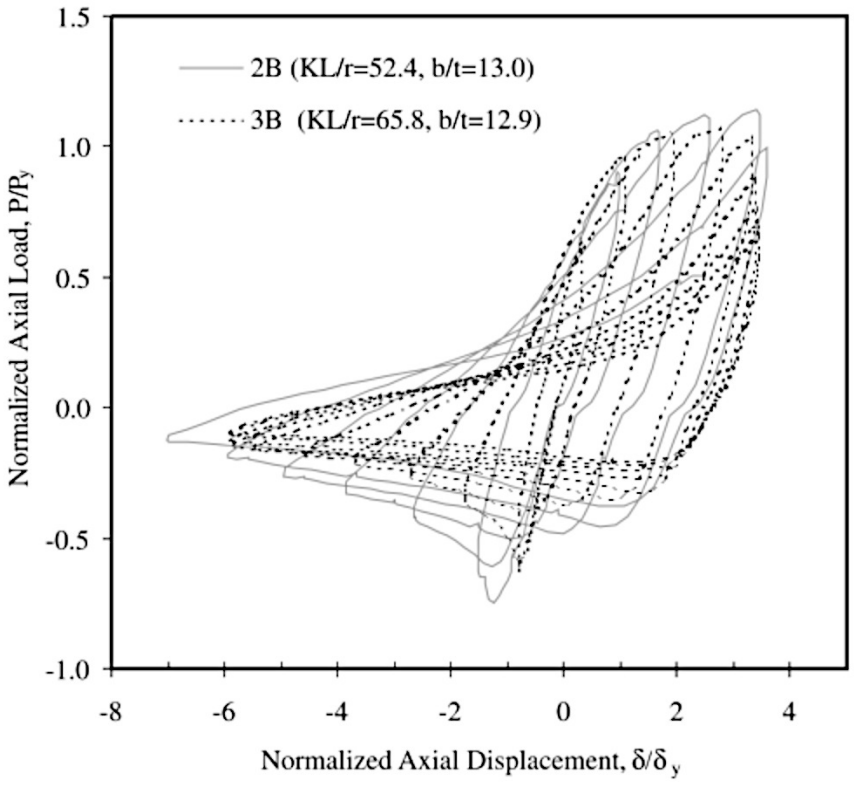

Figure 2.3 - Normalized Hysteretic Curve Comparison (Shaback and Brown, 2003)

Specimen 2B was stockier than 3B. Their hysteretic response shows that 2B exhibits better behavior in compression with fuller loops than 3B. It can be seen that as the effective slenderness ratio decreases, the stiffness degradation decreases, and energy dissipation per cycle increases (Shaback and Brown, 2003). The researchers found that the effective slenderness ratio had the most impact on a brace's hysteretic response. They also found that while the width to thickness ratio had minimal effect on the hysteretic response, it was influential on the brace fracture life. As the width to thickness ratio decreased, the specimens successfully completed more load cycles and reached greater maximum displacements than those with higher width to thickness ratios (Shaback and Brown, 2003).

2.3 Previous UW SCBF Research

While the research discussed in Section 2.2 mostly highlighted findings from testing brace sections, the research from the UW described herein, focused on full system behavior and brace connection design. The UW has conducted an extensive amount of research to promote better understanding of SCBF behavior and to influence connection design guidelines. Much of this research has been on fully welded gusset plate connections, as those are common in current west coast construction. However, bolted connections, rather than fully welded connections, are preferred by many engineers due to the perception of reduced construction time and labor costs. If they provide comparable ductility to welded SCBF connections, they could lead to an important development in SCBF design. The UW has conducted experiments on two types of bolted SCBF connections: bolted brace to gusset plate (HSS-16, HSS-19) and bolted end plates (HSS-20, HSS-21). The results from these bolted experiments as well as the results from the best performing welded SCBF specimen (HSS-05) are discussed below in their own subsections. Table 2.1 shows the connection drawings and test objectives for the specimens reviewed in this section. Figure 2.4 provides a drawing of the UW test setup for directional orientation such as "the NE corner".

Table 2.1 - Previous UW SCBF Test Specimens [Drawings: Johnson (2005), Kotulka (2007), Powell (2010)]

Specimen	Connection Drawing	Test Objective
HSS-05	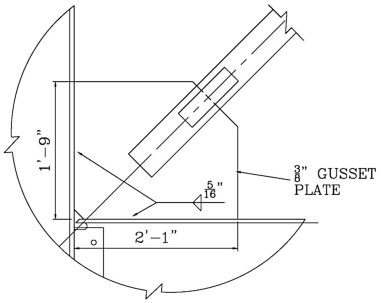	Specimen was designed to test the limits of the weld capacity design.
HSS-16	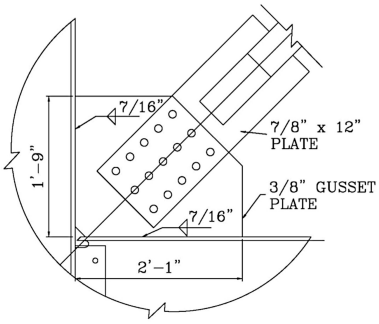	This specimen was designed with a bolted connection at the gusset plate to increase constructability.
HSS-19	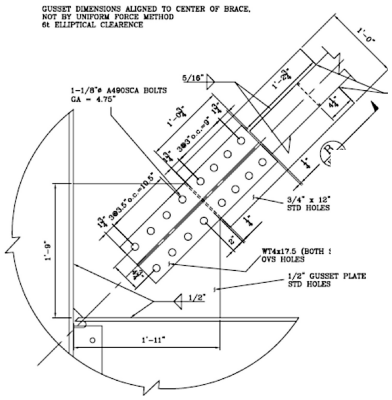	Specimen was designed to evaluate bolted brace to gusset plate connections for improved constructability.
HSS-20	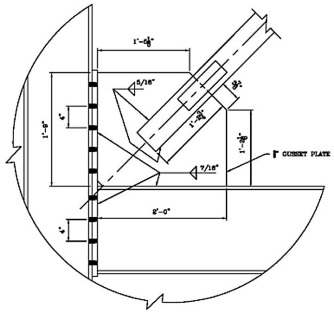	Specimen was designed with a bolted beam end plate connection for improved constructability.

Specimen	Connection Drawing	Test Objective
HSS-21	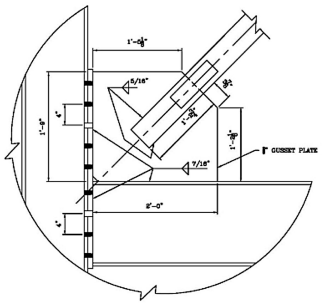	Specimen was designed with a bolted beam end plate connection for improved constructability and reduced bolt configuration.

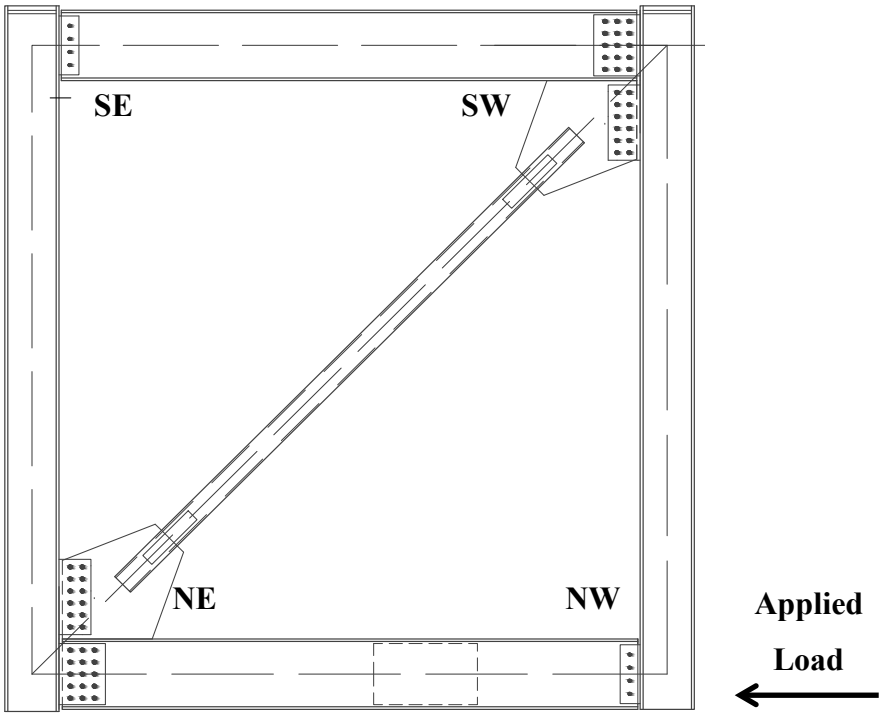

Figure 2.4 - UW Test Setup Orientation

2.3.1 HSS-05, Shawn Johnson [2005]

Specimen HSS-05 was designed using the BDP and was found to have the best SCBF performance of the specimens tested at the UW as it exhibited the greatest inelastic deformation capacity and ductility with brace fracture. Table 2.1 shows a drawing of the gusset plate connection. The gusset plate connections consisted of 3/8 in. thick gusset plates welded directly to the beam and column flanges with 5/16 in. fillet welds. The gusset plates provided a 6t elliptical rotational clearance rather than the standard 2t linear clearance as required by AISC.

The interface welds were designed for the plastic capacity of the plate, per the BDP. In the NE and SW corners, the beam was joined to the column with a complete joint penetration (CJP) weld. The force versus drift response for the specimen is shown in Figure 2.5. This specimen ultimately failed through brace fracture, but there was significant undesirable weld tearing in the gusset plate interface welds. At the end of the test, the gusset plate to column welds in the NE corner had fractured, the NE beam to gusset plate weld was torn 16% of its length, the SW beam to gusset plate weld was torn 19% of its total length, and the SW gusset plate to column weld had torn 21% of its length. Tearing of the welds is believed to have changed the support conditions of the specimen causing the brace to fracture on a diagonal and slightly offset from mid-span (Johnson, 2005).

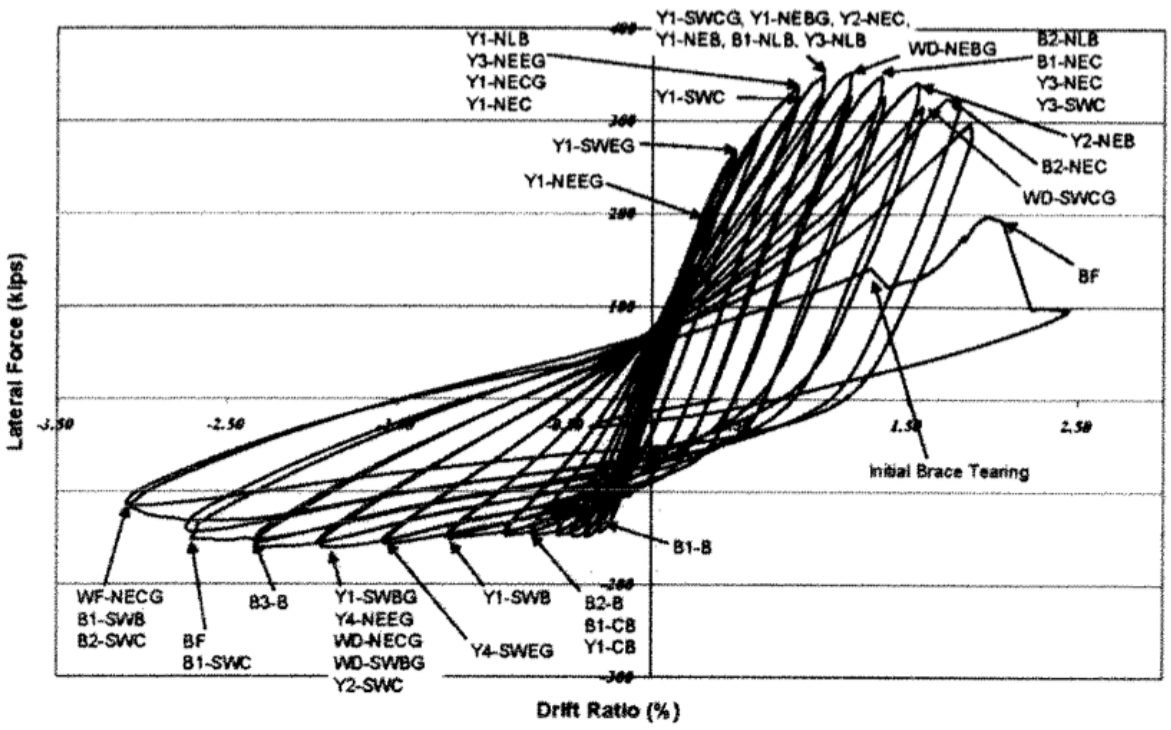

Figure 2.5 - Specimen HSS-05 Force vs. Drift Ratio Response (Johnson, 2005)

In addition to weld tearing in the gusset plate interface welds, both gusset plates sustained extensive yielding. The specimen's framing elements also experienced yielding and local flange buckling. The south beam underwent a downward rotation along the longitudinal axis of the beam due to the downward vertical brace force from the out-of-plane brace deformation (Johnson, 2005). The brace achieved a large, 17 in. of out-of-plane displacement prior to brace

fracture, due to the flexibility of the gusset plate weld tearing and the out-of-plane displacement of the gusset plates. HSS-05 reached a total drift range of 4.9% and had a total force range of 525 kip. The desirability of this specimen's performance stems from its high ductility, inelastic deformation capacity, and its ability to continue to gain compressive strength post-brace buckling. However, severe weld tearing is not encouraged in design, and was one negative outcome of this specimen. Throughout this thesis, the bolted specimens tested will be compared to the performance of this welded SCBF.

2.3.2 HSS-16, Brandon Kotulka [2007]

HSS-16 was the first of two bolted brace to gusset plate connections tested at the UW. A connection of this type would allow the brace to be shipped to the site with a pre-welded extension plate and field bolted to the gusset plate. This procedure, rather than field welding, can potentially save on construction costs as previously mentioned. Table 2.1 shows the gusset plate connection detail for HSS-16. It used a 7/8 in. extension plate bolted with (15) – 1 1/8 in. A490 slip critical bolts in oversized holes. The extension plate had a notch cut out to allow the brace to have its entire cross section for one third of its connection length to the extension plate to thereby eliminate a potential net section failure (Kotulka, 2007). Like HSS-05, this connection also used a 3/8 in. thick gusset plate with the same gusset plate to beam and gusset plate to column connection lengths as HSS-05. This connection used larger 7/16 in. welds to connect the gusset plate to the framing elements.

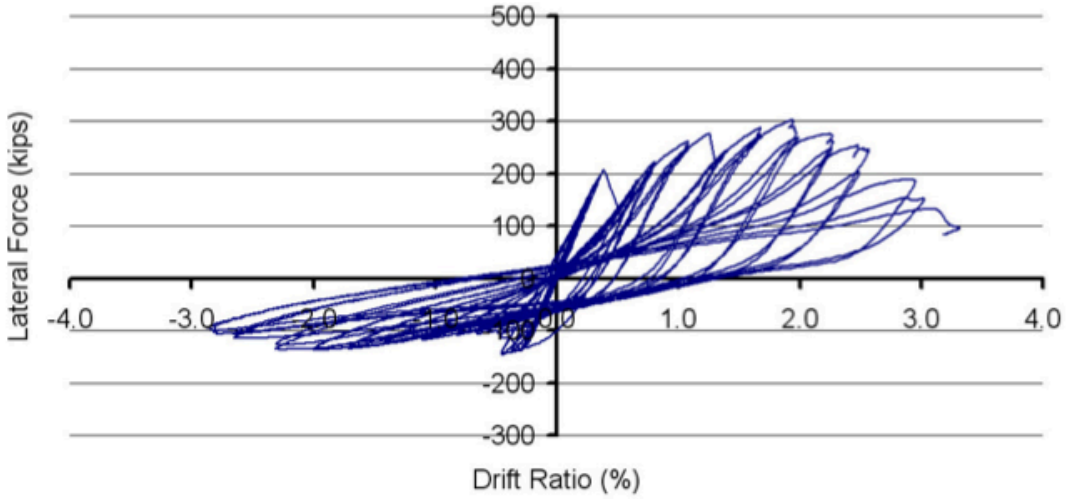

Figure 2.6 - Specimen HSS-16 Force vs. Drift Response (Kotulka, 2007)

The force versus drift response for specimen HSS-16 is shown in Figure 2.6. This specimen reached the highest drift range of any of the UW test specimens at 5.89%. On the other hand, it reached a much lower total force capacity than the other test specimens at 447 kip (78 kip less than HSS-05) and it had an undesirable failure mode of net section fracture in the brace to gusset plate extension plate. Figure 2.7 shows the plate cracking prior to full fracture. The smaller compressive capacity of the frame was due to the fact that the connection buckled before the brace capacity was developed (connection was weaker than brace) (Kotulka, 2007).

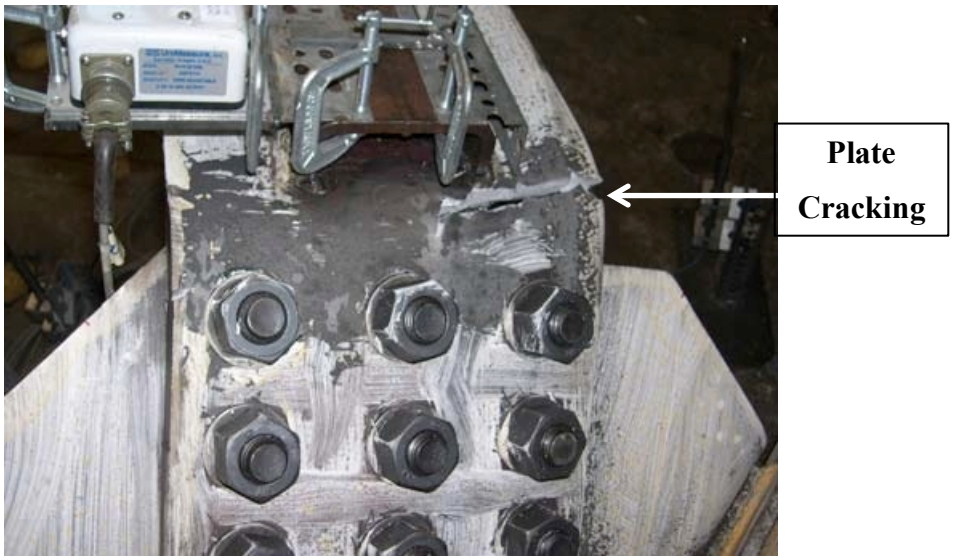

Figure 2.7 - Cracking in Extension Plate at -2.86% Drift (modified from Kotulka, 2007)

In addition to the net section fracture in the extension plate, there was significant cracking in the base metal and welds of both gusset plates, seen as early as -0.49% story drift. In both gusset plate connections, the base metal adjacent to the gusset plate to column weld fractured. Figure 2.8 shows the complete base metal fracture of the NE column to gusset plate connection. In the SW connection, the beam to gusset plate weld was torn 36% of its length at the end of the test. These outcomes are not desirable for seismic design.

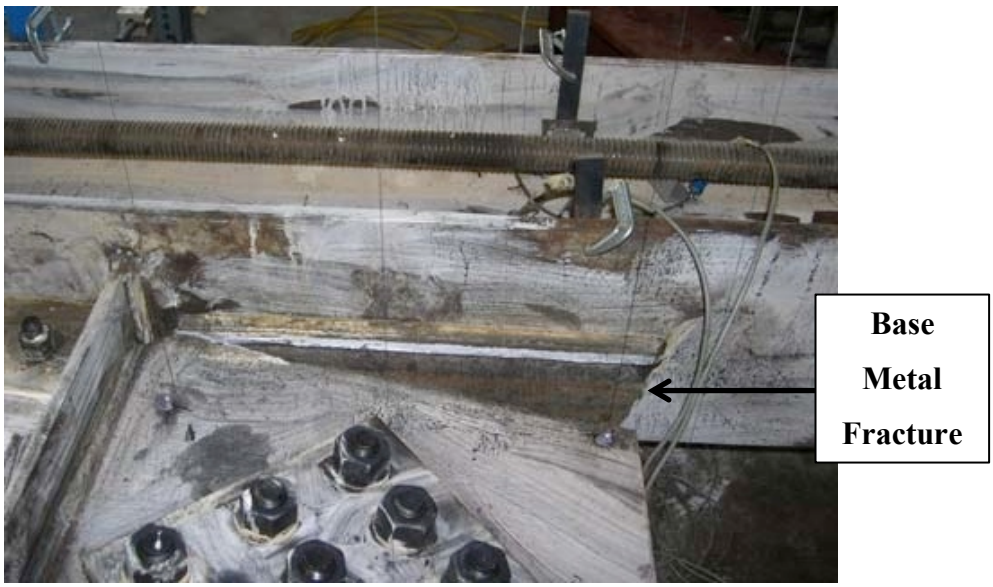

Figure 2.8 - NE Column Connection Base Metal Fracture at -2.66% Drift (modified from Kotulka, 2007)

2.3.3 HSS-19, Jake Powell [2010]

Specimen HSS-19 was the another bolted brace to gusset plate connection tested at the UW. The goal was to improve upon the performance of HSS-16, which had a high drift range but undesirable failure mode. This specimen was designed with consultation from AISC and practicing engineers. To improve the connection, two WT sections were chosen to connect the brace to the gusset plate because of their high out-of-plane stiffness. The connection for HSS-19 is shown in Table 2.1. The WT's were bolted through their flanges to the 1/2 in. gusset plate with (8) – 1 1/8 in. A490 slip critical bolts in standard holes. The WT's were also bolted to a 7/8 in. thick splice plate using the same number and size bolts as in the gusset plate. The brace was slotted and welded to the splice plate. The gusset plate was designed to provide a 6.8t elliptical clearance rather than the standard 2t linear clearance required by AISC.

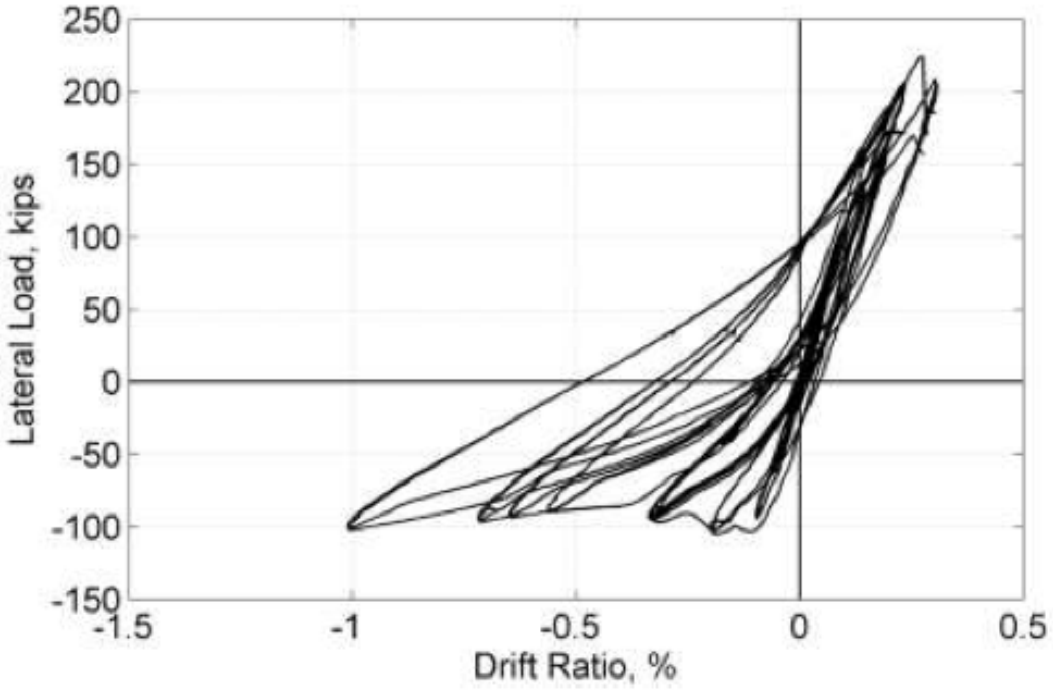

Figure 2.9 - Specimen HSS-19 Force vs. Drift Response (Powell, 2010)

The force versus drift response of the frame is shown in Figure 2.9. This frame reached a low total drift range of 1.32% and had a total force range in the frame of 326.2 kip. The failure mode of the test specimen was fracture of the splice plate connecting the WT's to the brace. While designed to improve upon the performance of HSS-16, this frame reached a significantly lower drift level, resisted a smaller force range by 121 kip, and also had an undesirable failure mode. There was minimal yielding in the framing elements and gusset plates throughout the test, failing to accomplish one of the testing goals of utilizing total ductility of the system components (Powell, 2010). All inelastic deformation was located in the splice plates, which led to plate fracture, shown in Figure 2.10.

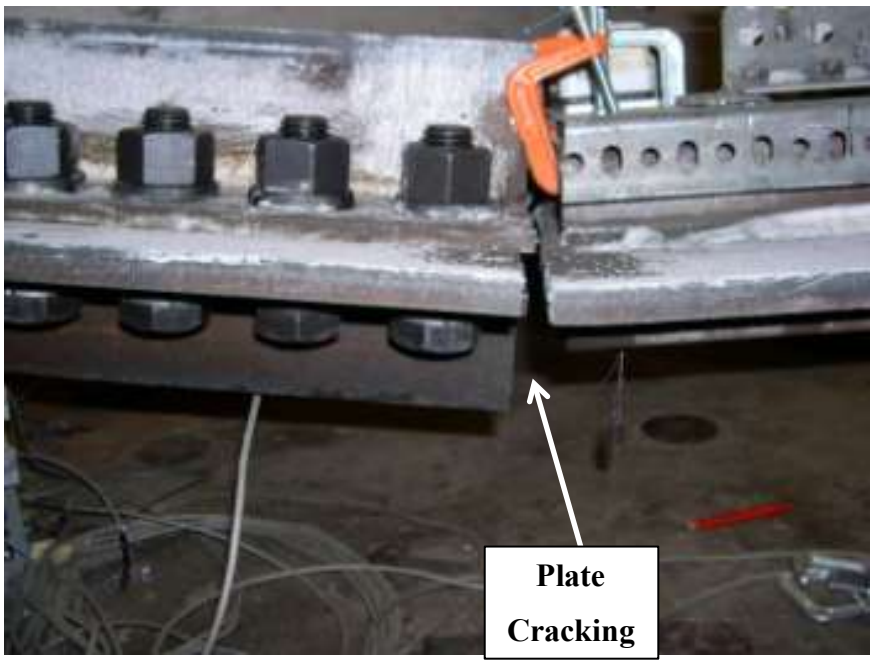

Figure 2.10 - Fractured Splice Plate at End of Test (modified from Powell, 2010)

2.3.4 HSS-20, Jake Powell [2010]

HSS-20 was the first of two bolted end plate connections tested at the UW to explore bolted SCBF options that could increase the rate of construction and decrease labor costs. This design was proposed by AISC and CANRON. The connection drawing is shown in Table 2.1. This specimen was the first of the tests within this chapter to not use a CJP weld to connect the beam to column in the NE and SW corners. Instead, the beam webs were welded directly to the 1 in. thick end plate. The 3/8 in. thick gusset plates were welded directly to the end plates and the beam flanges. The gusset plate provided a 6.8t elliptical clearance, rather than the standard 2t linear clearance. The end plate was bolted to the column flanges with (18) - 3/4 in. A490 bolts.

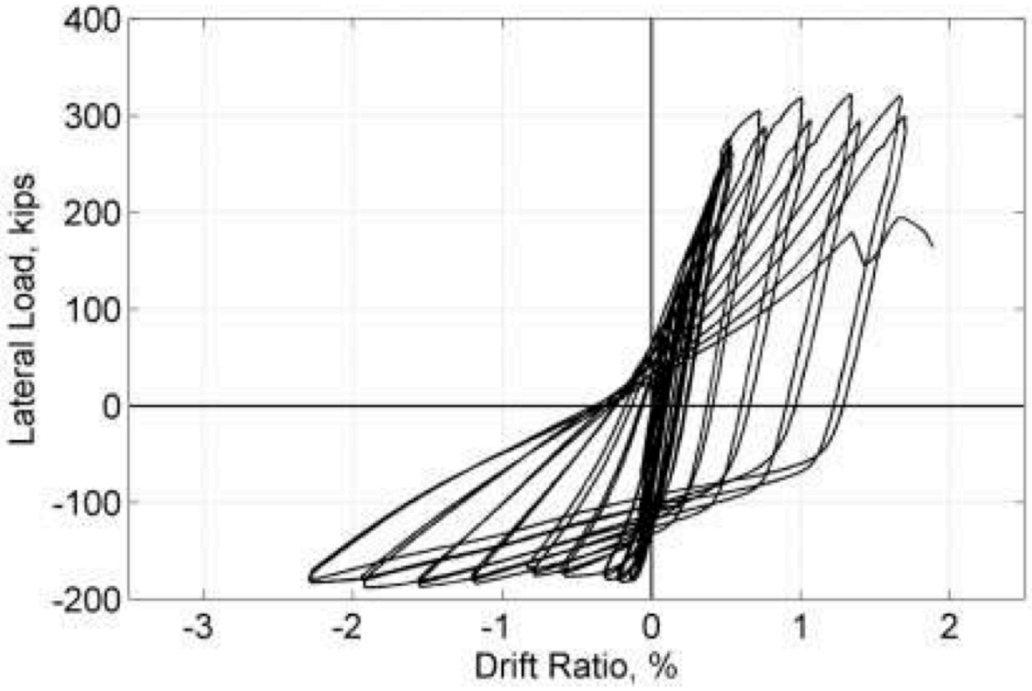

Figure 2.11 - Specimen HSS-20 Force vs. Drift Response (Powell, 2010)

Figure 2.11 shows the force versus drift response for specimen HSS-20. This specimen reached a total drift range of 3.97% and a total force range of 509.2 kip. While the specimen did not reach as high a drift range as HSS-05 or HSS-16, it achieved a higher force range than HSS-16 by 62 kip, and a slightly lower range than HSS-05 by 16 kip. Like HSS-05, this specimen experienced the desirable failure mode of brace fracture. This frame performed well in that it distributed some yielding through the gusset plates to the framing elements and did not have any gusset plate interface weld cracking.

2.3.5 HSS-21, Jake Powell [2010]

HSS-21 was the same connection design as HSS-20, but with one set of bolts removed from both the gusset plate and the beam connection to the endplate. With those bolts removed, HSS-21 used a 14-bolt end plate connection, as shown in the drawing in Table 2.1. It was assumed the tension from the brace would be evenly distributed amongst the bolts during cyclic loading (Powell, 2010). However, at +0.35% drift the two bolts in line with the brace's line of action fractured. This fracture indicates the bolts did not all resist the same amount of force. The bolt

fracture did not appear to inhibit the brace performance in any way. The force versus drift response for the specimen is shown in Figure 2.12. HSS-21 experienced a higher total drift range than HSS-20 at 4.14%, and a higher total force range of 511.3 kip. The frame ultimately failed through the desirable failure mode of brace fracture. Neither HSS-20 nor HSS-21 saw a loss in compressive resistance post-brace buckling.

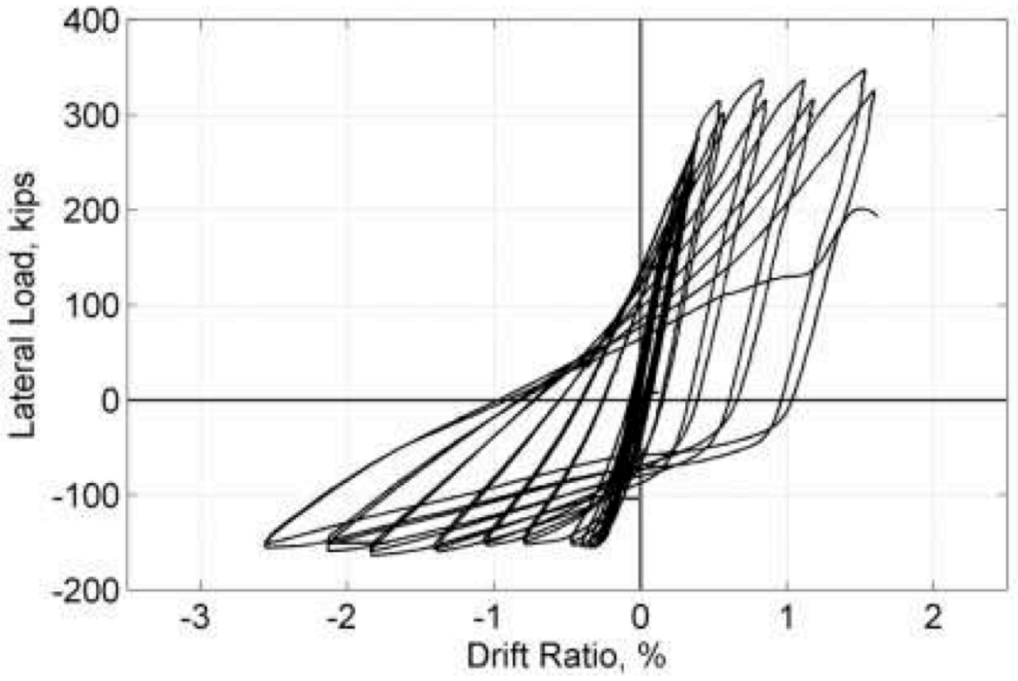

Figure 2.12 - Specimen HSS-21 Force vs. Drift Response (Powell, 2010)

2.4 Identification and Prior Testing of NCBF Deficiencies

The 1994 Uniform Building Code (UBC) introduced limited ductile detailing requirements for braced frames, and the 1997 AISC Seismic Design Provisions fully developed these concepts creating the "SCBF" (Hsaio et al., 2011). Prior to the 1988 UBC, there were no ductility requirements. Instead of encouraging ductility, the design philosophy for CBFs was to emphasize strength in the bracing members and their components, which may lead to poor CBF performance under severe ground motions (Rai and Goel, 2003). These NCBFs did not consider overstrength of the brace material nor did they include ductile detailing, which puts them at risk for brittle failures as previously mentioned. During the Northridge Earthquake, the main failure

modes seen in braced frames were: brace buckling, brace fracture, and brace connection failures. The connections failed due to the rotational demand on the gusset plate from the brace out-of-plane displacements (Rai and Goel, 2003).

To protect these vulnerable, older buildings, there is a large push in the engineering community for seismic retrofits. Retrofits vary in their level of intensity and expense, depending on the extent of work to the building. Creating a hierarchy of deficiencies in the NCBFs can be helpful to building owners trying to decide on a retrofit strategy. For example, one NCBF design might have multiple deficiencies, but they might not present the same level of risk in the event that aspect fails. To create this hierarchy and to develop an understanding of NCBF behavior, the UW first identified myriad perceived system deficiencies in the older buildings described in subsection 2.4.1. We then designed connections based on these deficiencies and conducted a series of NCBF full-scale single bay, single story tests in a similar experimental setup as the prior UW SCBF tests, described in Chapter 4. The design of these tests is presented in Chapter 3 and their test performance is described in Chapter 5. The first pilot NCBF specimen was tested by Jake Powell referred to as NCBF 32 (Hsiao et al., 2011), and discussed below in subsection 2.4.2.

Because the specimens in this thesis are all bolted beam to column and gusset plate to column connections, bolt yield mechanisms and failure modes are important to identify. Current design prevents these bolted limit states, as inelastic deformation is to occur in the brace. As seen in the previous UW bolted specimens described above, there was no mention of observed bolt limit states (except HSS-21, which had unexpected bolt fracture). It is expected that the older bolted designs with deficient connections could be susceptible to damage and failure from deficient bolt capacities. Subsection 2.4.3 describes the potential bolt yield mechanisms and failure modes.

2.4.1 Infrastructure Review

The three bolted NCBF experiments described in this thesis were developed from drawings of older buildings that were designed and constructed prior to the adoption of the 1988 UBC. Their design is discussed in detail in Chapter 3. Sloat (2014) conducted an extensive infrastructure

review of these older buildings that were located in high seismic zones. Using the official building drawings, he was able to identify and categorize the various NCBF configurations (such as Chevron, single diagonal and more) and categorize common connection types for the braced frames. He then analyzed both the braced frame subsystem as a whole, and the prominent connections individually using current AISC Seismic Requirements to find the system deficiencies. The results he found were enlightening, as many of the connections completely failed current AISC design standards in that their demand to capacity values were above 1. Chapter 3 provides an in depth discussion of the design of each NCBF specimen (NHSS-B1, NHSS-B2, NHSS-B3) and their controlling limit states for this thesis. The NCBF tests presented in this thesis, from Sloat (2014), and from Sen (2014) will analyze the results of the UW and NCREE NCBF experiments and will provide an evaluation of the braced frame performances (Chapter 7).

2.4.2 Pilot NCBF Experiment – NCBF 32 [Powell, 2010]

Pre-1988 NCBFs were designed without the special detailing requirements for SCBFs today, which ensure the connections to be stronger than the brace. Because of this absence, NCBFs are highly susceptible to connection failure and represent one of the largest potential seismic hazards in the US today (Hsiao et al., 2011). This pilot NCBF test was the first test conducted at the UW to begin improving the understanding of how NCBFs will respond to a seismic event. NCBF 32 was tested in the same setup in the UW SRL where previous SCBF specimens were tested. The full frame and connection drawings are shown in Figure 2.13.

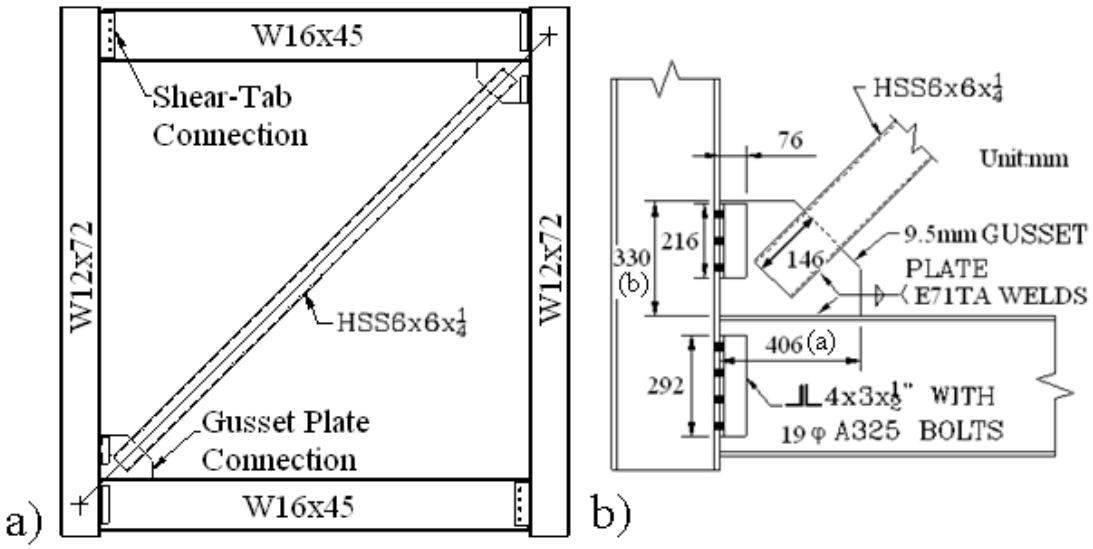

a. Full Frame Drawing **b. Gusset Plate Connection Drawing**

Figure 2.13 - NCBF 32 Test Details (Hsiao et al., 2011)

Unlike previous SCBF tests, this specimen used an HSS6x6x1/4, which is a non-seismically compact brace section. Additionally, the connections were not designed for the expected capacity of the brace as required for current SCBF design. They were instead detailed for the design compression strength of the brace using the nominal brace material strength (Hsiao et al., 2011). The gusset plate was not designed with elliptical or linear clearance as is required for SCBF design. The beam to column and gusset plate to column connections used field bolted double angles. The angles were welded to the gusset plates and beam webs. One significant difference between the test specimen and older field conditions is that NCBF 32 used demand critical welds. In older construction, the weld material did not have minimum toughness requirements as currently required for demand critical welds.

Figure 2.14 shows the applied load protocol, the force versus drift response, and photos at key points throughout the test. At +0.52% story drift, the fillet welds joining one side of the brace to the gusset plate fractured, resulting in a significant loss in lateral resistance by approximately 50%. A loss of strength in the frame greater than 20% is considered failure of the system. Nonetheless, the testing procedure was continued. After +0.52% story drift, the primary source of lateral resistance in the system was attributed to the beam to column connection in the corners

with the gusset plates (Hsiao et al., 2011). The bolted angle connections underwent large deformations, which led to angle fracture at +3.1% story drift. Weld fracture was also seen in the gusset plate to beam welds. For this NCBF, the strength of the connection controlled the system performance. The test exhibited an extremely brittle, unpredictable, and undesirable failure mode of weld fracture. Although the system was classified as "failed" early on, NCBF 32 retained some residual lateral resistance and drift capacity until the test was stopped.

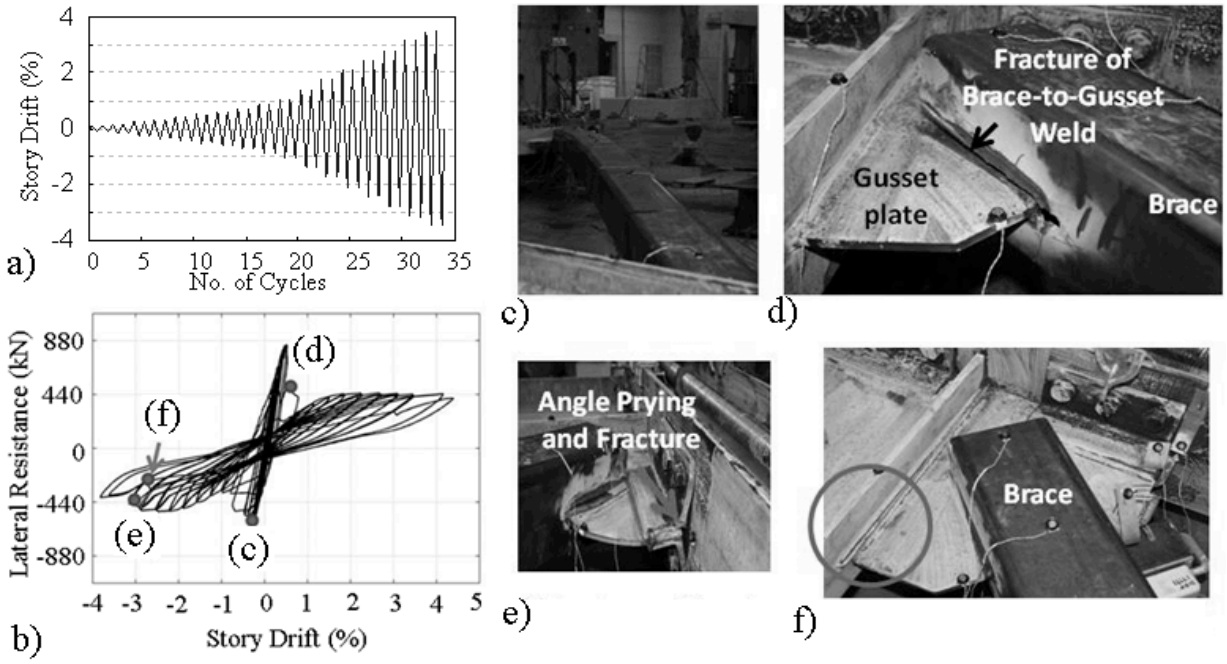

a. Load Protocol, b. Force vs. Drift Response, c. Brace Local Deformation at Plastic Hinge, d. Connection Fracture, e. Fracture of Gusset Plate Connecting Angle, f. Weld Tearing in Opposing Gusset Plate.

Figure 2.14 - Pilot NCBF 32 Behavior (Hsiao et al., 2011)

2.4.3 Bolted Connection Yield Mechanisms and Failure Modes

The calculations for many of these limit states are discussed in detail in Chapter 3 – those that are not will be detailed in this section. Bolted failures are brittle, and often sudden failure modes that could potentially be seen in NCBF performance. Bolted behavior is difficult to predict. A490 bolts have been found to have "remarkable ductility" when tension tests were performed on the bolt (Popov and Takhirov, 2002). At the same time, bolts subjected to cyclic loads can fail suddenly from fatigue, even at loads below the bolt strengths (Fastenal, 2009). Possible

secondary yield mechanisms for bolted connections are: bolt hole elongation from bolt bearing stresses, net section yielding, and deformation of the bolt. Possible failure modes are: bolt shear, bolt bearing (tearout), net section fracture, block shear, and tension failures from prying.

Yield Mechanisms:

- **Bolt Hole Elongation from Bolt Bearing**

  Figure 2.15 shows an illustration of bolt bearing and a photo taken of bolt hole elongation in the gusset plate from bolt bearing stresses in the NHSS-B3 experiment. In the photo shown from Specimen NHSS-B3 (performance described in Chapter 5), the bolt hole was originally 1 1/16 in. diameter and became elongated to an ovular major axis diameter of approximately 2 in. Bearing strength values are related to the strength of the material the bolt bears upon, not the bolt strength itself. According to the Commentary in the 14th Edition of the Steel Construction Manual's Specifications (referred to as the Specifications and the Manual), material bearing strength may be limited by bearing deformation of the hole, or by tearout of the material upon which a bolt bears. Frank and Yura (1981, commentary p.16.1-410) found bolt elongations of more than 1/4 in. occur when the bearing force is greater than $2.4dtF_u$ even though the material does not rupture. This behavior is visible especially when there is also high tensile stress on the net section.

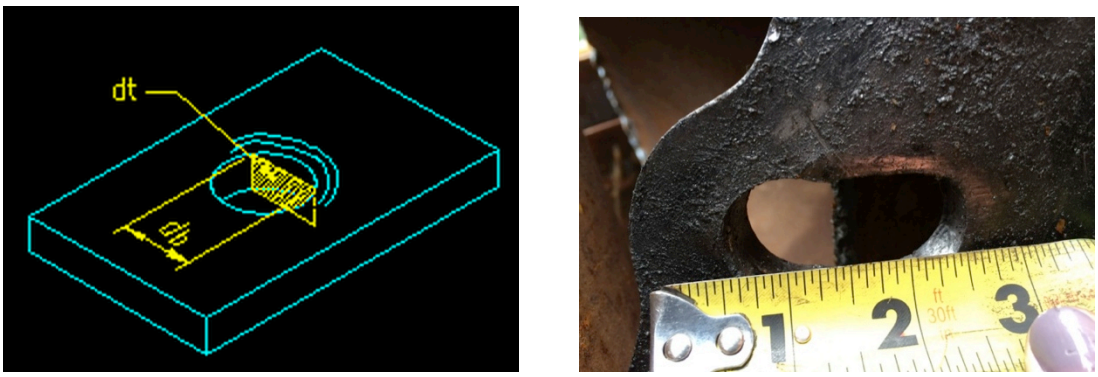

a. Bolt Bearing Schematic [20] **b. Bolt Bearing Deformation from NHSS-B3**

Figure 2.15 - Bolt Bearing Deformation

Section J10 in the Specifications provides the requirements for checking bearing strength at bolt holes. There are different requirements for standard, oversized and short-slotted holes versus long-slotted holes. Within the former group there are two different limitations for bearing strength depending on whether deformation of bolt holes at service load is a design consideration. This limit state is described in more detail in Chapter 3, but one of the two aforementioned equations from the Manual's Specification is reproduced below:

$$R_n = 1.2 l_c t F_u \leq 2.4 d t F_u \quad (2\text{-}1)$$

The left side of the equation is related to bolt tearout, discussed below. The right side of the equation is related to bolt bearing. The specified minimum tensile strength of the connecting material is multiplied by the area shown in Figure 2.15 (bolt diameter multiplied by the material thickness).

- **Bolt Deformation**

Figure 2.16 shows an illustration of a bolt in single shear undergoing bolt shear deformation, and a photo of bolt deformation from NHSS-B3 after the completed test. In the latter, there is a clear shear plane that developed in the bolt, but did not cause a bolt shear failure. All bolted specimens describes in this thesis were loaded in single shear. For bolts, the location of the shear plane is important to a bolt's shear strength. The shear strength of the bolts can either be calculated when the threads are excluded (resulting in a higher shear strength per bolt), or when the threads are included (resulting in a lower shear strength per bolt). Eventually, with increased force, this deformation can result in a bolt shear failure, discussed below.

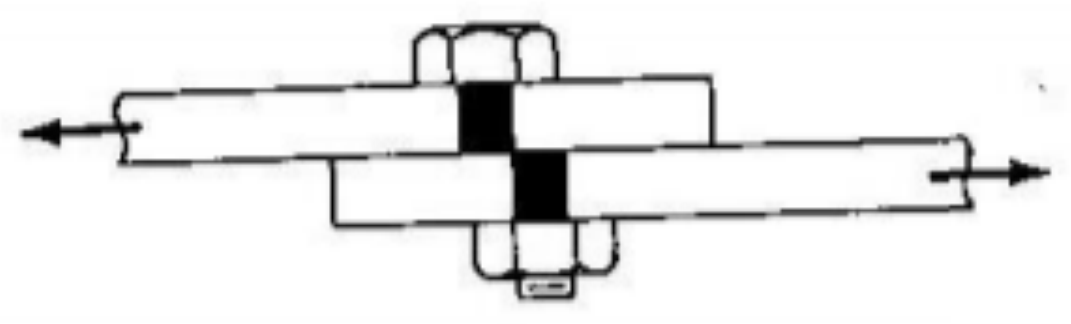

a. Illustration of Bolt Shear Deformation [17]

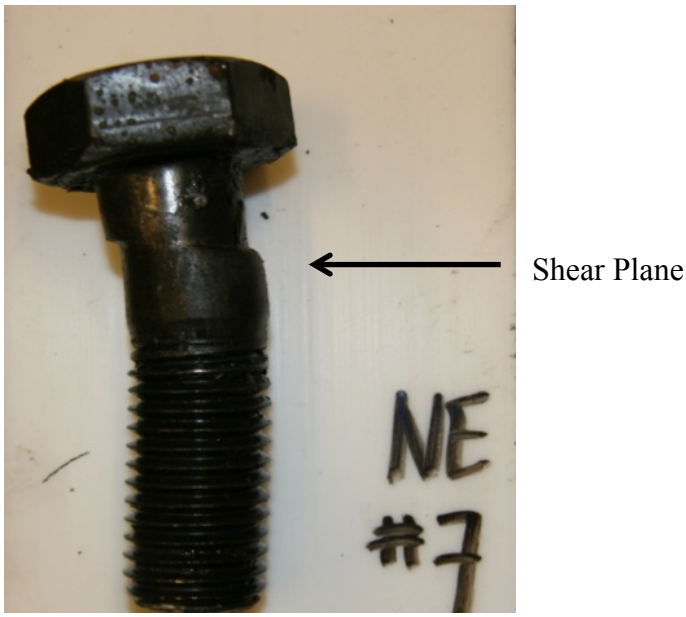

b. Bolt Deformation from NHSS-B3

Figure 2.16 – Bolt Deformation

Failure Modes:

- **Bolt Shear**

The bolt shear failure mode is discussed in detail in Chapter 3. Figure 2.17 shows two photos of a bolt from NHSS-B3 that fractured during the test from a bolt shear failure. Once the force on the bolt exceeds the bolt's shear capacity, the bolt will fail along its shear plane.

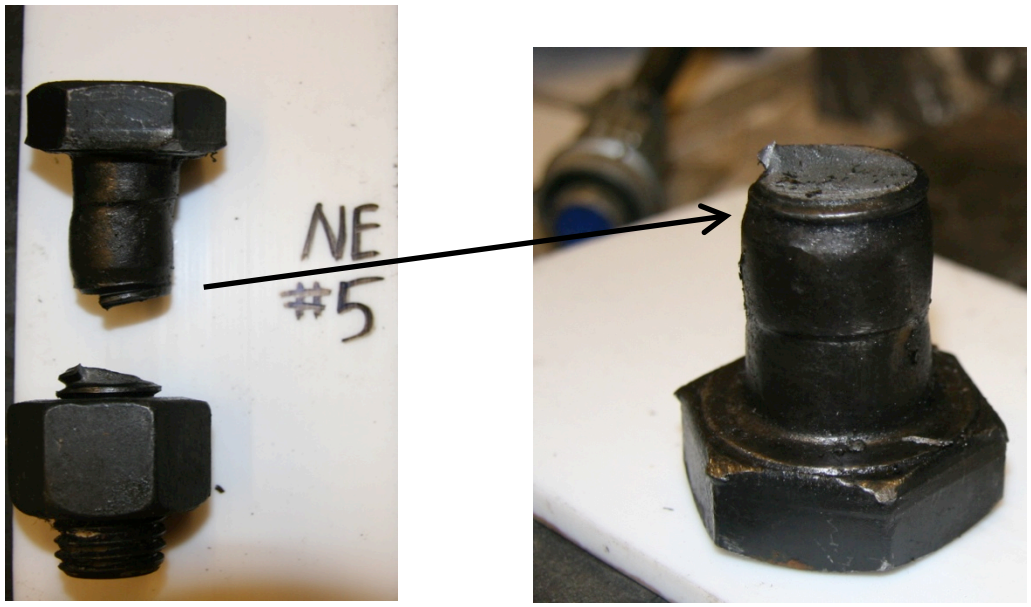

Figure 2.17 – Photos of Bolt Shear Failure from NHSS-B3

- **Bolt Bearing – Tearout**

The failure mode from bolt bearing is called tearout, which is a bolt-by-bolt block shear rupture of the connecting material (Manual's Commentary). Figure 2.18 shows an illustration of a bolt tearout failure. As mentioned, in Eqn. 2-1, the left side of the equation is related to tearout. It uses the ultimate tensile strength of the connecting material multiplied by the area shown in Figure 2.18 (the clear distance multiplied by the thickness of the material).

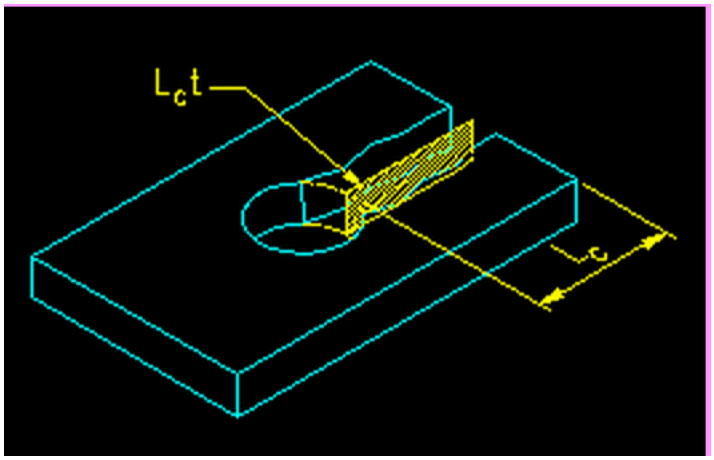

Figure 2.18 - Bolt Tear Out Failure [20]

- **Net Section Fracture**

Net section fracture is tensile rupture in the net area of the connecting elements. A diagram of this failure mode is shown in Figure 2.19 and the calculations are described in Chapter 3. In the case of bolted connections, net section fracture can occur when the cross sectional area is reduced from the bolt holes if the force on the connecting elements exceeds their tensile capacity.

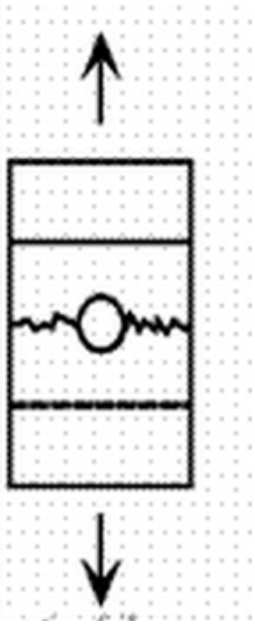

Figure 2.19 - Bolted Net Section Fracture [28]

- **Block Shear**

The block shear failure mode is similar to the net section failure mode except, as shown in Figure 2.20, there are now shear failure paths in addition to the tensile failure path. Additionally, it is similar to bolt tearout. Like a net section failure, when a bolted block shear failure occurs, part of the connection is torn away along the bolts from the rest of the connection. Block shear is a rupture or tearing failure mode, but gross yielding on the shear plane can occur when tearing on the tensile plane begins (Manual's Commentary). It is for that reason there are two sides to the equation J4-5 from the Manual's Specifications and discussed in detail in Chapter 3. The left side of the equation accounts for shear rupture and tensile rupture using the ultimate tensile strength of the material. The right side of the equation accounts for tensile rupture and shear yielding using the ultimate tensile strength and yield strength of the materials respectively.

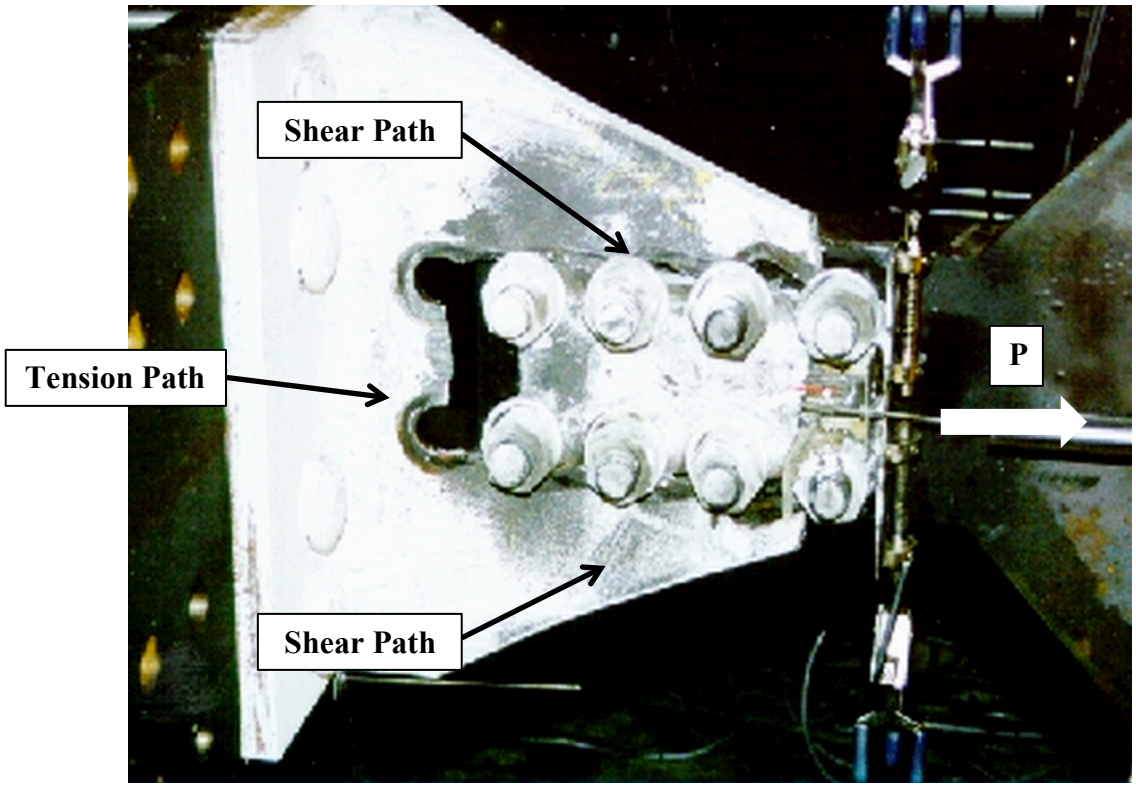

Figure 2.20 - Block Shear Failure [modified from Ref. 11]

- **Tensile Failure and Prying**

The final failure mode described in this section is bolt prying, illustrated in Figure 2.21. This failure mode usually occurs when there is a tee shape or angle in the connection. Prying was seen in NCBF 32 in the double angle connections, and to a lesser extent in the bolted end plate connections. The bolted end plate connections can be considered tee shapes, with the end plate as the "flange" and the gusset plate as the "web". As shown in Figure 2.21, when there is flexural deformation in the flanges or angle legs of the connection, a tensile force is engaged in the bolts as one connecting element pulls away from the other (or they pull away from each other) [6]. Prying is an added force in this situation. If this tensile force in the bolt exceeds the bolt's nominal tensile stress, the bolt will fail in tension.

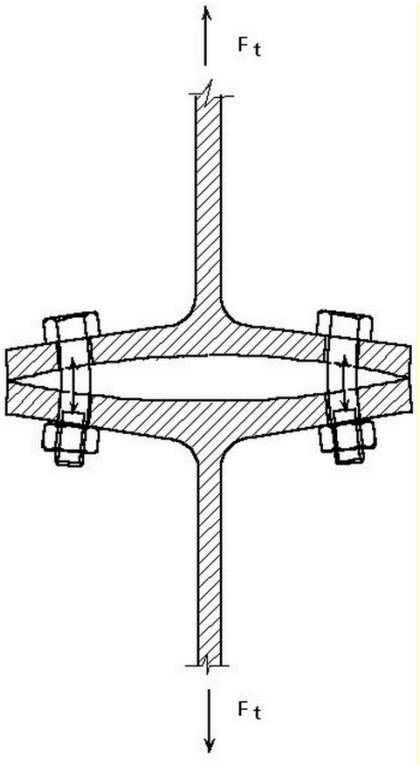

Figure 2.21 - Schematic Drawing of Bolt Prying [30]

2.5 Summary

This chapter served to provide motivation for the current research in this thesis. Five bolted gusset plate to column and beam to column connections were experimentally tested for the research purposes of this thesis. Two of these specimens were SCBFs designed by AISC and Cives to develop a baseline for bolted SCBF performance. Their design is discussed in detail in Chapter 3. The NCBF specimens were designed to replicate older connections with multiple perceived deficiencies discussed in Chapter 3, to improve understanding of NCBF behavior under seismic loading and identify the experimental severity of the deficiencies.

CHAPTER 3: SPECIMEN DESIGN

3.1 Introduction

The NCBF specimens were designed to model older, force-based design and construction practice with a focus on bolted beam to column and gusset plate to column connections. Section 3.2 explains the selected older bolted connections from the infrastructure review (described in Chapter 2) that were used to develop the three NCBF specimen designs. A demand-to-capacity analysis was conducted on the selected reference connections using the equations found in the 14th Edition of the AISC Steel Construction Manual (Manual referred to as "the Manual" and the specifications section is referred to as "the Specifications") and using the Balanced Design Procedure (BDP) (Roeder et al., 2011). The reference connections were checked for a number of limit states to identify perceived deficiencies to model in the NCBF specimens. These limit states were described in Section 3.3, and how the perceived deficiencies were incorporated into specimen development is described in Section 3.4. Section 3.5 concludes the chapter with the results from material tests on weld samples and coupon samples taken from each component of the specimens.

3.2 Bolted NCBF Connections from Infrastructure Review

The three NCBF specimens described within this thesis are part of a larger research project on evaluation and retrofit of older braced frames at the UW, UC Berkeley, and at NCREE in Taiwan (see Sloat (2014) and Sen et al. (2014)). The methodology for design prior to the early 1990s was largely force-based with a goal to create strong connections as opposed to the capacity-based design in SCBF theory, which encourages focus on ductility over strength. These tests aim to experimentally investigate the perceived deficiencies created from this older design philosophy that were found in braced frames designed and constructed in high seismic regions prior to the 1990s. From the experimental results, models for use in evaluation and retrofit will be developed in future work.

The buildings in the infrastructure review by Sloat (2014) were selected to represent a broad sample of older braced frame systems. The first existing braced frame connection detail that

inspired the NCBF bolted connection test series is from a four story building from 1982 and denoted NHSS-Ref-B1 herein. The gusset plate connection detail is shown in Figure 3.1. The connection detail gives a schedule (shown below the drawing) for varying brace sizes, gusset plate thicknesses, and number of high strength bolts at different locations within the structure. Standard, extra-strong pipe braces, and square tube steel ranging from a 6 in. diameter XS pipe to a TS12x12x1/2 were used, all with shallow brace angles from the horizontal. The larger brace sizes were used on lower stories and the smaller braces were used on the higher stories. The gusset plate increased in thickness, from 3/4 in. to 1¼ in. with increased brace size. The geometry of the tapered gusset plates and the length of the brace splice also increased with increased brace size.

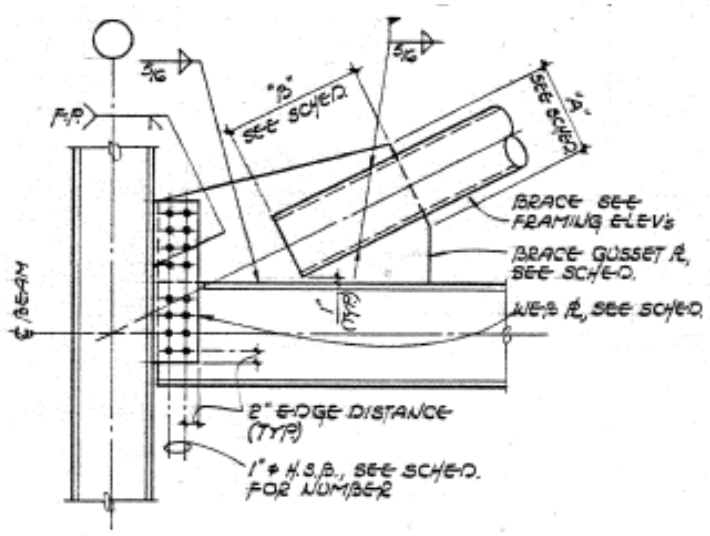

⚠ BRACE CONNECTION SCHEDULE

BRACE SIZE	BRACE GUSSET PL			WELD "C"	No. OF BOLTS	WEB PL THICK.
	PL THICK.	"A"	"B"			
TS 12 × 12 × ½	¼"	16"	27"	20"	16	¾"
12" ø XS PIPE	¼"	16"	24"	18"	14	¾"
12" ø STD. PIPE	1"	14"	18"	12"	12	¾"
10" ø XS PIPE	1"	14"	18"	–	12	¾"
10" ø STD. PIPE	1"	14"	18"	12"	12	¾"
8" ø STD. PIPE	¾"	10"	12"	–	8	¾"
6" ø STD. PIPE	¾"	8"	8"	–	6	¾"
6" ø XS PIPE	¾"	10"	12"	–	8	¾"

Figure 3.1 – Existing Bolted NCBF Connection NHSS-Ref-B1

There was a single shear plate welded to the column flanges with a complete joint penetration (CJP) weld that connected both the beam and gusset plate to the column. The columns were oriented with their strong axis resisting the brace forces. The 3/4 in. shear plate thickness remained the same regardless of the brace section or gusset plate thickness used. The brace to gusset plate and gusset plate to beam weld sizes remained the same (5/16 in. fillet welds) but the connection length varied with changing brace and gusset plate configurations. This reference connection did not use net section reinforcement on the brace and had no rotational clearance – both of which are required by current SCBF design specifications. The brace was typically connected with 1 in. clear space between the brace end and the beam to gusset plate interface, leaving minimal space for welding and placing high stress concentrations on the beam to gusset plate weld at that location.

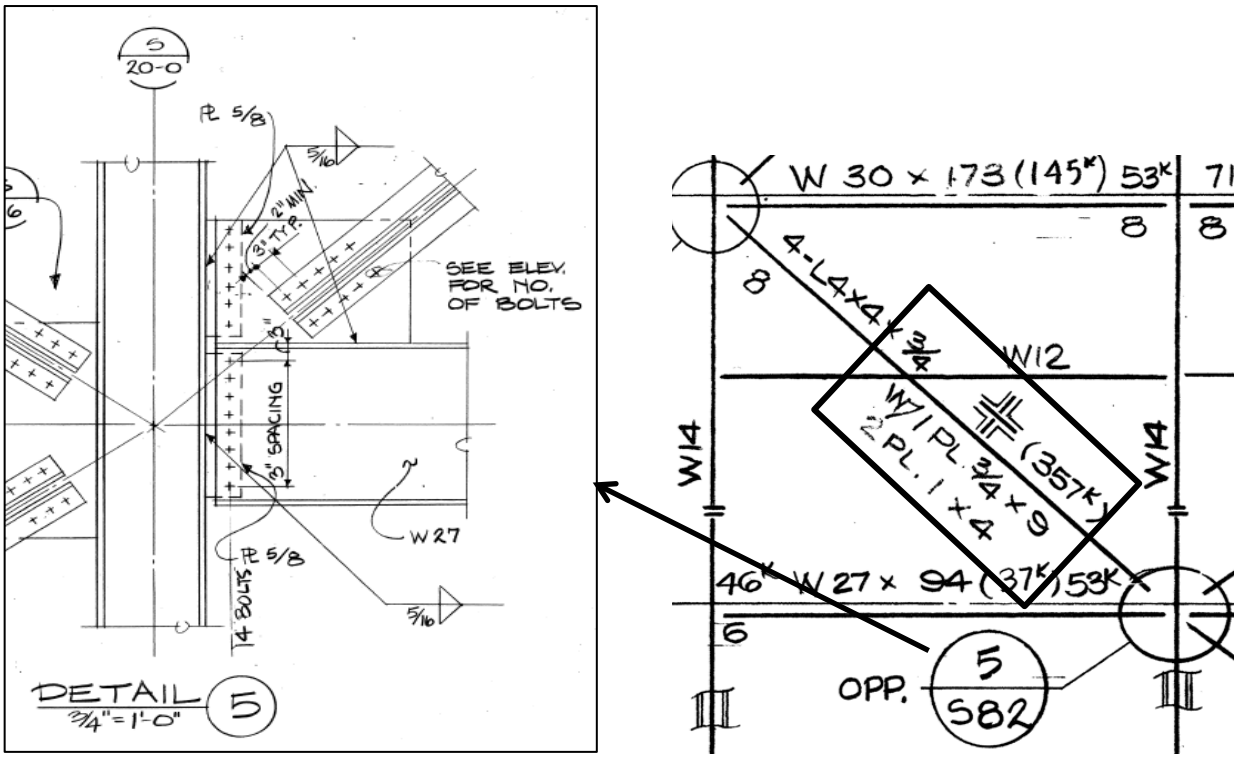

Figure 3.2 - Existing Bolted NCBF Connection NHSS-Ref-B2

The second connection studied for the design of the NCBF bolted specimens is from a hospital designed in 1980 and is herein referred to as NHSS-Ref-B2. The gusset plate connection is shown in Figure 3.2, along with an elevation view showing a sketch of the brace cross section (boxed). The braces in this configuration were a combination of plates and quad-angles bolted to

the rectangular gusset plates. The same combination of four L4x4x3/4 section braces was used through the height of the building. The columns in this braced frame systems were all strong-axis oriented to resist the brace forces. Similar to NHSS-Ref-B1, NHSS-Ref-B2 used a bolted connection to connect the beam and gusset plate to the column. However, this reference connection used two separate bolted plates rather than one continuous plate. The beam to column connection consisted of a 5/8 in. thick plate fillet welded to the column flange with a 5/16 in. fillet weld on both sides, and bolted to the beam flange with (8) 1 in. diameter A490 bolts. The gusset plate to column connection was similar but used (6) 1 in. diameter A490 bolts. The gusset plate was fillet welded to the beam with a 5/16 in. weld on both sides. It is not shown in Figure 3.2, but the gusset plate is 1 in. thick. Again, similar to the previous reference connection there was no rotational clearance in the gusset plate and the brace end was located very close to the beam to gusset plate interface weld.

An in-depth demand-to-capacity analysis was completed on NHSS-Ref-B1 and NHSS-Ref-B2 to identify potential deficiencies (Section 3.3) relative to current SCBF design criteria. The perceived deficiencies and common design characteristics of these two reference connections (such as the use of 1 in. diameter high strength bolts, split and shared shear plates, and no rotational clearance on the gusset plate) were used to develop the NCBF specimen designs. Other bolted connections were found in the infrastructure review and are provided in the Appendix.

3.3 Overview of UFM and Limit State Calculations

The UFM is an equilibrium method used to determine the distribution of forces through the multi-component braced frame system to design the gusset plate connections. These UFM demands from the expected brace capacity (using R_y factor) were used in a demand-capacity ratio (DCR) evaluation of the reference connections and design of the NCBF specimens. The Manual gives a description of the UFM on page 13-3 and says that the "essence of the Uniform Force Method is to select the geometry of the connection so that moments do not exist on the three connection interfaces; i.e. gusset-to-beam, gusset-to-column, and beam-to-column." Without these moments the engineer can design the connections for shear and/or tension only.

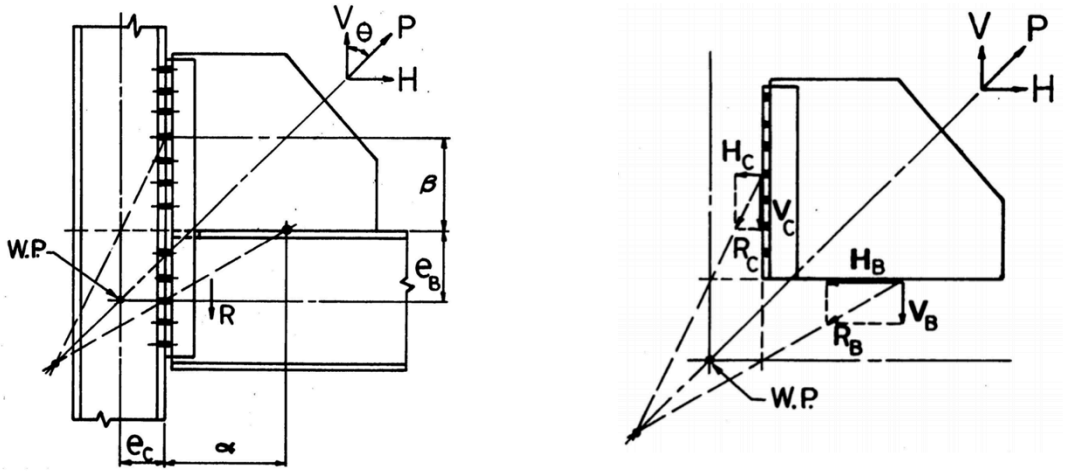

a. Diagonal bracing connection and external forces

b. Gusset free-body diagram

Figure 3.3 - Force transfer by the UFM [8]

The process for using the UFM is as follows. First, the geometry of the gusset plate is chosen by finding the parameters α and β. Figure 3.3 shows two free-body diagrams for the generic connection discussed in Part 13 of the Manual with key parameters labeled in the figures and defined in Table 3.1. To determine the gusset plate geometry, Eq. (3-1) must be satisfied to maintain equilibrium and ensure the connection interfaces do not have additional moments. The gusset plate geometry is set once α and β are determined and the required axial and shear forces on the connection can be calculated.

$$\alpha - \beta \tan\theta = e_b \tan\theta - e_c \qquad (3\text{-}1)$$

Next, the axial force in the brace is determined. In current SCBF design practice, the engineer is required to use the expected strength of the brace, R_yF_y to account for possible overstrength in the brace material. The connections must be designed for this expected strength in order to ensure the brace yields before any failure of the connection. Equations (3-2) and (3-3) below are used to calculate the expected brace tensile and compressive capacities and are found in sections D and E of the Specifications, respectively. For the compressive capacity, the Seismic Provisions state, "the expected brace strength in compression is permitted to be taken as the lesser of

$R_yF_yA_g$ and $1.14F_{cr}A_g$…" where F_{cr} is calculated from Chapter E of the Specifications but uses expected strength R_yF_y rather than F_y.

$$T = R_y \cdot F_y \cdot A_g \tag{3-2}$$

$$C = \min\left[R_y \cdot F_y \cdot A_g, 1.14 \cdot F_{cr} \cdot A_g\right] \tag{3-3}$$

Table 3.1 - Variables Used in UFM

Symbol	Description
P	Required axial force (either tension or compression capacity of brace)
θ	Brace angle from vertical
e_b	One-half the depth of the beam (in)
e_c	One-half the depth of the column (in)
β	Distance from the face of the beam flange to the centroid of the gusset-to-column connection (in)
α	Distance from the face of the column flange or web to the centroid of the gusset-to-beam connection (in)
r	$\sqrt{((\beta + e_b)^2 + (\alpha + e_c)^2)}$
V_c	Required shear force on the gusset-to-column connection
H_c	Required axial force on the gusset-to-column connection
V_b	Required axial force on the gusset-to-beam connection
H_b	Required shear force on the gusset-to-beam connection

The final step in the UFM is to determine the required axial and shear forces the connection must be designed to resist. These values are defined in Table 3.1 and calculated using Eq.'s (3-4) through (3-7) below. After these values are calculated, the connection limit states can be checked against these demands.

$$V_c = P \cdot \left(\beta/r\right) \quad (3\text{-}4)$$

$$H_c = P \cdot \left(e_c/r\right) \quad (3\text{-}5)$$

$$V_b = P \cdot \left(e_b/r\right) \quad (3\text{-}6)$$

$$H_b = P \cdot (\alpha/r) \quad (3\text{-}7)$$

With the demands throughout the connection defined, the limit states could be analyzed for each reference connection. A single bay, single story braced frame was isolated and analyzed using modern seismic design requirements for SCBFs. There are two current SCBF design methodologies used to evaluate the capacities of the connections. The first is the most widely accepted and is from the AISC Seismic Provisions. However, extensive experimental research on SCBFs at the UW with connections designed according to the AISC Seismic Design Provisions showed variable seismic performance, unintended failure modes, and limited deformation capacity (Roeder et al., 2011). The BDP was proposed as an alternate design methodology to improve the seismic performance of SCBF systems. While current AISC capacity-based design practice aims to concentrate the frame's inelastic behavior to the brace, the newly developed capacity-based design philosophy of the BDP aims to maximize ductile yielding in the frame, rather than limiting it to the brace. To increase drift capacity of the system by ensuring a desired yield and failure hierarchy, the BDP uses a series of balance factors that were validated from a broad range of experimental results on SCBFs (Roeder et al., 2011).

The limit state equations for AISC are shown in Table 3.2, and the corresponding equations for the BDP are in Table 3.3. All variables for these equations are defined in Table 3.4. Following the tables, each limit state is described in detail within its own section. Resistance factors were not included in these calculations because their absence added clarity in understanding the relative importance of various design deficiencies. Likewise, balance factors for the BDP were not included. Without balance and resistance factors, the limit state equations for the BDP and for AISC are very similar, allowing the limit state equations to be described in general with any differences in the procedures noted.

Table 3.2 - AISC Limit State Equations

Limit State	AISC Equation	ϕ	Reference
Net Section Fracture	$\phi \cdot F_u \cdot A_e = \phi P_n$	0.75	D2-2
Block Shear	$\phi[0.6 \cdot F_u \cdot A_{nv} + U_{bs} \cdot F_u \cdot A_{nt}] \leq \phi[0.6 \cdot F_y \cdot A_{gv} + U_{bs} \cdot F_u \cdot A_{nt}]$	0.75	J4-5
Gusset Plate Yielding in Tension	$\phi \cdot F_y \cdot A_g = \phi P_n$	0.90	J4-1
Gusset Plate Tensile Fracture	$\phi \cdot F_u \cdot A_e = \phi P_n$	0.75	J4-2
Gusset Plate Buckling	$\phi \cdot F_{cr} \cdot A_g = \phi P_n$	0.90	E3-1
Base Metal Fracture	$\phi \cdot F_{nBM} \cdot A_{BM} = \phi P_n$	0.75	J2-2
Brace to Gusset Plate Weld Fracture	$\phi \cdot 0.6 \cdot F_{exx}(1 + 0.5 \cdot \sin^2\theta) A_{we} \cdot N_w = \phi P_n$	0.75	J2-4 / J2-5
Interface Weld Fracture	$\phi \cdot 0.6 \cdot F_{exx}(1 + 0.5 \cdot \sin^2\theta) A_{we} \cdot N_w \geq Uniform\ Force\ Method$	0.75	J2-4 / J2-5
Bolt Shear	$\phi \cdot (F_{nv} \cdot A_b) \cdot N_b = \phi P_n$	0.75	J3-1
Bolt Bearing	$\phi[1.2 \cdot l_c \cdot t \cdot F_u] \leq \phi[2.4 \cdot d \cdot t \cdot F_u]$	0.75	J3-6a

Table 3.3 - BDP Limit State Equations

Limit State	BDP Equation*	β
Net Section Fracture	$\beta U\left[R_{tb} \cdot F_{ub} \cdot A_{nb} + F_{up} \cdot A_{gp}\right] = \beta P_n$	0.95
Block Shear	$\beta[0.6 \cdot F_u \cdot A_{nv} + U_{bs} \cdot F_u \cdot A_{nt}] = \beta P_n$	0.85
Whitmore Plate Yielding	$\beta \cdot R_y \cdot F_y \cdot A_w = \beta P_n$	1.0
Whitmore Plate Fracture	$\beta \cdot F_u \cdot A_w = \beta P_n$	0.85
Gusset Plate Buckling	Same as AISC	0.90
Base Metal Fracture	Same as AISC	0.75
Brace to Gusset Plate Weld Fracture	Same as AISC	0.75
Interface Weld Fracture	$1.5 \cdot \beta \cdot 0.6 \cdot F_{exx} \cdot (0.707) \cdot w_1 \cdot N_w \geq R_y F_y t$	0.75
Bolt Shear	N/A	-
Bolt Bearing	N/A	-

**subscripts: b [brace] and p [plate]*

Table 3.4 - Variables Used in Limit State Equations

Symbol	Description
ϕ	Strength reduction factor
θ	Angle between weld and applied force
β	Balance factor
A_b	Area of bolts
A_{BM}	Cross-sectional area of the base metal
A_e	Effective net area [$= A_n \cdot U$, *where A_n is net area and U is shear lag factor*]
A_g	Gross area of material
A_{gv}	Gross area subject to shear
A_{nt}	Net area subject to tension
A_{nv}	Net area subject to shear
A_w	Whitmore area
A_{we}	Area of weld [*= L(0.707)(D/16), where D is the weld size in sixteenths of an inch and L is the connection length*]
d	Nominal bolt diameter
F_{cr}	Critical stress as defined by equations E3-2, E3-3, or E3-4 in the Manual determined by member slenderness
F_{exx}	Weld electrode strength
F_{nBM}	Nominal stress of the base metal
F_{nv}	Bolt shear strength
F_u	Specified minimum tensile strength of material
F_y	Specified minimum yield strength of material
L	Connection length
l_c	Clear distance, in the direction of the force, between the edge of the hole and the edge of the adjacent hole or edge of the material
N_b	Number of bolts
N_w	Number of welds
P_n	Capacity of limit state in consideration
R_y	Ratio of expected to minimum specified yield stress of steel

Symbol	Description
t	Thickness of connected material
U_{bs}	1 if tension stress is uniform; 0.5 where tension stress is nonuniform
w_1	Weld size

3.3.1 Brace Net Section Fracture

A popular way of connecting an HSS section brace to the gusset plate is to cut a slot into two walls of the brace slightly longer than the splice length and weld the brace to the gusset plate. This procedure requires removal of a portion of the brace cross sectional area making this limit state a particular concern with thicker gusset plates (as in the reference connections) because more material is removed. Net section fracture is an undesirable failure mode as it is sudden and results in complete loss of brace resistance (Roeder et al., 2011). In SCBF construction, net section reinforcement is required to replace the material lost in the slotting procedure. In older frames, net section reinforcement of the brace typically was not included. The equation to calculate this limit state is shown in Table 3.2. It uses the ultimate tensile capacity of the brace, and the shear lag factor, U, which accounts for shear lag in the connection.

3.3.2 Block Shear

The block shear failure mode can occur at the brace to gusset plate connection, or in the bolted beam to column shear tab or gusset plate to column shear tab connections. Like the net section fracture limit state, the block shear limit state is greatly influenced by the thickness of the material used and the splice length (for brace to gusset plate connections). A thicker plate will have a higher resistance to block shear than a thinner plate. To calculate the block shear capacity of the connection, the AISC design methodology is to take the lesser of the results from the two sides of the inequality in Table 3.2. This inequality discourages shear yielding in the material. Alternatively, the BDP uses a single equation (shown in Table 3.3) to find the block shear capacity in order to instead, encourage gusset plate yielding.

3.3.3 Whitmore Gusset Plate Yielding

When gusset plate yielding is calculated, it uses the Whitmore width of the gusset plate. This parameter is shown in Figure 3.4 and is found using Eq. (3-8), where b is the brace width and L_w is the Whitmore width. This area was established by Whitmore (1952) and Part 9 of the Manual describes it as spreading the force from the start of the joint to 30° on each side in the connecting element, but the force cannot be distributed beyond an unconnected edge.

$$L_w = b + 2\tan 30 \tag{3-8}$$

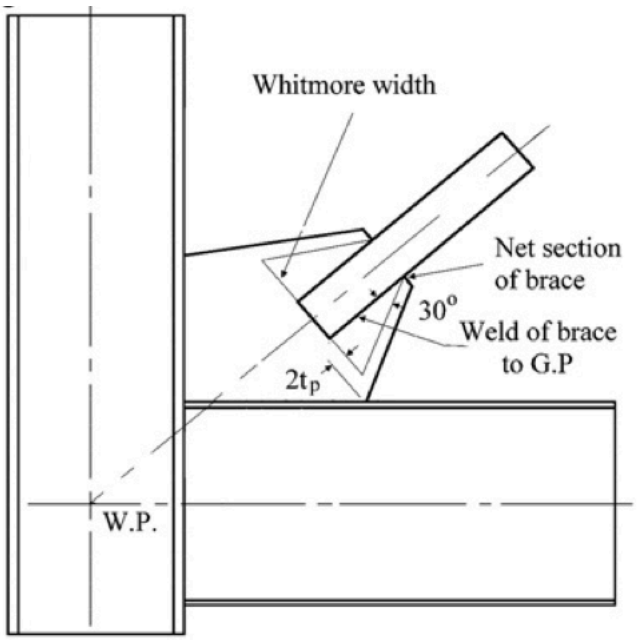

Figure 3.4 - Whitmore Width Illustration [modified from Roeder et al., 2011]

The AISC equation for this limit state is presented in Table 3.2. This equation gives the general calculation for a component under a tensile load. When applied to the gusset plate, A_g, refers to the Whitmore area of the gusset plate, as described above. This limit state depends on the gusset plate geometry and the plate thickness. A thicker plate will have a higher resistance to tensile yielding. As mentioned, AISC attempts to ensure the brace sustains the majority of inelastic deformation. On the other hand, in the BDP methodology, yielding is encouraged in the gusset plate along the Whitmore section, and is the desired secondary yield mechanism according to the BDP, following brace yielding and buckling (Roeder et al., 2011). The equation for the BDP

limit state is shown in Table 3.3. Research from the UW found that frames with thinner gusset plates were found to be the best at prolonging brace fracture life because they created a more flexible end condition for the brace, thereby increasing the experimental effective slenderness ratio (Roeder et al., 2011).

3.3.4 Whitmore Gusset Plate Fracture

The gusset plate fracture limit state stems from the gusset plate yielding limit state along the Whitmore area only instead of yielding, the plate tears. A photo of this failure mode is shown in Figure 3.5. The main difference is rather than using the yield stress of the material, both AISC and the BDP equations use the ultimate tensile strength of the material. The equations for this limit state are shown in Table 3.2 and Table 3.3, respectively.

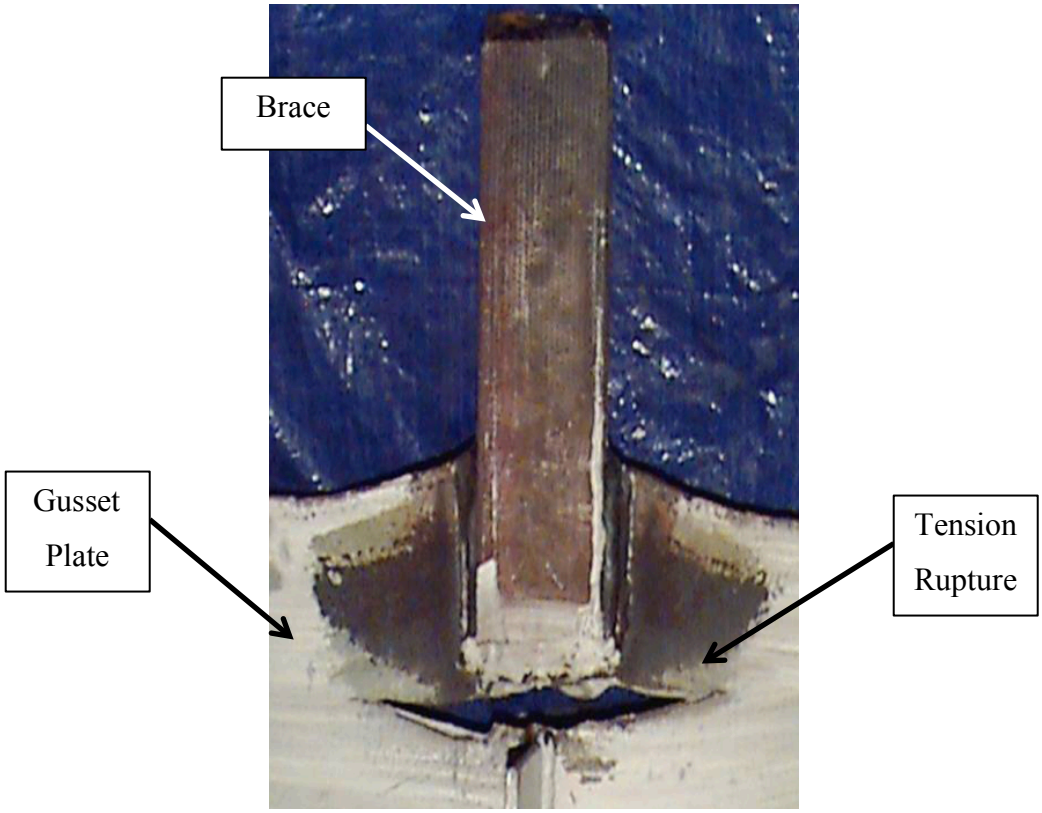

Figure 3.5 - Photo of Tension Rupture at Whitmore Section [31]

3.3.5 Gusset Plate Buckling

This limit state is checked against the expected buckling capacity of the brace. The AISC and BDP equations, presented in Table 3.2 and Table 3.3 respectively. The buckling stress, F_{cr}, is dependent on the slenderness of the plate. An effective length coefficient, k, of 0.65 is used for corner gusset plates. To determine the buckling length, the engineer can use either the average of three lengths, shown in Figure 3.6, or the sole length of L_2 shown in the same figure. The radius of gyration of the plate, r, is calculated using Eq. (3-9), where parameters I_w and A_w are about the Whitmore section. The slenderness ratio determines which equations from Chapter E in the Specifications are used to find the critical buckling stress. Gusset plate buckling is undesirable because it does not allow the brace to reach its full inelastic capacity and it weakens the connection.

$$r = \sqrt{I_w / A_w} \tag{3-9}$$

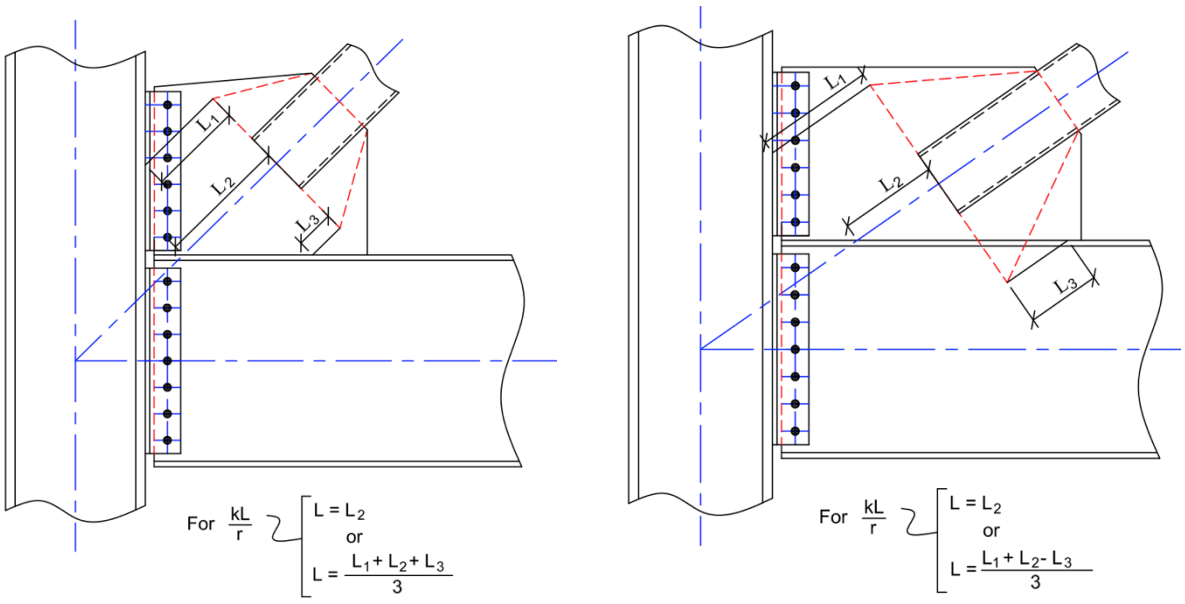

Figure 3.6 – Gusset Plate Buckling Length Determination [31]

3.3.6 Base Metal Fracture

Base metal fracture occurs in the heat affected zone of the material rather than in the weld itself. This weaker area is adjacent to the weld and may be prone to fracture because of reduced ductility from the welding process. This type of failure mode is equally as catastrophic and

undesirable as a weld fracture. From testing at the UW, overstrength of the welds did not negatively impact the SCBF performance (Roeder et al., 2011). The AISC and BDP equations for base metal fracture are shown in Table 3.2 and Table 3.3 respectively.

3.3.7 Interface Weld Fracture

The interface welds described in this section are those joining the gusset plate to the beam, the gusset plate to column shear tab, and the beam to column shear tab. SCBF design requirements mandate the welds to be AISC demand critical. However, in older frames filler metal with low or unspecified toughness was likely used because of their more rapid deposition rate and greater economy. The Charpy V-Notch (CVN) toughness of the weld metal is related to the energy required to induce fracture. The higher the toughness of the filler metal, the larger the crack length that can be sustained prior to unstable crack propagation. While this parameter is not included in the capacity calculation of the welds, it is important to note, as it influences the ability for ductile weld tearing. To accurately simulate older construction field conditions, the NCBF bolted test series used the weld product Fabshield® 21B E71T-11 from HOBART®, which is an all-position, non-demand critical weld metal with no minimum toughness requirements. The data sheet for this weld material is included in the Appendix. CVN tests were conducted on the different filler metals used in the tests to quantify the difference in actual toughness values. The results are presented in Section 3.5.

Current AISC provisions require the interface welds to develop the tensile capacity of the brace. Typically engineers use the UFM to distribute the brace force to the connection components. The UFM was originally developed for wind loading and later adapted to encompass seismic loading, but it still does not account for the inelastic rotational demands on the gusset plate from brace OOP displacements. Previous research at the UW has shown that welds designed using the UFM are actually subjected to stresses much larger than what the UFM predicts (Roeder et al., 2011). The AISC equation is shown in Table 3.2 and is a function of the load angle, the electrode strength, the area of the throat of the weld, and the number of welds connecting the components.

The BDP uses a similar, but modified version of the AISC interface weld equation. Rather than comparing the capacity against the UFM, the BDP uses the expected capacity of the plate, shown

in Table 3.3. Unlike the AISC equations, the BDP methodology accounts for the inelastic deformations of the plates and can protect the interface welds against fracture (Roeder et al., 2011). The BDP also includes the 1.5 factor present in the AISC equation because research shows that fillet welds in tension can resist about 50% more stress than those loaded in shear (Kotulka 2007, AISC 2005, AWS 2006). While the researchers at the UW found crack initiation began in the test specimens between 1.5% and 2% story drift regardless of the connection, and limited stable crack growth from demand critical welds permitted increased story drift capacity in the frames, interface weld fracture is not desirable.

3.3.8 Bolt Shear

The equation for the bolt shear capacity is shown in Table 3.2. Bolt shear can be a sudden and brittle, undesirable failure mode. There is uncertainty with using the UFM to determine force distributions of bolted connections that use a split shear tab versus a shared shear tab, stemming from whether the bolts act as one unit in both configurations.

For eccentric bolted connections, the Manual suggests using either the Inelastic Center of Rotation Method or the Elastic Method, discussed in Part 7 of the Manual. To determine the capacity of the bolted connection using the former method, the engineer can find the non-dimensional coefficient, *C*, from tables in Part 7 of the Manual. The Manual states that *C* represents the number of bolts effective in resisting the eccentric shear force. The eccentricity, *e*, of the brace force with respect to the centroid of the bolt group was calculated using Eq. (3-10), where *a* is the distance from the column flange to the centroid of the first row of bolts, *b* is the distance between vertical columns of bolts, and *n* is the number of vertical columns of bolts. An annotated drawing is shown in Figure 3.7. This eccentricity is used in the tables to determine *C*. The capacity of the bolt group can then be calculated using Eq. (3-11), where the parameter, r_n, is the shear capacity of the connection, $F_{nv}A_{b.}$ For this method, *C* replaces N_b in Table 3.2.

$$e = a + (n-1) \cdot \left({}^{b}/_{2}\right) \tag{3-10}$$

$$\phi R_n = C \cdot \phi r_n \tag{3-11}$$

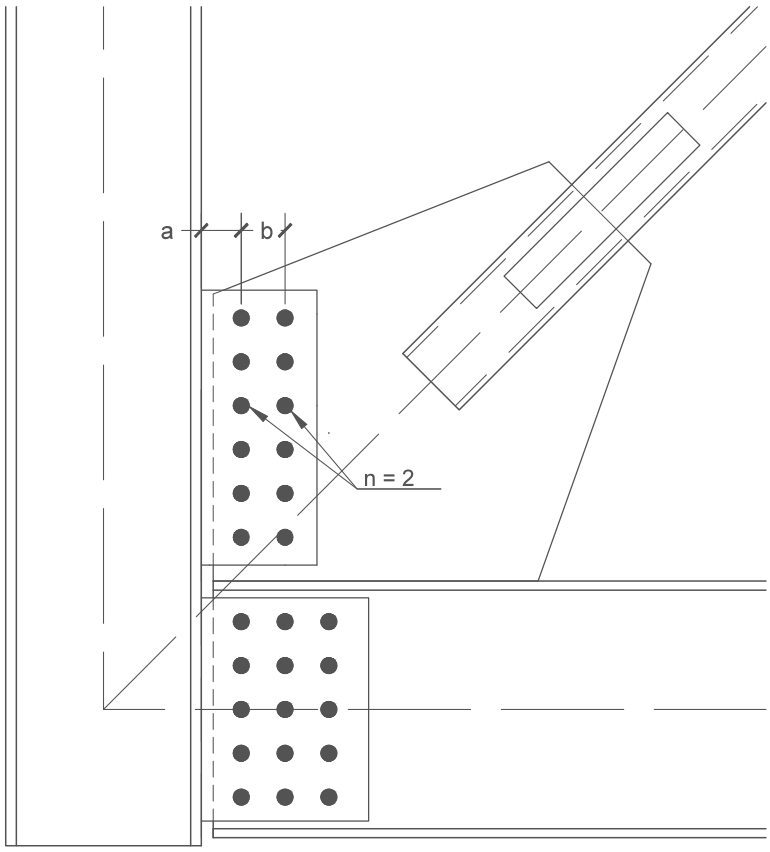

Figure 3.7 - Schematic Drawing of Variables a, b, n for Eccentricity Calculation

3.3.9 Bolt Bearing

The AISC bolt bearing limit state equation is shown in Table 3.2. The equation presented is used when the deformation at bolt holes is a design consideration as AISC attempts to concentrate inelastic behavior to the brace, not inelastic yielding in the connection. The inequality limits the bolt bearing capacity to the connection's resistance to bolt-by-bolt tearout (left side). Both parts of the inequality are functions of the ultimate tensile strength of the material and the material thickness. Tearout is a function of the clear distance, while bearing deformation is a function of the nominal bolt diameter.

3.4 Specimen Design Parameters

Target DCR values for key limit states of the test specimens were determined from analysis of the variations in the reference connections shown previously in Figure 3.1 and Figure 3.2. The equations for the limit states have been previously presented in Table 3.2 and Table 3.3. Table

3.5 shows the DCR values for NHHS-Ref-B1 (drawing in Figure 3.1), NHSS-Ref-B2 (drawing in Figure 3.2), and the average DCR values for both reference connections. The most severe limit states found from NHSS-Ref-B1 were brace block shear, brace to gusset plate weld fracture, bolt shear in both the gusset plate to column and beam to column connections, and in one instance, bolt bearing at the beam to column connection. The DCR values were more severe for NHSS-Ref-B2 - nearly all limit states in NHSS-Ref-B2 were above 1. When the DCR values from the reference specimens were averaged, the limit states above 1.0 were brace net section fracture, brace block shear, Whitmore gusset plate yielding, brace to gusset plate weld fracture, beam to gusset plate weld fracture, bolt shear at beam to column and gusset plate to column connections, and bolt bearing at beam to column and gusset plate to column connections.

Table 3.5 - DCR Values for Reference Connections

Limit State	NHSS-Ref-B1			NHSS-Ref-B2		Average
	6" XS Pipe	10" STD Pipe	12" XS Pipe	Angles + Plates	Angles	
Brace Net Section	0.84	0.83	0.83	**1.28**	**1.62**	**1.08**
Brace Block Shear	**1.08**	**1.25**	**1.05**	**2.16**	**1.29**	**1.36**
Gusset Plate Block Shear	0.51	0.36	0.35	**2.30**	**1.37**	**0.98**
Whitmore Gusset Plate Yielding	0.77	0.57	0.59	**2.04**	**1.22**	**1.04**
Whitmore Gusset Plate Fracture	0.59	0.44	0.45	1.**57**	0.94	0.80
Gusset Plate Buckling	0.15	0.28	0.35	**0.99**	0.74	0.50
Brace to Gusset Plate Weld Fracture	**0.98**	**0.96**	**1.10**	N/A	N/A	**1.02**
Brace to Gusset Plate Base Metal Fracture	0.63	0.73	0.61	N/A	N/A	0.66
Gusset Plate Shear Yielding	0.68	0.44	0.41	**1.09**	0.65	0.66

Limit State	NHSS-Ref-B1			NHSS-Ref-B2		Average
	6" XS Pipe	10" STD Pipe	12" XS Pipe	Angles + Plates	Angles	
Beam to Gusset Plate Weld Fracture	0.77	0.67	0.79	**2.49**	**1.48**	**1.24**
Column to Gusset Plate Bolt Shear	**1.20**	**1.16**	**1.49**	**2.74**	**1.64**	**1.55**
Column to Beam Bolt Shear	**1.25**	**1.01**	**1.12**	**2.78**	**1.66**	**1.66**
Column to Gusset Plate Bolt Bearing	0.43	0.42	0.54	**2.04**	**1.22**	**1.28**
Column to Beam Bolt Bearing	**1.47**	0.91	0.74	**1.52**	0.91	0.77

After potential deficiencies in the older connections were identified from the DCR analysis (bold values shaded in grey in Table 3.5 above), an iterative process began for the design of the first NCBF bolted specimen (NHSS-B1). This design aimed to match the key limit state DCR values from the average existing connection's DCR values. A similar DCR analysis was conducted for NHSS-B2 and NHSS-B3, but these specimens also considered the performance of the prior NCBF specimen tested. All three specimen's DCR results are shown in Table 3.7, with the most severe DCR values in bold and shaded in grey. Table 3.6 provides the test objective for each specimen along with key characteristics of the connection. The drawings of the NCBF specimens tested are shown in Figure 3.8 with boxes to highlight the parameters that changed for each experiment. It should be noted that in Table 3.7, for the NHSS-B2 specimen, the DCR values are lower than the NHSS-B1 in part due to the difference in brace size (NHSS-B1 used an HSS5x5x3/8 and NHSS-B2 used an HSS6x6x1/4). Following Table 3.7 is a more detailed discussion of how the NCBF specimens were developed from each limit state as compared to their DCR values.

Table 3.6 - Bolted Test Specimen Descriptions

Test Name	Test Objective	Shear Tab to Column Weld Size	Beam to Gusset Plate Weld Size and Length	Gusset Plate Thickness (in.)	Shear Tab Thickness (in.)
NHSS-B1	To explore perceived deficiencies of NCBF bolted connections (bolt shear, brace net section, & brace block shear) using a shared shear plate.	CJP	7/16 in. and 11.75 in.	3/4	3/4
NHSS-B2	To explore perceived deficiencies of NCBF bolted connections (bolt shear & bolt bearing, brace net section & block shear, and beam to gusset base metal fracture) using separate shear plates and does not meet brace seismic compactness requirements.	CJP	5/16 in. and 16 in.	3/4	3/4
NHSS-B3	To explore perceived deficiencies of NCBF bolted connections (bolt shear & bolt bearing, brace net section & brace block shear, and Whitmore & shear gusset plate yielding) using a split shear tab and thinner gusset plate.	CJP	5/16 in. and 15.25 in.	1/2	3/4

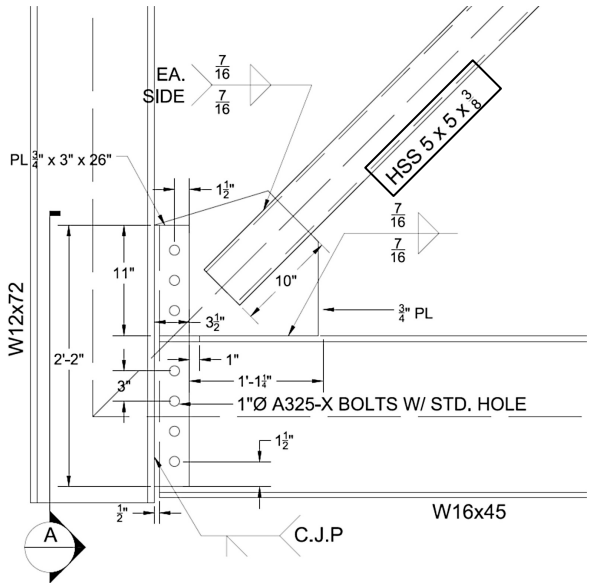

a. NHSS-B1

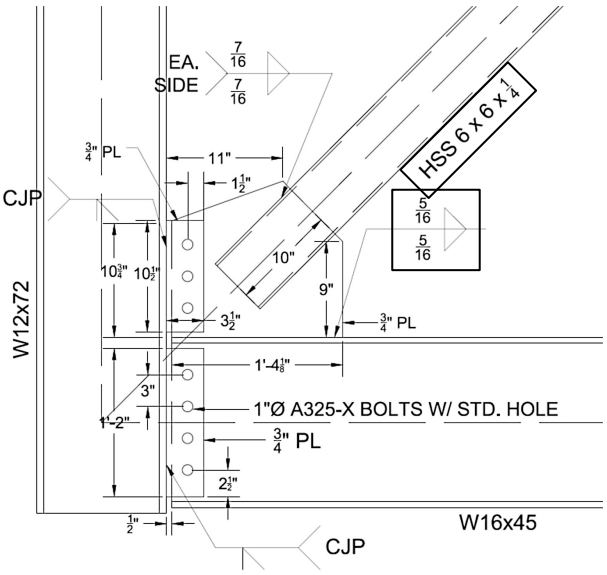

b. NHSS-B2

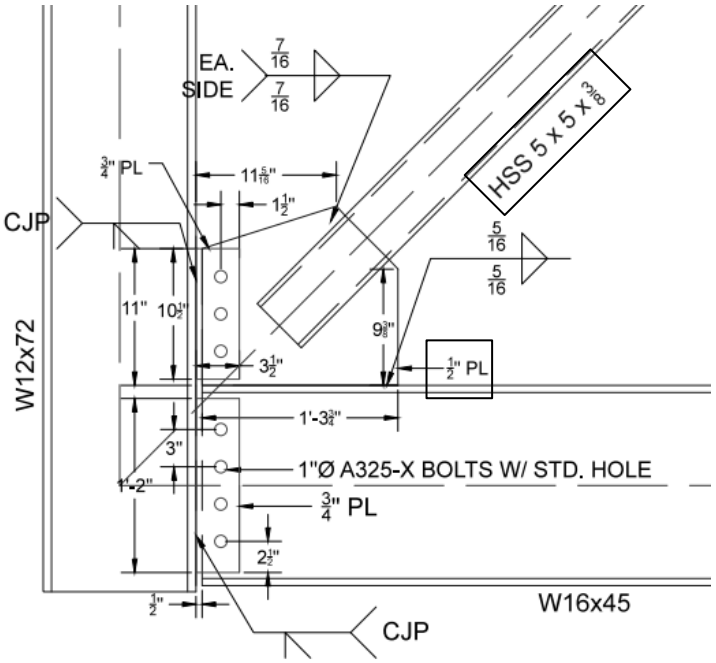

c. NHSS-B3

Figure 3.8 - Specimen Connection Drawings

Table 3.7 - NCBF Bolted Test Specimen DCR Values from AISC equations

Limit State	NHSS-B1	NHSS-B2	NHSS-B3
Brace Net Section	**1.2**	**1.2**	**1.1**
Brace Block Shear	**1.1**	**1.3**	**1.1**
Gusset Plate Block Shear	0.62	0.49	0.94
Whitmore Gusset Plate Yielding	0.75	0.61	**1.1**
Whitmore Gusset Plate Fracture	0.58	0.46	0.86
Gusset Plate Buckling	0.38	0.4	0.58
Brace to Gusset Plate Weld Fracture	0.83	0.71	0.83
Brace to Gusset Plate Base Metal Fracture	0.83	**1.1**	0.83
Gusset Plate Shear Yielding	0.96	0.6	**1.1**
Beam to Gusset Plate Weld Fracture	0.64	0.56	0.66
Column to Gusset Plate Bolt Shear	**1.90**	**1.63**	**1.92**
Column to Beam Bolt Shear	**1.56**	**1.30**	**1.55**
Column to Gusset Plate Bolt Bearing	0.98	0.84	**1.48**
Column to Beam Bolt Bearing	**1.73**	**1.45**	**1.73**
Block Shear Column to Gusset Plate and Beam	0.72	-	-

The net section DCR check for a HSS 5x5x3/8 used in NHSS-B1 and NHSS-B3 was above 1. Previous SCBF research found net section reinforcing plates were not required and did not influence SCBF performance (Powell, 2010), and therefore net section reinforcement was not included on the specimens.

One of the most prevalent deficiencies found in the infrastructure review by Sloat (2014) was the capacity of the beam to gusset plate weld. The average DCR value for this limit state was above

1. While the NCBF specimens did not achieve as high a DCR value, they maintained similar DCR values between the three specimens. To have this similarity, NHSS-B1 had a 11.75 in. long 7/16 in. fillet weld on the top and bottom of the plate, NHSS-B2 had a 16 in. long 5/16 in. fillet weld on the top and bottom of the plate, and NHSS-B3 had a 15.25 in. long 5/16 in. fillet weld on the top and bottom of the plate, as shown in Figure 3.8a-c. NHSS-B1 required a thicker weld due to the reduced connection length from the coped beam flange and shared shear plate.

The weld fracture limit state at the brace to gusset plate interface had previously been tested in NCBF 32 and found to control the specimen performance. To ensure the NCBF specimens did not repeat the same failure mode, the weld size at this location was increased. Weld fracture at the column to gusset plate shear tab connection was also not a deficiency considered in the NCBF design because many of the connections found in the infrastructure review used a CJP weld to connect the shear plates to the column. For that reason, NHSS-B1, NHSS-B2, and NHSS-B3 all used a CJP weld on the column to gusset plate shear tab weld.

The 2010 Seismic Provisions require clearance on the gusset plate for OOP brace rotation. None of the NCBF reference connections met current clearance requirements, and therefore, none of the NCBF bolted connection specimens tested were designed to meet these clearance requirements. This clearance localizes the damage on the gusset plate to a fold line (per AISC) or an elliptical region (per the BDP), forcing the gusset plate to deform rather than rotate as a rigid body.

Bolt bearing, calculated using the AISC equation in Table 3.2, at the beam to column connection was not a deficiency for the reference specimens because of the wide variety of framing elements used. The UW test setup used one type of beam section for all tests, a W16x45 with a thin 0.345 in. web. Because of this testing constraint, bolt bearing at the beam to column connection had DCR values greater than 1 for all NCBF bolted connections tested. Additionally, bolt bearing was not a deficiency for the older gusset plate to column shear tab connection because mostly thick plates were used as components. Likewise, bolt bearing at the gusset plate to column connection was not designed to be a deficiency for the NCBF bolted specimens because they

used 3/4 in. gusset plates. The one exception was NHSS-B3 because one of the test goals was to explore the effect of using a thinner gusset plate.

While all of the reference connections have bolted shear tab connections for the beam to column and gusset plate to column connections, they used two different methods – a single and a split shear plate. To investigate the significance of this shear tab discontinuity on braced frame performance, NHSS-B1 used a single shear tab (similar to NHSS-Ref-B1), while NHSS-B2 and NHSS-B3 used split shear tabs (similar to NHSS-Ref-B2). Of particular interest to these tests is how accurately the UFM predicts the limit states relevant to the shear tabs. A split shear tab is more susceptible to opposing eccentricities in the connection as opposed to a single, continuous shear tab across the connections. Further, a single shear plate has the potential to increase the integrity of the gusset plate to beam weld.

The impact of brace compactness was also studied. For current construction, the Seismic Provisions require the use of a seismically compact brace for SCBFs. However, many of the buildings from the infrastructure review were found to have braces with higher width-to-thickness ratios. The first NCBF welded test conducted by Sloat (2014) used an HSS7x7x1/4 brace section that exhibited this high local slenderness. This brace was not able to resist local buckling as well as a seismically compact brace and fracture at lower inelastic deformations. Due to the low total drift range prior to fracture, the brace was not able to impose significant demands on the connections. To place the highest demands on the connection, NHSS-B1 and NHSS-B3 used a seismically compact HSS5x5x3/8 brace. NHSS-B2 explored the effects of a non-compact brace section with a lower width-to-thickness ratio (compared to the HSS7x7x1/4) with an HSS6x6x1/4 brace section to develop a range of brace sections investigated.

A final important difference to be noted between the UW tests and the reference connections is the bay geometry. The UW setup uses a 12 ft x 12 ft bay with W12x72 columns and W16x45 beams, resulting in a 45° brace angle. The older, existing braced frame designs were often rectangular bays (width typically twice the height) with varying beam and column sizes through the height of the structure and varying, but often shallow, brace angles. Some drawings show beam sizes up to a W30, which is significantly different from a W16. Because of these

differences, the older designs had to be modified to fit into the UW test setup, but to ensure reflection of field conditions, the connections maintained a reasonable match with the DCR values found from the existing connections.

3.5 Material Properties

Samples were taken from three weld filler metals used for welding and subjected to CVN tests to assess relative average toughness values. The results of these tests are presented in Table 3.8. The weld electrode E71T-8 was the only demand critical weld type tested and was found to be about four times as tough as E71T-11 and about three times as tough as E70T-7. E71T-11 had the lowest average toughness value of all three electrodes. This electrode was also the one used most in the NCBF specimens because it is an all-position weld. A higher toughness value indicates more ductility in the material and a larger amount of energy absorption in the material.

Table 3.8 - Charpy V-Notch Test Results on Weld Material

Weld Material	Demand Critical?	Average Toughness (ft-lbs)
E71T-8	Y	81.75
E71T-11	N	20
E70T-7	N	27.7

CHAPTER 4: EXPERIMENTAL TEST SETUP

4.1 Introduction

This chapter describes the single bay, single story experimental test setup used for the nine NCBF tests and two SCBF tests conducted at the University of Washington between 2013 and 2014, also described in Sloat (2014). The setup was originally designed and constructed by Johnson (2005), modified by Powell (2010), and further modified by the author and Sloat (2014). Section 4.2 gives an overview of the test configuration. Section 4.3 details each of the test components. Section 4.4 discusses the instrumentation used in each experiment. Section 4.5 reviews the origins of the test protocol. Section 4.6 concludes the chapter with the preparation process for each test.

4.2 Overview of Experimental Configuration

Limitations imposed by the University of Washington Structures Research Laboratory (UW SRL) required the single story, single bay braced frames to be tested in the horizontal plane, parallel to the strong floor. The test setup was designed to replicate true field conditions as closely as possible to enable observation of the performance of the brace and connection behavior. Figure 4.1 shows a CAD drawing of the UW SRL test setup, with photo realizations shown in Figure 4.2. If the frame were tested upright, the south end would be the lower story, and the north end the upper story.

A general overview of how the system works is described here. The actuator is attached to a large concrete reaction block with threaded rods, and the block is anchored to the 3ft thick concrete strong floor through large post-tensioned Williams Anchor Rods. The lateral load from the actuator is applied to the frame through the short blue W21x62 steel load beam, which is bolted to the north beam of the frame. To resist the overturning moment from this force, the frame is tied back to the blue channel assembly through four large post-tensioned Williams Rods that also applied a simulated gravity load of 450 kip total to each column. The channel assembly is a system of two steel channels and welded plates post-tensioned to the 30 in thick concrete strong wall at the south end of the test setup.

Out-of-plane (OOP) restraints were used to prevent the beams, columns, and load beam from OOP movement, while still allowing the frame to move laterally. The applied lateral force travels through the frame system to the south shear connection. The bolts attaching the south beam to the channel assembly transfer the resulting base shear to the channel assembly and the strong wall. This force is then dissipated through the strong wall and the strong floor. These components will be discussed in detail in Section 4.3.

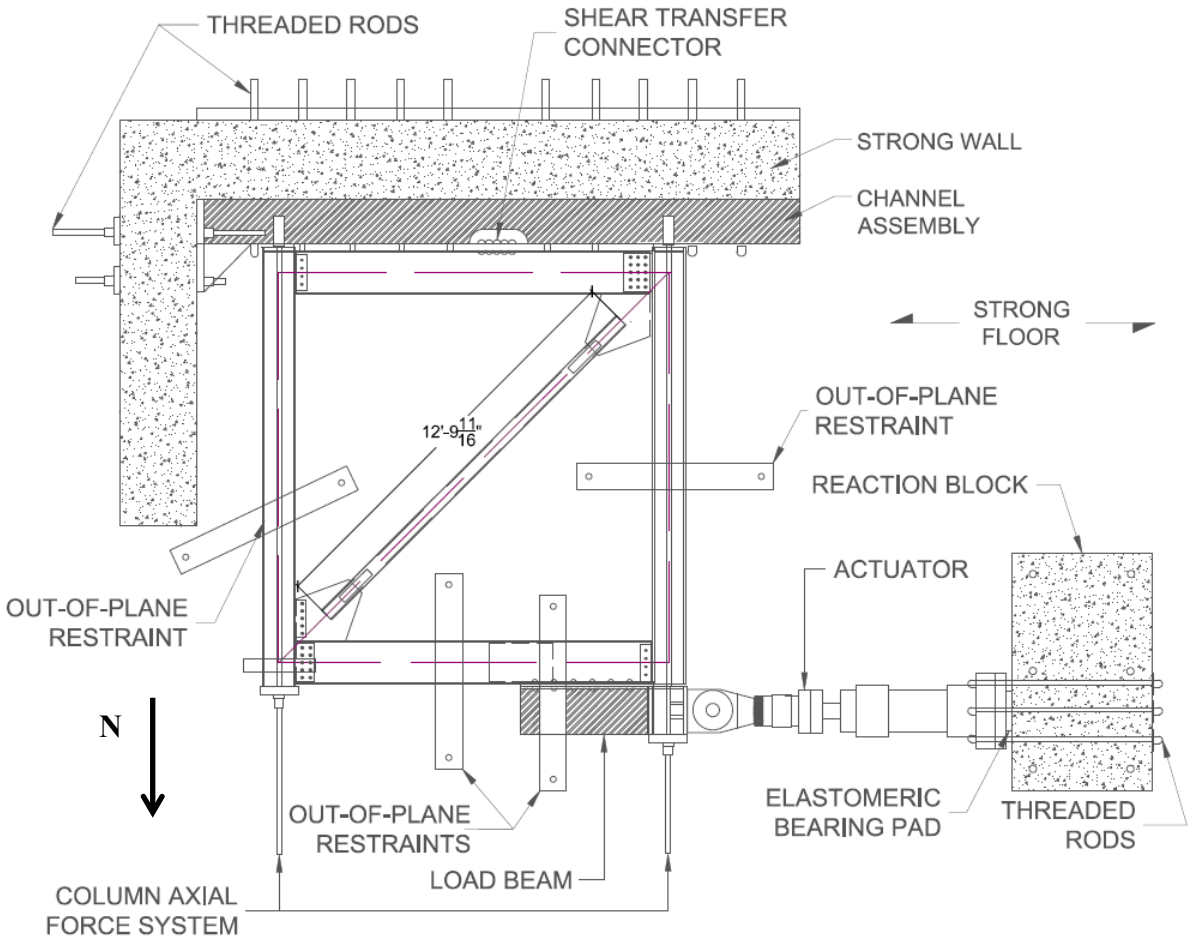

Figure 4.1 - CAD Drawing of the UW Test Setup

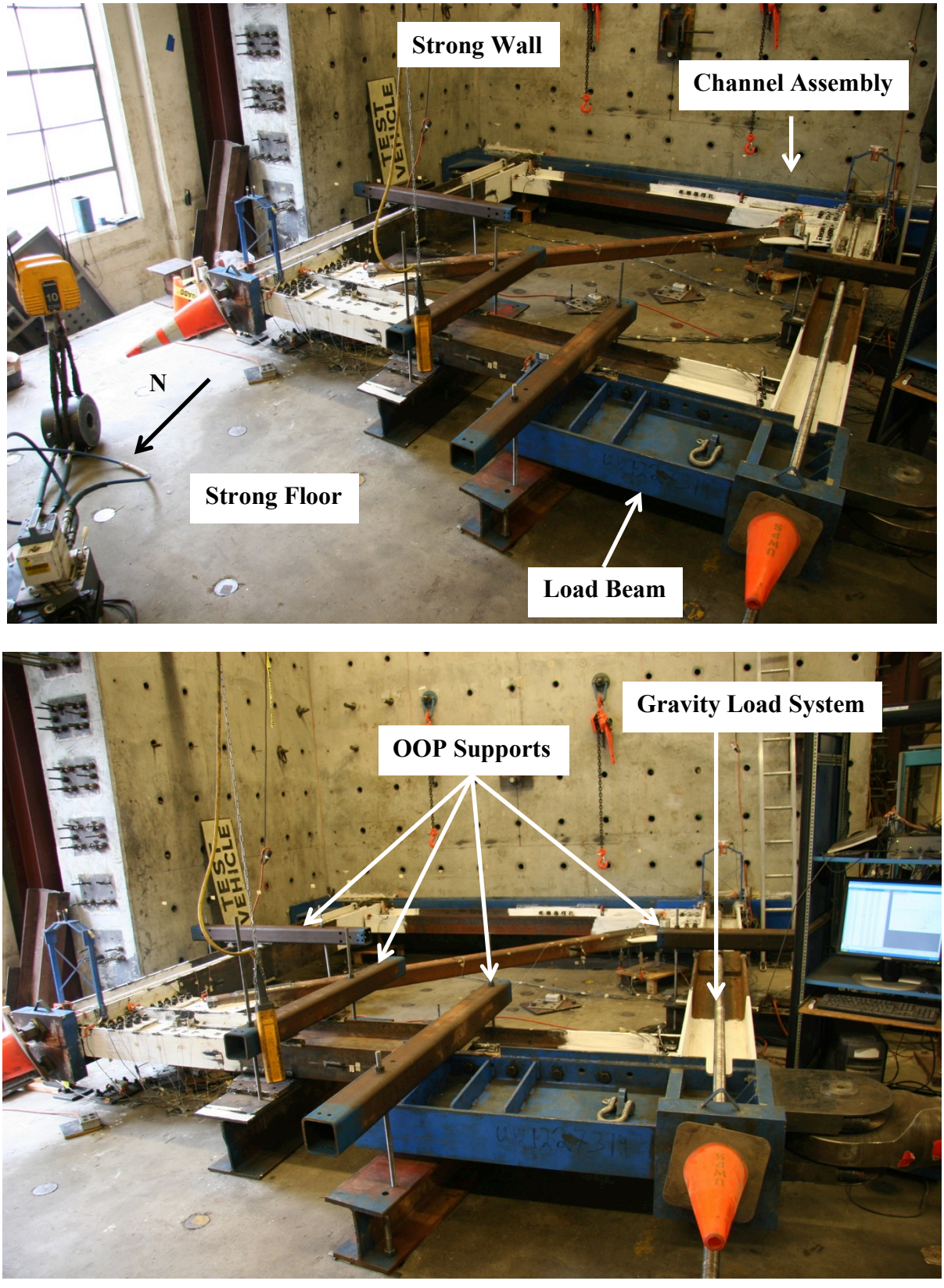

Figure 4.2 - UW Test Setup in the SRL

4.3 Test Setup Components

4.3.1 Strong Floor and Strong Wall

The tests took place on the concrete strong floor of the UW SRL. The strong floor is made of 3 ft thick concrete and acts as a rigid support for the frame, the reaction block, and the strong wall. It has evenly spaced holes in a grid pattern that are used to anchor the OOP supports. Unfortunately the floor has some unevenness in the surface, which required some effort to assure the frame was level and aligned parallel to a horizontal axis. The strong wall is L-shaped and composed of 30 in thick prestressed concrete. It also acts as a rigid support for the frame and was used to support some instrumentation for the experiments.

4.3.2 Channel Assembly

The channel assembly transfers the base shear and overturning moment from the braced frame to the strong wall. A cross sectional diagram of the channel assembly setup is shown in Figure 4.3, a plan view is shown in Figure 4.4, and photo realizations of the system in Figure 4.5. The system is composed of two C15x50 steel sections connected by 1/2 in. steel bearing plates on the north and south sides. At the shear connection in the middle of the south beam, the channel assembly has a 1.5 in. thick steel plate welded to the north face of the assembly. The channel assembly is stressed to both legs of the strong wall via a series of 1 in. and 1 5/8 in. diameter high strength threaded rods. As shown in Figure 4.3, there is also a C12x50 steel member on the south side of the strong wall to provide a base for the threaded connecting rods.

The braced frame is attached to the channel assembly through (10) – 1 in. diameter A490 bolts tightened using the turn-of-the-nut method (typically resulting in pressures between 3500 psi and 3700 psi) with the hydraulic torque wrench. The channel assembly also served as the anchorage for the 1.75 in. diameter William's rods that were used to apply axial load to the braced frame columns and as a rigid base to resist the overturning moment in the frame.

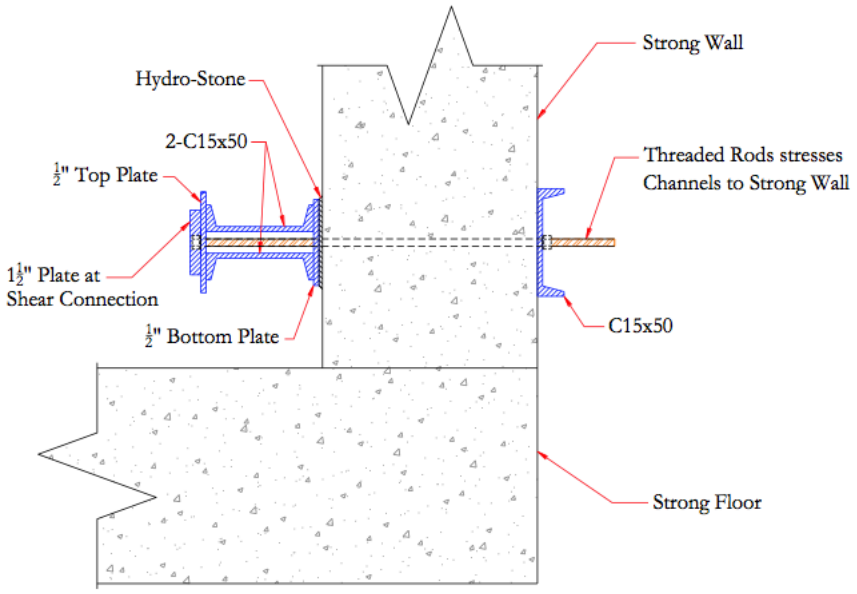

Figure 4.3 - Cross Section of Channel Assembly and Strong Wall [Powell, 2010]

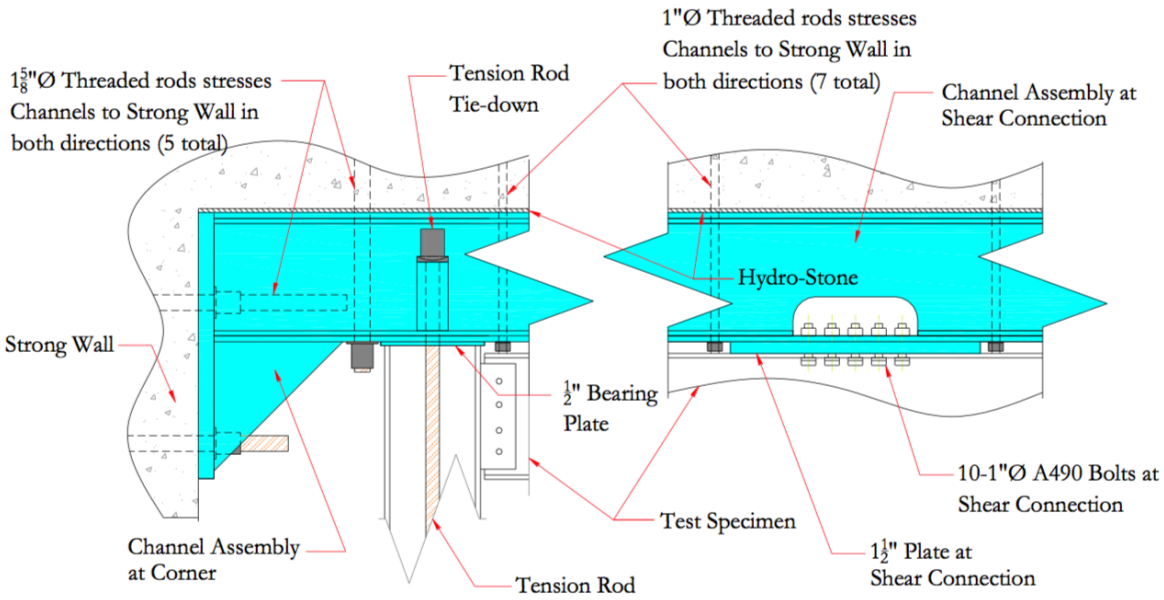

Figure 4.4 - Plan View of Channel Assembly and South Base Connection [Powell, 2010]

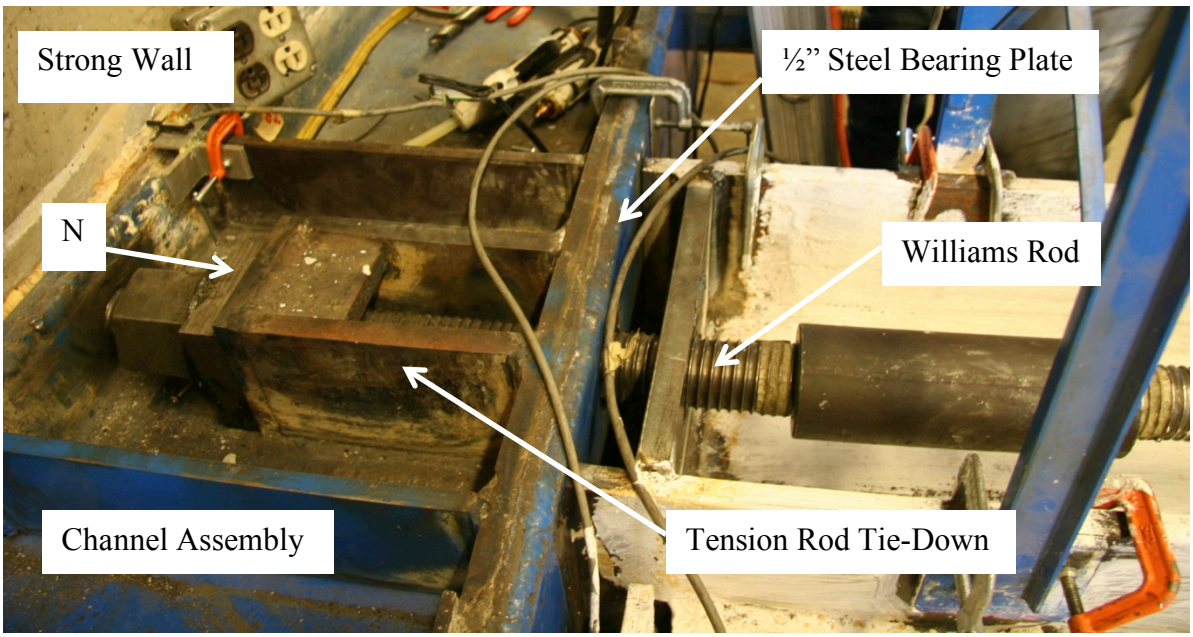

Figure 4.5 - Channel Assembly in SW Corner at West Column Base

4.3.3 Out-of-Plane Supports

Four OOP supports were required to hold the framing components in place vertically, while allowing in-plane, lateral movement of the frame. OOP supports were located on each column, on the north beam, and on the load beam. The south beam did not require an OOP support as it attached to the rigid channel assembly. A typical OOP restraint system is shown in Figure 4.6, which consisted of an HSS5x5x3/8 section on the top and a wide flange steel section on the bottom of the beam or column. As shown, nylon rods on the flanges of the beams or columns rested on greased stainless steel plates that were tack welded to the OOP restraints. The nylon rods and the stainless steel plates were greased to create an effectively frictionless surface. The wide flange OOP supports were anchored to the strong floor with threaded rods, and the HSS tubes were clamped to the wide flanges with wrench tightened threaded rods.

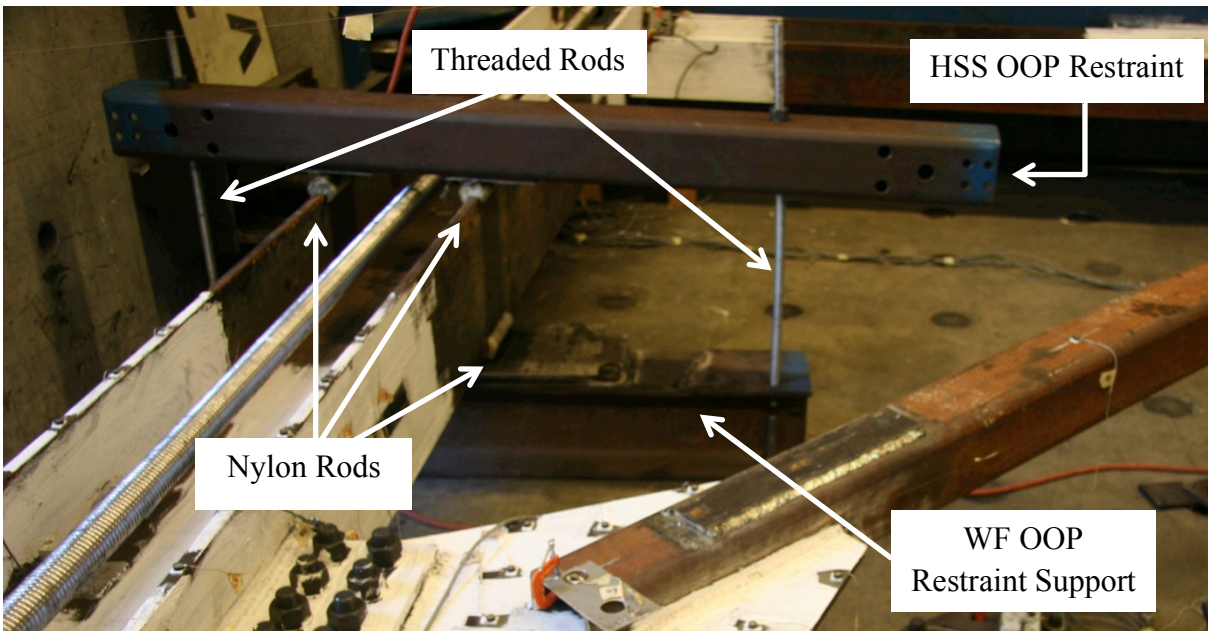

Figure 4.6 - OOP Restraint System

4.3.4 Gravity Load System

In a building, the gravity loads act to help prevent overturning of braced frames and add to the demands imparted from the braces. Gravity loads were simulated in the UW tests by post-tensioning each column to 450 kips with (2) – 1.75 in. diameter Williams Rods per column. Figure 4.7 shows the gravity load system layout with labeled components. The rods apply axial load to the braced frame and are anchored to the channel assembly to prevent braced frame overturning. In each column, the rods are centered with one rod positioned on top of the column web and one below the column web.

As shown in Figure 4.7, the post-tensioning rods are anchored at each end of the column with 1 in. thick dish washers and greased spherical hex nuts that allow rod rotation during frame loading. On the north end of the columns, a 4 in. thick cap plate is attached to the end of the east column, and to the side of the load beam for the west column. These thick cap plates allow for an even distribution of the applied axial load.

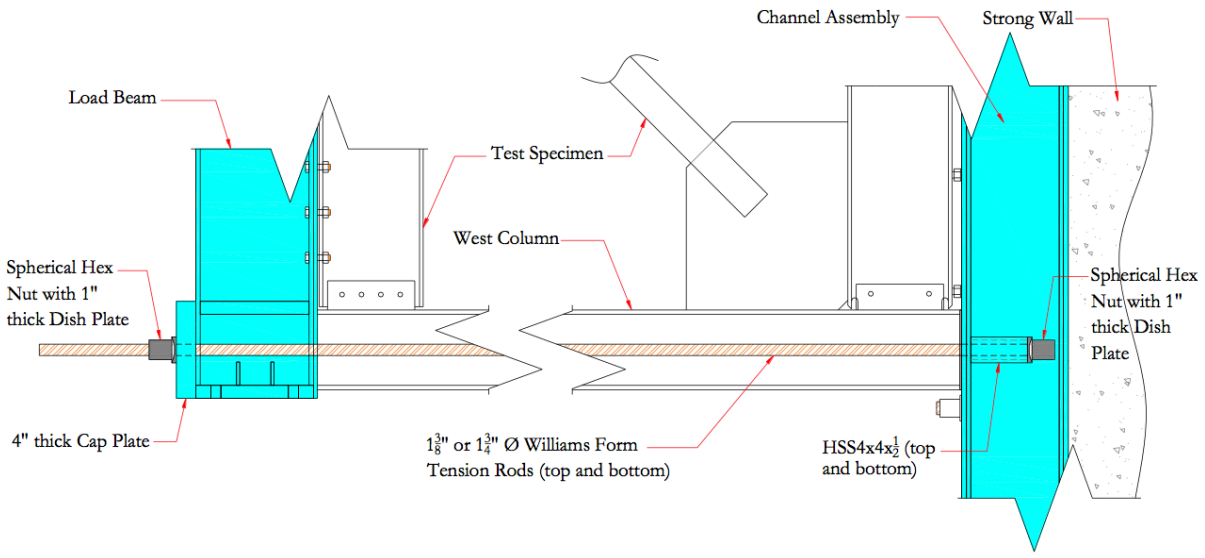

Figure 4.7 - Gravity Load System Layout in the West Column [Powell, 2010]

4.3.5 Reaction Block and Actuator

Figure 4.8 shows a drawing of the reaction block and the actuator and Figure 4.9 shows a photo of the same setup. The reaction block is a 6ft x 8ft x 4ft concrete block and it is anchored to the strong floor through (6) – 2 in. diameter Williams rods to the west of the test specimen. A thin layer of Hydro-Stone between the strong floor and the reaction block acts to uniformly distribute the load throughout the bottom surface. There is also a layer of Hydro-Stone, for the same reason, between the top of the reaction block and the washer plates for the anchor rods. The rods prevent overturning of the reaction block when the actuator pushes and pulls the braced frame test specimen. This reaction block serves as a rigid base for the attached hydraulic actuator that applies the lateral load to the braced frame system.

The actuator is secured to the reaction block with (6) - 1 1/8 in. threaded rods with an elastomeric bearing pad between the actuator and reaction block. The actuator has a capacity of 470 kips (pushing) and 350 kips (pulling), which informed the orientation of the frame; the frame is positioned with the brace in tension as the actuator is pushing and compression when the actuator is pulling to compensate for the force capacity differences. The actuator was displacement controlled through its internal LVDT and the loading followed a prescribed load

protocol, discussed in Section 4.5. A spacer plate was added to the end of the swivel head to ensure adequate stroke capacity for the braced frame specimens.

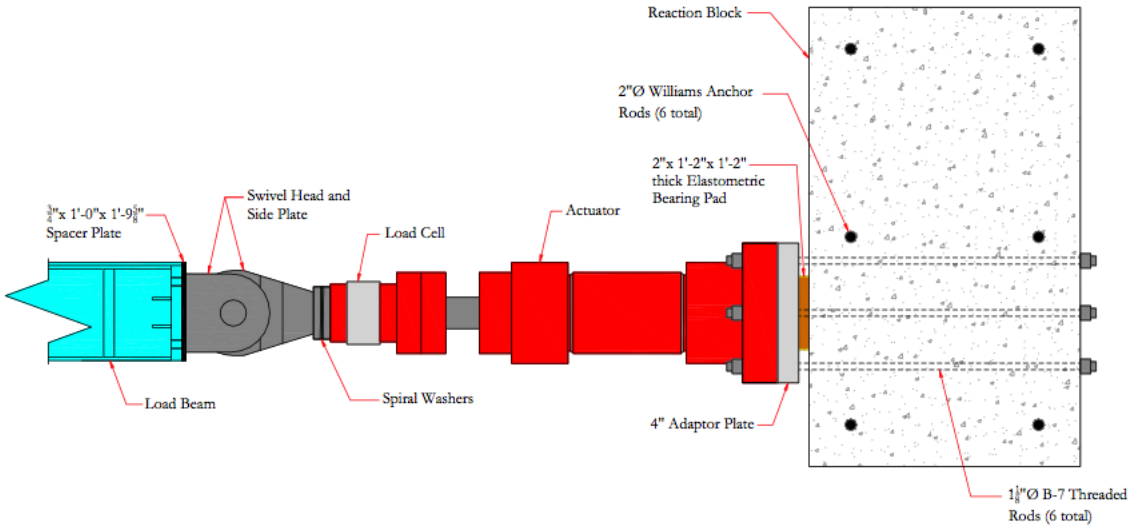

Figure 4.8 - Actuator and Reaction Block Components [Powell, 2010]

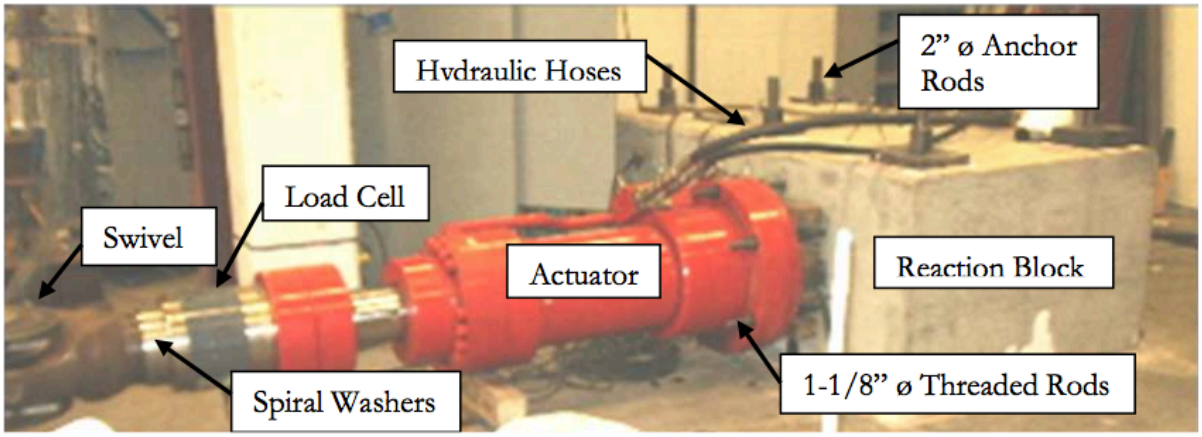

Figure 4.9 - Actuator and Reaction Block Components [Powell, 2010]

4.3.6 Load Transfer Beam

Figure 4.10 details the layout for the load transfer beam and its connection to the actuator and braced frame. The actuator applies force directly to the W21x62 load transfer beam and that horizontal applied load is transferred to the braced frame through a bolted shear connection. Note that relative to the center of the beam, the actuator eccentrically loads the frame with an eccentricity of 19 in.

As seen in Figure 4.10, the W21x62 load transfer beam has a 2 in. thick stiffener plate at each column flange and 1/2 in. thick stiffener plates along the length of the beam to stiffen the section. Four threaded rods connect the actuator and the load beam. The load transfer beam attaches to the north flange of the north beam in the braced frame through a bolted shear connection composed of (10) – 1 in. diameter A490 bolts.

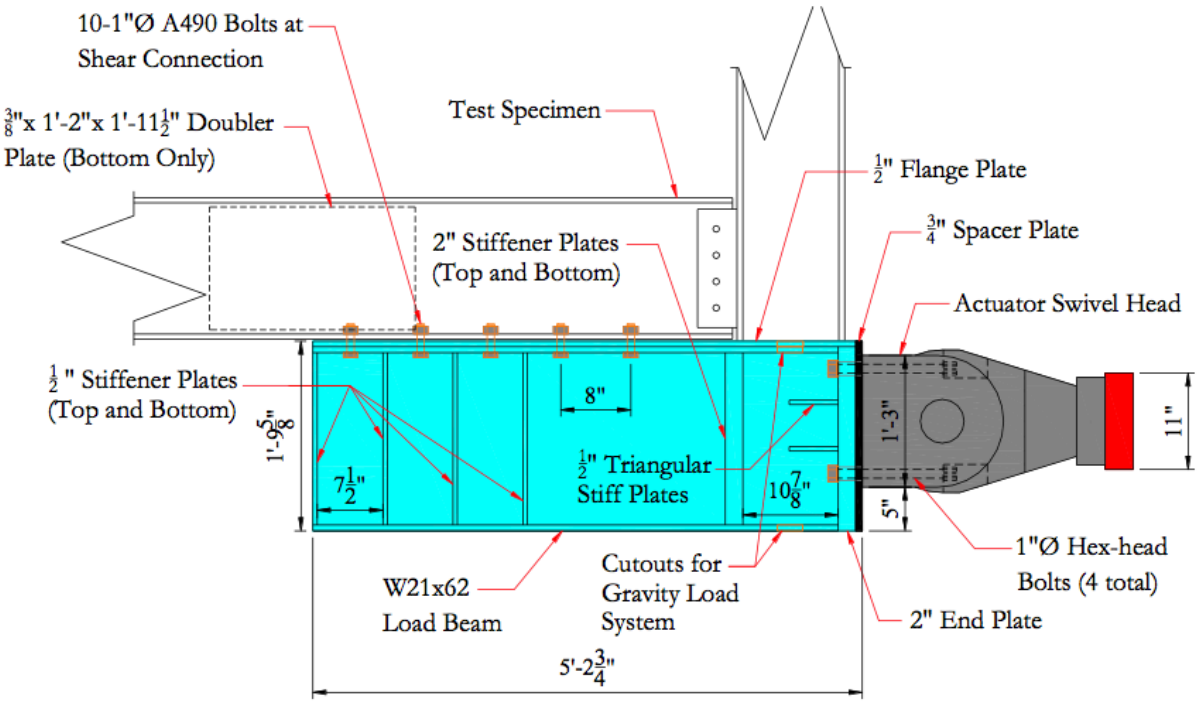

Figure 4.10 - Load Transfer Beam Layout [Powell, 2010]

4.3.7 Additional Test Specimen Details to Accommodate Test Setup

Special details were necessary in specific areas of the braced frame specimens to accommodate local demands imposed by the test setup. These details are not required in typical construction. The two components, a web doubler plate and column stiffener plates, are described in the subsections below.

4.3.7.1 Web Doubler Plate

As mentioned, the load transfer beam applied a load at an eccentric distance to the frame, which induces an in-plane moment in the beam web at the east end of the load beam. The compressive

force generated from the moment has the potential to buckle the beam web, as was seen in NCBF 1 (Sloat 2014) when a web doubler plate was not included. In this test the north beam web sustained significant local deformation and web buckling due to the eccentric loading. Subsequent tests included a 3/8 in. thick web doubler plate, shown in Figure 4.11, that was 2 ft. long, and as wide as the web depth. This plate is fillet welded on all four sides to the underside of the north beam – centered at the end of the transfer beam.

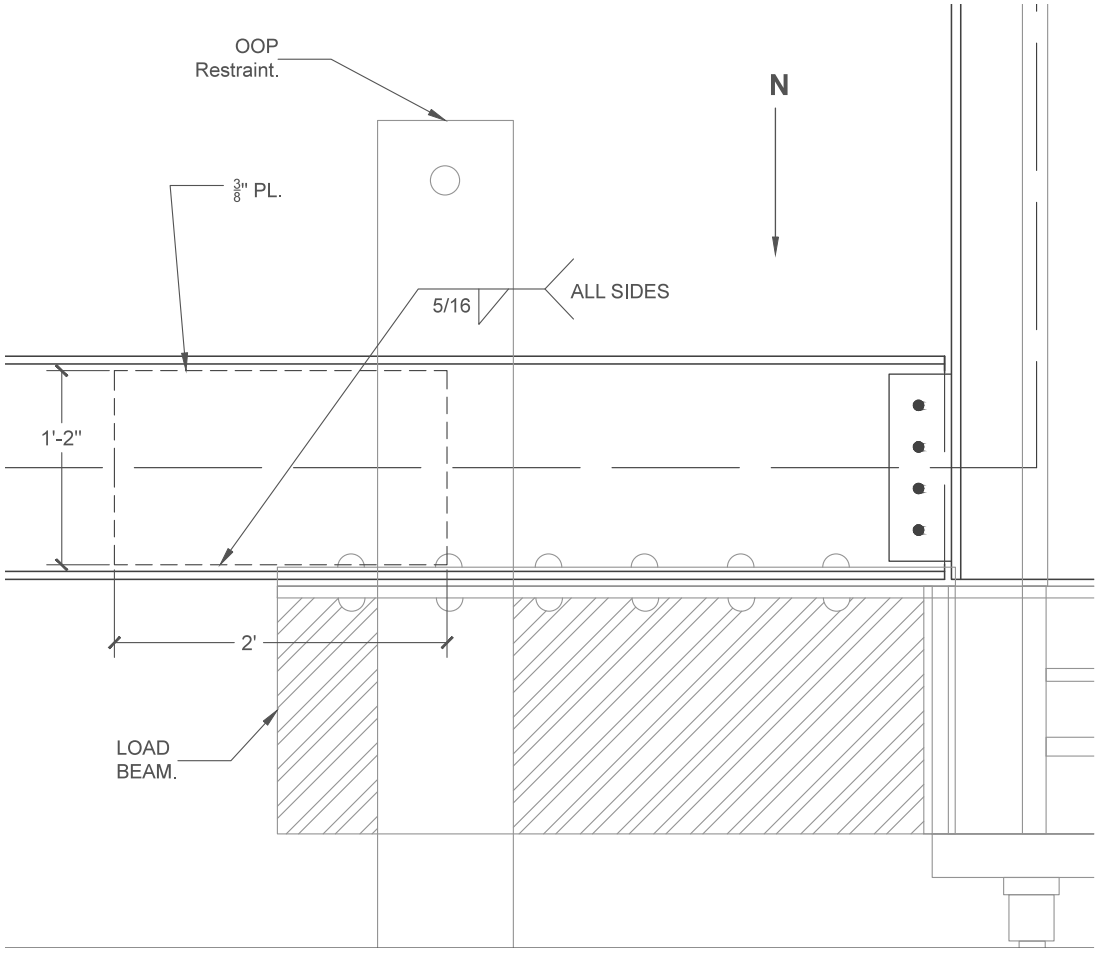

Figure 4.11 - Diagram of Web Doubler Plate in NW Corner of the Braced Frame

4.3.7.2 Column Stiffener Plates

Figure 4.12 shows a detail and photograph of a typical column stiffener. Four steel, 3/4 in. thick column stiffener plates were added to the south ends of the columns (two per column) to prevent local damage to the base of the columns seen in previous tests (Sloat, 2014). When the frame is loaded in tension or compression, one flange of each column has a high concentrated load due to

the overturning moment in the system. This concentrated load can cause local buckling in the column flanges. While these plates did not prevent all damage in the column bases, they appeared to be effective. Yielding of the column base around the stiffeners was observed in most tests (shown in Figure 4.12, within the rectangle) indicating that the stiffeners may have helped prevent local buckling at the column base.

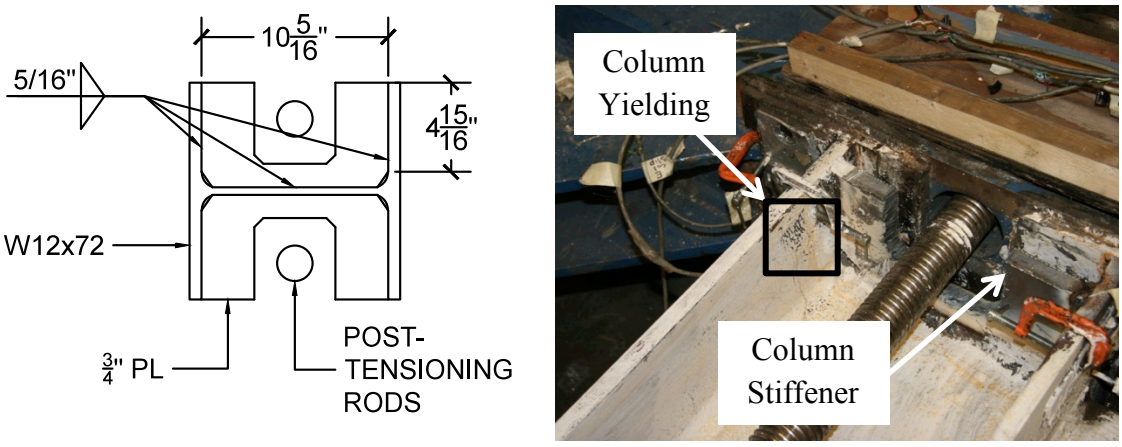

Figure 4.12 - Column Stiffener Detail

4.4 Instrumentation

Data from potentiometers and strain gauges was acquired using a National Instruments data acquisition (DAQ) system and was stored using LabView software on a desktop computer near the test setup. Each instrument had its own channel through which information was transmitted to the computer. All instruments were calibrated prior to their use. The calibration factors were used to convert the voltage readings into the desirable unit for forces, displacements, and strains. The Northern Digital, Inc (NDI) Optotrak system had a separate DAQ system to record the data from each individual sensor. These systems did not record data at the same frequency, which had to be corrected in the data to ensure simultaneous peaks in the data. The specific instrumentation used in the test is described further below.

Four different types of instruments were used to measure and record the behavior of the braced frame: strain gauges, potentiometers, the Northern Digital, Inc. (NDI) Optotrak systems, and visual observations. The first three types are discussed below with emphasis on the measurement

goals for each. Visual observations include photographs, whitewash yield patterns, and video. The overall instrumentation plan was consistent throughout the test series, with minor adjustments for the needs of different specimens. One significant change that was made for the later experiments was to eliminate a number of potentiometers in favor of Optotrak markers.

4.4.1 Strain Gauges

Strain gauges were adhered to the brace, both columns, and the north beam as shown in Figure 4.13. Exact locations for each test are tabulated in the Appendix. The strain gauge measurements on these components, coupled with the results from the coupon tests allowed the determination of:

- Moments in the columns and the north beam [Strain Gauges #5-8, #9-12, and #13-16]
- Shear in the columns and the north beam [Strain Gauges #5-8, #9-12, and #13-16]
- Brace axial force [Strain Gauges #1-4]

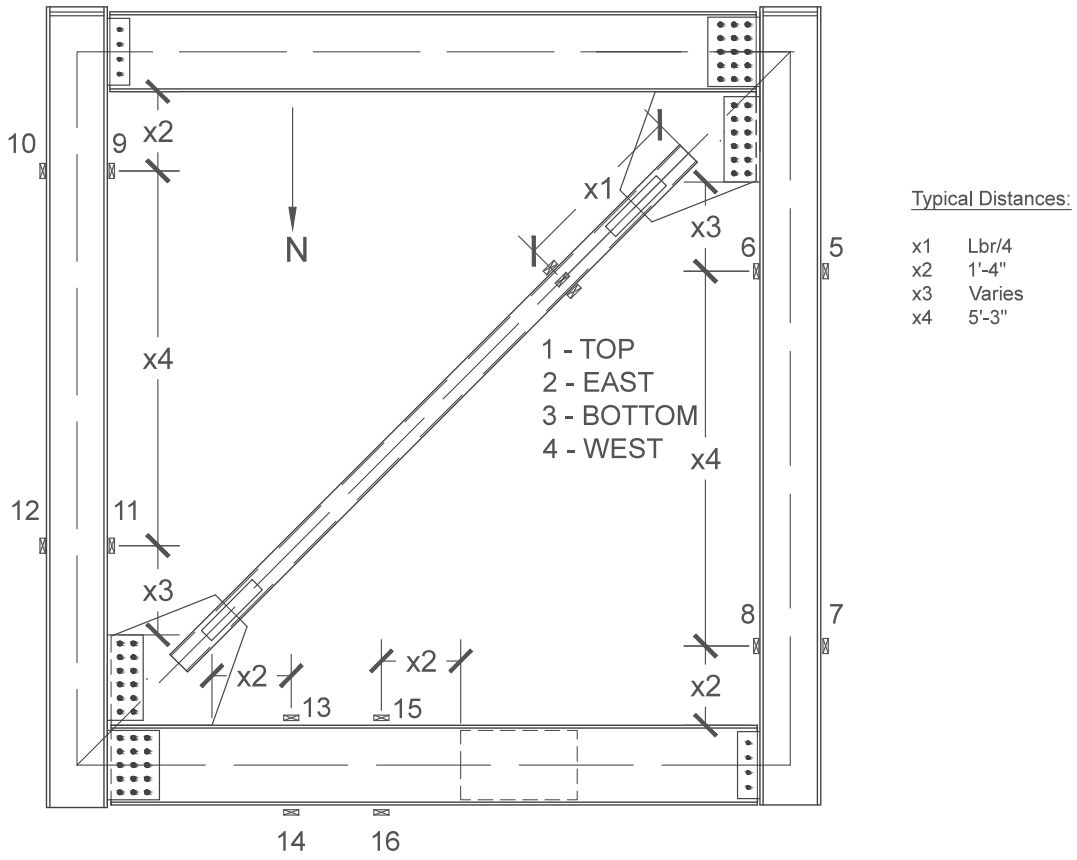

Figure 4.13 - Typical Strain Gauge Layout

It is important to calculate the moments in the framing elements to better quantify the extent of damage they withstood during the experiments. By calculating the moments at each strain gauge pair on the beam and columns we can project a moment diagram over the length of the component assuming linear behavior. The moment diagram can be extended to the ends of the gusset plate where it can be determined whether a plastic hinge formed in the framing elements in addition to the brace midspan. This knowledge can shed light on the comparative behavior of the beams and columns and whether there was a "weak beam-strong column" scenario or vice versa.

Strain gauge data also makes it possible to trace the load through the system. Using the column shears calculated from strain gauge pairs on the columns and the applied load, the brace axial force can be determined. This value can be verified with the strain gauges on the brace and the

brace material properties from coupon tests that serve as a more direct measurement of the brace axial force.

To determine the quantities listed above, the strain gauges were located as follows: four gauges were attached to the brace, one on the midpoint of each wall, 1/4 of the brace length from the SW end of the brace; four gauges were placed on each column at mid-depth of the flange; in some cases, two sets of gauges were placed for redundancy for a total of eight gauges on each column; and four gauges were attached to the north beam between the west end of the NE gusset plate and the east end of the load beam. The exact calculations using the strain gauges are detailed in Chapter 6. Tokyo Sokki Kenkyujo Co., Ltd. FLA-6-11-5L uni-axial strain gauges were used with a 6mm gauge length, nominal gauge factor of 2.12, and high reliability for strain ranges between ±1%.

4.4.2 Potentiometers

Three types of potentiometers were used in each tests: UniMeasure, Inc. model P510 string potentiometers, the 9600 Series (for small displacements, ±1/4 in. to ±2 in.) BEI Duncan linear conductive potentiometer, and the BEI Duncan 600 Series (medium displacements, ±2 in. to ±5 in.) BEI Duncan. The potentiometers were used to record the quantities listed below and their typical layout is shown in Figure 4.14. Exact locations for each test are tabulated in the Appendix.

String potentiometers were used for the following measurements:

- Brace out-of-plane midspan displacement [#8]
- Brace elongation and shortening [#6]
- Frame diagonal [NE to SW frame work points] [#15]
- Frame corner work point vertical displacements [#18, 19, 34, 35]
- Lateral frame displacement [#4]

BEI Duncan potentiometers were used for the following measurements:

- Uplift (2 locations) and slip of the channel assembly from the strong wall [#38, 39, 40]
- Uplift and slip of each flange of both columns from the channel assembly [SW: #43, 51, 44. SE: #41, 53, 42]

- Horizontal slip of the south beam to channel assembly connection [#45]
- Horizontal slip of the north beam to the load beam [#52]
- Horizontal slip of the reaction block at the base to the strong floor (3 locations) [#47-49]
- Movement of the actuator at the reaction block
- Rotation of all NW, SE beam to column shear tabs [NW: #30, 31. SE: #32, 33]
- Rotation of the SW gusset plate from the west column
- Rotation at plastic hinge locations in north beam and west column (in SW corner) [Beam: #24, 25. Column: #26, 27]

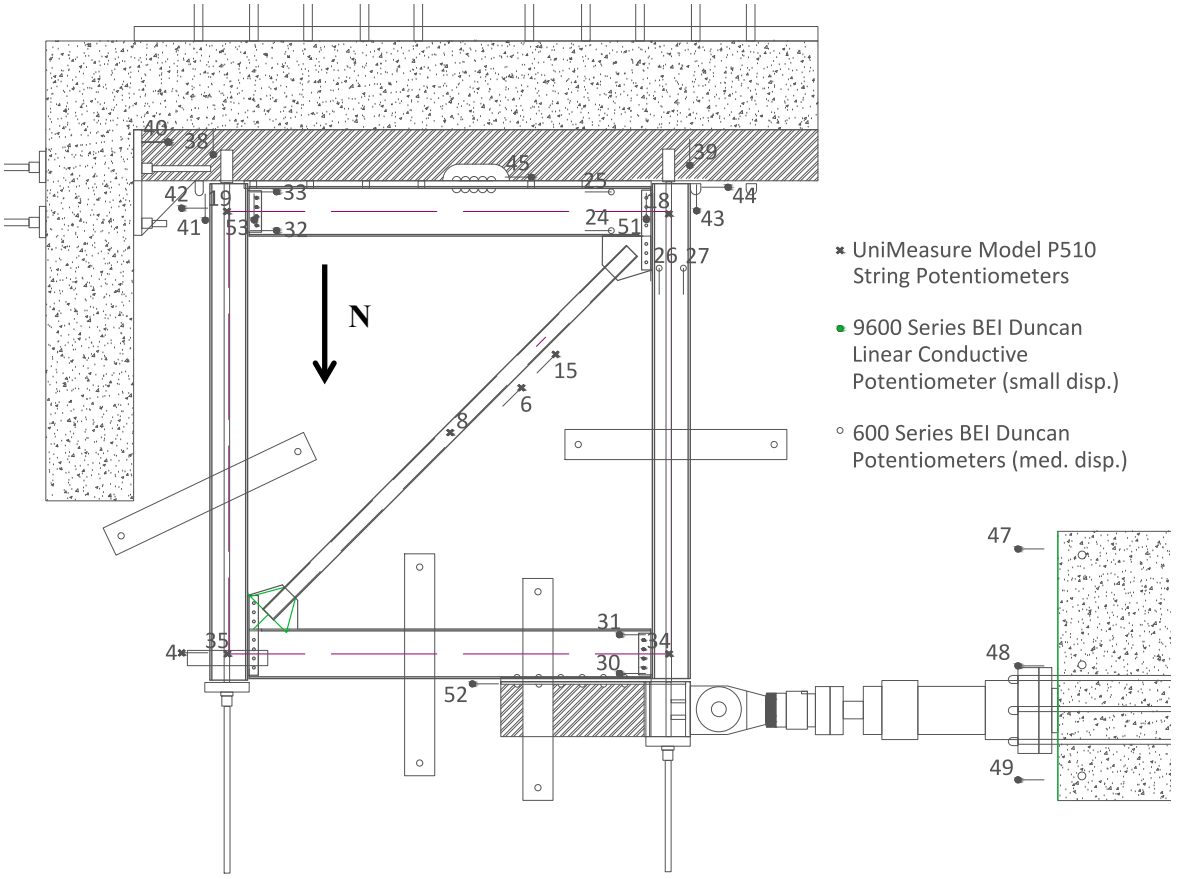

Figure 4.14 - Typical Potentiometer Layout

The frame diagonal measurement is one of the most important in the test setup as it is used to calculate the frame drift. The other potentiometers used to calculate various brace behaviors are important to understanding the brace response. Potentiometers combined with Optotrak sensors along the length of the brace can record the brace deflected shape. This shape can visually aid in

giving information about the brace end conditions, discussed more in Chapter 6. The brace elongation measurement compared to the frame diagonal measurement can give an indication of how much elongation and shortening is occurring in the connection (combination of gusset plate, shear tabs, bolts and welds, and corner framing elements) as compared to the brace itself. Knowing how much deformation the connection is incurring is of particular importance to the NCBF specimens.

The lateral frame measurement (#4), combined with uplift and slip measurements of the testing assembly can provide an indication of where losses are occurring throughout the system, and can begin to quantify the loss values at each measured location. In previous UW SCBF experiments, these losses were not trivial, and are the reason we cannot use the lateral frame string pot measurement.

The pots used to measure connection rotations allow the calculation of the amount each corner is opening and closing throughout the experiment. Likewise, the potentiometers used to measure the uplift at the base of the columns can quantify the base rotation of the frame. These instruments can also be used to identify if any complete uplift of a column base occurred during the testing procedure.

A number of corrections using geometry had to be applied to the potentiometer data when measuring OOP movement of components to account for the lateral movement of the frame. The calculations made from the potentiometers for the quantities listed above are detailed in Chapter 6.

4.4.3 Northern Digital, Inc. - Optotrak

The Optotrak system manufactured by Northern Digital Inc. was used to measure displacements at critical locations on the frame. It is composed of two overhead cameras, one mounted to each leg of the strong wall, that read the 3-D positions (x, y, and z coordinates) of each the light emitting diodes (LEDs). The two cameras are used to cover a majority of the brace and the NE corner. The two cameras are required to have an overlapping volume to establish a shared coordinate system. The Optotrak was used to record the quantities listed below and a typical

layout is shown in Figure 4.15, where the "+" symbols represent Optotrak markers. Exact locations for each test are tabulated in the Appendix.

- Brace out-of-plane buckled shape (including midspan displacement)
- Rotation at plastic hinge locations in south beam and east column (in NE corner)
- NE gusset plate out-of-plane displaced shape
- Movement of the NE corner frame diagonal stand
- Rotation of the NE beam to column shear tab
- Rotation of the NE gusset plate to column shear tab

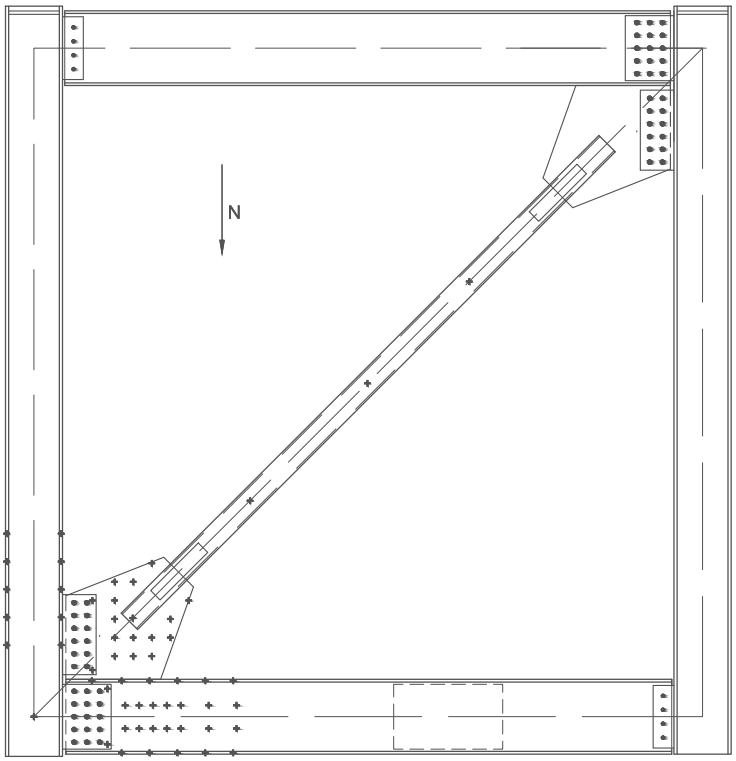

Figure 4.15 - Typical Optotrak LED Layout

The LED sensor layout varied the most on the gusset plate and shear tabs in the NE corner to accommodate changes in gusset plate geometry, but Figure 4.16 shows a sample configuration. As mentioned, the LEDs along the brace length are critical to quantifying and visually representing the brace out-of-plane displaced shape. A pair of these LEDs can also be used to determine the brace end rotation. The LEDs on the gusset plate can also visually represent the out-of-plane rotation of the gusset plate. Measuring the connection behavior is of particular

importance to the NCBF connections where the brace will not necessarily concentrate the majority of the inelastic deformation. Because the NE corner of the frame is not as restrained as the SW corner, identifying any movement in the tower used to measure the frame diagonal elongation was also important. The calculations made from the Optotrak measurements are described in detail within Chapter 6.

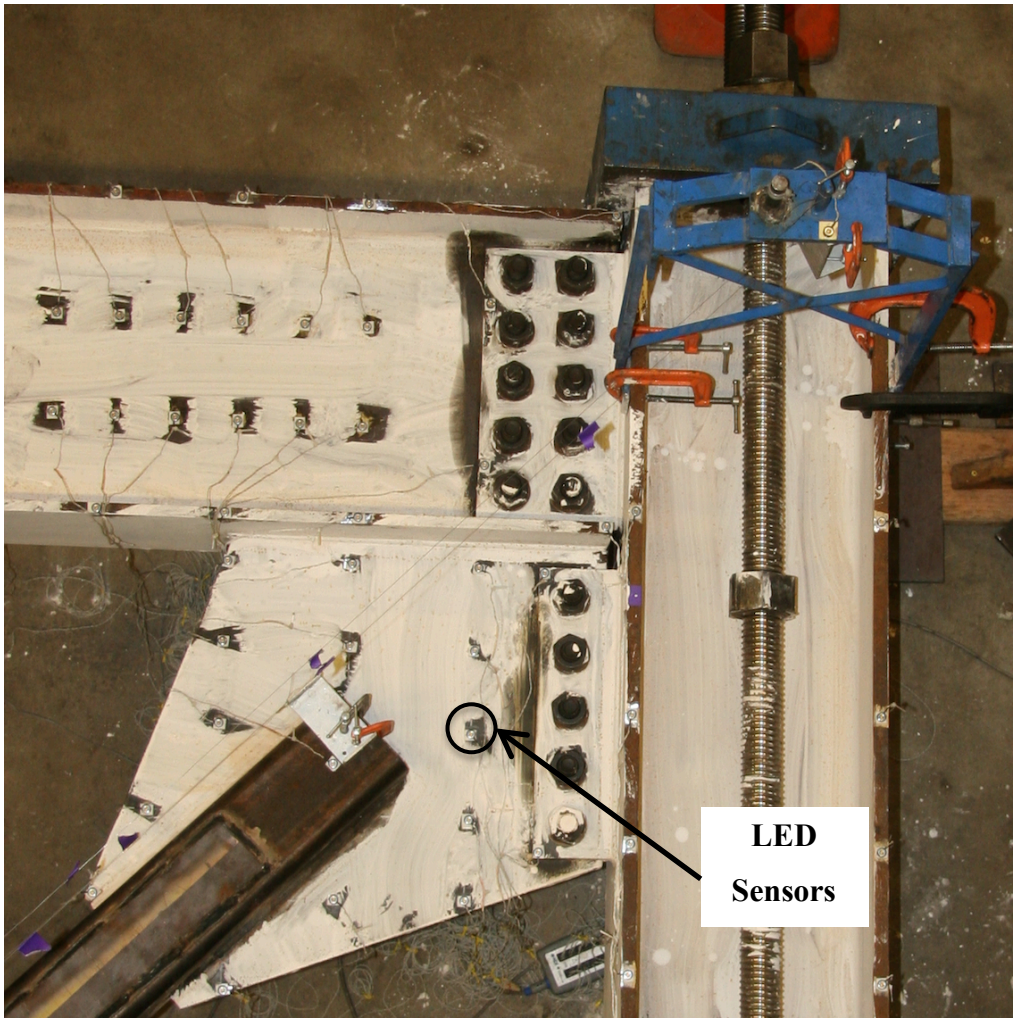

Figure 4.16 - Sample LED Layout from SHSS-B2

4.4.4 Visual Observations

The final instrumentation type was visual observations, which included photographs, whitewash yield patterns, and video. Photographs were taken at each pause in the loading protocol either at a peak tensile load, or peak compressive load. They provided an excellent and unambiguous form of test documentation that can tell a clear visual story of damage progression.

Whitewash – a mix of lime and water – was painted on the hot rolled steel beams and columns. As these elements yielded, the mill scale flaked off, along with the whitewash. The HSS braces were not whitewashed because they are cold formed steel and therefore do not have mill scale. The whitewash is critical for visual observations of yield patterns, which helped determine shear or tensile yielding, and provides a visual indication of the extent of member yielding.

4.5 Load Protocol

The load protocol used for the test was built on and adapted from previous SCBF tests in the UW SRL (Johnson, 2005). The target protocol has been reproduced below in Figure 4.17, with the target displacement (in) on the y-axis and the cycle number on the x-axis, and in and Table 4.1. In Table 4.1 a "cycle" consists of equal positive and negative displacements. For instance, cycle 1 consists of displacing the frame +0.125 in. and then through zero to -.125 in. The protocol consisted of two cycles at increasing displacements; a cycle consisted of a tensile displacement followed by an equal compressive displacement. There are more cycles at smaller displacements in order to establish the elastic stiffness of the frame. The original protocol was created by Shawn Johnson in 2005 which he developed from recommendations from ATC-24 [6] and the SAC Steel Project [24]. The actuator was pushed to the peak in either tension or compression and held while photographs and visual observations were made.

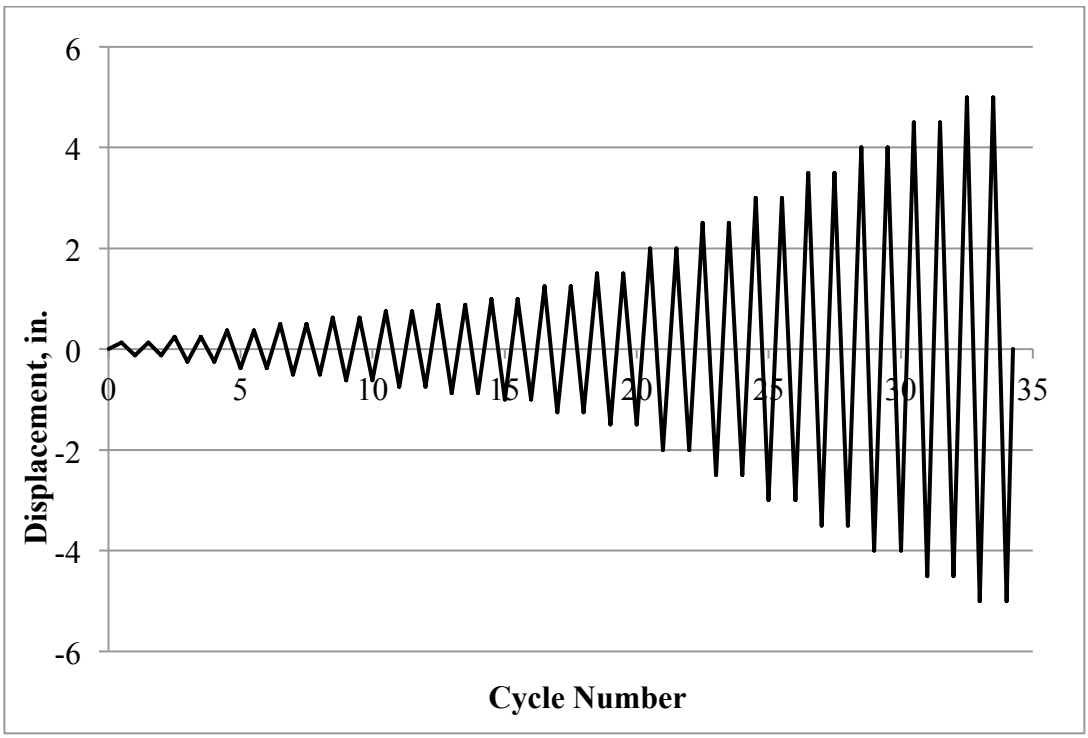

Figure 4.17 - General Testing Load Protocol

Table 4.1 - Target Displacement per Cycle for Applied Loading Protocol

Cycle	Displacement (in).
1-2	0.125
3-4	0.25
5-6	0.375
7-8	0.5
9-10	0.625
11-12	0.75
13-14	0.875
15-16	1.0
17-18	1.25
19-2-	1.5
21-22	2.0
23-24	2.5
25-26	3.0

27-28	3.5
29-30	4.0
31-32	4.5
33-34	5.0

There were significant differences between the applied displacement history and the measured displacement history in each test. Larger differences were seen in tests that sustained higher tensile forces. This discrepancy was from losses throughout the system through column uplift, bolt slip in the connection to the south beam to channel assembly and from the north beam to the load transfer beam, and is discussed further in Chapter 6. The actual applied load histories for each specimen are given in the Appendix.

4.6 Testing Preparation

A brief overview of the test preparation procedure is listed below:

- The steel columns, beams, and braces were fabricated in the lab; cut to length with an oxy-acetylene torch.
- The frame was leveled and aligned using a jig setup on the strong floor.
- The members were flipped in order to weld the plates downhand.
- Once welded or bolted together completely, the frame was lifted onto a cart at the north end and the crane on the south end and rolled to the south end of the strong floor.
- The frame was leveled using the nylon rods to be approximately 11 3/4” vertical distance between the strong floor and the bottom of the flange and then bolted to the channel assembly.
- The OOP restraints were placed while strain gauges and Optotrak sensors were applied.
- The columns were tensioned and the frame was whitewashed the day before the test.
- Before testing, the frame underwent elastic cycles to ensure all instruments were recording properly.

CHAPTER 5: TEST RESULTS & OBSERVATIONS

5.1 Introduction

This chapter discusses test results and detailed observations for the three bolted NCBF test specimens. Section 5.2 briefly describes the nomenclature used to quantify the damage found throughout the test and to provide a uniform method of defining damage. Figure 5.1 shows locations on the frame called out in the text during damage observations. For additional information on the setup, see Chapter 4.

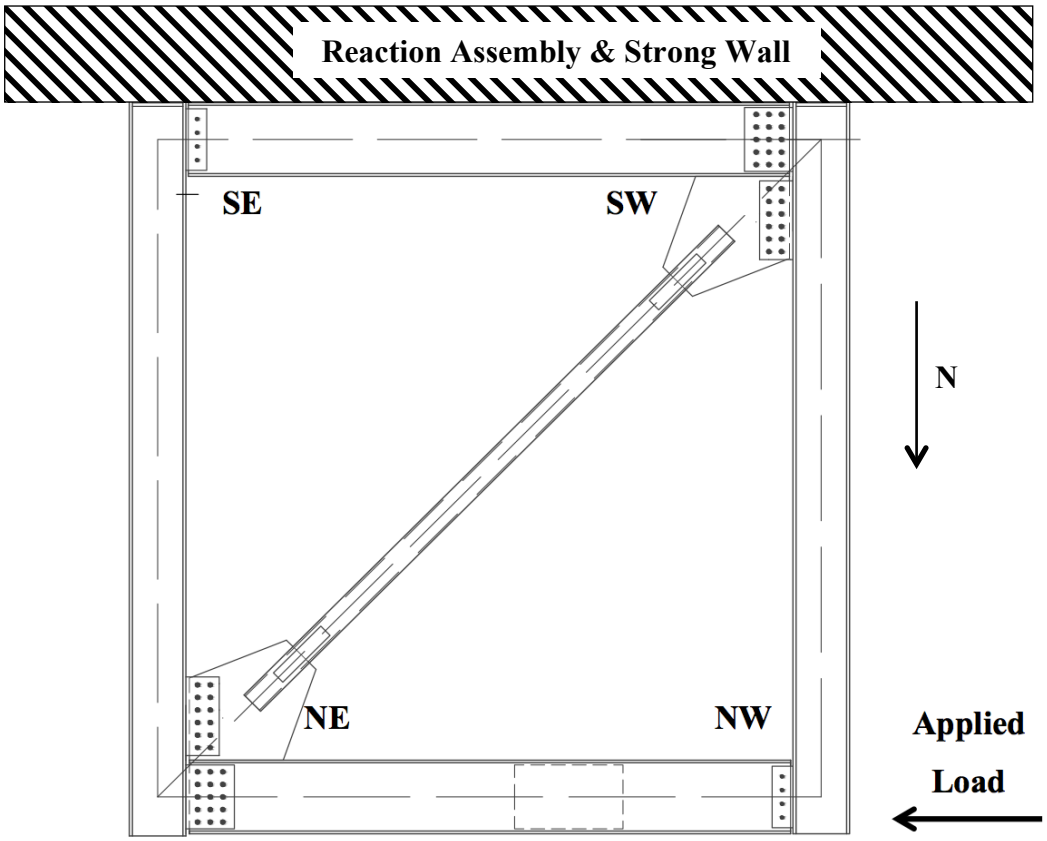

Figure 5.1 - Frame Orientation

Subsections of 5.3 begin with an overview of the specific specimen's design and are then divided into two sections describing performance at moderate damage states (DS1 & DS2) through severe damage states (DS3 & DS4). Each damage state was observed at the peak drift, where a

“+” drift value indicates the brace was in tension and a “-” value indicates the brace was in compression. The drift values are the measured drifts obtained from the elongation of the frame diagonal. The story shears noted in this chapter are the horizontal applied loads from the actuator. Each specimen’s section concludes with a summary of the key observations during the test. Table 5.1 provides a brief description of each specimen. Figure 5.2 summarizes the total drift ranges achieved by each test, with their respective maximum tensile drifts shown in hatched grey (“+” values) and maximum compressive drifts in solid grey (“-” values).

Table 5.1 – Overview of Specimen Test Matrix

Test Name	Test Objective	Shear Tab to Column Weld Size	Beam to Gusset Plate Weld Size and Length	Gusset Plate Thickness (in.)	Shear Tab Thickness (in.)
NHSS-B1	To explore perceived deficiencies of NCBF bolted connections (bolt shear, brace net section, & brace block shear) using a shared shear plate and HSS5x5x3/8 brace section.	CJP	7/16 in. and 11.75 in.	3/4	3/4
NHSS-B2	To explore perceived deficiencies of NCBF bolted connections (bolt shear & bolt bearing, brace net section & block shear, and beam to gusset base metal fracture) using separate shear plates and an HSS6x6x1/4 that does not meet brace seismic compactness requirements.	CJP	5/16 in. and 16.125 in.	3/4	3/4
NHSS-B3	To explore perceived deficiencies of NCBF bolted connections (bolt shear & bolt bearing, brace net section & brace block shear, and Whitmore & shear gusset plate yielding) using a split shear tab, thinner gusset plate and HSS5x5x3/8 brace section.	CJP	5/16 in. and 15.75 in.	1/2	3/4

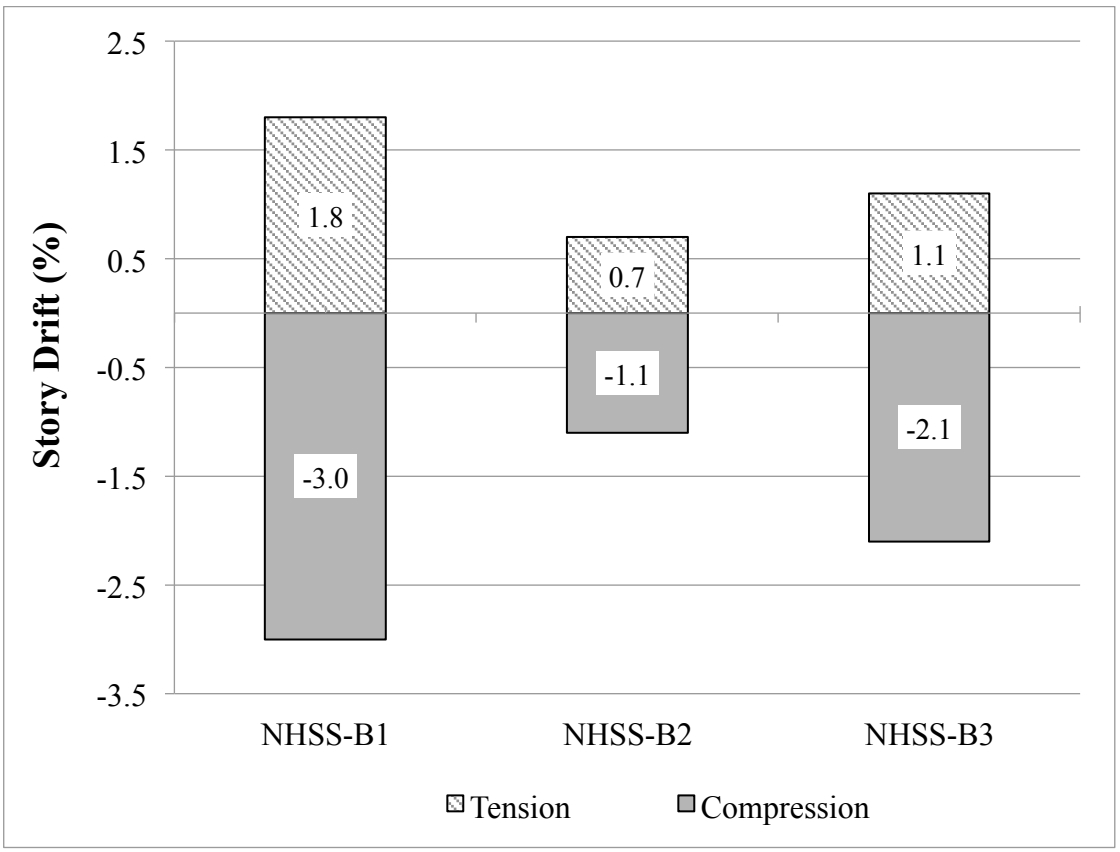

Figure 5.2 - Specimen Drift Ranges

5.2 Overview of Performance States

The major performance states defined for observed damage in these tests are yielding, buckling (both local and global), weld damage, bolt hole elongation, and bolt deformation. The performance states are summarized in Table 5.2. The photographs accompanying the descriptions should be used as a reference throughout the text when different performance states are stated in test descriptions. As mentioned, these observed performance states are used to classify the frame into four different damage states based on observed damage. These damage states are presented in Table 5.3 following the performance state descriptions.

Table 5.2 - Performance State Descriptions

Symbol	Label	Detailed Description
Y1	Initial Yielding	Yield lines are visible and cover less than one half the gusset plate or member depth.
Y2	Moderate Yielding	Yield lines cover more than one half the gusset plate or member depth, but not the entire member.
Y3	Severe Yielding	Yield lines cover the entire gusset plate or member depth to the extent much of the white wash might have flaked off.
B1	Initial Buckling	*Framing Elements*: Local buckling is first visible but does not exceed the buckled steel element's thickness. *Brace*: Global buckling does not exceed the member depth
B2	Moderate Buckling	*Framing Elements*: Local buckling exceeds the buckled steel element's thickness. *Brace*: Global buckling exceeds the member depth
B3	Severe Buckling	*Framing Elements*: Local buckling exceeds twice the buckled steel element's thickness. *Brace*: Global buckling exceeds twice the member depth
BT	Brace Tearing	Tearing has initiated on at least one corner of the brace in the plastic hinge region.
BF	Brace Fracture	Brace is completely fractured.
WC1	Initial Weld Cracking at Column	A weld crack has initiated on the gusset plate to column or beam to column weld but is only torn on one side or it has not exceeded 5% of the weld length.
WC2	Moderate Weld Cracking at Column	The weld crack on the gusset plate to column or beam to column weld is on both the top and bottom of the plate or it has not exceeded 25% of the weld length.
WC3	Severe Weld Cracking at Column	The weld crack on the gusset plate to column or beam to column weld is on both the top and bottom of the plate or it has not exceeded 50% of the weld length.

Symbol	Label	Detailed Description
WCF	Weld Fracture at Column	Complete weld fracture on the beam to column or gusset plate to column connection.
WB1	Initial Weld Cracking at Beam	A weld crack has initiated on the gusset plate to beam weld but is only torn on one side or it has not exceeded 5% of the weld length.
WB2	Moderate Weld Cracking at Beam	The weld crack on the gusset plate to beam weld is on both the top and bottom of the plate or it has not exceeded 25% of the weld length.
WB3	Severe Weld Cracking at Beam	The weld crack on the gusset plate to beam weld is on both the top and bottom of the plate or it has not exceeded 50% of the weld length.
WBF	Weld Fracture at Beam	Complete weld fracture on the gusset plate to beam connection.
WBc	Base Metal Damage on Column	There is base metal damage [usually a tear] at the beam to column or gusset plate to column connection.
WBb	Base Metal Damage on Beam	There is base metal damage [usually a tear] at the beam to gusset plate connection.
BoE	Bolt Elongation in Connecting Materials	There is bolt hole elongation in either the beam web, the gusset plate, or the shear tabs.
BD	Bolt Deformation	There is at least 1/16” measured bolt deformation.
BoF	Bolt Fracture	One or more of the bolts has fractured in a connection.

Table 5.3 - Damage State Descriptions

Damage State	DS1	DS2
Observable Damage	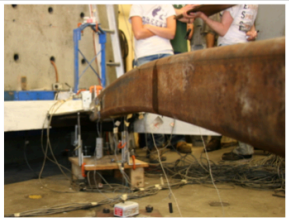 *B1 - brace*	 *WC1 or WB1*  *Y2 - gusset*
	 *Y1- gusset*	 *B2*
Maximum Seismic Response	Initial yielding, but no physically discernable damage. Brace OOP buckling less than brace depth.	OOP brace buckling is less than twice the brace depth. Crack initiation in welds less than 5% total weld length. Gusset yielding around fold line. Limited frame yielding. Initial bolt hole elongation >1/16 in.

Damage State	DS3		DS4	
Observable Damage	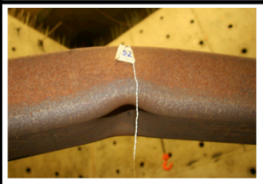 *B3 - local deformation*	 *Y3 - column*	 *B3 - beam flange*	 *BoE >1/4 in. and/or BoF*
	 *WB2 or WC2*	 *BoE <1/4 in.*	 *WB3, WC3, WBF, WCF*	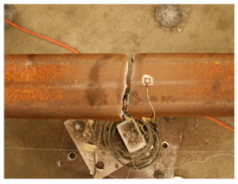 *BT or BF*
Maximum Seismic Response	OOP brace buckling less than three times brace depth - visible damage localization. Gusset plate yielded over 50% of the area. Weld tears have propagated between 25% and 50% of length. Framing members yielded over entire depth. Flange and web local buckling less than the thickness. Bolt hole elongation less than 1/4 in.		Brace has fractured or severe plastic hinge with OOP displacement more than three times the brace depth. Widespread yielding or buckling of gusset plates - over 75%. Weld torn more than 50% of length or fully fractured. Visible plastic hinging in framing elements. Flange and web local buckling less than twice the thickness. Bolt hole elongation greater than 1/4 in., or bolt fracture.	

5.2.1 Plate and Frame Yielding (Y)

Strain gauge measurements (described in Chapter 6) and whitewash yield patterns (described in Chapter 3) are used for measuring and observing yielding in the UW braced frame system experiments. To compare damage levels and to expand upon the notation in Table 5.2, samples of yield progression in the gusset plates and framing elements are shown through photos in Figure 5.3 and Figure 5.4, respectively.

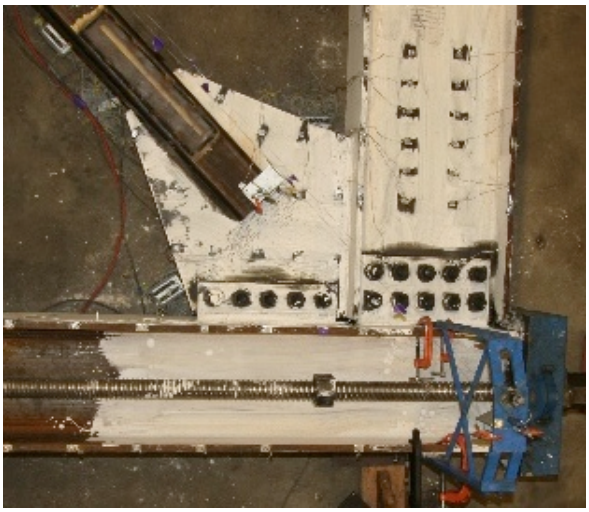

a. Initial Yielding, Y1

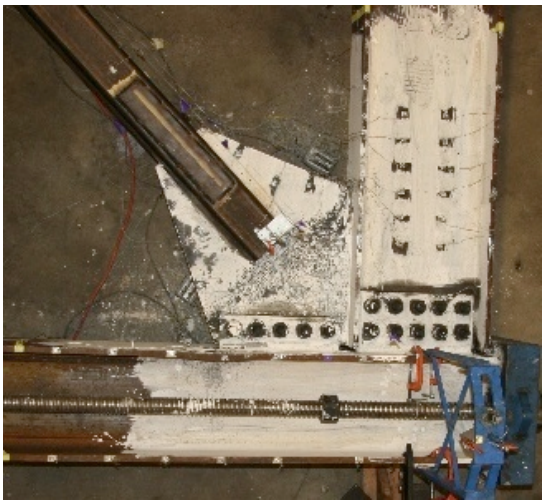

b. Moderate Yielding, Y2

c. Severe Yielding, Y3

Figure 5.3 - Typical Yield Progression on Gusset Plate (from Specimen SHSS-B2)

In most tests initial yield lines (Y1) on the gusset plate were perpendicular to the brace axis, resulting from the gusset plate bending out-of-plane (OOP) to accommodate brace buckling, shown in Figure 5.3a. These yield lines increased in density with increased brace buckling. Moderate yielding (Y2) is defined when yield lines have covered over 50% of the gusset plate, as shown in Figure 5.3b. Yield patterns were visible on both the top and the bottom of the gusset plates. In the majority of the tests, severe yielding (Y3) occurred in the gusset plates when almost all the whitewash had been removed, as seen in Figure 5.3c.

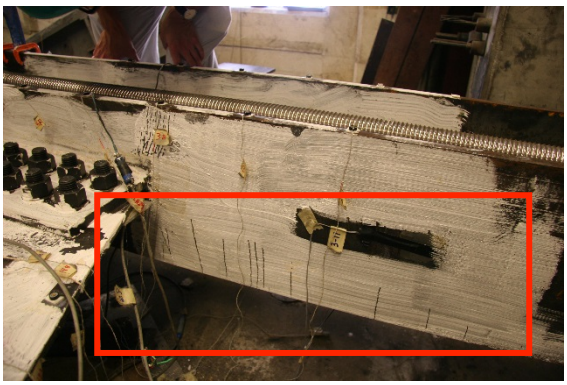

a. Initial Yielding, Y1

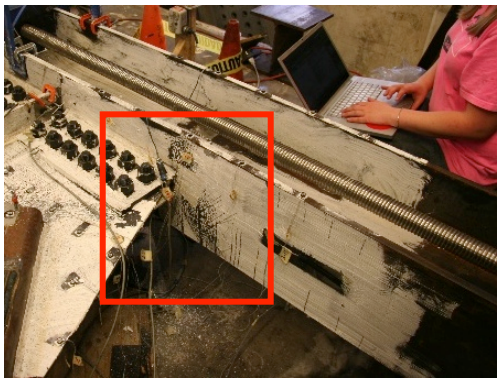

b. Moderate Yielding, Y2

c. Severe Yielding, Y3

Figure 5.4 - Typical Yield Progression in Columns (from Specimen SHSS-B1)

In most tests, initial yielding (Y1) formed in the framing elements from the flange tips propagating towards the web at the edge of the gusset plate, as shown in Figure 5.4a. State Y2 is defined when these lines increased in density and length to half of the member depth (Figure 5.4b). Severe yielding (Y3) was defined when the yield lines had propagated the entire member depth, and the width of the yield lines was approximately one member depth, as shown in Figure 5.4c. In this condition, a large band of whitewash had flaked off. Framing element yielding was observed on both sides of the beam or column flanges in the connection regions and the beam/column webs within the connection region.

5.2.2 Buckling (B)

Global brace buckling also occurred, and is illustrated in Figure 5.5. Figure 5.5a shows initial visible brace buckling (B1). With increased drift levels, the brace OOP displacement progressed to larger than the brace depth (B2), shown in Figure 5.5b. After the brace exceeded two times the brace depth it was in B3, shown in Figure 5.5c.

A plastic hinge occurs in the brace when it has fully yielded due to a combination of axial load and P-δ moment. Ultimately, plastic deformation may lead to a concentration of damage near midspan, and local deformation occurs in all four walls of the HSS brace sections. At this severe deformation (B3), there is cupping in the top and bottom brace walls and bulging in the side walls, shown in Figure 5.5d. Severe strain concentrations develop in the corners of these brace sections and brace tearing (BT) initiates from the corners of the brace during tension cycles, as seen in Figure 5.5e. The tearing leads to brace fracture (BF) when it penetrates through the depth of the brace as shown in Figure 5.5f.

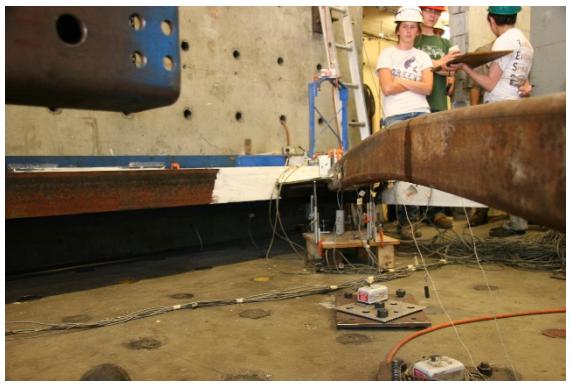
a.

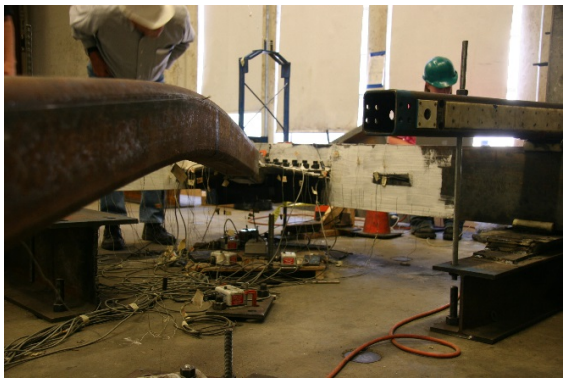
b.

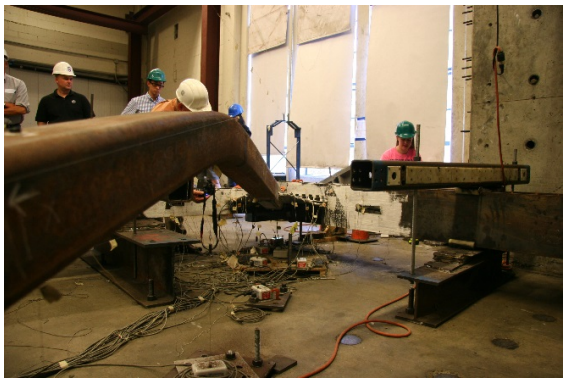
c.


d.

e. 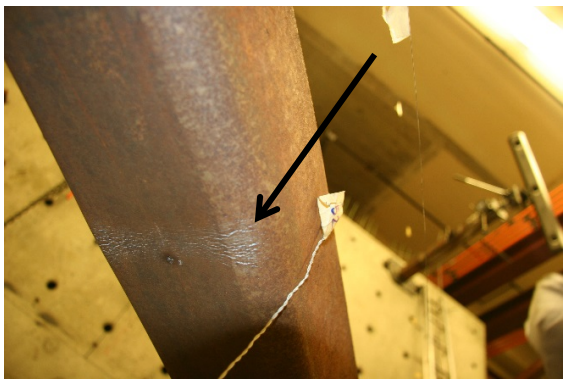 f. 

Figure 5.5 - Typical Brace Fracture Progression: a. B1, b. B2, c. B3, d. B3-Hinge, e. BT, f. BF

Every test resulted in local buckling of a column or beam flange near the edge of the gusset plate, after significant flange yielding as discussed in Table 5.2. In Figure 5.6a, the beam flange had visible local buckling (B1), where the amplitude of the buckle was less than the element thickness. In Figure 5.6b, with increased drift levels, the flange continued to buckle to more than the thickness of the beam flange (B2). For severe damage (B3), the flange buckle had an amplitude more than twice the flange thickness, as shown in Figure 5.6c.

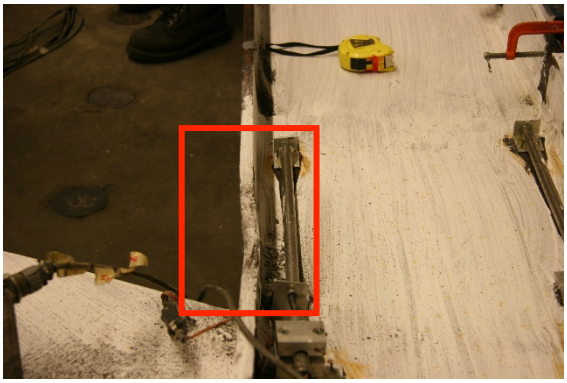

a. Initial Buckling, B1

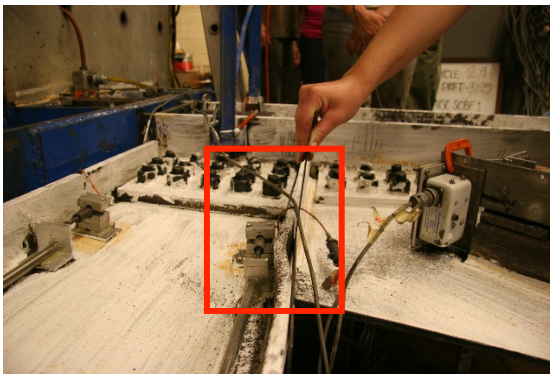

b. Moderate Buckling, B2

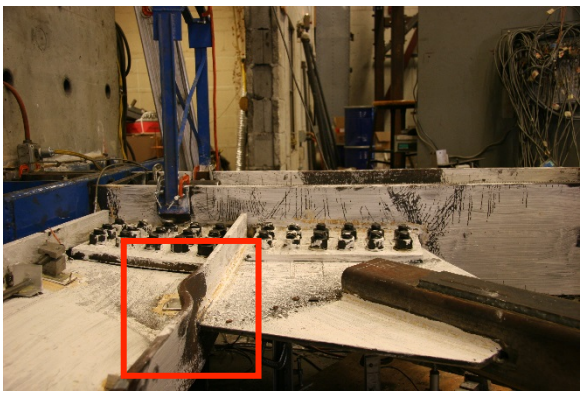

c. Severe Buckling, B3 (Post-fracture cycles)

Figure 5.6 - Typical Local Buckling Progression in Beam (from Specimen SHSS-B1)

5.2.3 Weld Tearing and Fracture (W)

Weld tearing was prominent in all specimens, but the extent of the tearing varied. With stable crack growth, weld tearing is tolerable and can accommodate increased drift levels without strength degradation. Weld fracture implies the weld has torn along its entire length and no longer joins the two welded parts. The resistance to unstable weld fracture is related to the CVN toughness of the weld metal. The E71T-11 weld metal used for the specimens is not demand critical weld material and has limited resistance to fracture.

Progression of weld tearing is defined by the performance states from Table 5.2. The photo series in Figure 5.7 shows the development of weld tearing at the beam to gusset plate connection (WB), but weld tearing at the gusset plate to column shear tab (WC) also occurred and followed a similar progression through performance states. Initial weld cracking (WB1), shown in Figure 5.7a, is designated when the crack was visible and had propagated less than 5% of the total weld length. Once it grown to between 5% and 25% it was considered moderate weld cracking (WB2), as seen in Figure 5.7b. Cracks longer than 50% of the total connection length were considered severe weld cracking (WB3), shown in Figure 5.7c. Figure 5.7d shows the connection after the beam to gusset plate weld fractured (WBF).

a. Initial Weld Tearing, WB1

b. Moderate Weld Tearing , WB2

c. Severe Weld Tearing, WB3

b. Weld Fracture, WBF

Figure 5.7 - Progression of Weld Fracture (from Specimen SHSS-B2)

5.2.4 Bolt Damage States (Bo)

Bolted connection yield mechanisms and failure modes were described in Chapter 2. Bolt hole elongation (BoE) and to a much lesser extent, bolt shear deformation can add drift capacity to the system. However, bolt fracture (BoF) is a clear, undesirable failure mode that should be avoided. The bolt performance states presented in Table 5.2 are illustrated in Figure 5.8. Additionally, at the end of each subsection of Section 5.3, diagrams for each bolted connection of the frame illustrate the bolt damage in the bolts, the beam web and/or gusset plate, and the shear tabs. Bolt fracture is dictated with an "X", elongation/deformation between 1/16 in. and 1/4 in. is hatched with diagonal lines, and bolt elongation/deformation greater than 1/4 in. is fully shaded. For

system orientation, Figure 5.1 has previously identified the four corners of the frame. Figure 5.9 shows an example of these bolt damage diagrams.

a. Bolt Hole Elongation, BoE (shown in GP)

b. Bolt Deformation, BD

c. Bolt Fracture, BoF

Figure 5.8 - Bolt Performance State (from Specimen NHSS-B3)

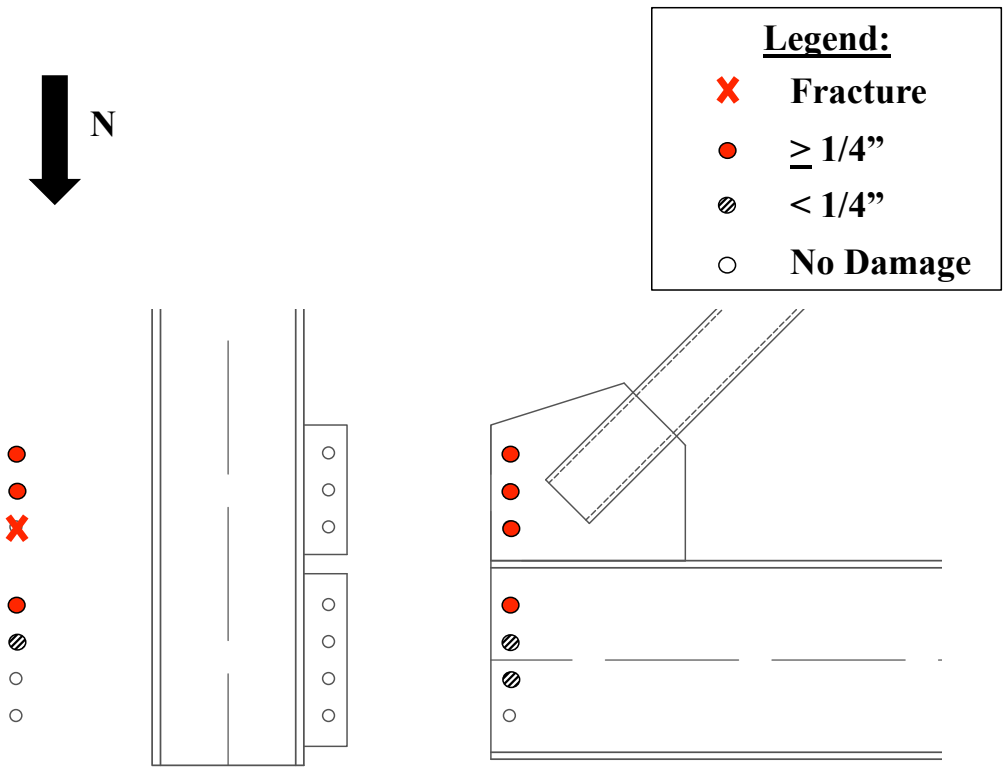

Figure 5.9 - Bolt Damage from Specimen NHSS-B3, Left to Right: Bolt Damage, Shear Tab Damage, Beam Web & Gusset Plate Damage

5.3 Bolted NCBF Test Observations

This section reports the test observations from the three bolted NCBF specimens NHSS-B1, NHSS-B2, and NHSS-B3. The calculations behind the designs were summarized in Chapter 3. These connections were all designed to be deficient in a number of limit states to model older pre-1988 connections. The demand to capacity values developed from AISC equations (shown in Chapter 3) without using resistance factors are shown in Table 5.4. Also, shown in Table 5.5, is a comparison between the DCR values calculated using the Balanced Design Procedure (BDP) without the beta factors and the AISC equations without resistance factors.

Table 5.4 - Demand to Capacity Ratios with AISC Equations

Limit State	NHSS-B1	NHSS-B2	NHSS-B3
Brace Net Section	**1.2**	**1.2**	**1.1**
Brace Block Shear	**1.1**	**1.3**	**1.1**
Gusset Plate Block Shear	0.62	0.49	0.94
Whitmore Gusset Plate Yielding	0.75	0.61	**1.1**
Whitmore Gusset Plate Fracture	0.58	0.46	0.86
Gusset Plate Buckling	0.38	0.4	0.58
Brace to Gusset Plate Weld Fracture	0.83	0.71	0.83
Brace to Gusset Plate Base Metal Fracture	0.83	**1.1**	0.83
Gusset Plate Shear Yielding	0.96	0.6	**1.1**
Beam to Gusset Plate Weld Fracture	0.64	0.56	0.66
Column to Gusset Plate Bolt Shear	**1.90**	**1.63**	**1.92**
Column to Beam Bolt Shear	**1.56**	**1.30**	**1.55**
Column to Gusset Plate Bolt Bearing	0.98	0.84	**1.48**
Column to Beam Bolt Bearing	**1.73**	**1.45**	**1.73**

Table 5.5 – Comparison of BDP and AISC DCR Values for Beam to Gusset Plate Weld

Limit State	NHSS-B1	NHSS-B2	NHSS-B3
AISC	0.64	0.56	0.66
BDP	1.1	1.5	1.4

5.3.1 NHSS-B1

5.3.1.1 Specimen Overview

Specimen NHSS-B1 was tested on October 2nd, 2013, and was the first in a series of bolted NCBF tests that were designed to model a common bolted connection from the building survey described in Chapter 3. NHSS-B1 was designed to be deficient in brace net section rupture, brace block shear, bolt bearing, and bolt shear, and the design is illustrated in Figure 5.10. The BDP recommends that welds be designed to develop the tensile yield capacity of the plate, and this method results in larger DCR values as seen in Table 5.5. The most severe limit state for this connection is bolt shear. In addition to the deficiencies in the limit states listed above, the gusset plate was not designed to have a buckling rotation clearance as required by SCBF criteria. Although the brace was slotted for the welded connection to the gusset plate, net section reinforcing plates were not used, as required by the current Seismic Provisions. The E71T-11 weld material used does not meet demand critical requirements.

Key components of the frame included a single (7) bolt, 3/4 in. thick shear tab connecting the column to both the beam (with 4 bolts) and the 3/4 in. thick gusset plate (with 3 bolts); all bolts were A325, 1 in. diameter bolts with F436 structural washers. The shear tabs were connected to the column flanges via complete joint penetration welds (CJP). The gusset plates were connected to the beam flanges with 7/16 in. fillet welds. The brace was also connected to the gusset plates with 7/16 in. fillet welds. One difference between NHSS-B1 and the reference specimens (shown in Chapter 3) is the brace type. NHSS-B1 used a seismically compact brace because NCBF1 (Sloat, 2014) showed that using a non-seismically compact brace fails at small drift levels and does not develop the capacity of the connection.

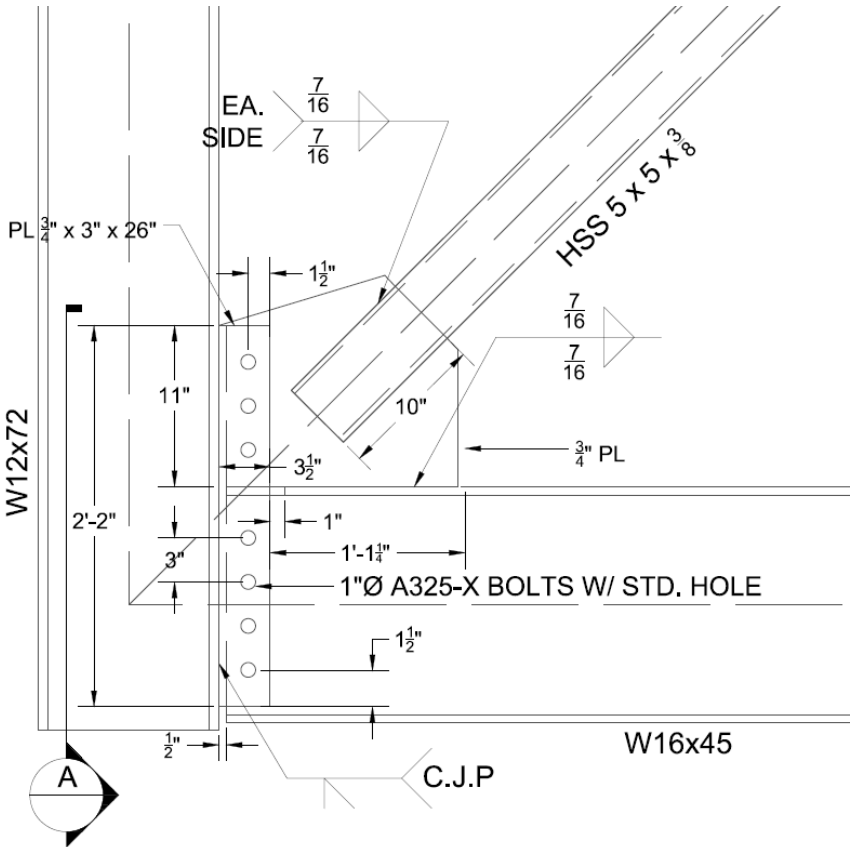

Figure 5.10 - NHSS-B1 Connection Drawing

NHSS-B1 had a surprising performance – it was able to sustain a maximum applied force with the brace in tension of 362 kip and -171 kip when the brace was in compression. The maximum drift levels achieved were 1.9% in tension and -3.0% in compression for a total drift range of 4.9% prior to brace fracture. The specimen's hysteretic response is shown in Figure 5.11. The system experienced brace fracture, the failure mode typical of SCBFs. Table 5.6 through Table 5.8 show the progression of performance states at each cycle of NHSS-B1. They present information on each component of the system and it's yielding, buckling, or failure modes throughout the experiment.

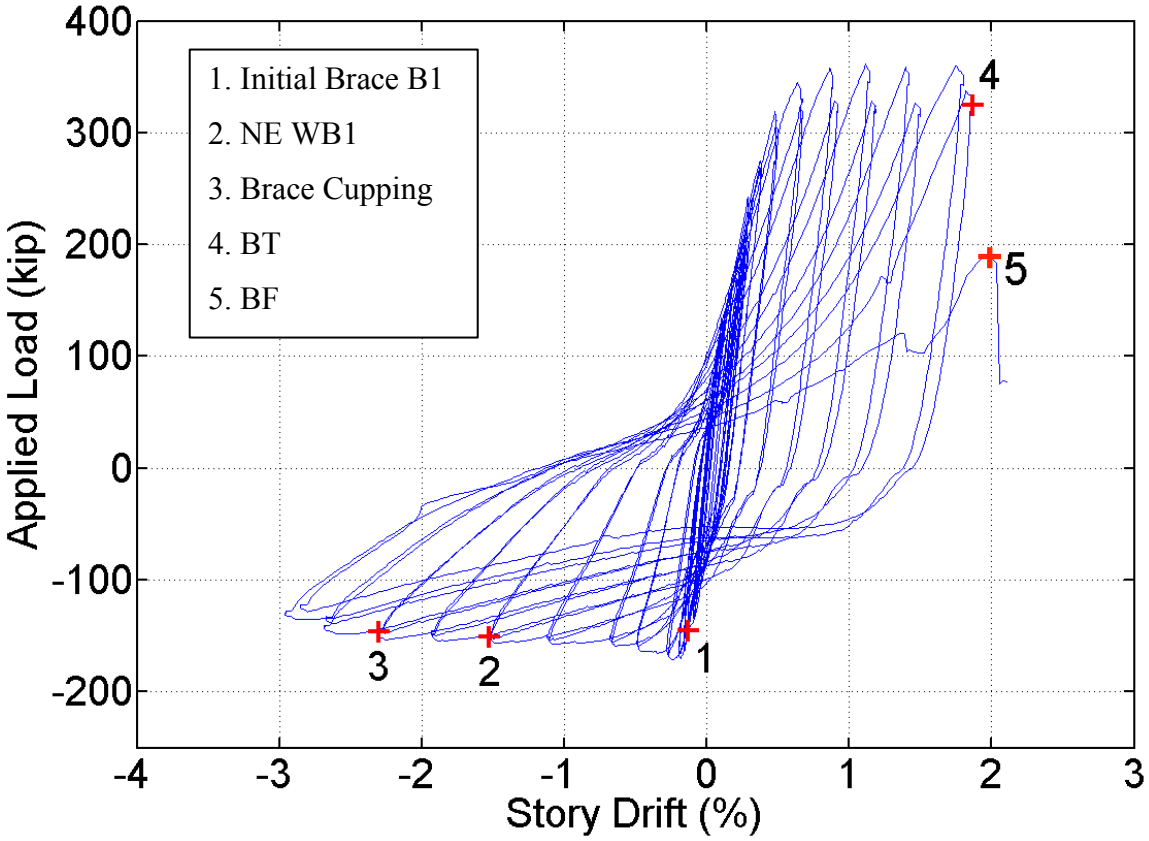

Figure 5.11 - Specimen NHSS-B1 Applied Story Shear vs. Story Drift Hysteretic Behavior

Table 5.6 - Progression of Damage in NE Corner

CYCLE	True Tension Drift (%)	True Compression Drift (%)	Brace	NE CORNER			
				Gusset Plate	Beam/Gusset to Column Shear Tab	N Beam	E Column
1	0.01	-0.03					
2	0.01	-0.04					
3	0.04	-0.07					
4	0.04	-0.07					
5	0.08	-0.08					
6	0.07	-0.08					
7	0.11	-0.09					
8	0.12	-0.09					
9	0.17	-0.13					
10	0.17	-0.13					
11	0.21	-0.16					
12	0.23	-0.16		Y1			
13	0.27	-0.20	B1				
14	0.27	-0.20					
15	0.30	-0.27					Y1 - W flange
16	0.28	-0.28					
17	0.32	-0.49					
18	0.28	-0.50					
19	0.38	-0.67	B2				
20	0.37	-0.68					B1 - flange
21	0.49	-1.10					
22	0.50	-1.12					
23	0.66	-1.53	B3	WB1			
24	0.67	-1.53					
25	0.87	-1.92					
26	0.92	-1.94					
27	1.10	-2.29	B3-hinge				
28	1.16	-2.30					Y2- W flange
29	1.42	-2.68		Y2, WB2			
30	1.48	-2.67					
31	1.80	-2.94					
32	1.86	-2.83	BT				
33	2.21		BF - END				
34							
35							
36							
37							
38							

Table 5.7 - Progression of Damage in SW Corner

CYCLE	True Tension Drift (%)	True Compression Drift (%)	Brace	SW CORNER				
				Gusset Plate	Gusset Plate to Column Shear Tab	Beam to Column Shear Tab	S Beam	W Column
1	0.01	-0.03						
2	0.01	-0.04						
3	0.04	-0.07						
4	0.04	-0.07						
5	0.08	-0.08						
6	0.07	-0.08						
7	0.11	-0.09						
8	0.12	-0.09						
9	0.17	-0.13						
10	0.17	-0.13						
11	0.21	-0.16						
12	0.23	-0.16						
13	0.27	-0.20	B1	Y1				
14	0.27	-0.20						
15	0.30	-0.27						
16	0.28	-0.28						
17	0.32	-0.49						
18	0.28	-0.50						
19	0.38	-0.67	B2		Y1			
20	0.37	-0.68						B1 - E flange, Y1 - W flange
21	0.49	-1.10						Initial Uplift
22	0.50	-1.12					Y1	
23	0.66	-1.53	B3					
24	0.67	-1.53						
25	0.87	-1.92						
26	0.92	-1.94						
27	1.10	-2.29	B3-hinge	WB1				B2 - E flange, Y2- W flange
28	1.16	-2.30						
29	1.42	-2.68						
30	1.48	-2.67			WC1			
31	1.80	-2.94						
32	1.86	-2.83	BT					B1 - W flange, Y3 - W flange
33	2.21		BF - END					
34								
35								
36								
37								
38								

Table 5.8 - Progression of Damage in Brace, NW Corner, and SE Corner

CYCLE	True Tension Drift (%)	True Compression Drift (%)	Brace	NW CORNER			SE CORNER		
				N Beam	W Column	Beam to Column Shear Tab	E Column	Beam to Column Shear Tab	S Beam
1	0.01	-0.03							
2	0.01	-0.04							
3	0.04	-0.07							
4	0.04	-0.07							
5	0.08	-0.08							
6	0.07	-0.08							
7	0.11	-0.09							
8	0.12	-0.09							
9	0.17	-0.13							
10	0.17	-0.13							
11	0.21	-0.16							
12	0.23	-0.16					Initial Uplift		
13	0.27	-0.20	B1						
14	0.27	-0.20							
15	0.30	-0.27							
16	0.28	-0.28							
17	0.32	-0.49							
18	0.28	-0.50							
19	0.38	-0.67	B2						
20	0.37	-0.68							
21	0.49	-1.10							
22	0.50	-1.12							
23	0.66	-1.53	B3						
24	0.67	-1.53							
25	0.87	-1.92				Y1			
26	0.92	-1.94							
27	1.10	-2.29	B3-hinge				Y1 - E flange		
28	1.16	-2.30							
29	1.42	-2.68			B1 - flange, Y1 - W flange				
30	1.48	-2.67		B1 - flange				Y1	
31	1.80	-2.94							
32	1.86	-2.83	BT						
33	2.21		BF - END						
34									
35									
36									
37									
38									

5.3.1.2 Moderate Damage States (DS1 & DS2)

Initial brace buckling (B1) was observed at -0.2% drift. There was slight initial visible uplift of the east flange of the east column at this drift. Uplift of a single flange at the column bases continued throughout the remainder of the test and grew in magnitude. At this same drift level, initial yielding on the NE gusset plate (Y1) and whitewash flaking (Y1) on the NE beam to column and gusset plate to column shared shear tab was observed, as shown in Figure 5.12. The SW gusset plate also began yielding from the OOP brace rotation demands around -0.2% drift at the brace end.

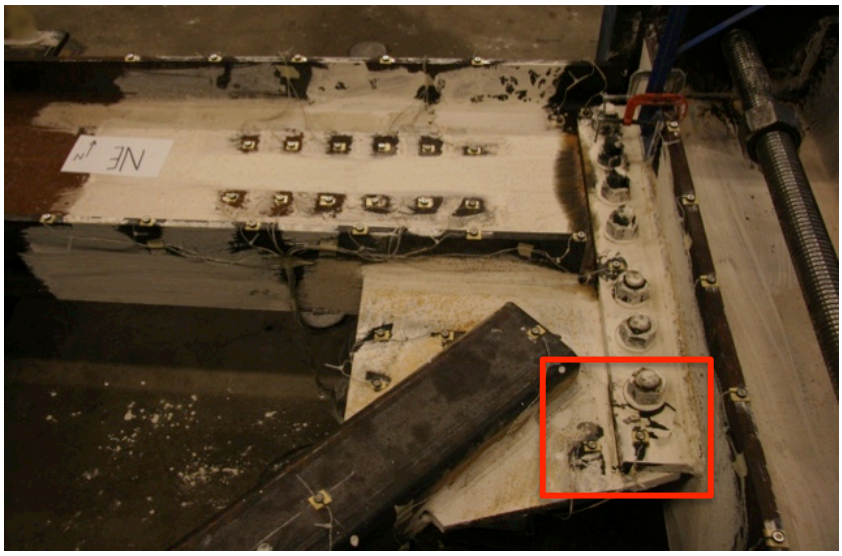

Figure 5.12 - Yielding in NE Gusset Plate and Shear Tab at +0.2% Drift

As the cycles continued, the NE corner sustained more yielding and damage than the SW corner. In the NE corner at +0.4% drift, local buckling (B1) of the west flange of the east column at the south end of the gusset plate to shear tab connection occurred, as shown in Figure 5.13. At this same drift level and location in the SW corner (west column, east flange), there was also local buckling of the column flange (B1). After reaching -0.7% drift, the brace had buckled upwards OOP at the midspan 6.1 in. (B2).

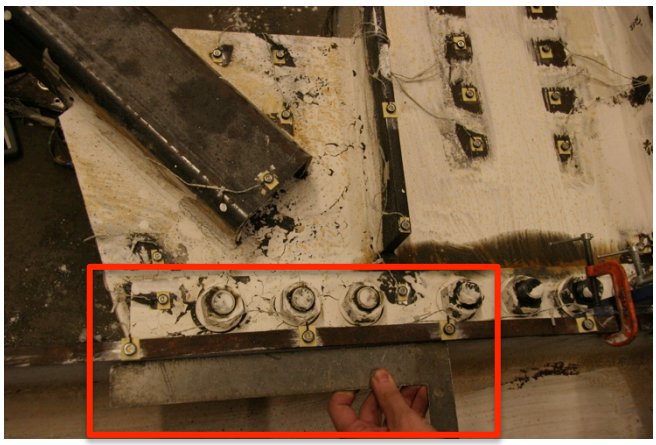

Figure 5.13 - NE Corner Local Flange Buckling (B1) at -1.0% Drift

At -0.7% drift, along the gusset plate to beam connection in the SW corner, the north flange of the south beam was rotating – the top of the flange rotated north and the bottom of the flange rotated south, shown in Figure 5.14 by the gap between the level and the beam flange. This rotation was noted in previous SCBF tests and attributed to the downward force from the brace. For this specimen, the shared shear tab did not provide much stiffness or resistance against the OOP rotational demand, and this caused the whole corners to be affected and rotate.

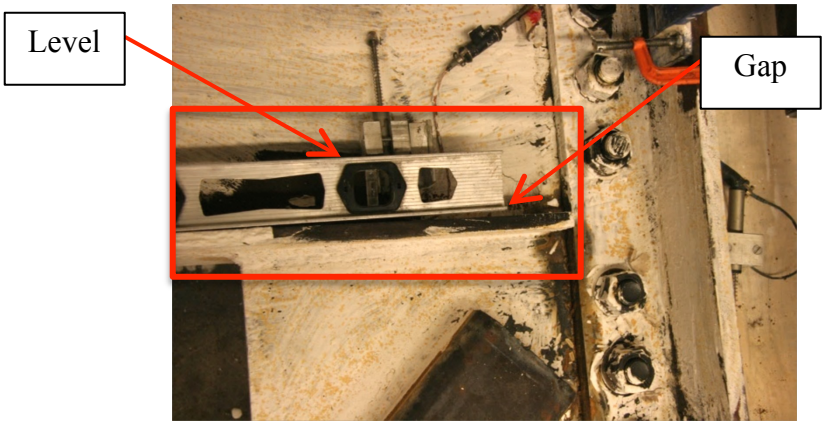

Figure 5.14 - Rotation of North Flange of South Beam in SW Corner

The framing elements sustained increased yielding with increased drift levels. On the west flange of the west column, there was increased widespread yielding (Y2) at the south base of the column at -1.1% drift. As the brace buckled to larger OOP displacements it placed more rotational demand on the connections. The rotation of the south beam in the SW corner increased, and the east flange on the west column was visibly rotating as well - the top of the

flange was twisting east while the bottom of the flange was twisting west as shown in Figure 5.15. The flexibility in the shared shear tab allowed all components within the corner to rotate.

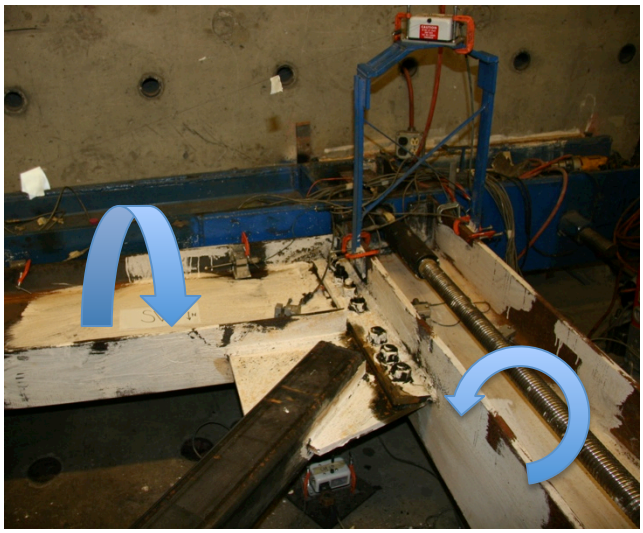

Figure 5.15 - Illustration of the SW Corner Beam and Column Rotations with Brace in Compression

At +0.5% drift there was a 1/8 in. vertical gap between the gusset plate and shear tab in the SW corner of NE connection, shown in Figure 5.16. This gap indicated that the shear tab was bent upward, sustained inelastic deformation, and did not straighten back out in tension. The gap was only located at the free end of the shear tab, since bolt clamping forces held the plates together at other locations. At +0.7% drift, yield lines (Y1) began to form in the SW gusset plate that ran 45° in each direction from the end walls of the brace.

Figure 5.16 - Gap Between Shear Plate and Gusset Plate in NE Corner

At -1.5% drift, a 1/8 in. weld crack initiated on the bottom of the NE gusset plate to beam weld (WB1). At the next compressive cycle, -1.5% drift, this weld crack propagated to 3/4 in. in length (WB1). At this drift level, there was rotation of the south flange of the north beam in the NE corner, similar to the behavior observed in the SW corner. The top of the flange was rotating south while the bottom of the flange was rotating north. At this compression cycle the potentiometer measuring the brace midspan OOP displacement value broke. The last measured displacement was 10.3 in. (B2) at -1.5% drift, but the Optotrak sensor continued to measure this OOP displacement.

5.3.1.3 Severe Damage States (DS3 & DS4)

The rotations in the SW corner became more pronounced at +1.1% drift with a 1/2 in. measured displacement of the east flange in the west column, shown in Figure 5.17. At -2.2% drift, the weld crack in between the beam and the NE gusset plate continued to grow to 3.25 in. (WB1), but was still only on the bottom side. An approximately 1/8 in. long weld crack initiated (WB1) in the SW beam to gusset plate (east propagating west) at this drift level. The brace walls experienced visible local deformation at the brace plastic hinge location at the midspan.

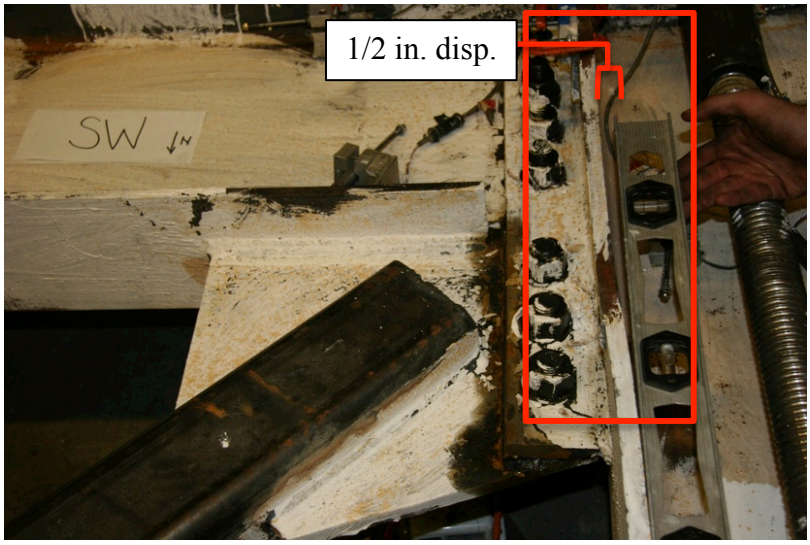

Figure 5.17 - Rotation of the East Flange of the West Column at +1.1% Drift

The NE shear tab remained appreciably bent upward in the SW corner of the plate at +1.2% drift. There was a 4 in. long weld crack (WB2) in the NE corner between the beam to gusset plate that

propagated through to the top fillet weld at -2.3% drift. More local buckling of the framing elements occurred at -2.7% drift on the west flange of the west column at the north end (against load beam).

At -2.7% drift, the severity of the hinge at midspan of the brace increased (B3-cupping) with the bottom wall cupping inward as shown in Figure 5.18. A 1 in. weld crack on the underside of the SW beam to gusset plate developed (WB1). In the SW corner, a 3 in. long weld crack also developed in the CJP weld (WC1) joining the shear plate to column beginning at the north end of the connection and propagated south. In compression at -2.9%, the weld crack in the NE beam to gusset plate connection had grown to 4.25 in. on top and 6.5 in. on the bottom fillet weld (WB2).

Figure 5.18 - Brace Local Deformation (B3-Cupping) at Midspan at -2.7% Drift

The bottom corners of the brace began to tear at midspan at +1.9% drift (shown in Figure 5.19), while framing element rotations increased in both corners. The west column in the SW corner sustained significant yielding over the full depth of the column (Y3) and the west flange of the west column in the SW corner locally buckled (B1) at -2.8% drift, both shown in Figure 5.20. Additionally, the CJP weld crack in the SW corner grew to 5 in. in length but only 3 in. cracked fully through the thickness (WC1). At this compression drift level, there was severe increased local buckling of the brace (B3-cupping) at midspan. At +2.2% drift, the brace fractured (BF), shown in Figure 5.21.

Figure 5.19 - Brace Tearing (BT) at Midspan at +1.9% Drift

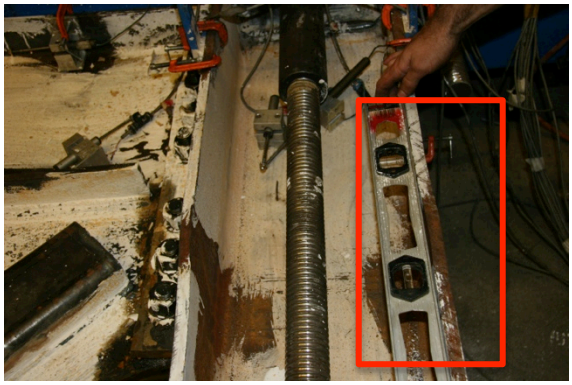

a. Local Buckling (B1) on West Flange

b. Severe Yielding (Y3) on West Flange

Figure 5.20 - Damage in West Column in SW Corner at -2.8% Drift

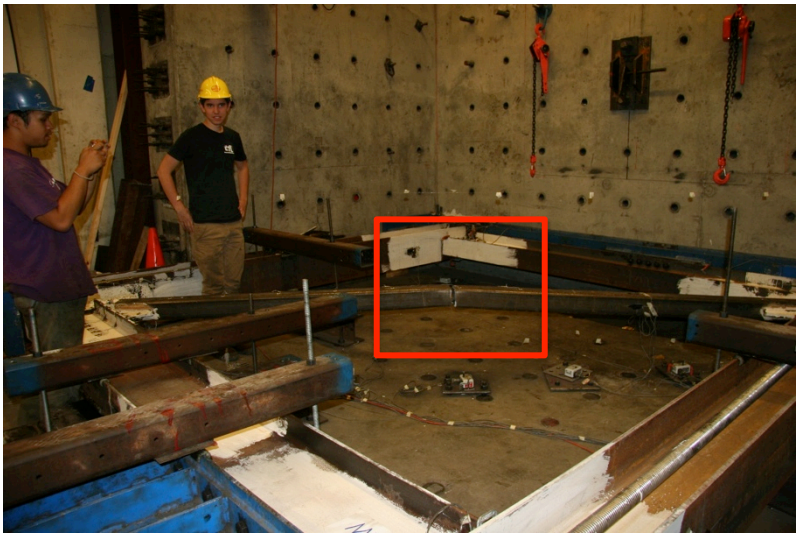

Figure 5.21 - Brace Fracture (BF) at +2.2% Drift

5.3.1.4 Specimen Summary of Results

The brace achieved a 17.5 in. OOP displacement at midspan before failing through brace fracture. The framing elements sustained damage and the specimen's unexpected ductility was likely due to local deformation in the columns, weld fracture, bolt hole elongation, and bolt ductility. The OOP rotation of the brace was not localized to the gusset plate bending alone – the beam and column flanges attached to the gusset plate also were rotating. There was weld tearing in the south gusset plate to column shear tab weld, in all gusset plate to brace splice welds (minimal <1/4 in.), and in the north beam to gusset plate weld. The damage to the CJP weld was extensive and moved between the heat affected zone of the plate, the weld metal, and finally fully into the plate (latter in post fracture cycles). The gusset plate to brace welds were small and did not propagate a notable amount. The damage to the beam to gusset plate weld in the NE corner is described below.

At the NE beam to gusset plate connection, weld crack initiation was observed at -1.5% drift and increased with increased story drift (see Figure 5.22). At the completion of the -2.7% drift compressive cycle, the weld crack was 5.125 in. long on the bottom (Figure 5.22c) and 2.25 in. long on the top (Figure 5.22d). The weld crack was 6.5 in. long on the bottom (Figure 5.22e) and 4.25 in. (Figure 5.22f) on the top at brace fracture. The weld crack did not fracture despite the use of welds with low CVN toughness.

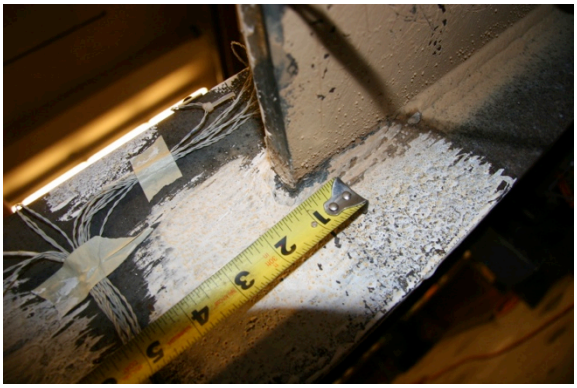

a. 3/4 in. weld crack (WB1) at -1.5% drift

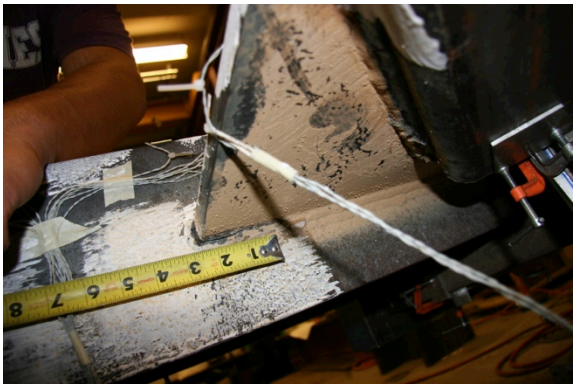

b. 2.125 in. weld crack at -1.9% drift

c. 5.125 in. weld crack (bottom, WB2) at -2.7% drift

d. 2.25 in. weld crack (top) at -2.7% drift

e. 6.5 in. weld crack (bottom) at -2.9% drift

f. 4.25 in. weld crack (top) at -2.9% drift

Figure 5.22 - Progression of Weld Cracking in NE Beam to Gusset Plate Connection

Post-fracture cycles were completed after brace fracture on the frame to quantify the residual system strength and stiffness. Continued rotation was observed in the connections. The post-fracture cycles were stopped because of the 10.5 in. crack in the CJP weld at the SW shear plate to column connection. The crack at the north end opened to 3/4 in. Additionally, the south beam developed a severe hinge in the SW corner adjacent to the gusset plate connection. Also during post-fracture cycles a bolt in the SE corner fractured. During these cycles, the frame was able to sustain story shears of 100 kip and -100 kip.

After post-fracture cycles, the frame was disassembled and the bolts and bolt holes were studied with findings displayed in Figure 5.23 through Figure 5.26. A few bolts in the gusset plates had visible bearing deformation (BD) and well-defined shear planes as shown in Figure 5.24a. In the NE and SW connections, there was significant bolt hole elongation (BoE) (most notably in the

beam web as it was the thinnest component). The largest elongation seen was 5/16 in. shown in Figure 5.24c. There was no tearing, bolt pull out, or block shear. One bolt fractured (BoF) in the SE beam to column connection during the post-fracture cycles, shown in the illustration in Figure 5.23. A detailed photo summary of bolt damage can be found in the Appendix.

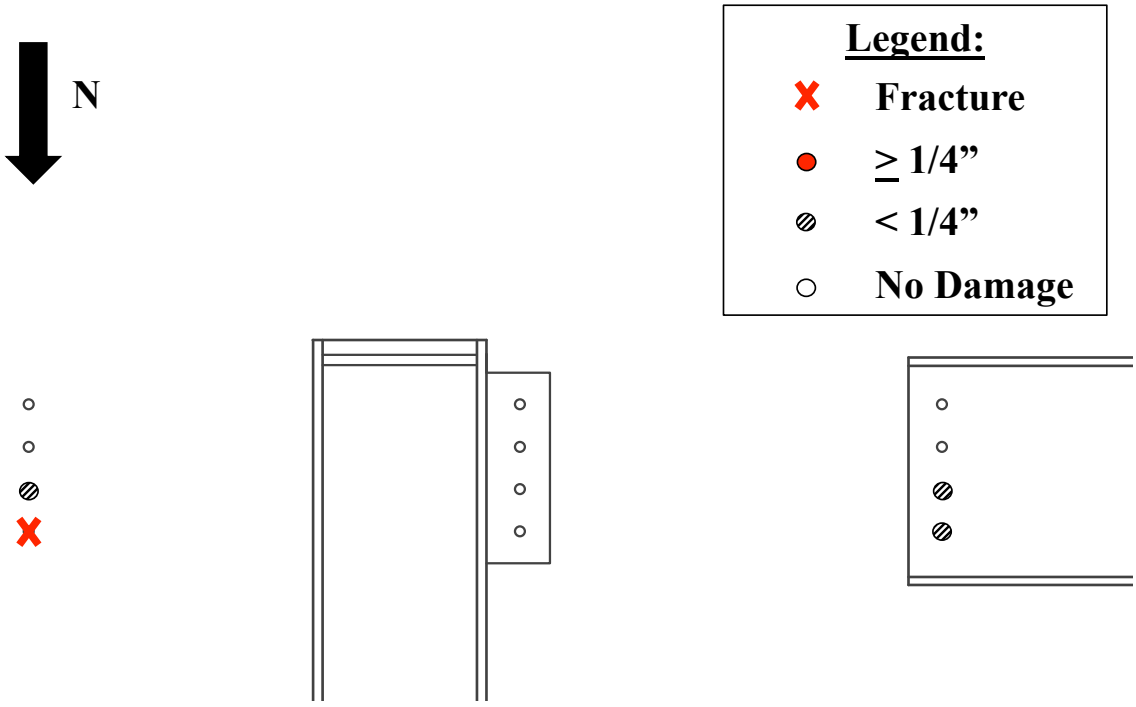

Figure 5.23 - SE Corner Bolt Damage

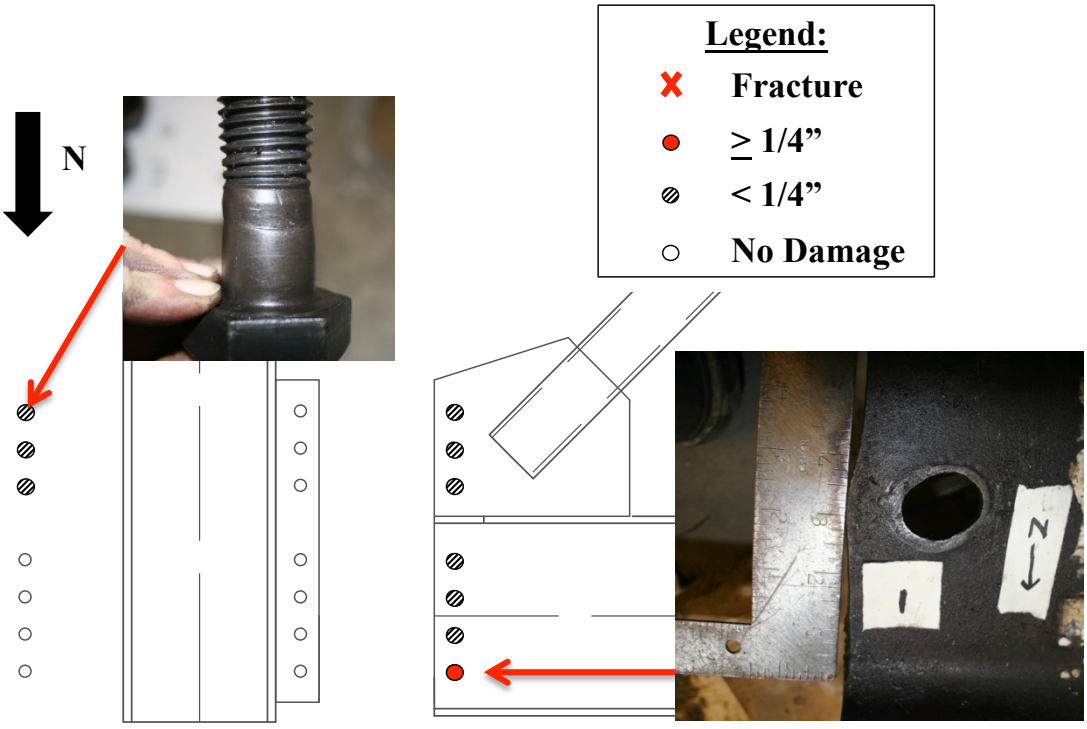

a. Bolts b. Shear Tab c. Beam Web/Gusset Plate

Figure 5.24 - NE Corner Bolt Damage

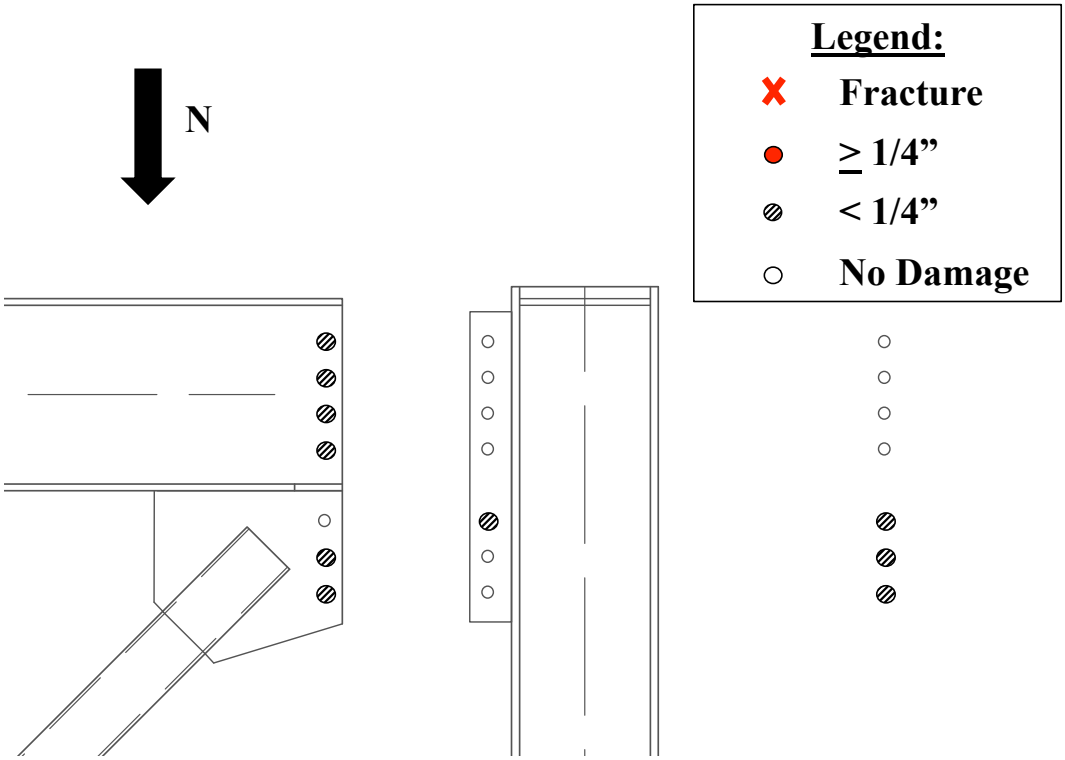

a. Beam Web/Gusset Plate b. Shear Tab c. Bolts

Figure 5.25 - SW Corner Bolt Damage

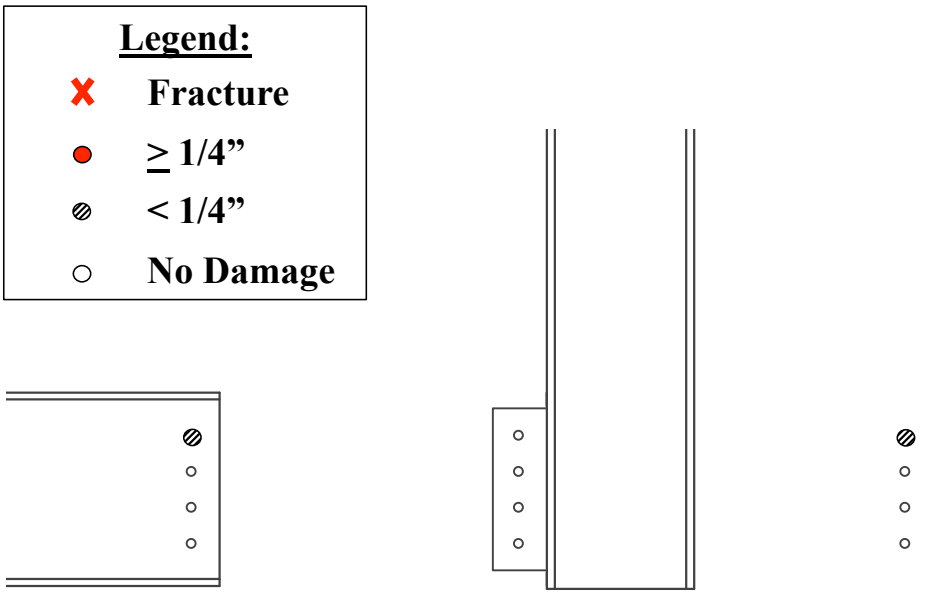

a. Beam Web b. Shear Tab c. Bolts

Figure 5.26 - NW Corner Bolt Damage

5.3.2 NHSS-B2

5.3.2.1 Specimen Overview

Specimen NHSS-B2 was tested on November 18th, 2013. It was the second in a series of bolted NCBF tests, and modified NHSS-B1 to have a split shear tab rather than a shared beam to column and gusset plate to column shear tab. The goal of this test was to examine the effects of this change in connection configuration. Additionally, NHSS-B2 used an HSS6x6x1/4 (non-compact) brace to explore whether the brace would resist local damage at the plastic hinge long enough to reach the full capacity of the connection.

As seen in Table 5.4, NHSS-B2 was designed to be deficient in brace net section rupture, brace block shear, brace to gusset plate base metal fracture, bolt shear, column to beam bolt bearing, and brace local slenderness. The BDP predicts a DCR value of 1.5 for the weld joining the gusset plate to the beam, since the BDP recommends that welds be sized to the tensile strength of the gusset plate. The most severe limit states for this connection are the beam to gusset plate weld fracture according to the BDP, and bolt shear for AISC. In addition to the deficiencies in the limit states listed above, the gusset plate was not designed to have linear (AISC) or elliptical (BDP) clearance. Although the brace was slotted for the welded connection to the gusset plate, no net section reinforcing plates were included as required by the current Seismic Provisions. The welds were E71T-11 and did not meet demand critical requirements.

Key components of the frame included (2) 3/4 in. thick bolted shear tabs – one to connect the column to the beam (with 4 bolts) and the other to connect the 3/4 in. thick gusset plate (with 3 bolts) to the column; all bolts were A325, 1 in. diameter bolts with F436 structural washers. The shear plates were connected to the column flanges via CJP welds. A drawing of the connection is shown in Figure 5.27. The gusset plate and shear plate width and thickness, and number and size of bolts were identical to NHSS-B1.

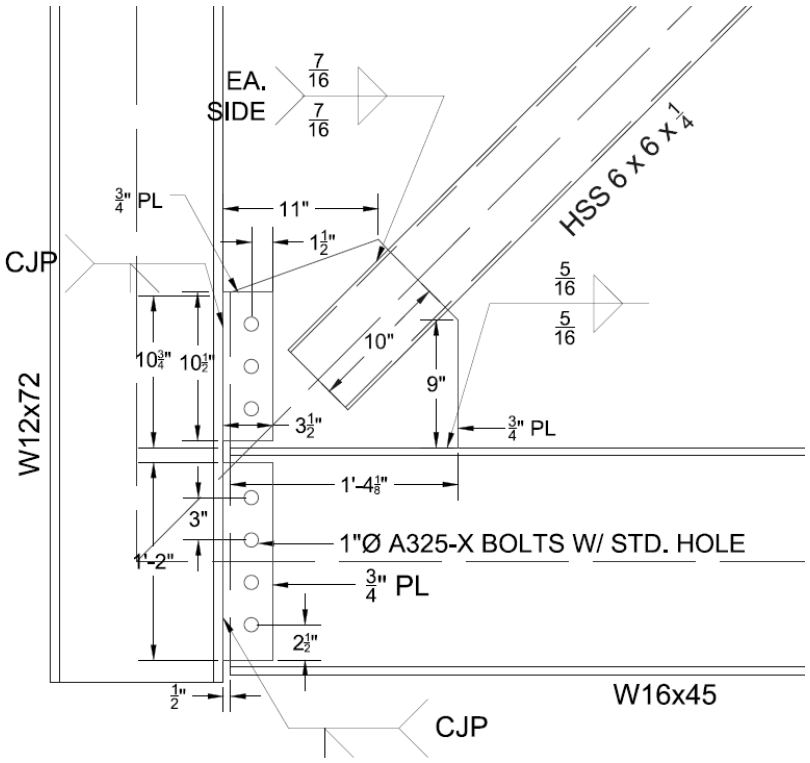

Figure 5.27 - Specimen NHSS-B2 Connection Drawing

The non-compact brace of NHSS-B2 was able to fracture the NE gusset plate connection. NHSS-B2 reached a maximum applied force of 292.9 kip, and -164.4 kip when the brace was in tension and compression, respectively. The maximum story drifts were 0.69% in tension and -1.1% in compression for a total drift range of 1.79% prior to connection failure. The specimen's hysteretic behavior is found in Figure 5.28. The frame exhibited a brittle and undesirable failure mode of bolt fracture (BoF) and gusset plate to beam weld fracture (WBF) for the NE gusset plate. Table 5.9 though Table 5.11 show the progression of performance states at each cycle of NHSS-B2. They present information on each component of the system and its yielding, buckling, or failure modes throughout the experiment.

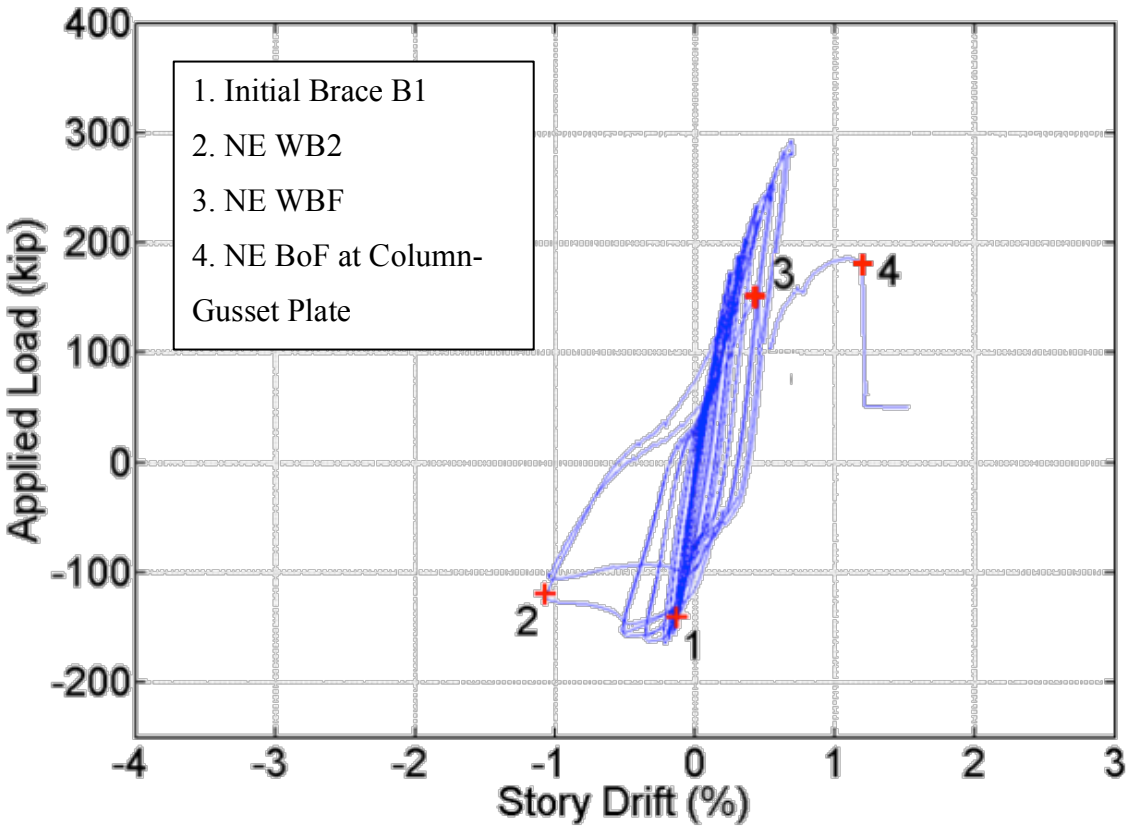

Figure 5.28 - Specimen NHSS-B2 Applied Story Shear vs. Story Drift Hysteretic Behavior

Table 5.9 - Progression of Damage in NE Corner

CYCLE	True Tension Drift (%)	True Compression Drift (%)	Brace	NE CORNER			
				Gusset Plate	Beam to Column Shear Tab	N Beam	E Column
1	0.04	-0.03					Y1 - inside W flange
2	0.04	-0.03					
3	0.08	-0.07					
4	0.08	-0.07					
5	0.13	-0.09					
6	0.13	-0.08					
7	0.17	-0.11					
8	0.17	-0.11					
9	0.21	-0.13					Y1 - outside W flange
10	0.21	-0.12					
11	0.25	-0.16					
12	0.25	-0.15					
13	0.31	-0.19	B1				
14	0.32	-0.19					
15	0.36	-0.23					
16	0.36	-0.23					
17	0.44	-0.36					
18	0.44	-0.36					
19	0.56	-0.52		Y1			
20	0.54	-0.53					
21	0.69	-1.07	B2 - hinge	WB2			Y2, B1
22	0.64	-1.05		WB3			
23				Y2, WBF, BoF - END			
24							
25							
26							
27							
28							
29							
30							
31							
32							
33							
34							
35							
36							
37							
38							

Table 5.10 - Progression of Damage in SW Corner

CYCLE	True Tension Drift (%)	True Compression Drift (%)	Brace	SW CORNER			
				Gusset Plate	Beam to Column Shear Tab	S Beam	W Column
1	0.04	-0.03					
2	0.04	-0.03					
3	0.08	-0.07					
4	0.08	-0.07					
5	0.13	-0.09					
6	0.13	-0.08					
7	0.17	-0.11		Y1			
8	0.17	-0.11					
9	0.21	-0.13					
10	0.21	-0.12					
11	0.25	-0.16					Y1
12	0.25	-0.15					
13	0.31	-0.19	B1				
14	0.32	-0.19					
15	0.36	-0.23					
16	0.36	-0.23					
17	0.44	-0.36					
18	0.44	-0.36					
19	0.56	-0.52					
20	0.54	-0.53					
21	0.69	-1.07	B2 - hinge				
22	0.64	-1.05					
23							
24							
25							
26							
27							
28							
29							
30							
31							
32							
33							
34							
35							
36							
37							
38							

Table 5.11 - Progression of Damage in NW & SE Corners

CYCLE	True Tension Drift (%)	True Compression Drift (%)	Brace	NW CORNER			SE CORNER		
				N Beam	W Column	Beam to Column Shear Tab	S Beam	E Column	Beam to Column Shear Tab
1	0.04	-0.03							
2	0.04	-0.03							
3	0.08	-0.07							
4	0.08	-0.07							
5	0.13	-0.09							
6	0.13	-0.08							
7	0.17	-0.11							
8	0.17	-0.11							
9	0.21	-0.13							
10	0.21	-0.12							
11	0.25	-0.16							
12	0.25	-0.15							
13	0.31	-0.19	B1						
14	0.32	-0.19							
15	0.36	-0.23							
16	0.36	-0.23							
17	0.44	-0.36							
18	0.44	-0.36							
19	0.56	-0.52						Initial Uplift	
20	0.54	-0.53							
21	0.69	-1.07	B2 - hinge	Y1 - at load beam					
22	0.64	-1.05							
23									
24									
25									
26									
27									
28									
29									
30									
31									
32									
33									
34									
35									
36									
37									
38									

5.3.2.2 Moderate Damage States (DS1 & DS2)

The columns sustained initial yielding (Y1) due to the compression force from column tensioning and bolt pretensioning. When the bolts were tightened, the shear plate and the gusset plate and beam web were clamped together. Because the shear plate was not initially perpendicular to the column (at a slight angle from welding process), the column flange deformed to accommodate the induced rotation. This initial yielding occurred in the NE corner, on the inside of the east column, west flange along the length of the connection, shown in Figure 5.29. Additional initial yield lines appeared in the SW corner on the west column east flange along the gusset plate to column shear tab region.

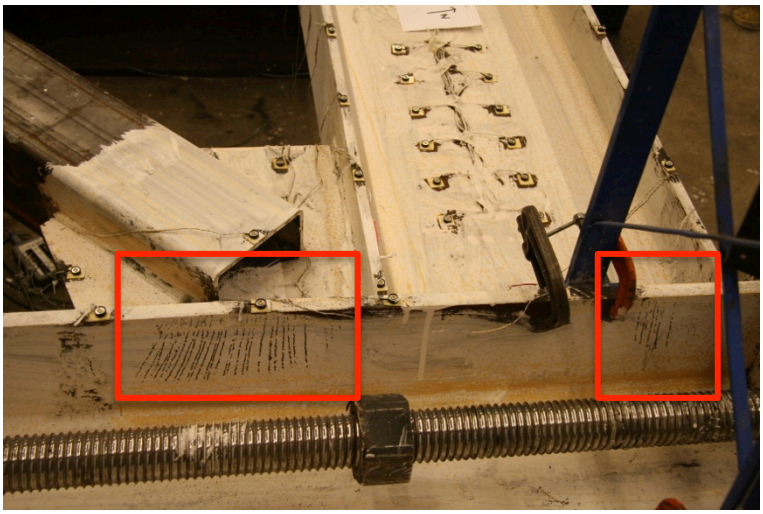

Figure 5.29 - Pre-Test Yielding in NE Corner on East Column

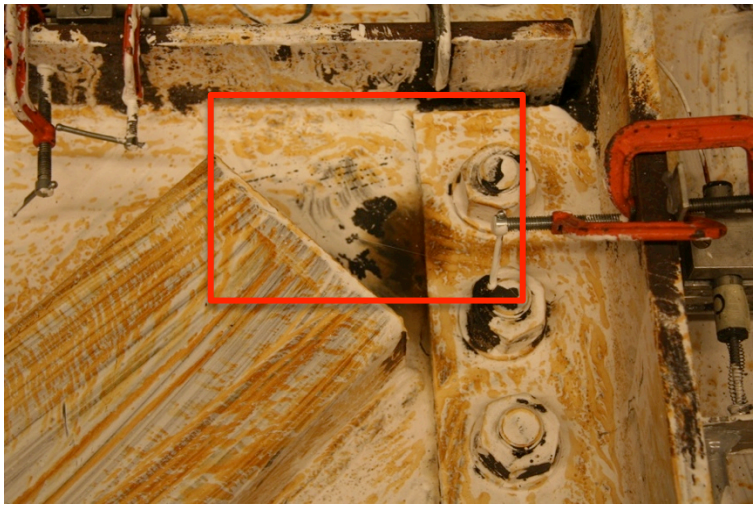

Figure 5.30 - Initial Yielding (Y1) on SW Gusset Plate

Initial yield lines (Y1) developed in the SW gusset plate at +0.2% drift as seen in Figure 5.30. Additionally, the brace buckled OOP (B1) at -0.2% drift. Minor initial weld tearing was observed at +0.4% drift in the brace to gusset plate welds at both the NE and SW corners. Yield lines in the framing elements increased at +0.6% drift on the west flange of the east column at the south end of the gusset plate to column connection. In the NE corner, yielding increased (Y1) between the walls of the brace on the gusset plate around +0.6% drift. The early weld tearing in the brace to gusset plate welds remained stable with no signs of growth over these cycles.

5.3.2.3 Severe Damage States (DS3 & DS4)

The damage sustained at -1.1% drift is shown in Figure 5.31. There was local buckling (B1) at the NE corner on the west column flange of the east column (Figure 5.31b) and increased yielding (Y2) in the same location (Figure 5.31a). During this same cycle there was visible yielding in the north flange of the north beam on both the inside and outside adjacent to the load beam. At the brace plastic hinge there was visible local deformation in the walls (B2-cupping), shown in Figure 5.31c. In the NE corner, a 6 in. weld crack (WB2) appeared suddenly in the beam to gusset plate connection through the top and bottom of the fillet welds as seen in Figure 5.31d.

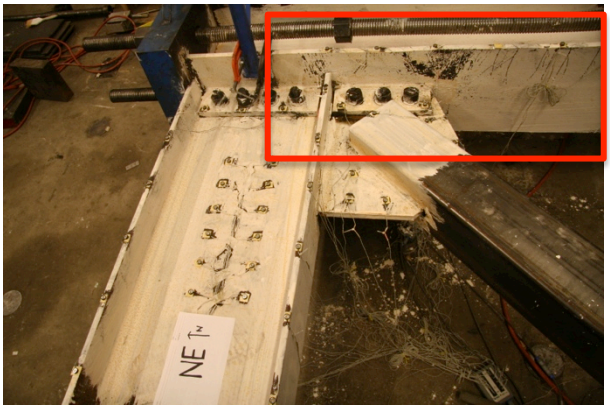

a. Yielding (Y2) on West Flange of East Column

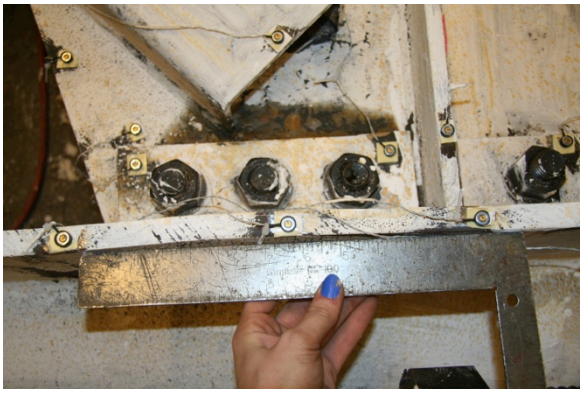

b. Local Buckling (B1) on West Flange of East Column

c. Brace Hinge (B2-Hinge)

d. 6 in. Weld Crack (WB2) at Beam to Gusset Plate

Figure 5.31 - Increased Damage in the NE Corner at -1.1% Drift

When the brace was in tension at +0.7% drift, there was slight residual local deformation in the brace hinge at midspan, but no increase in lengths of weld tearing. At the next compressive cycle at the same drift level, the hinge at brace midspan increased in severity, (B2-cupping). At -1.1% drift, the weld tear in the NE corner had grown to 12 in. long on top and 11.125 in. long on the bottom. The NE gusset plate dislocated upward OOP out of the weld seat by 1/4 in. During the following tensile cycle at a higher drift level, complete fracture of the beam to gusset plate weld in the NE connection occurred (Figure 5.32a). While investigating the weld fracture during the pause in the load cycle, initial tearing was observed on the bottom of the brace at midspan in the corners (Figure 5.32b). The tension cycle was continued, and simultaneous fracture of the 3 bolts connecting the column to gusset plate shear tab in the NE corner occurred (Figure 5.32c). The test did not reach the full tensile cycle. This full failure progression is shown in Figure 5.32.

a. Complete Fracture of Beam to Gusset Plate Weld

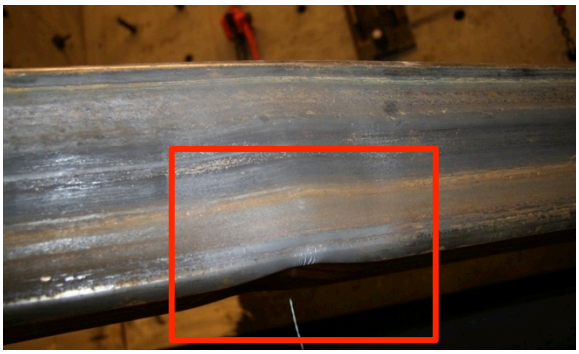

b. Brace Tearing

c. Complete Connection Failure

Figure 5.32 - NE Connection Failure in Final Tensile Cycle

5.3.2.4 Specimen Summary of Results

NCBF 1 (Sloat, 2014) used the seismically non-compact HSS7x7x1/4, and the local strain concentrations at the corners of the locally slender brace due to brace buckling resulted in early, sudden brace fracture before the connection was fully developed. NHSS-B2 also had a locally slender brace with a slightly lower b/t ratio. NHSS-B2 was only able to reach a total drift of 1.79% (0.27% higher than NCBF1) but the connection failed before the brace fractured.

This specimen saw comparatively little yielding in the framing components. The inelastic deformation was largely constrained to the brace plastic hinge. The 6 in. weld crack that propagated in the NE beam to gusset plate weld developed quickly and led to sudden weld fracture. The 3 bolts joining the gusset plate to the shear plate fractured shortly thereafter. The failure mode of this specimen was extremely brittle and swift. The connection failed on the third cycle after the weld crack was first observed in the NE beam to gusset plate weld.

Once the connection failed, a portion of the brace was cut out. Post-fracture cycles were completed on the specimen to determine the residual stiffness of the frame. During these cycles, the frame was able to sustain story shears of 70 kip and -50 kip with the brace in tension and compression respectively. After these cycles, the frame was disassembled and the bolts and their connecting members were investigated. Diagrammatic sketches of the bolt damage found in the four corners can be found in Figure 5.33 through Figure 5.37. Aside from the 3 fractured bolts in

the NE gusset plate to column shear tab connection, shown in Figure 5.34a and Figure 5.35a, there was limited bolt damage and bolt hole elongation. Maximum elongation from bearing stresses of 3/16 in. was found in the NE gusset plate to column shear tab in all holes, shown in Figure 5.34b and Figure 5.35b. There was no observed deformation at the edge of the plate from bolt bearing stresses, as seen in NHSS-B1. The beam web only had one hole with less than 1/4 in. elongation (comparable to that found in the shear tab), as shown in Figure 5.34c and Figure 5.35c. Overall, the performance of this frame did not appear greatly influenced by bolt deformation and bolt hole elongation.

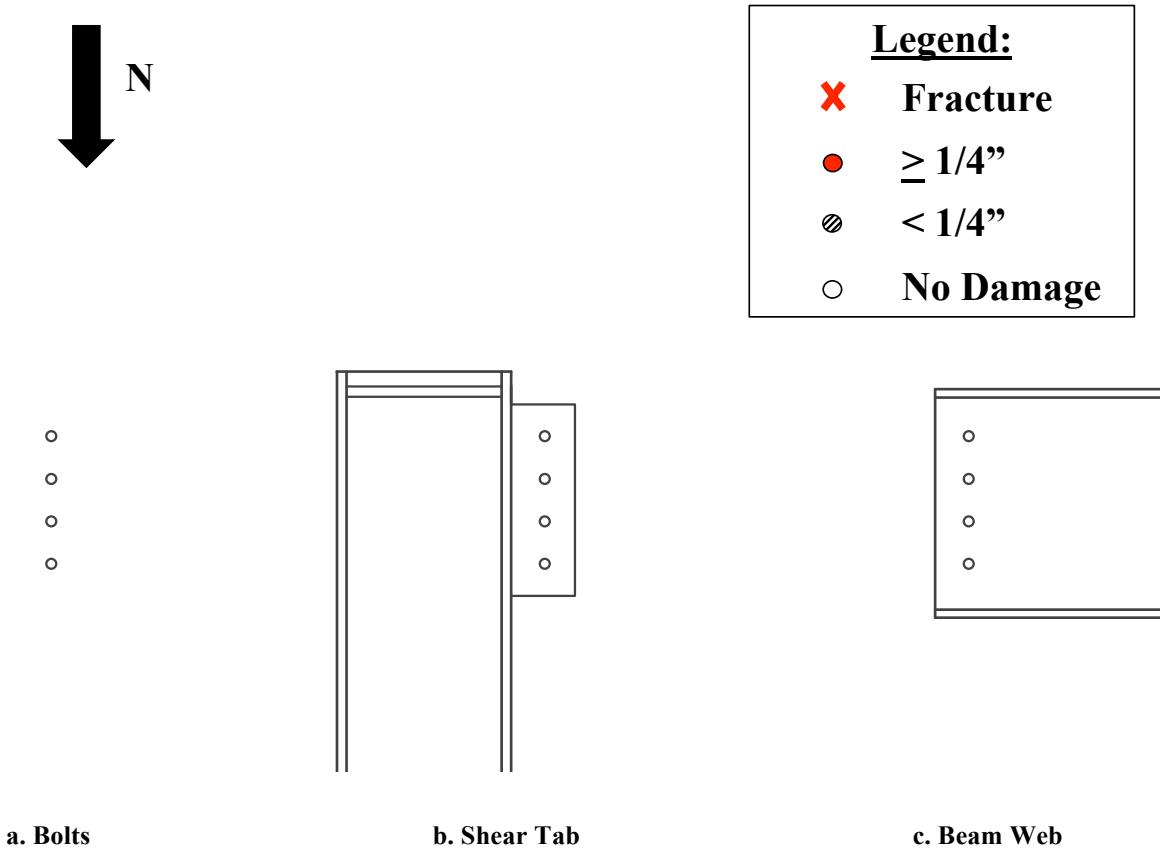

Figure 5.33 - SE Corner Bolt Damage

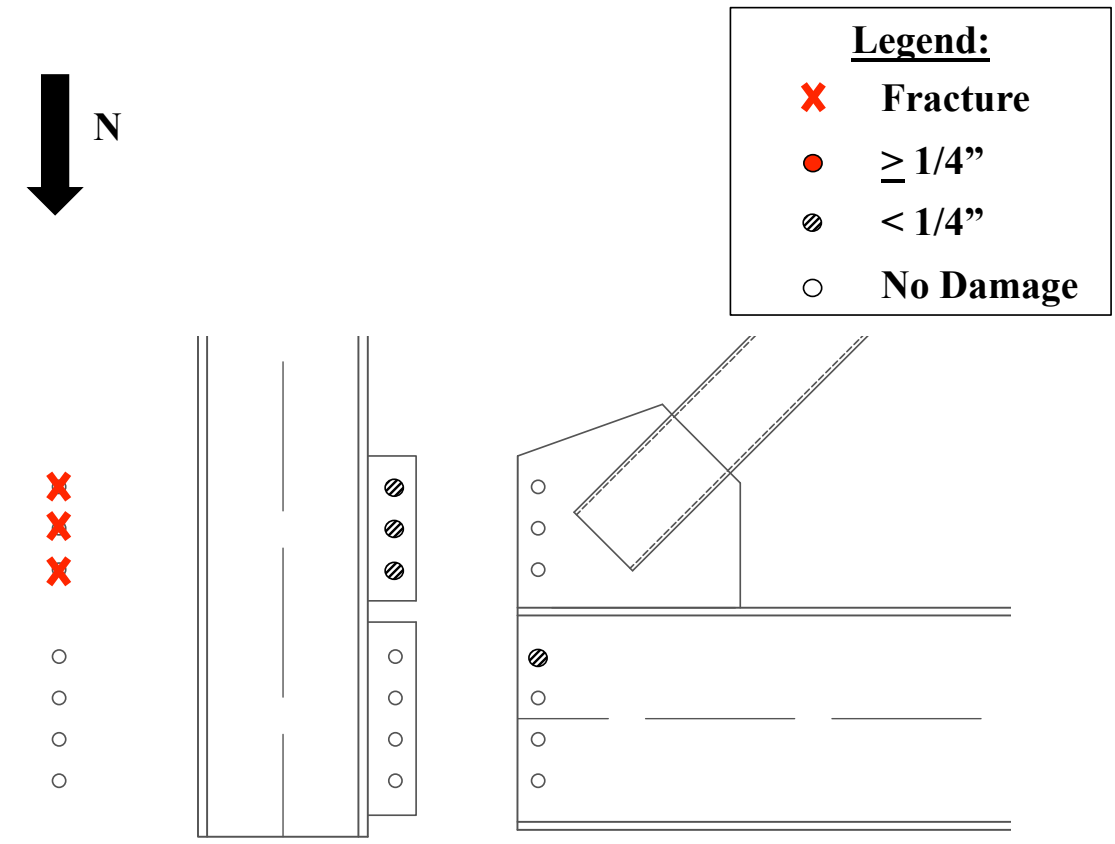

a. Bolts b. Shear Tab c. Beam Web/Gusset Plate

Figure 5.34 - NE Corner Bolt Damage

a. GP to Col. Bolts b. Southern-most GP to Col. Shear Tab Bolt Hole c. Beam Web

Figure 5.35 - Photo Evidence of Bolt Damage in NE Corner

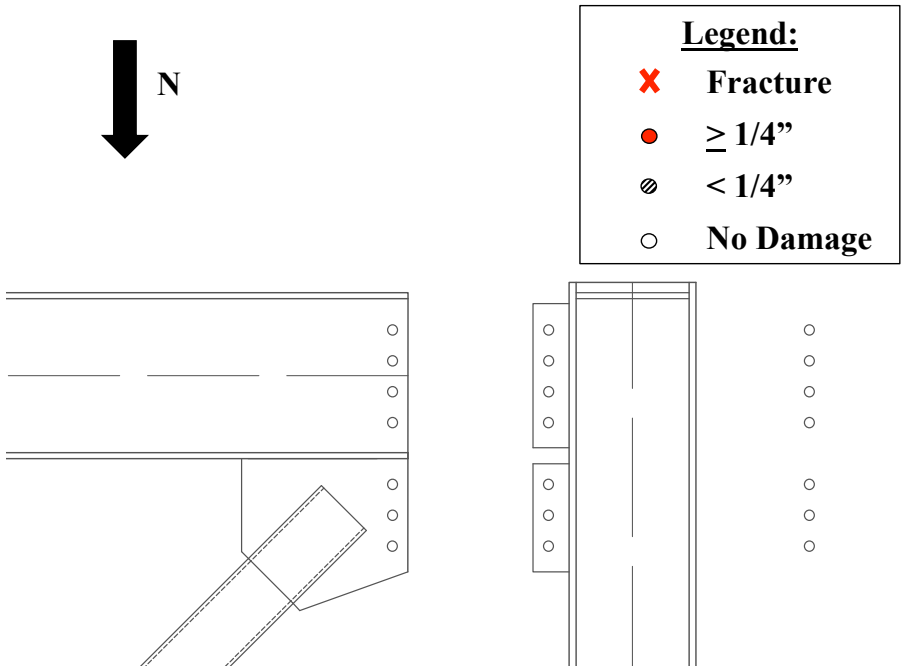

Figure 5.36 - SW Corner Bolt Damage

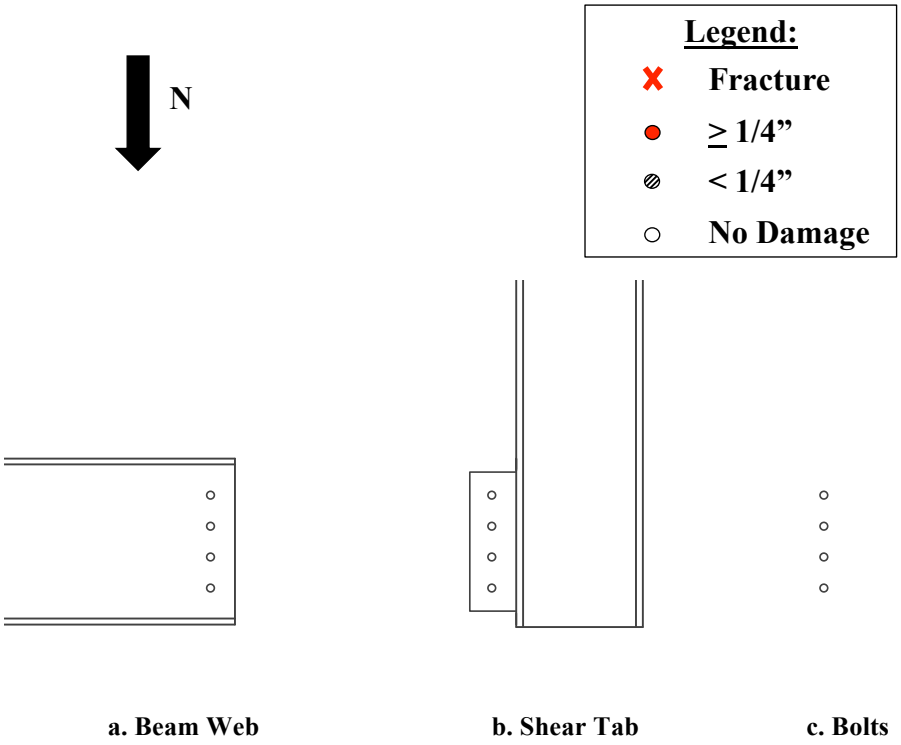

Figure 5.37 - NW Corner Bolt Damage

5.3.3 NHSS-B3

5.3.3.1 Specimen Overview

The third bolted specimen, NHSS-B3, was tested on December 19th, 2013. NHSS-B3 resembled NHSS-B2, except it used a seismically compact HSS 5x5x3/8 brace and with a thinner 1/2 in. thick gusset plate to explore the effects of using a thinner gusset plate on the connection performance.

As seen in Table 5.4.1, NHSS-B3 was designed to be deficient in brace net section rupture, brace block shear, Whitmore gusset plate yielding, gusset plate shear yielding, bolt shear, and bolt bearing. The AISC equation shows a DCR of 0.64 for beam to gusset plate weld strength, but the BDP resulted in a DCR value of 1.4, because of the recommendation that weld strength should develop the tensile yield capacity of the gusset. The most severe limit state for this connection is bolt shear and bolt bearing.

In addition to the deficiencies in the limit states listed above, the gusset plate was not designed to have linear (AISC) or elliptical (BDP) clearance. Although the brace was slotted for the welded connection to the gusset plate, no net section reinforcing plates were included as required by the current Seismic Provisions. The E71T-11 welds were not demand critical.

Key components of the frame included: 3/4 in. thick bolted beam to column shear tabs (4 bolts) and 3/4 in. thick bolted gusset plate-to-column shear tabs (3 bolts); all bolts in those components were A325, 1 in. diameter bolts, with F436 structural washers. The shear tabs were connected to the column flanges via CJP welds. The gusset plates were connected to the beams with 5/16 in. fillet welds. The brace was connected to the gusset plate with 7/16 in. fillet welds. The connection drawing is shown in Figure 5.38.

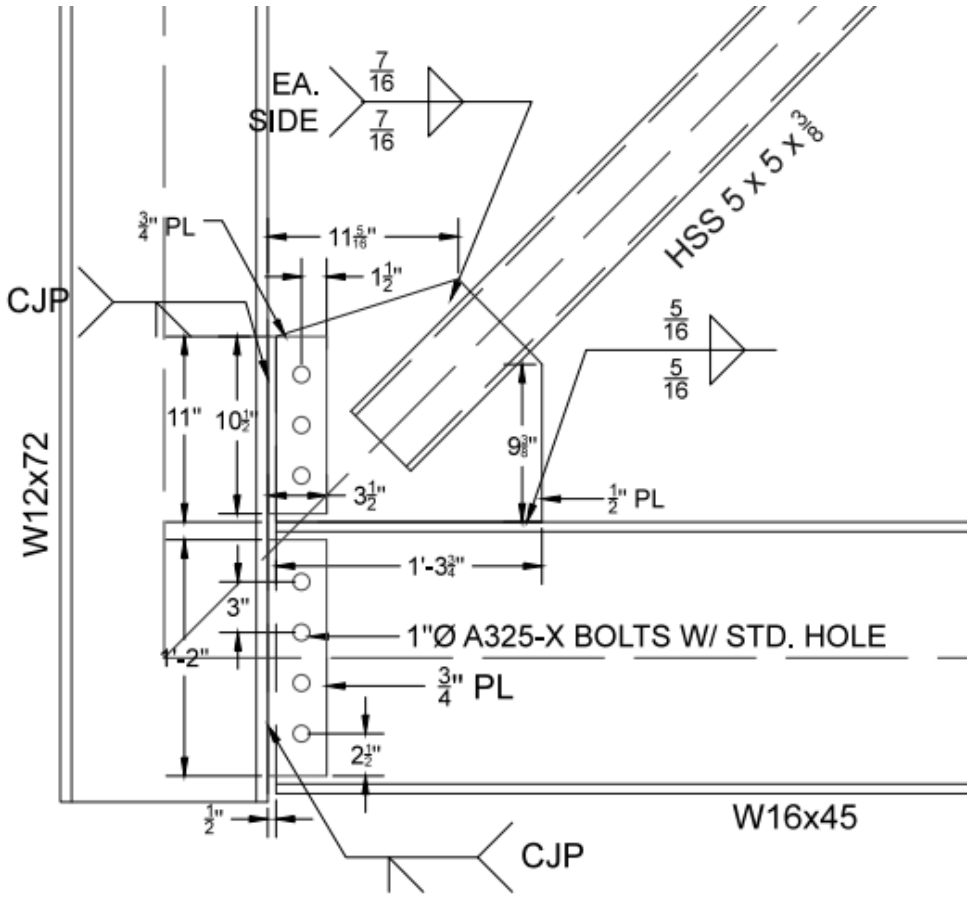

Figure 5.38 - Specimen NHSS-B3 Connection Drawing

NHSS-B3 failed due to fracture of the beam to gusset plate welds in the NE and SW corners which caused a loss of more than 20% in lateral resistance. The test was continued after the welds fractured and the frame was able to reach higher drift levels. Prior to the connection failures, the maximum load resisted in the frame with the brace in tension was 341 kip and -176 kip with the brace in compression. After these fractures, when the brace was in tension the frame was able to sustain loads of about 200 kip, and when in compression the frame resisted a little over 100 kip. The brace remained connected to the column through the 3 bolts in each gusset plate to column shear tab. Even with only 3 bolts in each corner, the brace was still able to continue buckling OOP at increased displacements to eventually reach 17.8 in. midspan OOP displacement.

Prior to connection failure, the maximum story drifts achieved were 1.1% and -2.1% with the brace in tension and compression respectively, for a total range of 3.2%. As mentioned, the test was continued after these fractures and the maximum story drifts achieved at the completion of the test were 2.6% in tension and 3.8% in compression for a total drift range of 6.4%. The specimen's hysteretic response is shown in Figure 5.39. Table 5.12 through Table 5.14 show the progression of performance states at each cycle of NHSS-B3. They present information on each component of the system and it's yielding, buckling, or failure modes throughout the experiment.

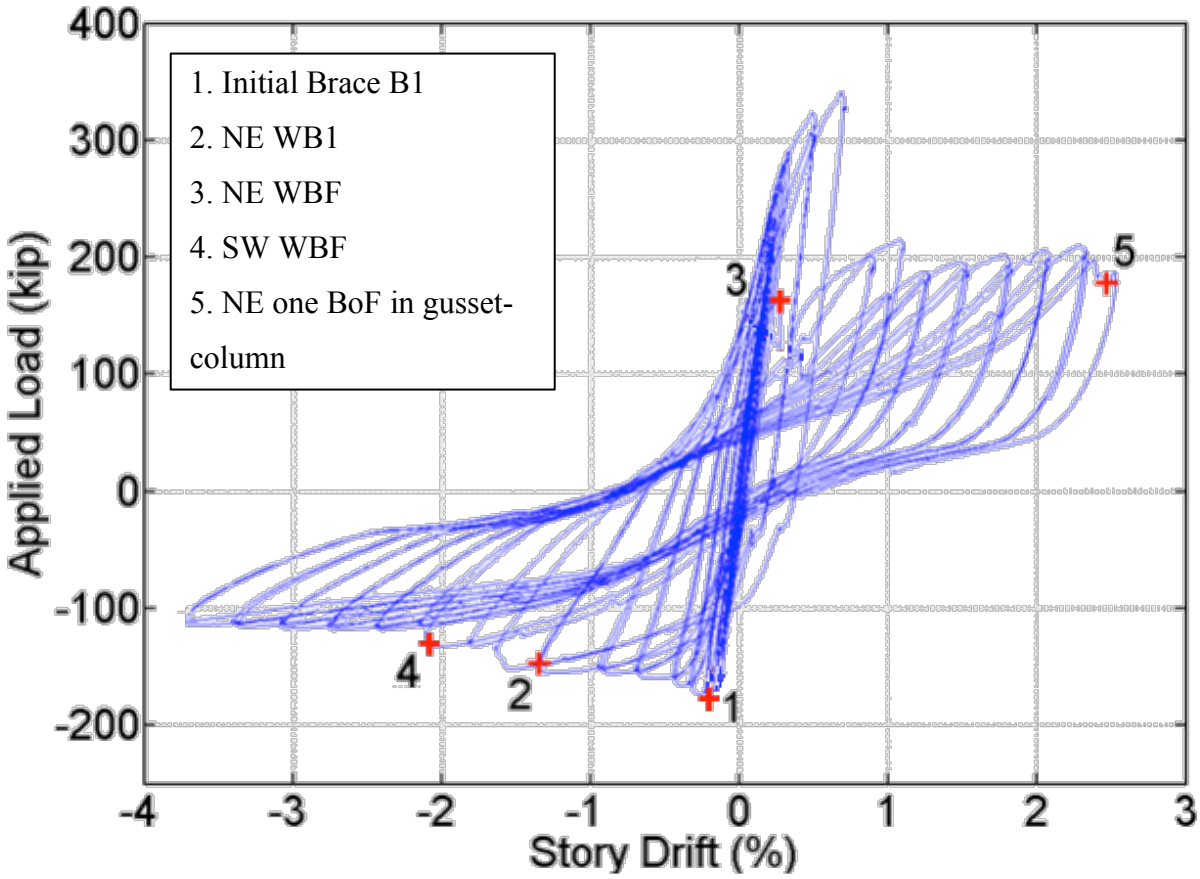

Figure 5.39 - Specimen NHSS-B3 Applied Story Shear vs. Story Drift Hysteretic Behavior

Table 5.12 - Progression of Damage in NE Corner

CYCLE	True Tension Drift (%)	True Compression Drift (%)	Brace	NE CORNER				
				Gusset Plate	Gusset to Column Shear Tab	Beam to Column Shear Tab	N Beam	E Column
1	0.03	-0.04						
2	0.03	-0.04						
3	0.05	-0.07						
4	0.05	-0.07						
5	0.08	-0.09						
6	0.08	-0.09						
7	0.12	-0.12						
8	0.12	-0.12						
9	0.16	-0.16						
10	0.16	-0.16						
11	0.21	-0.22	B1					Y1
12	0.19	-0.23						
13	0.23	-0.32						
14	0.20	-0.34						
15	0.24	-0.44						
16	0.21	-0.45						
17	0.28	-0.68	B2					
18	0.25	-0.69						
19	0.32	-0.92		Y1	Y1			
20	0.30	-0.94						
21	0.50	-1.35		WB1				
22	0.49	-1.35		WB2				
23	0.70	-1.63	B3	WB3				B1 - flange
24	0.88	-1.81		WBF, BoEg, Y2				
25	1.10	-2.10						
26	1.01	-2.14						
27	1.27	-2.44	IPB1					Y2
28	1.25	-2.45						
29	1.53	-2.77						
30	1.53	-2.75						
31	1.82	-3.09						
32	1.83	-3.07						
33	2.08	-3.38						
34	2.07	-3.40					Y1 - web	
35	2.33	-3.75	B3 - hinge					Y3
36	2.33	-3.73						
37				BoF - END			B1 - web	
38								

Table 5.13 - Progression of Damage in SW Corner

CYCLE	True Tension Drift (%)	True Compression Drift (%)	Brace	SW CORNER				
				Gusset to Column Shear Tab	Gusset Plate	Beam to Column Shear Tab	S Beam	W Column
1	0.03	-0.04						
2	0.03	-0.04						
3	0.05	-0.07						
4	0.05	-0.07						
5	0.08	-0.09						
6	0.08	-0.09						
7	0.12	-0.12						
8	0.12	-0.12						
9	0.16	-0.16						
10	0.16	-0.16						
11	0.21	-0.22	B1					Y1
12	0.19	-0.23						
13	0.23	-0.32						
14	0.20	-0.34						
15	0.24	-0.44						
16	0.21	-0.45						
17	0.28	-0.68	B2				Y1 - web	
18	0.25	-0.69						
19	0.32	-0.92		Y1				
20	0.30	-0.94						
21	0.50	-1.35						
22	0.49	-1.35			WB1			
23	0.70	-1.63	B3		WB2			Y2
24	0.88	-1.81						
25	1.10	-2.10			WB3			
26	1.01	-2.14			WBF			
27	1.27	-2.44	IPB1		BoEg			
28	1.25	-2.45						
29	1.53	-2.77						
30	1.53	-2.75						
31	1.82	-3.09						
32	1.83	-3.07						
33	2.08	-3.38						
34	2.07	-3.40						
35	2.33	-3.75	B3 - hinge					
36	2.33	-3.73						
37								
38								

Table 5.14 - Progression of Damage in NW & SE Corner

CYCLE	True Tension Drift (%)	True Compression Drift (%)	Brace	NW CORNER			SE CORNER		
				N Beam	W Column	Beam to Column Shear Tab	S Beam	E Column	Beam to Column Shear Tab
1	0.03	-0.04							
2	0.03	-0.04							
3	0.05	-0.07							
4	0.05	-0.07							
5	0.08	-0.09							
6	0.08	-0.09							
7	0.12	-0.12							
8	0.12	-0.12							
9	0.16	-0.16							
10	0.16	-0.16							
11	0.21	-0.22	B1						
12	0.19	-0.23							
13	0.23	-0.32							
14	0.20	-0.34							
15	0.24	-0.44							
16	0.21	-0.45				Y1		Y1	
17	0.28	-0.68	B2		Y1				
18	0.25	-0.69							
19	0.32	-0.92							
20	0.30	-0.94							
21	0.50	-1.35							
22	0.49	-1.35							
23	0.70	-1.63	B3					Initial Uplift	
24	0.88	-1.81							
25	1.10	-2.10							
26	1.01	-2.14							
27	1.27	-2.44	IPB1						
28	1.25	-2.45							
29	1.53	-2.77							
30	1.53	-2.75					Y1		
31	1.82	-3.09			B1				
32	1.83	-3.07							
33	2.08	-3.38			Y2				
34	2.07	-3.40			Y3				
35	2.33	-3.75	B3 - hinge						
36	2.33	-3.73							
37									
38									

5.3.3.2 Moderate Damage States (DS1 & DS2)

The brace buckled upward OOP (B1) at -0.2% drift. Initial yield lines (Y1) on the inside of the east flange of the west column were observed at +0.21% drift. Framing element yielding (Y1) continued at +0.54% drift in the NE corner on the west flange on the east column at the south end of the gusset plate, shown in Figure 5.40. As the cycles continued at larger drifts, yielding in the framing elements increased.

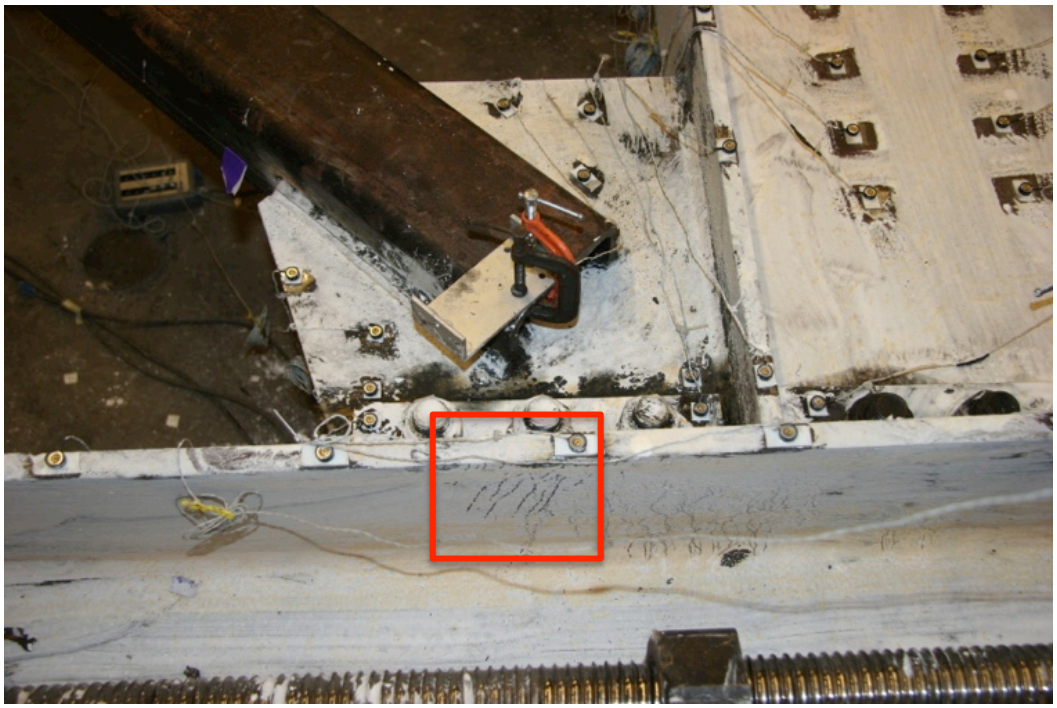

Figure 5.40 - Initial Yielding (Y1) in NE Corner

By -0.45% drift, a 4 in. x 3 in. area of yield lines on the outside of the west flange of the base of the west column was seen. On the east column, yield lines formed at both the top and bottom of the east flange. Additionally, the gusset plate was observed to be bending OOP – but not bending the shear tab with it as in NHSS-B1, shown in Figure 5.41. At -0.92% drift, yielding (Y1) in the NW corner on the east flange of the west column as seen in Figure 5.42 was observed.

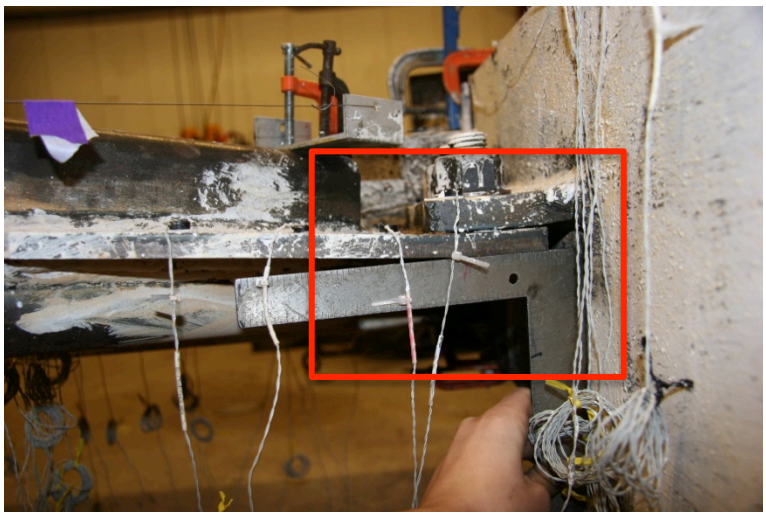

Figure 5.41 - Gusset Plate Bending in NE Corner at -0.92% Drift

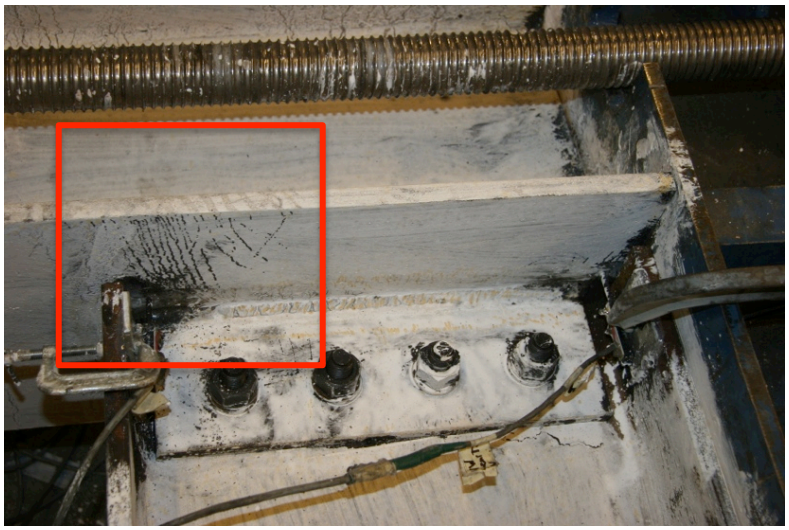

Figure 5.42 - Yielding (Y1) in the NW Corner

At the next compressive cycle at -0.94% drift, yield lines (Y1) also formed on the north flange of the north beam about 8 in. east of the load beam. The brace continued to buckle upwards OOP and at -0.68% drift, the brace midspan had displaced 5.7 in. (B2). At -1.3% drift, there was increased yielding (Y1) at the base of the west column on the west flange. Also at this drift level, a 1 in. long weld crack (WB1) initiated in the NE corner at the west end of the gusset plate to beam weld on the bottom of the plate, shown in Figure 5.53a. The OOP rotation of the gusset plate in the NE corner is shown in Figure 5.43. Tensile yield lines were observed on the

underside of the NE gusset plate at +0.49% drift. On the SW gusset plate, radial yield lines formed around all 3 bolts.

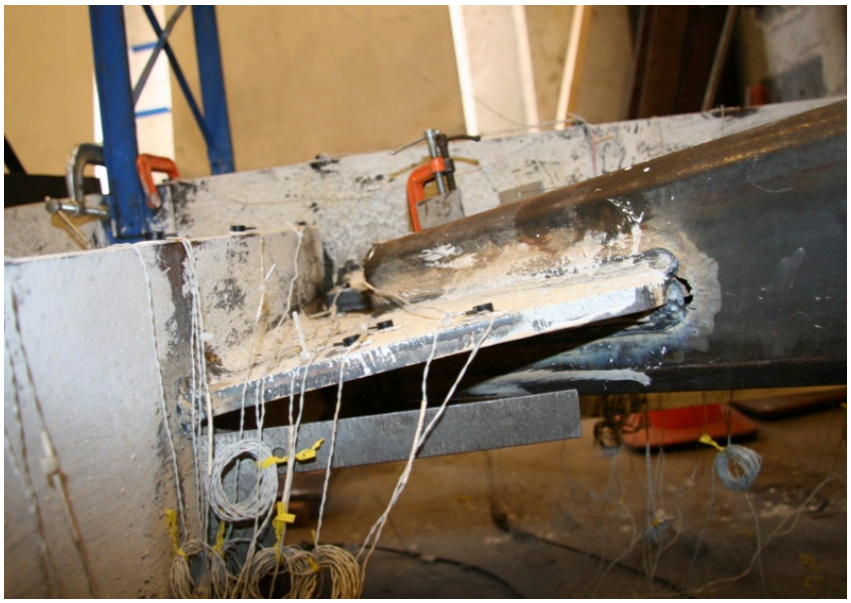

Figure 5.43 - Gusset Plate Rotation at -1.3% Drift

By the second compressive cycle at the above drift, the crack in the NE beam to gusset plate weld had propagated to 3/4 in. and 4.125 in. long (WB2) on the top and bottom, respectively, as shown in Figure 5.53b. In the SW corner, the beam to gusset plate weld crack (WB1) had propagated to 2.75 in. long on the bottom, as seen in Figure 5.54a. After this compression cycle, there was increased yielding in the NW beam to column shear tab at the southern end. Moving to the tension cycle, at +0.70% drift there was significant yielding in the NE gusset plate and about 40% of the whitewash had flaked off.

5.3.3.3 Severe Damage States (DS3 & DS4)

During the compressive cycle at -1.6% drift, the NE weld tearing propagated to 11.25 in. (WB3) through both welds and the gusset plate had dislocated OOP at the west end by 1/2 in., as seen in Figure 5.53c. The SW corner beam to gusset plate weld tearing had propagated to 4 in. and 1 in. long on the top and bottom fillet weld (WB2), respectively, shown in Figure 5.54b. In this corner, the east flange of the west column had rotated over the entire depth of the SW

connection. Yield lines continued propagating on the west column flange of the west column (Y2), shown in Figure 5.44.

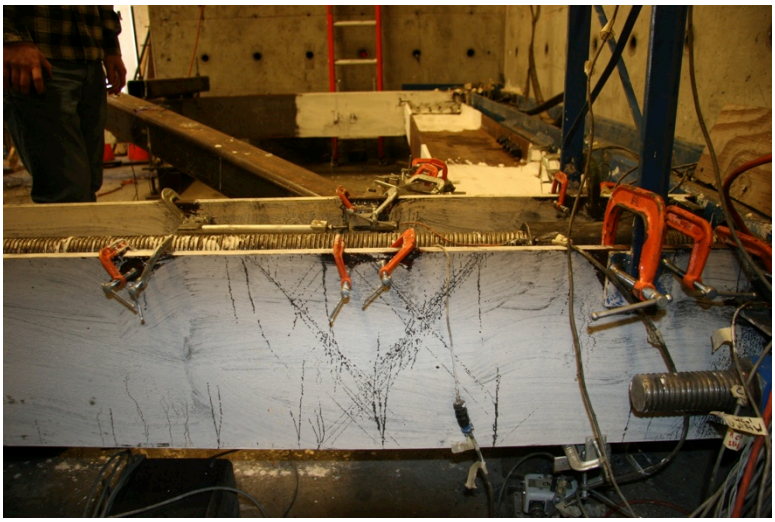

Figure 5.44 - Moderate Yielding (Y2) on the West Flange of the West Column at -1.6% Drift

The test was paused during the +0.88% drift cycle when the beam to gusset plate weld in the NE corner fractured, as seen in Figure 5.53d. Once the tensile drift peaked at +0.88%, there was a residual 2 in. vertical OOP displacement of the brace. The fully fractured weld crack in the NE corner opened a gap of 1 in. at the far west side, seen in Figure 5.45. On the underside of the NE gusset plate three bulges formed east of the bolt heads caused by bolt hole elongation, shown in Figure 5.46. On the south ends of the brace to gusset plate splice, small weld cracks initiated. At -1.6% drift, the brace had increased in vertical OOP displacement to 11.2 in. (B2). At -1.8% drift, the SW beam to gusset plate connection now had a 5 in. long weld crack on the bottom and 2.5 in. long weld crack on the top, shown in Figure 5.54c.

Figure 5.45 - 1 in. Gap Between NE Gusset Plate and Beam at +0.88% Drift

Figure 5.46 - Bolt Hole Elongation in the Gusset Plate in the NE Corner

In the following cycles, the SW beam to gusset plate weld continued to deteriorate, and at -2.1% drift it had cracked 8.5 in. on top and 11 in. on the bottom (WB3), as shown in Figure 5.54d, and the east flange of the west column continued to rotate. By the second cycle at +1.0% drift, the bottom weld crack fractured and the crack length was 14 in. on top. In these larger compression drift cycles, the brace began to buckle in-plane to the NW due to the eccentricity from the connection weld fractures. When stretched in tension, the brace developed into an "S" shape, shown in Figure 5.47. The photo shows that in the SW corner the brace was displaced towards the west, and in the NE corner the brace was displaced towards the east.

Figure 5.47 - Brace "S" Shape at +1.0% Drift

At the second compressive cycle at -2.1% drift, the SW beam to gusset plate weld fractured, as shown in Figure 5.54e and the gusset plates were attached to the columns by 3 bolts at each gusset. After this event, the specimen lost significant lateral resistance, but the test was still continued. At -2.1%, a gap of 1/8 in. between the load beam and the north beam flange at the east end was first observed. The NE bolt holes continued to elongate at increasing drift levels. Bolt hole elongation (BoE) was first seen at in the SW corner at -2.4% drift.

At +1.5% drift, the north flange of the south beam in the SW corner came in contact with the east flange of the west column. The SW corner of the gusset plate was also bearing on the east flange of the west column. This contact continued throughout the rest of the test. Figure 5.48 shows the local buckling (B1) that formed at -2.8% drift on the east flange of the west column at the south end of the NW shear tab.

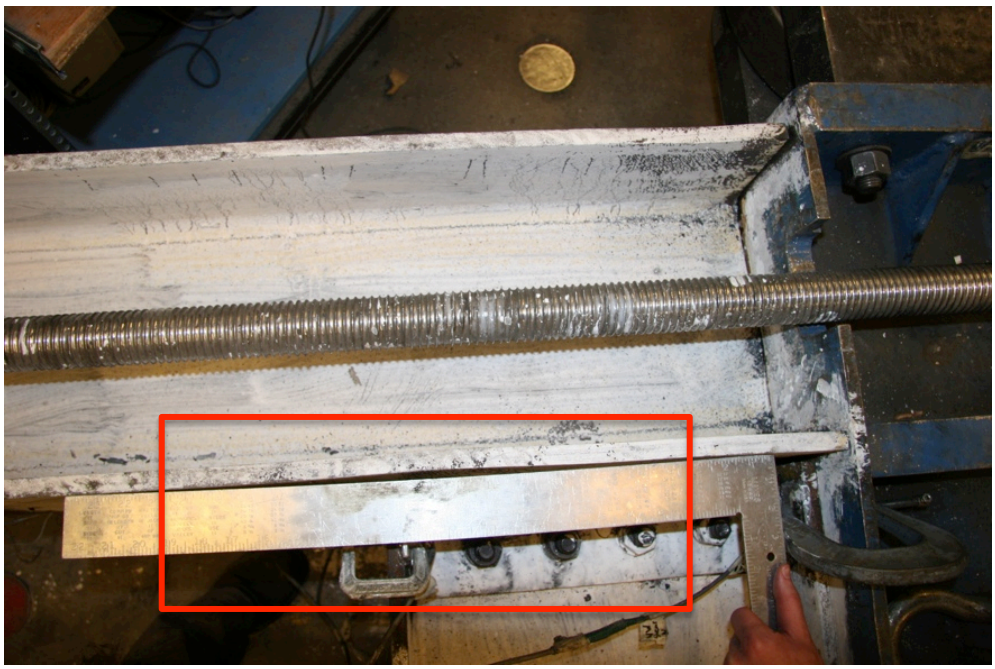

Figure 5.48 - Local Buckling (B1) in the NW Corner of the Frame at -2.8% Drift

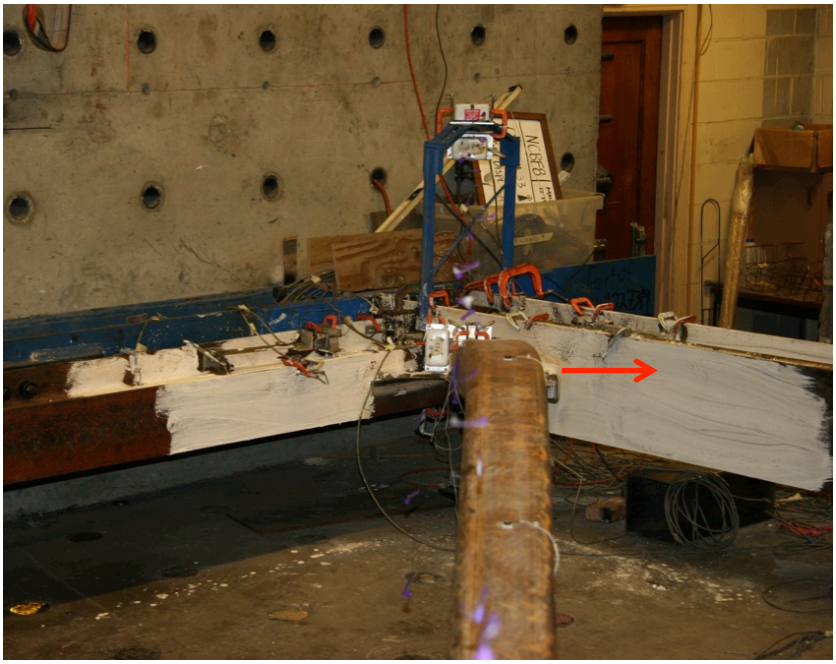

Figure 5.49 - In-plane Brace Buckling at -3.1% Drift

By -3.1% drift, the brace in-plane buckling increased at its midspan from the first observation (shown in Figure 5.49), likely due to the flexibility and eccentricity caused by the beam to gusset plate weld fracture. The brace appeared to be developing slight local deformations in the brace

walls (B3-cupping) and it was warm to the touch. By the second cycle at this drift, both flanges at the base of the north column were bowed outward (local deformation) as shown in Figure 5.50. The NE corner continued to suffer extreme damage at +2.3% drift with the west end of the gusset plate separated 1.5 in. to the south and moved 1.5 in. to the west from its original location, as seen in Figure 5.51.

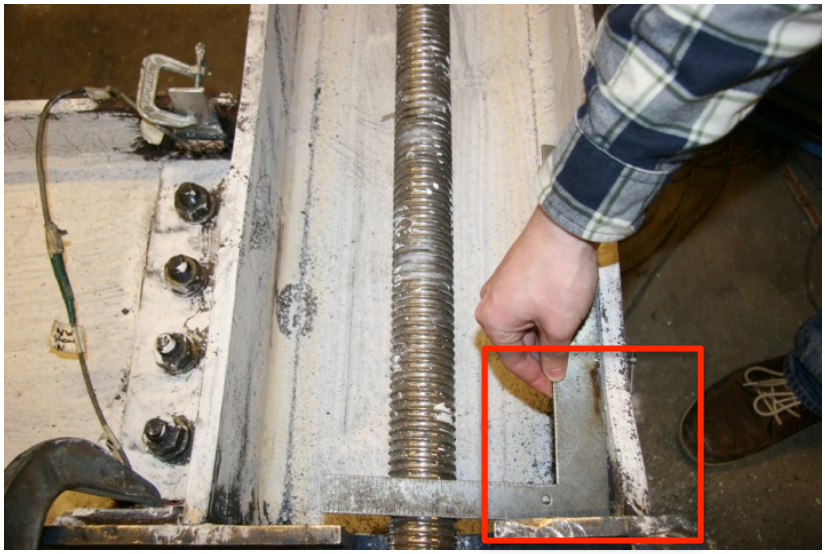

Figure 5.50 - Local Buckling (B1) of the West Flange of the West Column

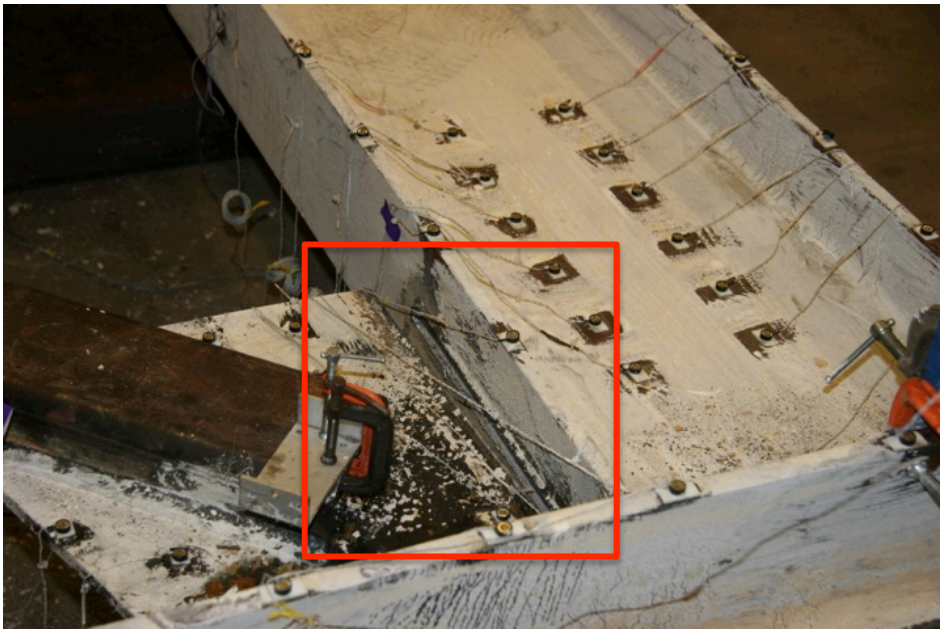

Figure 5.51 - Visible Gap in Gusset Plate to Beam at +2.3% Drift

At -3.7% drift, slight beam web local buckling (B1) in NE beam to column connection occurred, as shown in Figure 5.52a. This behavior was seen because of the eccentricities induced by weld fractures in the gusset connections. The free edge of the gusset plate at the beam to gusset plate connection had displaced out of the weld seat significantly as shown in Figure 5.52b and Figure 5.53e. The elongation of the bolt holes and deformation in the bolts in the gusset plate to column shear tab was so severe the bolts were pointing diagonally – towards the west; and in viewing from below, the edge of the bolt hole was visible from around the bolt head, as shown in Figure 5.52c. The brace continued to develop deformation at the plastic hinge at midspan, with a total vertical displacement of 17.8 in (Figure 5.52d). The actuator reached its full stroke capacity and the test was stopped at +2.6% drift. There was one bolt fracture in the NE gusset plate to column shear tab connection (the northernmost bolt). The test was stopped after this bolt fracture – a photo summary of the last compression cycle is below in Figure 5.52.

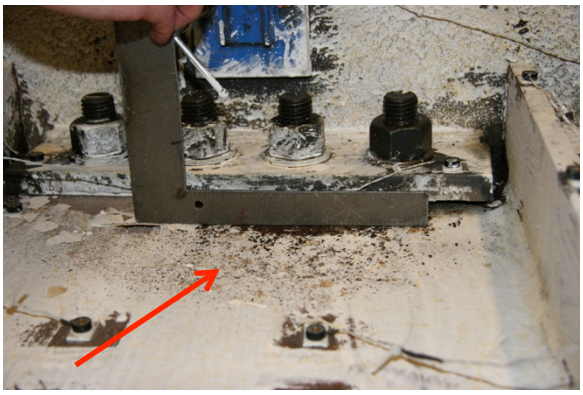

a. Local Buckling of Beam Web NE Corner

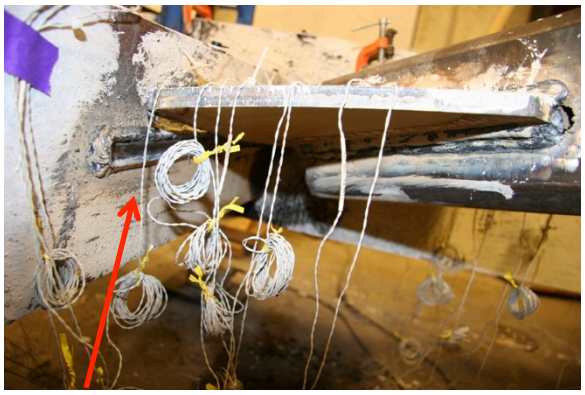

b. OOP Rotation of North Gusset Plate

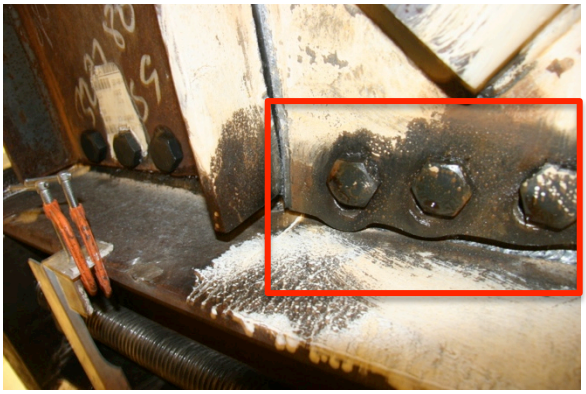

c. Bolt Hole Elongation from Below the North Gusset Plate

d. Brace Hinge at Midspan

Figure 5.52 - Final Test Photos at -3.7% Drift

5.3.3.4 Specimen Summary of Results

While NHSS-B3 was able to achieve the highest drift range of all the tests, it had an undesirable failure mode and sustained significant loss of resistance at a much lower drift range. The frame's resilience after weld fracture was due to increased flexibility in the gusset plate connections, extreme bolt hole elongation, and bolt deformation. Once the beam to gusset plate welds fractured, the brace achieved larger OOP displacements due to the significant OOP rotation of the free sides of the gusset plate.

In NHSS-B2, once the NE beam to gusset plate weld fractured, the bolts joining the gusset plate to column shear tab fractured in the same tensile cycle. The same three bolts in this NHSS-B3 did not fracture. Changing to a 1/4 in. thinner gusset plate allowed bolt hole elongation and bolt deformation that contributed to increased frame story drift capacity. In the previous tests, bolt hole elongation concentrated in the thinnest connecting member, but in NHSS-B3, both the gusset plate (1/2 in.) and the connecting shear tab (3/4 in.) deformed.

Post-fracture cycles were completed as part of the full test cycles. Typically, to conduct post-fracture cycles, the testing had to be stopped and a portion of the brace cut out to prevent binding. The beam to gusset plate weld fracture in both corners was the cause of the loss in resistance, but the gusset plates remained connected to the columns. Because of this connectivity, the test did not have to be stopped prior to post-fracture cycles. At the conclusion of the test, the frame was disassembled and the bolts and bolt holes were studied. The diagrammatic sketches below in Figure 5.55 through Figure 5.60 document the bolt damage found with key photos included. Additionally there are photographs of all bolts and connecting plates in the Appendix. A few bolts in the gusset plates withstood significant deformation (BD) from bearing stresses and looked close to shear failures, as seen in Figure 5.57 and Figure 5.58.

There was significant elongation of bolt holes (BoE) from bearing stresses, most notable in the NE gusset plate. Those three holes elongated to a final ovular diameter of between 2.125 in. (closest to the beam), which is double the original diameter, and 1.625 in. (southernmost), which is 9/16 in. larger than the original diameter. With these elongations, it is clear that bolt hole elongation contributed a large portion of the maximum story drift. The edges of the NE gusset

plate and NE beam web were deformed significantly from bolt bearing. Photos of these elongated bolt holes are shown in Figure 5.57. Bolt #5, located closest to the beam in the gusset plate connection, fractured during the final tension cycle, seen in Figure 5.58, making bolt shear failure the controlling failure mode over individual bolt tearout.

a. 1 in. long weld crack at -1.3% drift

b. 4.125 in. (bottom) & 0.75 in. (top) weld crack at -1.3% drift

c. 11.25 in. (bottom) & 11.25 in. (top) weld crack at -1.6% drift

d. Weld fracture at +0.88% drift

e. Post weld fracture at -3.7% drift

Figure 5.53 - Progression of NE Beam to Gusset Plate Weld Fracture

a. 2.75 in. long weld crack at -1.3% drift

b. 4 in. (bottom) & 1 in. (top) weld crack at -1.6% drift

c. 5 in. (bottom) & 2.5 in. (top) weld crack at -1.8% drift

d. 11 in. (bottom) & 8.5 in. (top) weld crack at -2.1% drift (first cycle)

e. Weld fracture at -2.1% drift (second cycle)

Figure 5.54 - Progression of SW Beam to Gusset Plate Weld Fracture

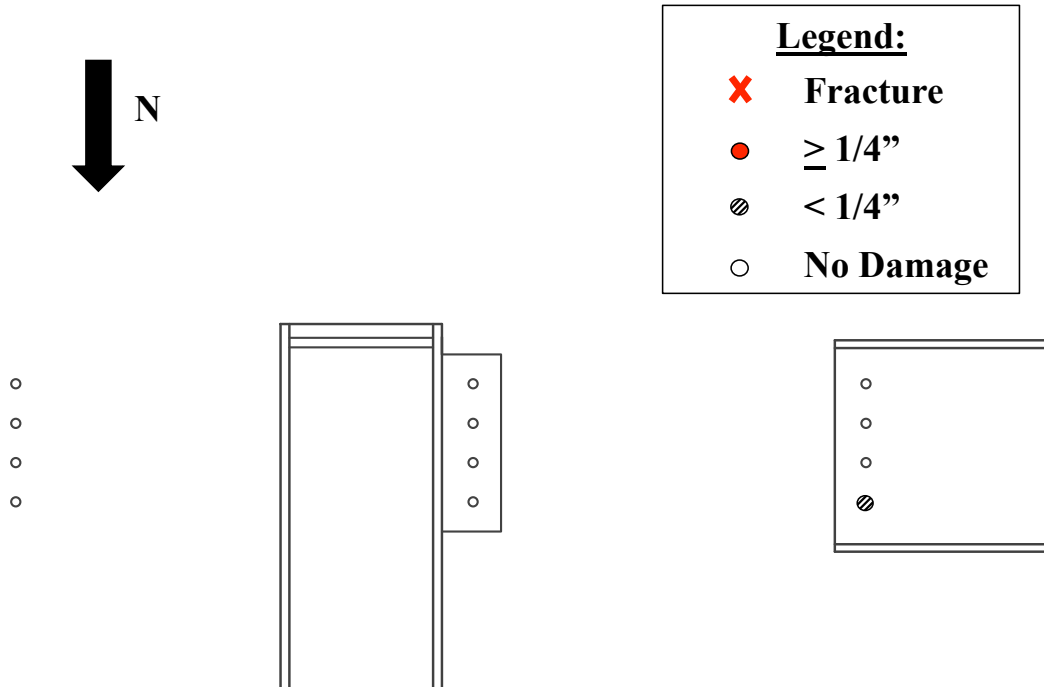

Figure 5.55 - SE Corner Bolt Damage

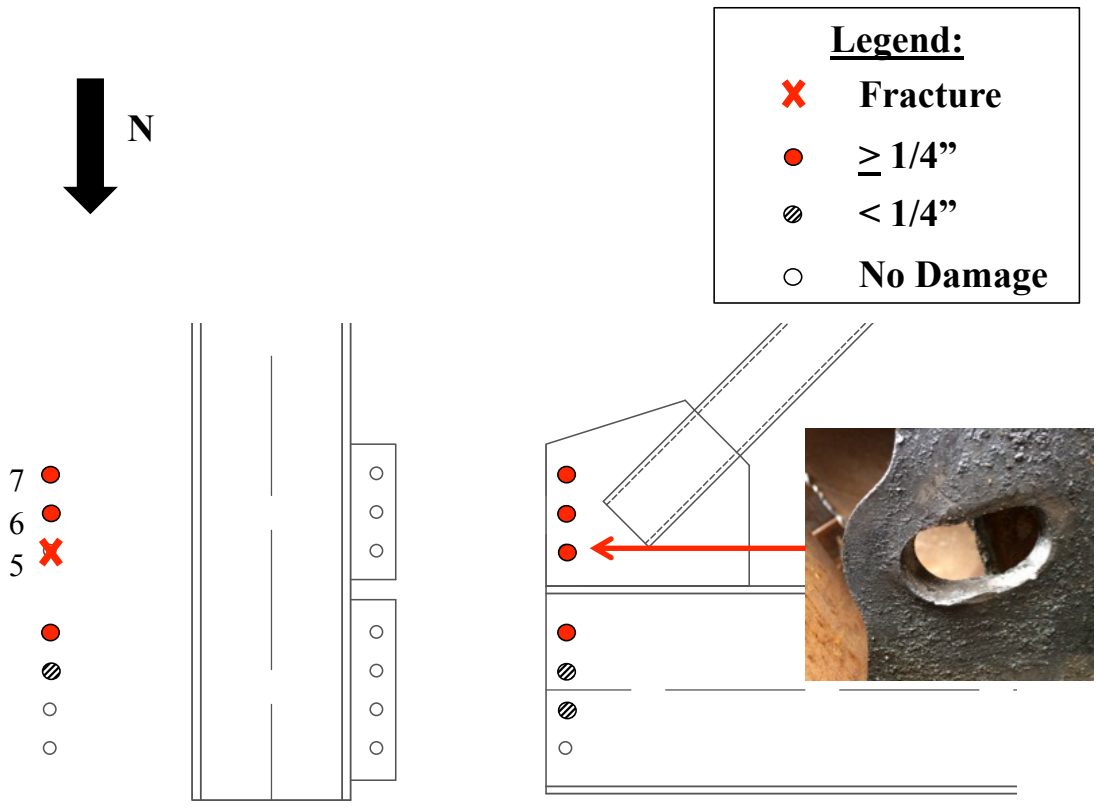

Figure 5.56 - NE Corner Bolt Damage

Figure 5.57 - Bolt Hole Elongation in NE Gusset Plate

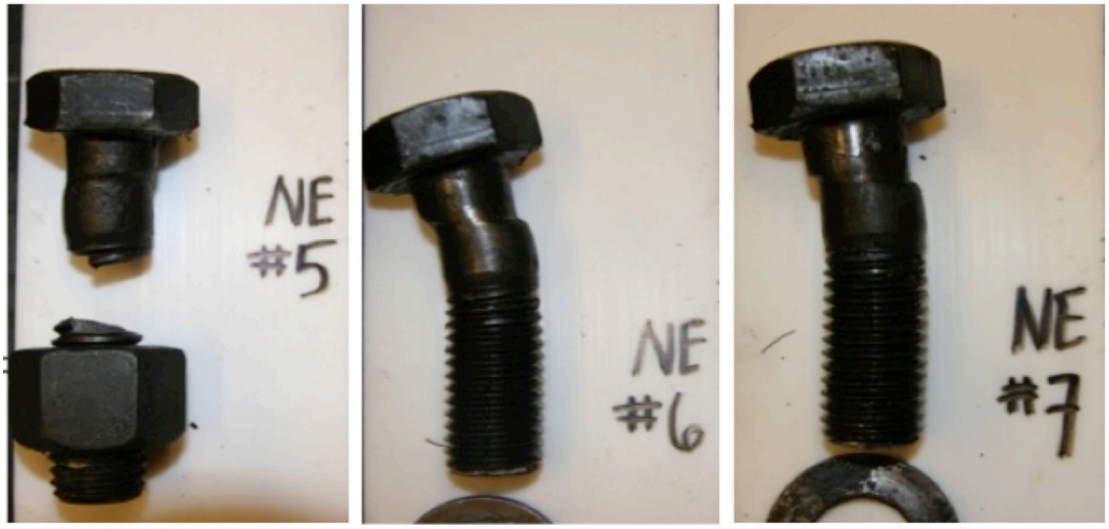

Figure 5.58 - Bolt Damage in NE Gusset Plate

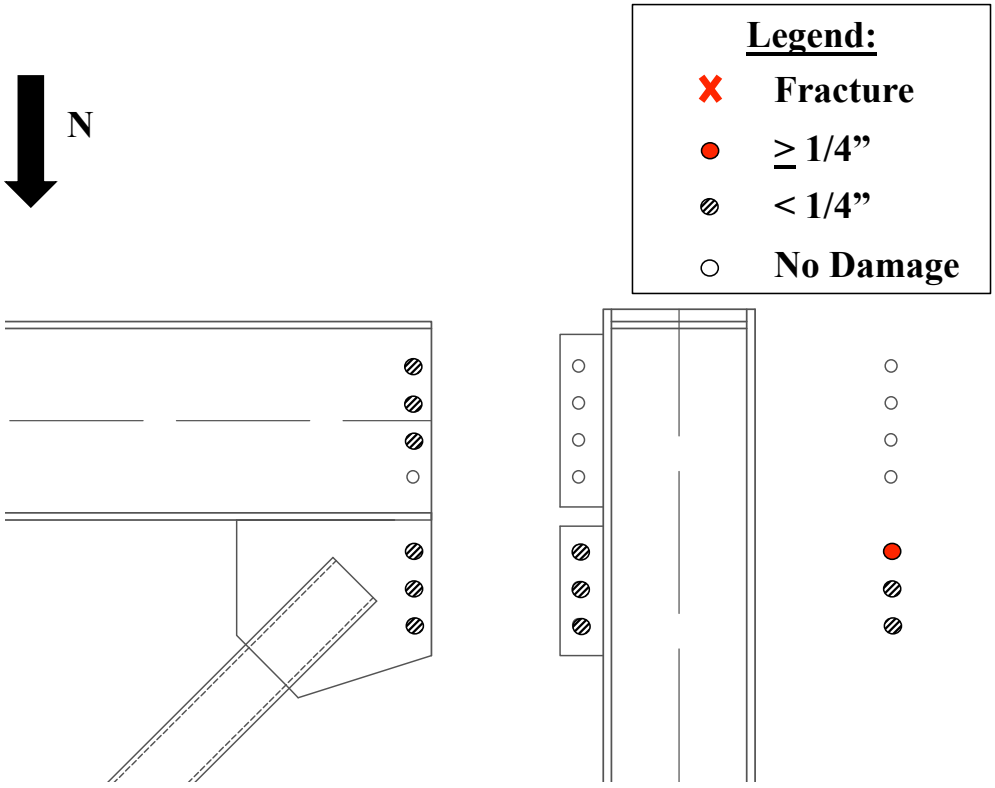

Figure 5.59 - SW Corner Bolt Damage

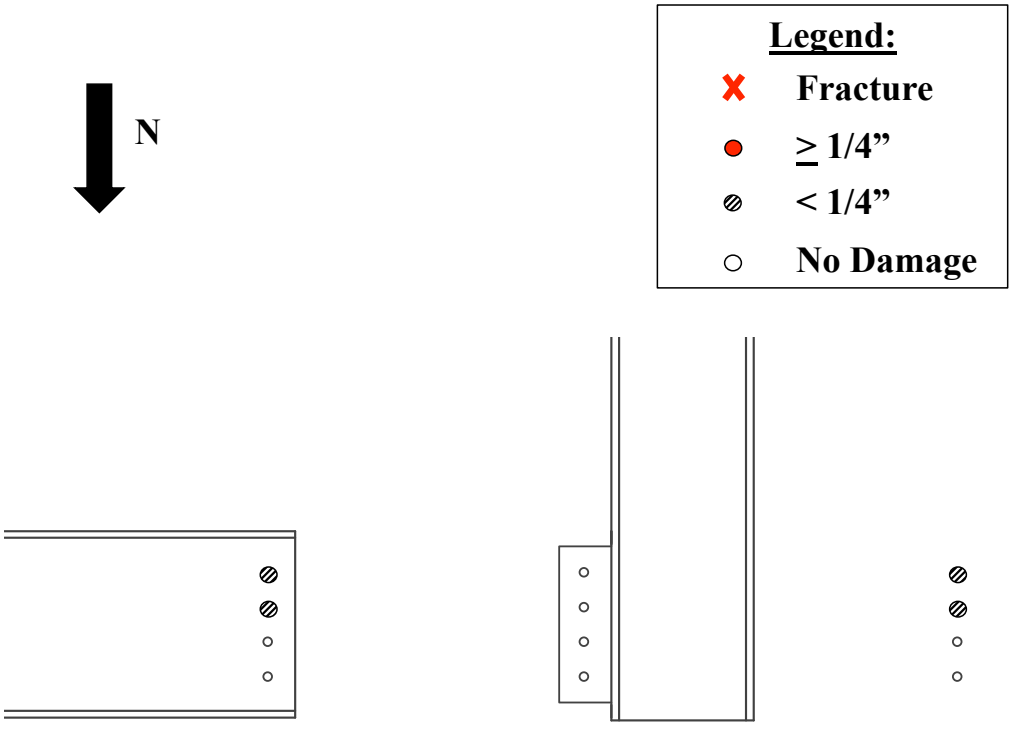

Figure 5.60 - NW Corner Bolt Damage

CHAPTER 6: DATA ANALYSIS

6.1 Introduction

This chapter focuses on analyzing the data from each specimen and drawing conclusions about system performance. The instrumentation layout was described in Chapter 4, but will be elaborated on in this chapter as necessary to accompany sample calculations. Data analysis utilized Matlab Version R2013a and Microsoft Office Excel. Occasionally, instrumentation was damaged or electronic errors occurred during the test. This flawed data was not included in the analysis.

The total braced frame system behavior is evaluated in Section 6.2, with subsections investigating the applied lateral load versus story drift responses, system stiffness comparisons, energy dissipation comparisons, and post-failure system behavior. Section 6.3 discusses the NE and SW connection responses (the corners with the gusset plate connection), in particular the gusset plate OOP displaced shape, gusset plate OOP rotation angle, and shear tab rotations. Section 6.4 discusses bolt damage seen in the test and its impact on system performance, and Section 6.5 discusses weld damage for each test specimen.

Section 6.6 describes the analysis of the brace response for each test specimen. It is broken into several subsections that describe finding the experimental effective length factor, k, the brace buckled performance state comparisons, the brace axial force versus story drift response, the brace buckled shape, and the brace elongation. Section 6.7 discusses the NW and SE connection responses (the corners without the gusset plate connection).

6.2 Braced Frame System Behavior

When assessing the performance of a braced frame, its ultimate drift capacity and its lateral load resistance are two important factors. The braced frame's drift capacity can be a direct measure of its ductility. The desired performance for a braced frame is one that can survive large drift levels while maintaining its lateral load resistance. Braced frame systems achieve their ductility through inelastic brace buckling and yielding of the brace, however, yielding of other

components can add ductility and inelastic deformation capacity to the system. In order to develop the brace capacity and maximize brace performance, the connection must be able to withstand the large forces and inelastic rotational demands from the brace. Connection failures in several tests had detrimental effects on the frame's lateral drift and resistance capabilities.

Table 6.1 provides a summary of each test, including their experimental goals, drift and load capacities, and ultimate failure modes. The applied lateral load versus story drift response for the specimens are asymmetric and could be misleading. The asymmetry is due to different factors, including the difference between the brace's tensile and compressive capacities and losses and slip that occur within the system. The total drift range is reported and is a better measure to use because it more closely relates the strain in the outer fiber of the braces.

From the results presented in Table 6.1, NHSS-B1 achieved the largest ductility, total force range and total drift capacities. It also had the most desirable failure mode of brace fracture, despite significant tearing at the gusset plate to beam weld. NHSS-B2 and NHSS-B3 were less ductile and neither was able to achieve brace fracture. NHSS-B3 had comparable lateral resistance to NHSS-B1, and NHSS-B2 had the lowest lateral resistance. The hysteretic force-drift response of these specimens is described in more detail in Section 6.2.1.

Table 6.1 - Summarized Test Specimen Performance

Specimen	Test Goal	Drift (%)			Load Capacity (kip)			Failure Mode
		T	C	Range	T	C	Range	
NHSS-B1	Specimen was designed to explore perceived deficiencies of NCBF bolted connections (bolt shear, brace net section, brace block shear) using a shared shear tab.	1.9	-3	4.9	362	-171	533	Brace Fracture
NHSS-B2	Specimen was designed to explore perceived deficiencies of NCBF bolted connections (bolt shear & bearing, brace net section & block shear, beam to gusset base metal fracture) using a split shear tab and non-seismically compact brace.	0.69	-1.1	1.8	293	-164	457	Weld/Bolt Fracture
NHSS-B3	Specimen was designed to explore perceived deficiencies of NCBF bolted connections (bolt shear, brace net section & block shear) using a split shear tab and thinner gusset plate.	2.6[a]	-3.8[a]	6.4[a]	213[c]	-133[c]	345[c]	Weld Fractures
		1.1[b]	-2.1[b]	3.2[b]	341[d]	-176[d]	517[d]	

a. Drift values for entire test, however failure (20% strength loss) occurred at lower drift values, see note b.

b. Drift values at failure (20% strength loss) due to weld fractures in NE & SW connections.

c. Peak story shear values after failure (20% strength loss) from weld fractures.

d. Peak story shear values at failure (20% strength loss).

6.2.1 Applied Story Shear versus Story Drift Response

Figure 6.1 shows the applied story shear versus story drift response for the three specimens with their failure mode noted on the plot (refer to Chapter 5 for definitions of the notation). The axes for each specimen are at the same scale for visual comparison. The lateral load plotted on the y-axis is the measurement recorded directly from the load cell in the actuator during the test. The frame drift was calculated as the true horizontal displacement divided by the frame height. The true horizontal displacement of the frame was calculated using the frame diagonal elongation measurement divided by the cosine of the original brace angle. This measurement was used instead of the string pot measuring the lateral displacement in the NE corner, because it requires minimal corrections and is easily and accurately determined.

Comparisons can be made of the total drift range, the maximum tensile and compressive capacities of the system, the strength degradation, and the energy dissipation (qualitative observations) from these plots. The energy dissipation capability of the tests can be compared from the hysteretic responses as tests with wider loops indicate more energy dissipated than those with more narrow, pinched loops.

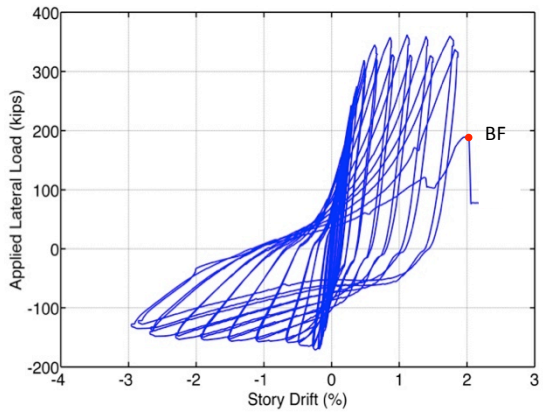

a. NHSS-B1

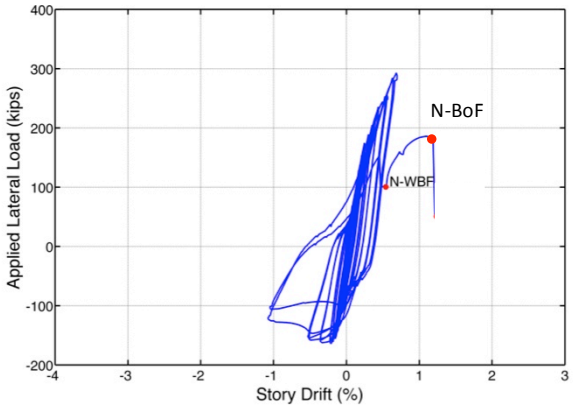

b. NHSS-B2

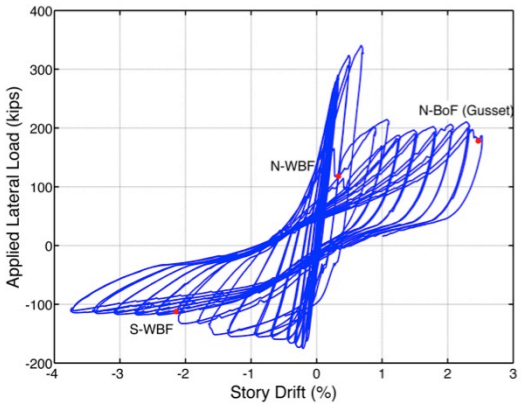

c. NHSS-B3

Figure 6.1 - Applied Story Shear vs. Story Drift Hysteretic Response

Brace fracture was the ultimate failure mode for NHSS-B1, and the other two specimens had less ductile failure modes of weld/bolt fractures in the NE and SW gusset plate connections. Despite its connection deficiencies, most notably the DCR values for bolt shear of 1.6 in the beam to column shear tab and 1.9 in the gusset plate to column shear tab, NHSS-B1 had reasonably good hysteretic behavior as compared to previous SCBF research (Johnson, 2005). Nevertheless, it experienced weld tearing at the beam to gusset plate interface in the NE corner, which was unexpected due to its low DCR value of 0.64 (per AISC equations in Chapter 3). If the strength of the gusset plate in tension is substituted for the expected tensile brace capacity for the demand, as recommended in Roeder et al. (2011), the DCR value was 1.1 and more closely reflects the specimen performance.

NHSS-B1 achieved 362 kip and -171 kip lateral load with the brace in tension, and compression, respectively. Prior to weld fracture in both NE and SW corners, NHSS-B3 reached a total load capacity range 16 kip less than NHSS-B1, with a comparable compressive buckling load. Its hysteretic behavior changed dramatically after beam to gusset plate welds in both the NE and SW connections fractured. After weld fracture, the system remained connected through the bolted gusset plate to column shear tabs, but the lateral load resistance decreased significantly. Again, NHSS-B3 had DCR values for bolt shear of 1.9 and 1.6 for the gusset plate to column and beam to column shear tabs, respectively, and yet these failure modes were not seen. NHSS-B2

had the least ductile response of the three NCBF specimens. It suffered rapid strength degradation shortly after brace buckling. The hysteretic loops indicate little damage or yielding prior to a 6 in. weld crack (WB2) that formed in the beam to gusset plate weld in the NE connection at -1% story drift. Weld fracture occurred shortly thereafter, but was not expected for this specimen because the AISC DCR value for interface weld fracture was only 0.56. Using the gusset plate strength however, NHSS-B2 had a DCR value of 1.5 for interface weld fracture, which was only slightly lower than the 1.6 DCR value for bolt shear in the column to gusset plate shear tab. These bolts failed immediately after weld fracture in the NE corner (same tension cycle).

Powell (2012) tested a pilot NCBF specimen (NCBF 32 as discussed in Chapter 2) and its applied lateral load versus story drift response was previously shown in Figure 2.14. Its response was similar to NHSS-B3, where despite an early connection failure resulting in large strength degradation, the system was able to continue to much higher drift levels at a decreased lateral load capacity. Prior to failure of the gusset plate to brace welds, the system resembled a combination of NHSS-B2 and NHSS-B3, with very narrow, tight hysteretic loops. At connection failure and large strength degradation, NCBF 32 had achieved a drift range of 1.3%. Its low total drift range also indicates it was the least ductile system.

6.2.2 Stiffness Comparisons

For each test the backbone envelope curve of the applied lateral load-displacement data was plotted. From these curves, the elastic stiffness (k_e), the post-yield stiffness (k_{pt}), and the post-buckling stiffness (k_{pc}) of the system were found using a linear fit to the segments; the slope of the applied lateral load versus displacement plot is the stiffness. The elastic stiffness is of interest to engineers when the braced frame system is subjected to smaller, more frequent earthquakes, as the system remains elastic at the lower displacement values. The post-buckling and post-yield stiffness values for the systems are more important when considering larger, more infrequent earthquakes. The stiffness values found for each of the specimens is shown in Table 6.2. A sample calculation of these values is illustrated with specimen NHSS-B1, shown in Figure 6.2.

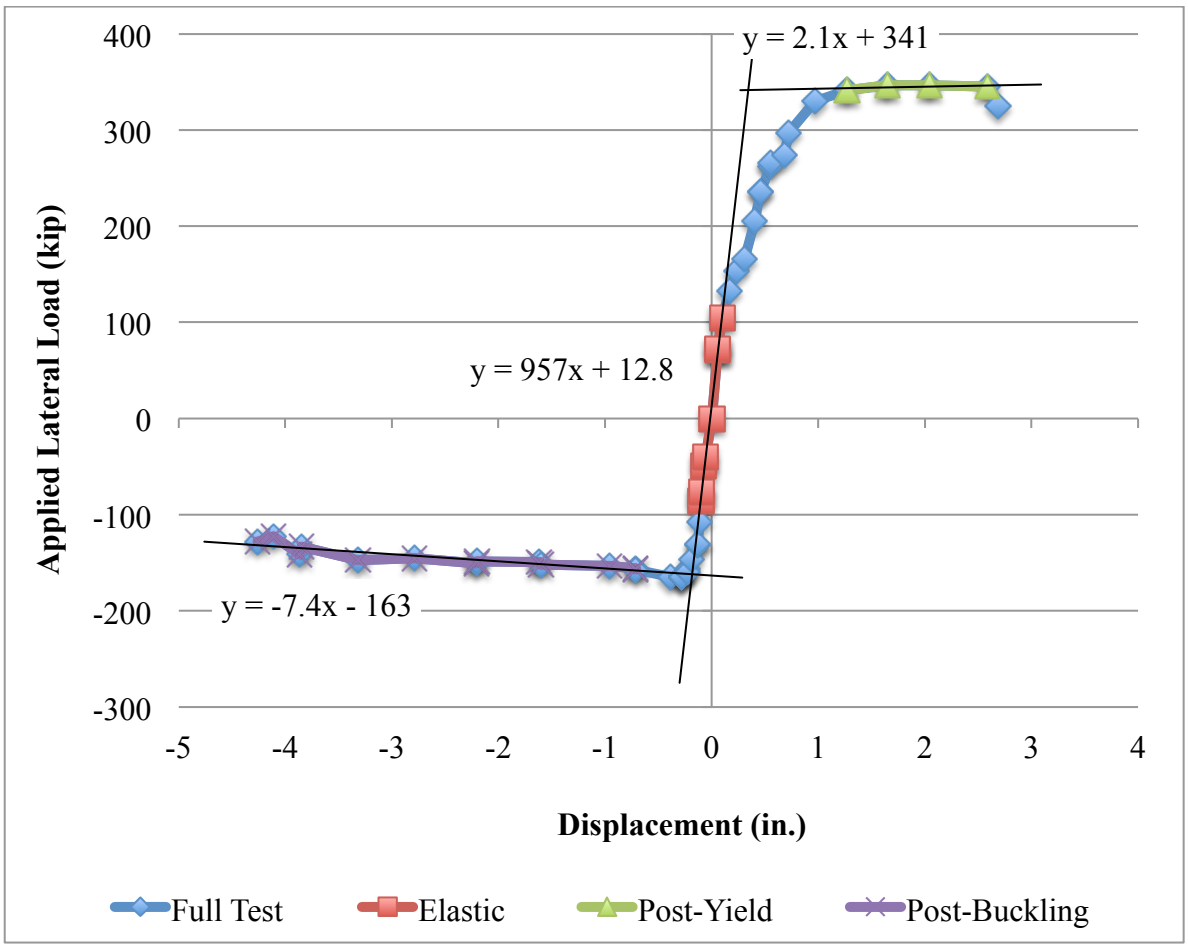

Figure 6.2 – Sample Stiffness Calculation for Specimen NHSS-B1

Table 6.2 – Stiffness Comparison of Test Specimens

Test Specimen	Elastic, k_e (k/in)	Post-Yield, k_{pt} (k/in)	Post-Buckling, k_{pc} (k/in)
NHSS-B1	957	2.1	-7.4
NHSS-B2	545	N/A	-39
NHSS-B3	807	13*	-14.7

**Post-weld fractures*

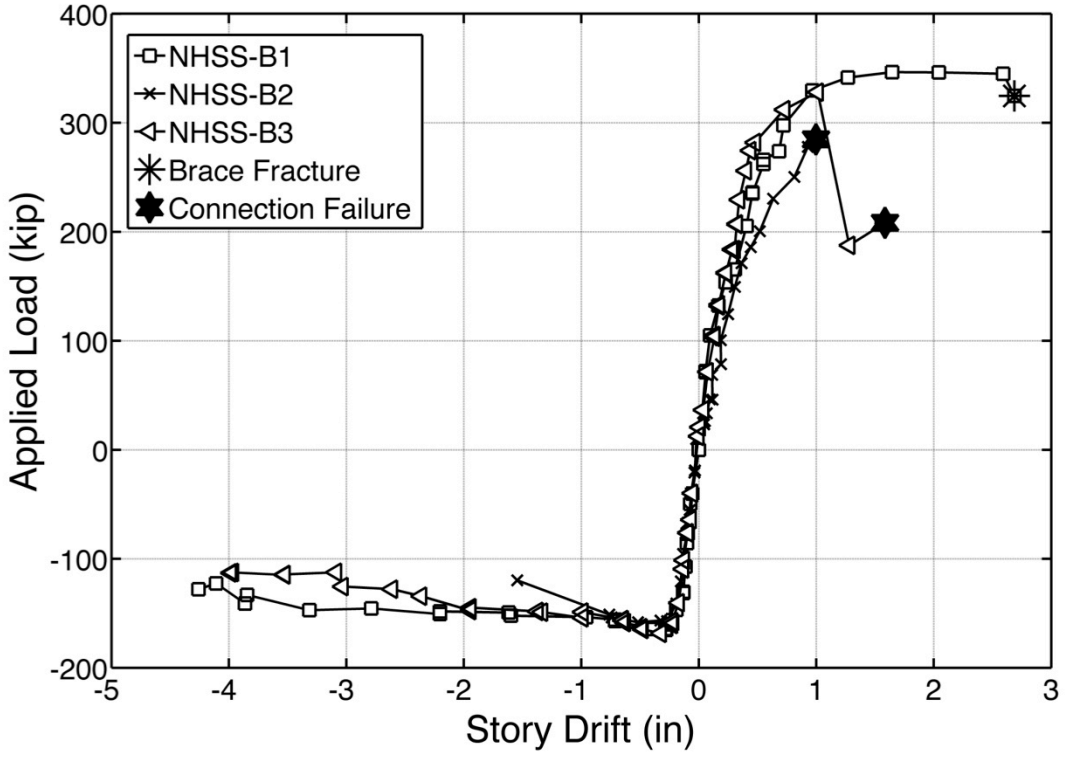

Figure 6.3 - Backbone Curves for NCBF Bolted Specimens

Figure 6.3 shows the backbone envelope curves for the three NCBF specimens. NHSS-B1 had the highest elastic stiffness, followed by NHSS-B3, and then NHSS-B2. The differences between NHSS-B3 and NHSS-B1 are that NHSS-B3 used a split shear tab to connect the beam and gusset plate to the column, and used a 1/2 in. thick gusset plate, while NHSS-B1 used a shared shear tab and a 3/4 in. thick gusset plate. The higher elastic stiffness for NHSS-B1, could be attributed to the thick plates and connecting the beam and gusset plate to the column with a single combined shear plate, since this configuration creates a more restrained corner connection. A value for the post-yield stiffness of NHSS-B2 and NHSS-B3 was not calculated as the frames' connections had brittle failures at lower drift levels. The post-yield stiffness value reported for NHSS-B3 in Table 6.2 was based upon the data collected after both the NE and SW connections beam to gusset plate weld's had fractured, and these fractures resulted in a drastic strength loss (not shown in Figure 6.3 for clarity). NHSS-B2 had an HSS6x6x1/4 brace section that was designed to have a lower kL/r value and saw more severe stiffness degradation in the system.

NHSS-B1 had the highest post-buckling stiffness value, followed by NHSS-B3, and then NHSS-B2. The increased flexibility of the NHSS-B2 system post-buckling could be attributed to the 6 in. weld crack that appeared suddenly in the NE beam to gusset plate connection around -1% story drift (-1.5in). NHSS-B1 had twice as high a post-buckling stiffness as NHSS-B3, again possibly because the shared shear tab and thicker gusset plate in NHSS-B1 provided a more restrained connection after brace buckling able to better distribute the load.

6.2.3 Energy Dissipation

A braced frame system dissipates energy through the inelastic buckling and yielding of its braces with secondary yielding of other elements. Energy dissipation is crucial to seismic lateral-load resisting systems because it dampens the structure's dynamic response to an earthquake. While a system with higher energy dissipation improves seismic performance, it does not guarantee a satisfactory performance. Systems that absorb large amounts of energy also sustain significant damage. This section compares the calculated total braced frame energy dissipated for each of the three specimens. The total energy is divided into energy dissipated from the brace and from other components of the system (framing elements, connection ductility, bolt deformation).

Energy dissipation is calculated using the applied lateral load and horizontal displacement values for each specimen. The energy dissipated per cycle is the area within one full hysteretic loop. The sum of these cycles gives the cumulative energy dissipated for the specimen. The trapezoidal rule, shown in Eq. (6-1) was used to calculate the area of the hysteretic loops. Figure 6.4 shows the calculation graphically. One caveat of this energy calculation is that the total energy dissipated is directly dependent on the number of cycles completed – the higher the drift achieved and the more cycles completed, the larger the total energy dissipated. Losses vary from test to test, and two frames can have different energy dissipation by virtue of differences in their deformation capacity and history.

$$E = \sum \left[\left(\frac{P_i + P_{i+1}}{2} \right) \cdot (\Delta_{i+1} - \Delta_i) \right] \quad (6\text{-}1)$$

where: $E =$ *total energy dissipated*

$P =$ *applied lateral load*

$\Delta =$ *displacement in direction of applied force*

$i =$ *increment*

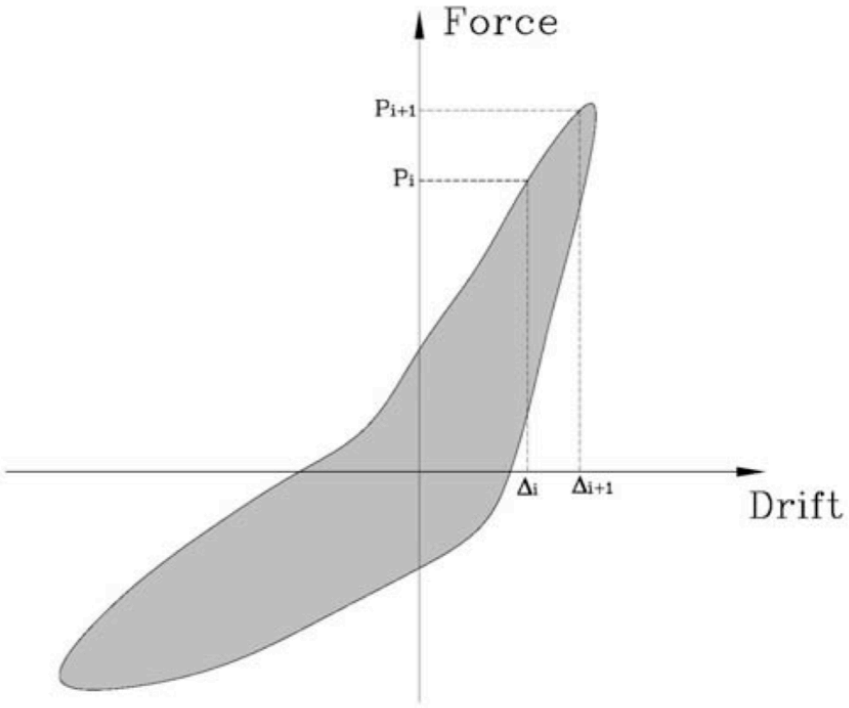

Figure 6.4 - Energy Dissipation Calculation (Kotulka, 2007)

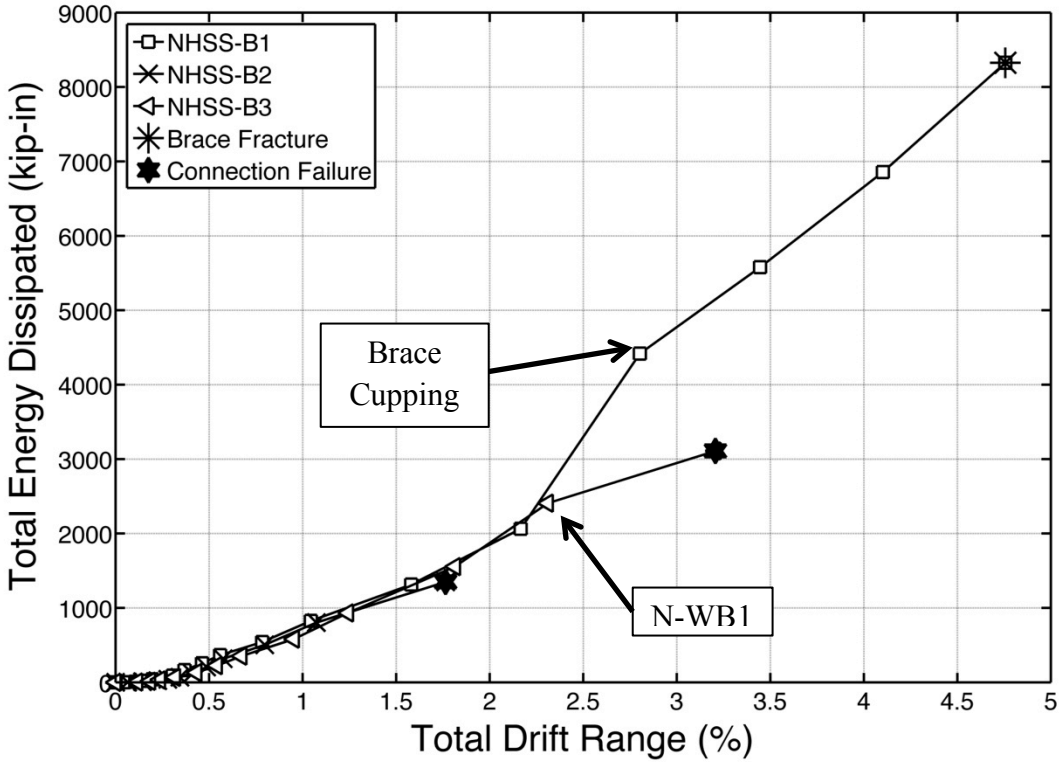

Figure 6.5 - Cumulative Braced Frame System Energy Dissipated for NCBF Specimens

Figure 6.5 shows the energy dissipated by the full braced frame system for the three bolted NCBF specimens, with failure modes indicated on the plot. The three specimens follow a similar energy versus total drift range curve until NHSS-B2 sustained weld fracture at the NE gusset plate to frame connection at the 1.75% total drift range with 1350 kip-in of energy dissipation. NHSS-B1 and NHSS-B3 continued to follow similar curves until the 2.25% drift range. NHSS-B3 sustained a sequence of weld fractures first in the NE then the SW gusset plate to beam connection at slightly larger drift ranges. By the second fracture at 3.2% total drift range, NHSS-B3 had dissipated 3110 kip-in.of energy dissipation. There was a large increase in energy dissipated at approximately 2.8% total drift range in NHSS-B1 when cupping developed at the plastic hinge. Following this drift range, the rate of energy dissipation in NHSS-B1 decreased. The local deformations in the brace walls at midspan increased in severity for NHSS-B1 until the brace fractured at close to 5% total drift range with 8325 kip-in energy dissipated.

Table 6.3 - Energy Dissipation Comparison

Specimen	Description	Total Energy Dissipated (kip-in)	% Energy Distribution		Total Drift Range (%)
			Brace	Other	
HSS-05	Specimen was designed during development of Balanced Design Procedure with a thinner gusset plate than AISC design procedures allow and 8t elliptical clearance.	6000*	80%	20%	4.3*
NCBF 32	Specimen was designed as a pilot NCBF test with a brace that did not meet current b/t limits for SCBFs and connections that were not designed for the expected brace capacity as required for SCBFs.	3057[a]	-	-	1.3
NHSS-B1	Specimen was designed to explore perceived deficiencies of NCBF bolted connections (bolt shear, brace net section, brace block shear) using a shared shear tab.	8325	69%	31%	4.9
NHSS-B2	Specimen was designed to explore perceived deficiencies of NCBF bolted connections (bolt shear & bearing, brace net section & block shear, beam to gusset base metal fracture) using a split shear tab and non-seismically compact brace.	1350	92%	8%	1.8
NHSS-B3	Specimen was designed to explore perceived deficiencies of NCBF bolted connections (bolt shear, brace net section & block shear) using a split shear tab and thinner gusset plate.	3110	83%	17%	3.2

[a]*This is the total energy dissipated for the system past 1.3% at which there was significant loss in lateral resistance.*

**Instrumentation problems did not allow for data collection after 4.3% drift range, however this connection reached close to 5% total drift range.*

Table 6.3 gives tabulated results for these bolted NCBF specimens. In addition, a previously tested NCBF (NCBF 32) and an SCBF with nearly optimal performance (HSS-05) are included. These additional specimens have nearly the same member sizes allowing energy dissipation to be

directly compared, where the difference largely reflects specimen behavior. HSS-05 is considered the "upper-bound" of previously tested SCBF specimens at the UW because of its optimal performance. However, the full energy dissipation of HSS-05 is not included because key instruments were not functional in the final cycles of that test. The table provides a brief description of each specimen, the total energy dissipated, the total drift range achieved, and distributes the total energy into energy dissipated by the brace and other sources, including frame yielding, plate yielding, bolt deformation, bolt hole elongation, and other system inelastic deformations.

NHSS-B1 had a desirable failure mode of brace fracture and also dissipated more energy than the other NCBF specimens, despite its numerous deficiencies. Comparing NHSS-B1 to HSS-05 at the drift range of about 4.3%, HSS-05 had a total energy dissipation of 6000 kip-in while NHSS-B1 had a total energy dissipation of about 7000 kip-in. This observation is significant because NHSS-B1 had a highly deficient connection (described in Chapter 3) and HSS-05 was designed to meet current seismic requirements.

The horizontal component of the brace axial force versus displacement plot was used to determine the energy dissipated by the brace. The energy was calculated as the area within one hysteretic loop and the total energy as the sum of all hysteretic loops. 80% of HSS-05's energy dissipation capacity came from the brace, whereas NHSS-B1 only dissipated 69% of its energy through the brace. NHSS-B2 dissipated 92% of its energy through the brace, which was the most of the specimens. NHSS-B3 dissipated 83% of its energy through the brace. NHSS-B1 also dissipated energy through significant yielding, local flange buckling sustained in both columns and the south beam, and bolt hole elongation and deformation.

NHSS-B1 was the only specimen with a shared shear tab configuration, and this may have benefited the distribution of energy dissipation. This shared shear tab more evenly distributed the brace demand to the bolts connecting the beam to column and gusset plate to column connections, resulting in widespread bolt hole elongation and bolt deformation in the majority of the bolts. NHSS-B3 had even more bolt hole elongation and deformation, but only after the

specimen had lost a significant amount of its load capacity and was therefore not considered in the energy calculations.

NHSS-B2 used a non-compact brace with thin walls unable to resist the large strain demands at the plastic hinge location. There was very little other yielding or deformation in the system aside from the brace plastic hinge. The weld tearing that occurred and resulted in a connection failure was sudden and brittle and therefore did not absorb much energy. Similarly, NHSS-B3 did not see much frame or gusset plate yielding in early cycles. NHSS-B3 had similar brittle weld tearing that led to a connection failure at early cycles. NCBF 32 also failed at a small, 1.5% total drift range due to weld fracture at the brace to gusset plate connection. The specimen then functioned at dramatically reduced strength for significantly larger drift levels, and its total energy was comparable to NHSS-B3 (Hsiao et al., 2011).

6.2.4 Post-Failure Behavior

When the beam to column connections remained connected after initial fracture of the brace or welded joints, the frame was cycled to increasing drift levels, to determine the residual strength and stiffness of the system after the initial failure mode. This residual performance is important in the event of large, infrequent earthquakes that fail a connection or fracture a brace during the seismic event. The applied lateral load versus displacement response was generated for each specimen with post-fracture data. The residual stiffness of the frame was calculated from the slope of the entire post-failure data. Table 6.4 reports the stiffness results from the specimens, and Figure 6.6 shows the applied lateral load versus story drift responses for the tests.

The post-failure strength and stiffness values were primarily based on moment frame action. NHSS-B3 was the only specimen that did not result in brace fracture or a complete disconnection of the gusset plate from its framing elements. No portion of the brace was removed, and the post-failure cycles to the frame were completed continuously, as shown in Figure 6.1e.

NHSS-B3 had a much larger residual strength and stiffness value than the other two NCBF specimens, as the brace remained connected to the framing elements. NHSS-B2 had the higher post-weld fracture stiffness of 32 kip/in, despite a complete loss of the NE gusset plate due to

weld fracture. NHSS-B1 had the lowest post-failure stiffness of 21 kip/in, despite having a brace fracture with the gusset plates partially in tact. One contributor to the low stiffness value could have been from the SW corner, which had a weld crack that grew in the CJP weld and base metal for the entire length of the gusset plate to column shear tab connection. This frame also had considerable bolt hole elongation, which could have contributed to the low post-failure stiffness.

Table 6.4 - Post-Failure Stiffness Comparison

Specimen	Test Goal	Failure Mode	Post-Failure Stiffness (k/in)	Percent of Initial Stiffness (%)
NHSS-B1	Specimen was designed to explore perceived deficiencies of NCBF bolted connections (bolt shear, brace net section, brace block shear) using a shared shear tab.	Brace Fracture	21	2.2%
NHSS-B2	Specimen was designed to explore perceived deficiencies of NCBF bolted connections (bolt shear & bearing, brace net section & block shear, beam to gusset base metal fracture) using a split shear tab and non-seismically compact brace.	Connection Failure	32	5.9%
NHSS-B3	Specimen was designed to explore perceived deficiencies of NCBF bolted connections (bolt shear, brace net section & block shear) using a split shear tab and thinner gusset plate.	Connection Failure	N/A	N/A

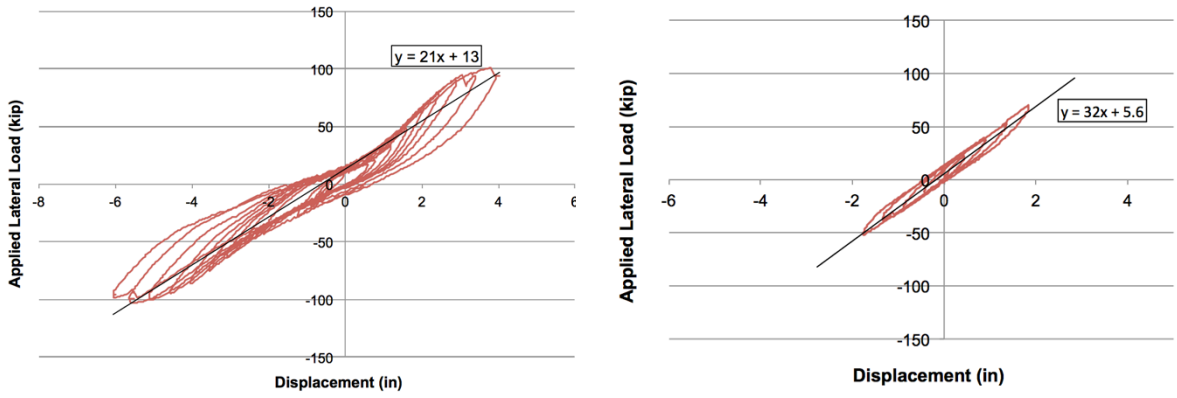

a. NHSS-B1 **b. NHSS-B2**

Figure 6.6 - Post-Fracture Applied Lateral Load vs. Displacement Response

6.3 Gusset Plate Connection Response

Modern SCBF connections are required to provide rotational clearance on the gusset plate (typically linear $2t_p$) to accommodate the demand from the brace end rotation, but older NCBF specimens, such as described in this thesis, were not required to provide this clearance for rotational demand.

The OOP gusset plate rotations were determined using Optotrak LED sensors placed on top of the gusset plate. Figure 6.8 shows an example of the LEDs used to plot the gusset plate OOP displaced shape. For the maximum OOP gusset plate rotation, the LEDs marked #1 and #2 in Figure 6.8 were used. The rotation (θ) was found by taking the arcsine of the OOP displacement at #2 (d_z) divided by the distance between the two markers (R), as shown in Eq. (6-2) and Figure 6.7. The gusset plate distance between the two markers was assumed to remain constant (ignoring any elongation in the plate) and the OOP displacement was taken as the changing variable. The hysteretic response for these maximum OOP displacements are shown in Figure 6.9. These plots were not obtained for NHSS-B2 because of limitations in the test data.

$$\theta = \sin^{-1}\left({}^{d_z}/_{R}\right) \tag{6-2}$$

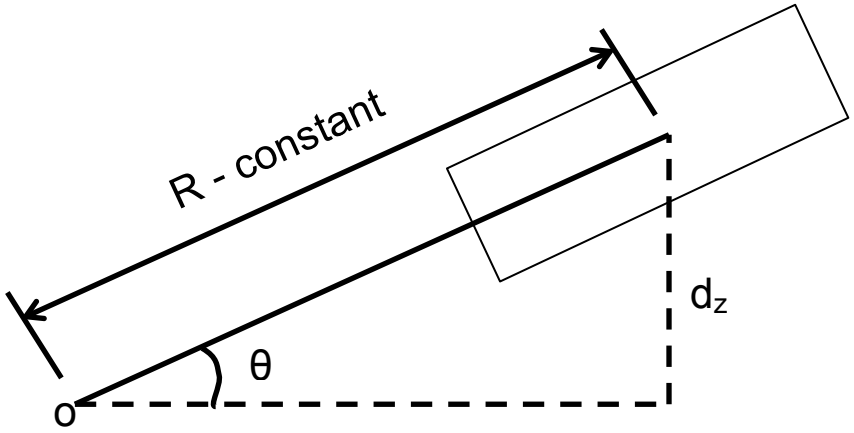

Figure 6.7 - Diagram of OOP Gusset Plate Rotation

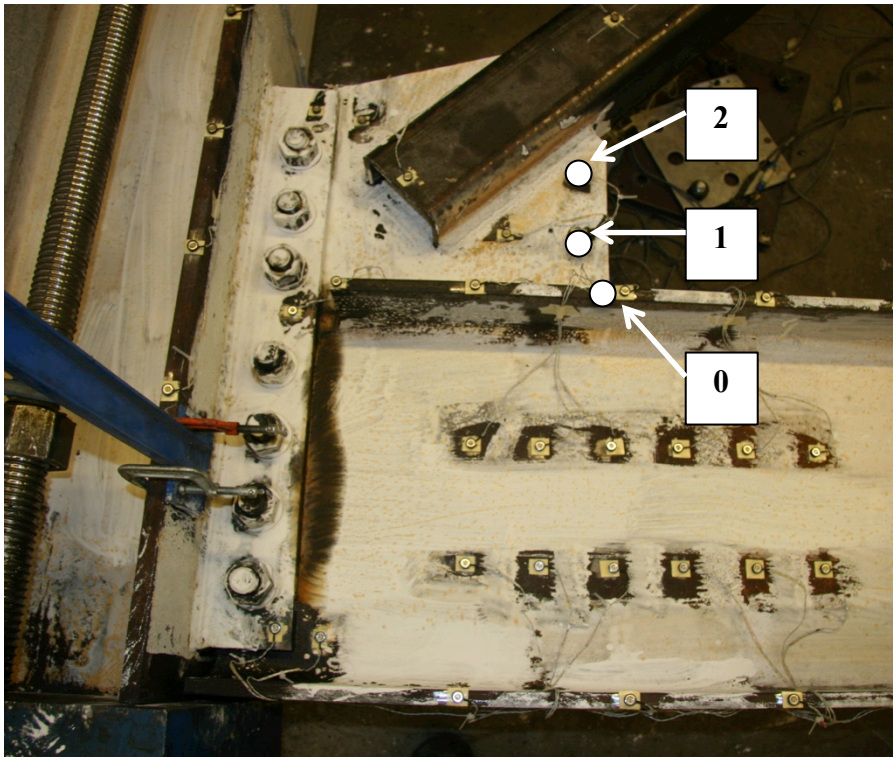

Figure 6.8 - LEDs used to Plot Gusset Plate OOP Displaced Shape (from Specimen NHSS-B1)

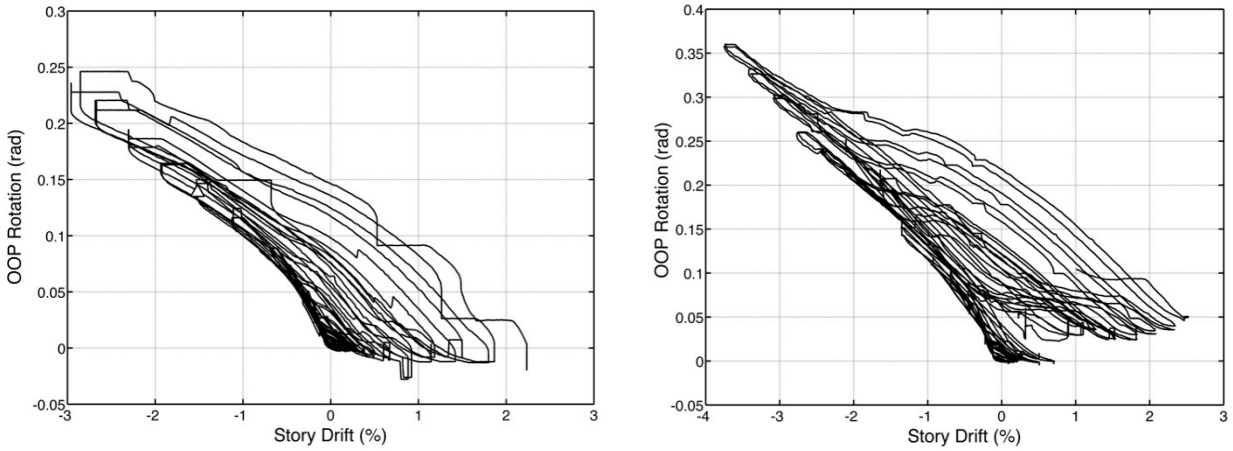

a. NHSS-B1 **b. NHSS-B3**

Figure 6.9 - Hysteretic Response for Maximum Gusset Plate OOP Rotation

Figure 6.9 shows that NHSS-B3 had the highest gusset plate OOP rotation. However, the beam-gusset interface welds fractured fairly early in the experiment. The fracture allowed a large portion of the gusset plate to rotate because it was no longer fixed to the beam. Further, these markers have some inherent inaccuracy because the gusset plate became disconnected from the beam flange at larger drift levels.

Additionally, the OOP displacement of the gusset plate was plotted along the length of the gusset plate connection at each LED marker, shown in Figure 6.10. The marker on the beam is at the "0 in." length along the gusset plate. These displacements are compared with photos from the specimen to provide assurance the calculations were reasonable and are also shown in Figure 6.10. From Figure 6.10, it can be seen the photos have a generally good correlation with what the data reflects. NHSS-B1 had somewhat smaller gusset plate rotations and displacements as shown in Figure 6.9 and Figure 6.10. Additionally, between markers "0" and "1" there is a line with the same slope as between "1" and "2" when the gusset plate to beam weld had not fractured. NHSS-B3 has a kink in these lines at -3.7% drift, after the weld had fractured and was moving OOP disconnected from the beam.

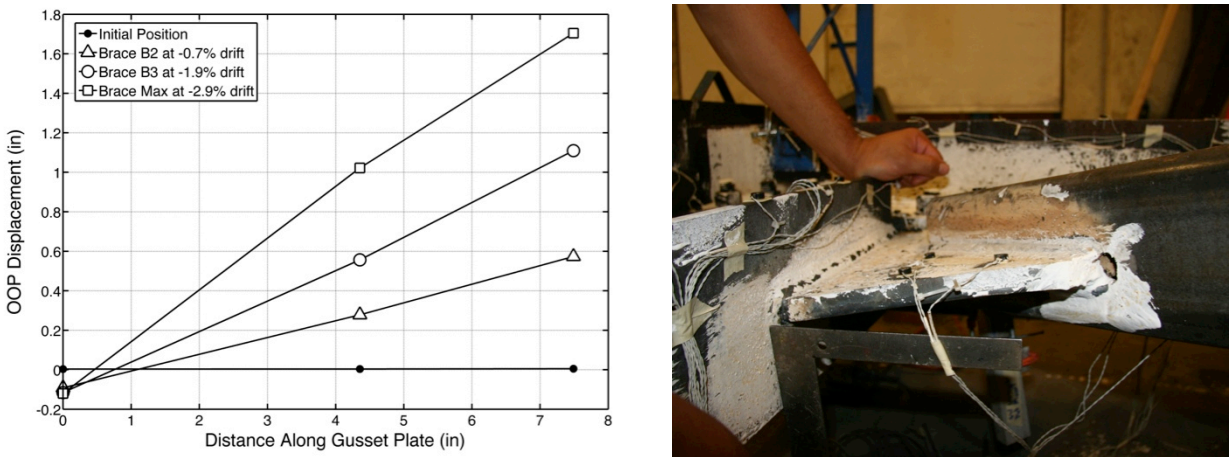

a. NHSS-B1 (Photo at -2.3%)

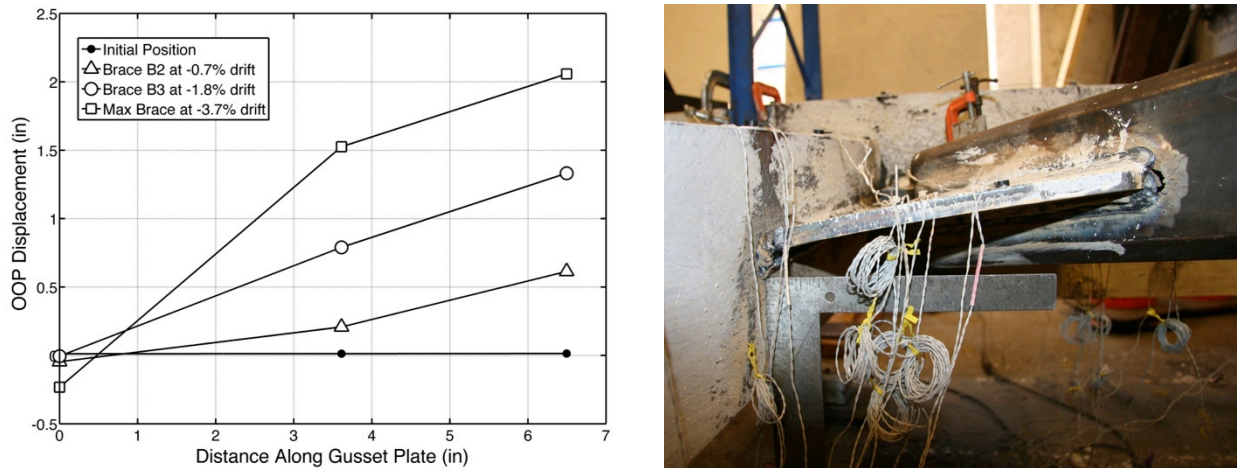

b. NHSS-B3 (Photo at -1.6%)

Figure 6.10 - Gusset Plate OOP Displacement along Gusset Plate Length

6.4 Bolt Damage

NCBF specimens used 1 in. diameter A325 bolts whose yield mechanisms and failure modes were previously described in Chapter 2, and their bolt damage photos and diagrams were shown in Chapter 5. A tabulated presentation of this data for the NCBF specimens is given in Table 6.5 and Table 6.6, with the bolts and bolt holes are numbered in Figure 6.11.

All three NCBF specimens had DCR values between 1.6 and 1.9 for bolt shear. These high DCR values were perceived as the primary deficiency of all three specimens. However, bolt shear was not the failure mode for any of these tests. Bolt shear failures in the gusset plate connection occurred in NHSS-B2 after the gusset plate to beam weld in the NE corner had fractured. Additionally, one bolt fractured in NHSS-B3 in the last tension cycle of the frame well after there was a significant loss in strength in the system caused by weld fractures.

These specimens also had high bolt bearing DCR values for the beam to column connection, and bolt hole elongation was visible in the beam web in all three specimens to varying degrees of severity. NHSS-B3 also had a high DCR value for gusset plate to column bolt bearing (due to the thinner gusset plate), and it had significant bolt hole elongation in the gusset plate. However, bolt tearout did not occur in any specimen. Note that the beam web thickness for the NHSS specimens was thinner than the reference connections, and therefore, there would likely be less bolt hole elongation in those reference connections.

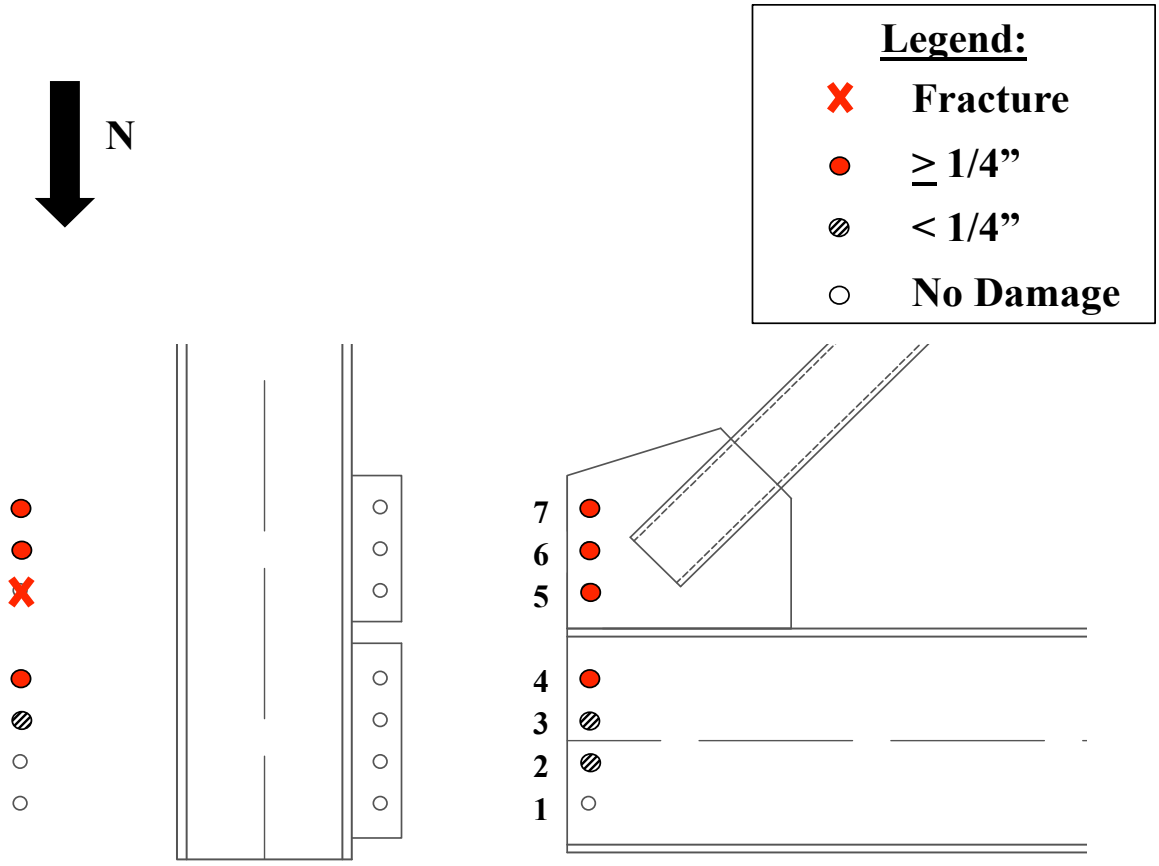

Figure 6.11 - Bolt/Hole Numbering for NCBF Specimens

Table 6.5 - Bolt Hole Elongation per NCBF Specimen

Bolt Hole Number	Amount of Elongation (in.)	NHSS-B1	NHSS-B2	NHSS-B3
1	None		X	X
	<1/4			
	≥1/4	X		
2	None		X	
	<1/4	X		X
	≥1/4			
3	None		X	
	<1/4	X		X
	≥1/4			

4	None			
	<1/4	X	X	
	≥1/4			X
5	None			
	<1/4	X	X (ST)	
	≥1/4			X
6	None			
	<1/4	X	X (ST)	
	≥1/4			X
7	None			
	<1/4	X	X (ST)	
	≥1/4			X

Table 6.6 - Bolt Deformation of NCBF Specimens

Bolt Number	Behavior	NHSS-B1	NHSS-B2	NHSS-B3
1	None	X	X	X
	Deformation			
	Fracture			
2	None	X	X	X
	Deformation			
	Fracture			
3	None	X	X	
	Deformation			X
	Fracture			
4	None	X	X	
	Deformation			X
	Fracture			

5	None			
	Deformation	X		
	Fracture		**X**	**X**
6	None			
	Deformation	X		X
	Fracture		**X**	
7	None			
	Deformation	X		X
	Fracture		**X**	

6.5 Weld Damage

As seen from the test observations in Chapter 5, weld tearing and fracture was significant in these specimens. This weld tearing was surprising, as the specimens all had beam to gusset plate interface weld DCR values between 0.6 and 0.7. The welds connecting the shear tabs to the columns were CJP welds and were not deficient. Figure 6.12 shows a bar chart of the extent of weld tearing for each specimen and HSS-05 at the interface welds at the end of each test. The chart is normalized on the y-axis by the total interface weld length. Welds with a measure of 1 experienced complete weld fracture. The welds were measured throughout the test as they were observed. There was no observed weld tearing in the beam to column shear tab welds. As mentioned from Chapter 2, HSS-05 was considered the best SCBF performance by a BDP designed connection, but this connection had ductile weld tearing in multiple locations throughout the experiment.

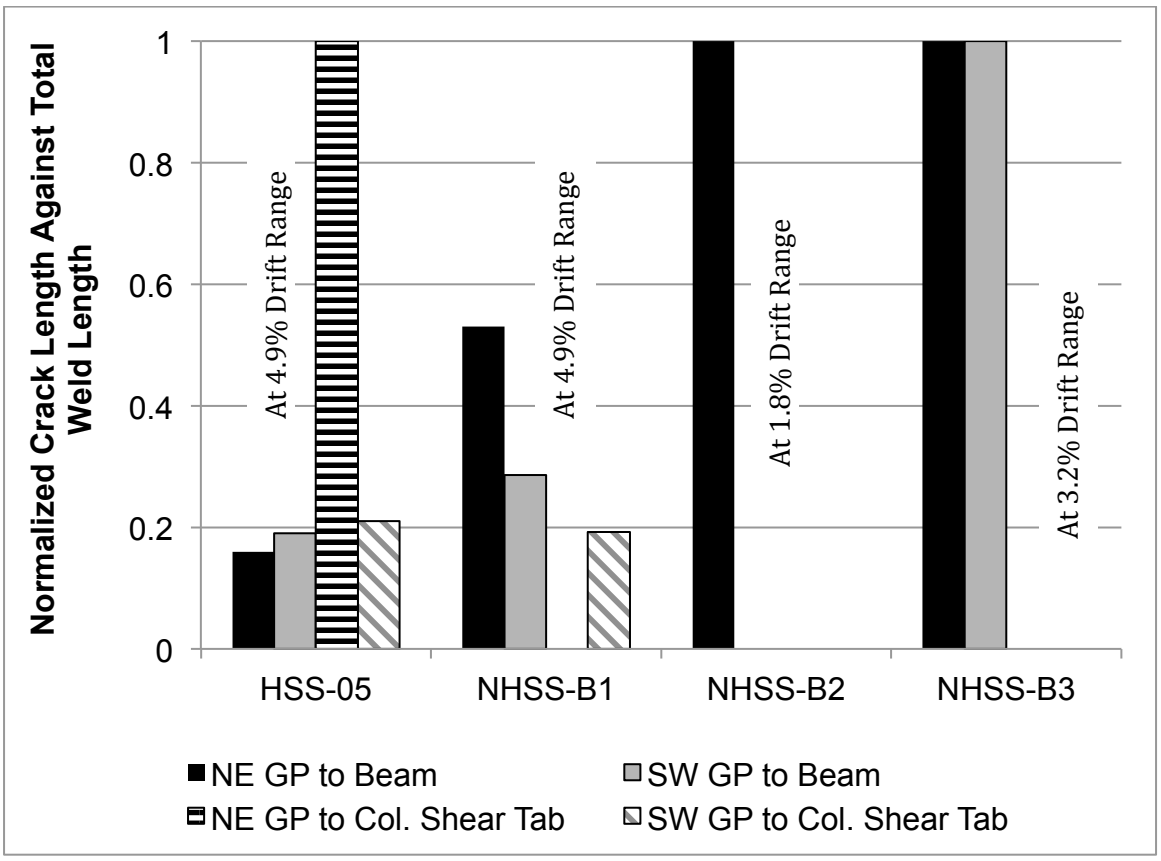

Figure 6.12 - Normalized Weld Crack Length for Each Specimen Compared to HSS-05

Weld fracture of the NE beam to gusset plate weld was the failure mode for two of the three specimens. Specimens NHSS-B2 and NHSS-B3 had concentrated weld tearing at that interface weld, and NHSS-B3 also had weld tearing in the SW gusset plate to beam weld. NHSS-B1, on the other hand, had more distributed weld tearing throughout all gusset plate and shear tab interface welds (except the NE gusset plate to column shear tab weld). NHSS-B1 developed a weld tear in the CJP weld in the SW shared gusset plate shear tab and as the weld propagated, it crossed from the base metal (in the heat affected zone) back through the CJP weld.

The DCR values computed with the brace strength as the demand were compared to those found using the strength of the gusset plate as the demand in Table 6.7. The DCR values using the gusset plate strength are consistently higher than the AISC DCR values (using the brace strength) and for all specimens the fillet weld sizes were under-designed. The BDP calculates this weld based on the expected tensile capacity of the gusset plate, which allows for inelastic deformation

of the plate within the weld calculation. NHSS-B2 and NHSS-B3 had fracture of the beam to gusset plate weld, and similarly, also had the highest DCR values using the gusset plate strength.

Table 6.7 - Comparison of Beam to Gusset Plate Weld DCR using Different Demands

Demand	NCBF Specimens			
	Average NHSS-Ref	NHSS-B1	NHSS-B2	NHSS-B3
AISC (strength of brace)	1.24	0.64	0.56	0.66
BDP (strength of gusset plate)	**2.69**	**1.1**	**1.5**	**1.4**

With the discrepancy from using two different demands noted, the data was used to investigate whether there were commonalities between all specimens that could be related to weld tearing initiation. Table 6.8 provides data on initial weld tearing correlations in the beam to gusset plate weld in the NE corner. It lists the initial weld crack length observed and the total drift range at which this initial crack appeared. Both the brace end rotation and the gusset plate rotation in the NE corner were calculated and are presented in the table at the rotation value when initial weld tearing occurred. Finally, the table compares the cycle number where initial weld tearing appeared.

Table 6.8 - Initial Weld Tearing Correlations in NE Beam to Gusset Plate Weld

Specimen	Initial Weld Crack Length (in)	Total Drift Range (%)	Brace End Rotation (rad)	GP Rotation (rad)	Cycle
NHSS-B1	1/8	2.2	0.15	0.14	23
NHSS-B2	6	1.8	0.10	0.10	21
NHSS-B3	1	1.9	0.14	0.14	21

Regardless of the gusset plate geometry, connection configuration, brace size, or initial crack length, initial weld tearing occurred at very similar total drift ranges for all specimens. NHSS-B1 saw initial weld tearing at the highest total drift range (with the lowest DCR from the gusset plate demand). As expected, the brace end rotation and the gusset plate rotation yielded consistent values for observation of initial weld tearing. The table shows that, NHSS-B2 had the lowest OOP gusset plate and brace end rotation value at initial weld tearing, and NHSS-B1 had the highest OOP gusset plate and brace end rotation values at initial weld tearing, because it was able to achieve the highest drift range prior to initial weld tearing. The shared shear tab in NHSS-B1 likely relieved stress on the beam to gusset plate weld, allowing increased OOP rotation and increased drift ranges prior to weld tearing initiation.

Table 6.8 can be used in conjunction with Table 6.9 to draw further conclusions about the beam to gusset plate weld tearing. Table 6.9 lists the number of cycles completed after initial weld tearing prior to weld fracture, and lists whether this weld fracture was the failure mode of the specimen. The two NCBF specimens that had beam to gusset plate weld fracture were only to achieve two to three cycles before weld fracture, due to the low toughness weld material. As seen from this section, the gusset plate to beam weld presents a severe vulnerability for older CBFs.

Table 6.9 - Weld Propagation Information for NE Beam to Gusset Plate Weld

Specimen	Cycles to Failure after Initial Weld Tearing	Cause of Failure?
NHSS-B1	Did Not Fail.	NO
NHSS-B2	2	YES
NHSS-B3	3	YES

6.6 Brace Response

A typical progression of brace fracture from cyclic loading (as typical for SCBFs) is illustrated in Figure 6.13 and was only seen in specimen NHSS-B1. Stage 1 shows the initial buckling of the brace, which occurred when the brace was loaded in compression and surpassed its buckling capacity. As the compressive drift levels increased, the brace OOP displacement increased and a plastic hinge formed at the brace midspan, shown in Stage 2. Stage 3 occurred as the brace was loaded in tension after a plastic hinge had formed and there was residual OOP displacement at midspan due to high strain concentrations in the plastic hinge region at zero applied load. In Stage 4, as the brace was pulled towards a peak tension displacement, there was again increased strain concentrations at the plastic hinge location. In Stage 5, there was uneven tensile yielding in the brace, mostly concentrated near the plastic hinge region. Finally, in Stage 6 the brace began to tear in tension at the corners of the plastic hinge region where the strain concentrations were the highest. As the brace was pulled further in tension, the tears propagated through the thickness of the brace and the brace fractured.

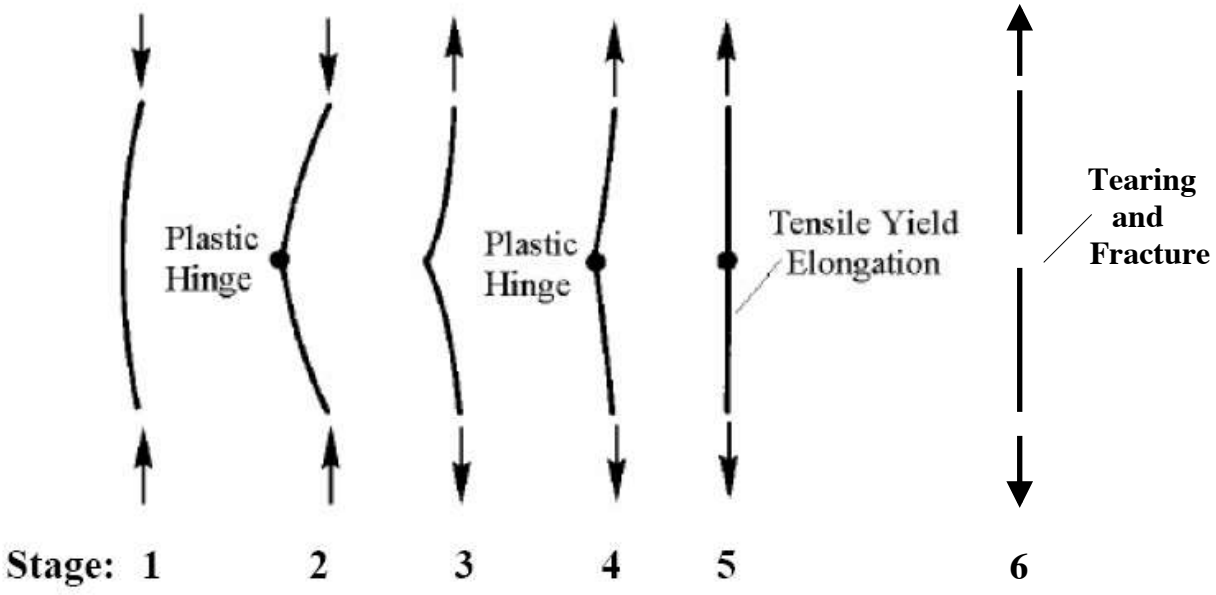

Figure 6.13 - Idealized Inelastic Brace Behavior Under Cyclic Loading [Modified from Powell, 2010]

Although brace fracture only occurred in one of the three bolted NCBF specimens, brace response is still important to observe in the NCBF specimens. Table 6.10 shows the buckling and damage progression of each brace for the test specimens. The specific drift ranges for each performance state can be found in the respective specimen sections in Chapter 5. All specimens used an HSS5x5x3/8 except for NHSS-B2, which used a non-seismically compact HSS6x6x1/4. The performance states in the table were defined in Chapter 5. The brace axial force versus displacement plots shown in Figure 6.16 were used to identify when the brace initially buckled, B1. Initial brace buckling occurred at the drift when the brace axial force reached a maximum compressive value.

Table 6.10 - Comparison of Brace Performance States

CYCLE	Brace		
	NHSS-B1	NHSS-B2	NHSS-B3
1 2			
3 4			
5 6			
7 8			
9 10			
11 12			B1
13 14	B1	B1	
15 16			
17 18			B2
19 20	B2		
21 22		B2 - cupping	
23 24	B3		B3
25 26			
27 28	B3 - cupping		IPB1
29 30			
31 32	BT		
33 34	BF - END		
35 36			B3 - cupping
37 38			

NHSS-B1 and NHSS-B2 are directly comparable for brace performance states as both used an HSS5x5x3/8. The differences between the two connections were NHSS-B1 used a shared shear tab, while NHSS-B3 used a split shear tab to connect the beam and gusset plate to the column. In addition, NHSS-B1 used a 3/4 in. thick gusset plate while NHSS-B3 used a 1/2 in. thick gusset plate. The two braces appeared to buckle around the same cycle, and reach B2 and B3 around the same cycle, as seen in Table 6.10. NHSS-B3 experienced weld fractures connecting the gusset plate to beam in both gusset plate connections at cycle 26 and subsequently lost a substantial amount of its resistance. Because of the significantly increased flexibility in gusset plate corners caused by weld cracking, the curvature at brace midspan for NHSS-B3 was not as concentrated as in NHSS-B1. NHSS-B1 developed cupping in the brace walls at midspan during cycle 27 and eventually the brace fractured in cycle 33, as noted in Table 6.10. NHSS-B3 did not appear to show local deformation in the brace walls until cycle 35. The brace for NHSS-B3 never fractured.

NHSS-B2 used a non-seismically compact brace HSS6x6x1/4 but buckled around the same drift value as the HSS5x5x3/8 braces, as noted in Table 6.10. The brace developed cupping earlier than the other specimens – at performance state B2 rather than B3, shown in Table 6.10. The seismically compact braces were able to sustain much larger OOP displacements, over 7 in. more OOP displacement than in NHSS-B2. The tests with seismically compact braces were also able to resist local damage to the brace in the hinge location for more cycles than NHSS-B2. Ultimately, while the brace was beginning to tear, the specimen had a connection failure when the beam to gusset plate weld fractured causing the bolts in the gusset plate to column shear tab to fracture. Because of the evidence of tearing, it is suspected that the brace would have failed within a couple cycles.

6.6.1 Experimental effective length factor, *k*

In practice, an effective length factor, *k,* of 1.0 is often assumed to estimate the expected brace buckling capacity. This capacity depends upon the effective slenderness, kL/r, of the brace members, where *k* is the effective length coefficient, *L* is the true length of the brace, and *r* is the

radius of gyration of the brace. The AISC Seismic Provisions place an upper limit to preclude dynamic effects associated with extremely slender braces.

Table 6.11 compares the experimental brace buckling load (P_{cr}) to the expected AISC critical buckling load (P_n), where P_n uses R_yF_y in place of F_y. The experimental brace buckling load was found from the brace axial force versus story drift graphs and this experimental brace buckling load was used to calculate the experimental effective length factor, k_{exp}, for each test. A k_{exp} value around 1 represents gusset plate connections that behave similar to a theoretical pinned end connection. A k_{exp} value greater than 1 indicates a larger effective length and a k_{exp} value less than 1, represents a smaller effective length. These experimental effective length factors were then used to compute the experimental slenderness ratios ($k_{exp}L/r$) for each test.

Table 6.11 - Comparison of Experimental Brace Quantities

Test Specimen	L_{br} (in)	Experimental P_{cr} (kip)	AISC $P_n=F_{cr}A_g$ (kip)	P_{cr}/P_n	Experimental Effective Length Factor, K_{exp}	Experimental Slenderness Ratio, $K_{exp}L_{br}/r$
NHSS-B1	167.3	186	191	0.98	1.1	94.8
NHSS-B2	167.3	201	217	0.92	1.1	77.2
NHSS-B3	167.3	199	191	1.04	0.97	86.8

Table 6.11 shows that experimental effective length factors of close to 1.0 were found for all specimens. Therefore, using the brace length as the true end-to-end length and a *k* value of 1.0 is recommended for computing the compressive strength in braced frames for these types of NCBF bolted gusset plate connections.

6.6.2 Brace Axial Force versus Drift Response

The brace axial force was calculated by two different methods. The first method measures the strain of four gauges placed one quarter of the brace depth from the SW corner on the center of each brace wall. While the brace remains elastic, an average of the four readings can be used to

find the brace axial force. Once the brace had yielded, a bilinear constitutive model following the coupon data results was used to model the non-linear behavior. The brace axial force calculation for the first method is shown in Eq. (6-3).

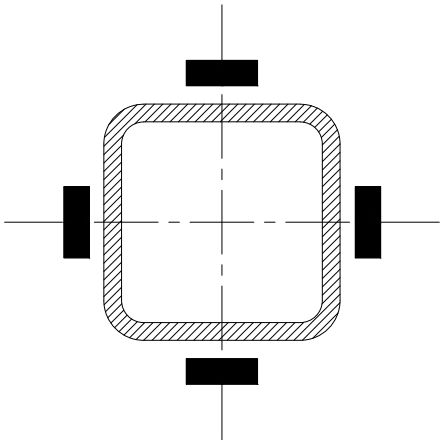

Figure 6.14 - Cross Section of Brace Showing Strain Gauge Layout

$$P_{brace} = \left[\frac{(\varepsilon_1 + \varepsilon_2 + \varepsilon_3 + \varepsilon_4)}{4}\right] \cdot E \cdot A_{brace} \tag{6-3}$$

where: $P_{brace} =$ *brace axial force (kip)*

$\varepsilon =$ *brace strain from gauge*

$E =$ *brace elastic modulus (ksi)*

$A_{brace} =$ *brace area (in^2)*

The second method for calculating the brace axial force is by equilibrium – using the column shears and the applied actuator load. The column moments were determined from two sets of strain gauges placed on the two extreme fibers at the center of the column flanges and located at each end of the column where the column was anticipated to remain elastic. Once the moments were found at each end of the column, the constant shear along the column (no external forces

applied) is determined by equilibrium. The sum of the two column shears represents the total shear force due to flexure of the frame. This shear in the frame was subtracted from the applied lateral load from the actuator and divided by the cosine of 45° (original brace angle). Figure 6.15 illustrates these calculations from the second method.

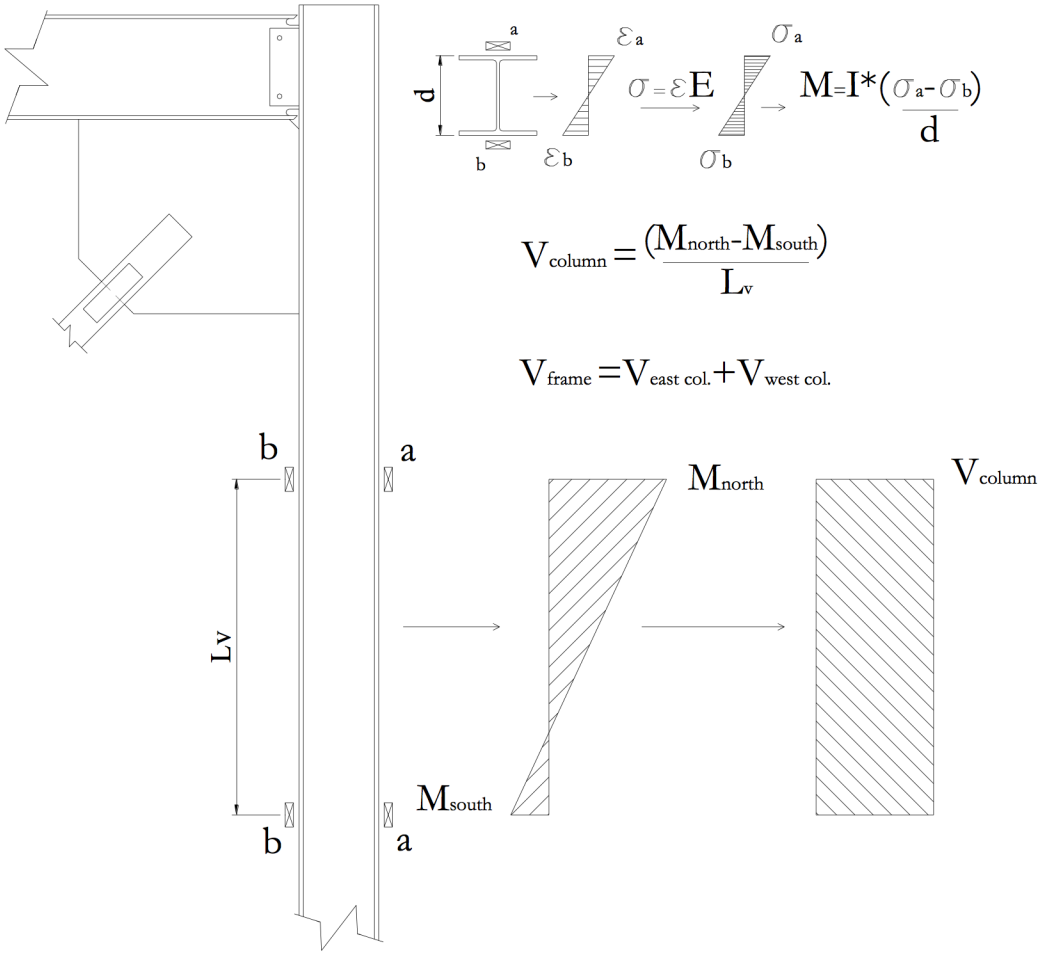

Figure 6.15 - Column Shear Calculations from Strain Gauges

Figure 6.16 shows each specimen's brace axial force normalized by the expected brace tensile capacity, $P_y = R_y F_y A_g$, plotted against the story drift. The axial forces for NHSS-B2 and NHSS-B3 were calculated using method 2, but NHSS-B1 used method 1 and the expected brace material properties. Table 6.12 highlights the peak tension and compression brace force normalized by the expected yield strength of the brace. This table also includes the maximum brace OOP displacement.

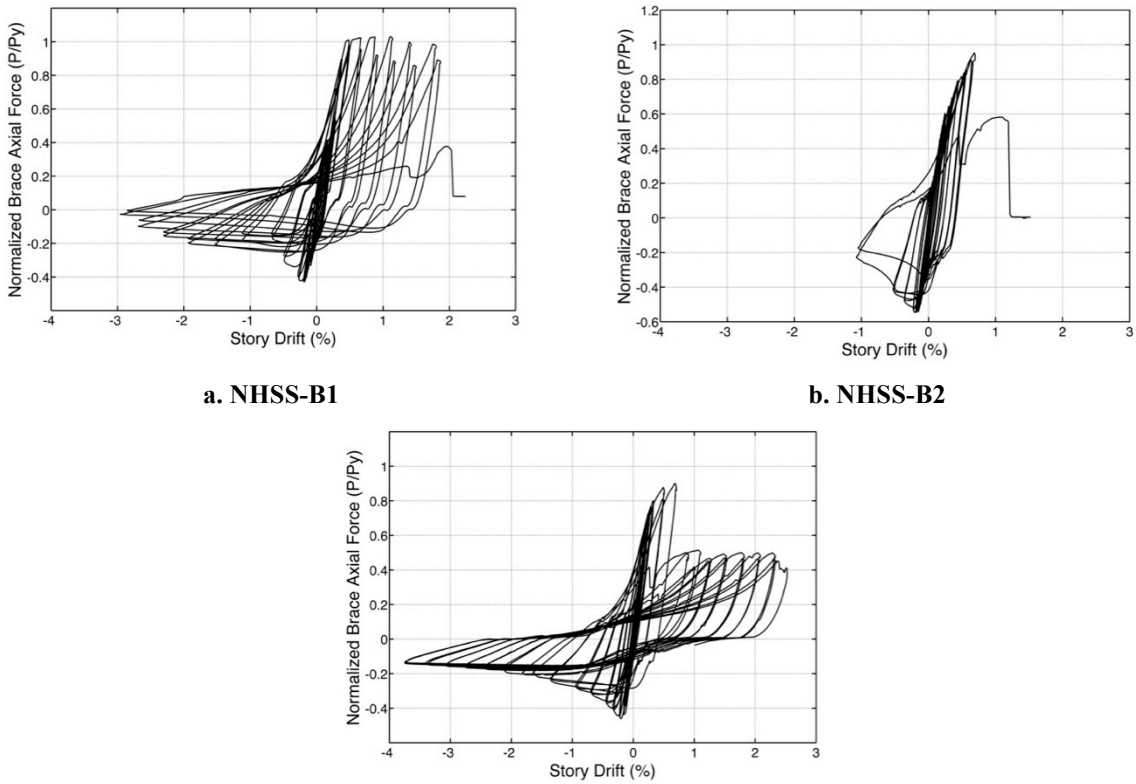

a. NHSS-B1

b. NHSS-B2

c. NHSS-B3

Figure 6.16 – Normalized Brace Axial Force (P/Py) vs. Story Drift (%) for Each Test Specimen

Table 6.12 - Brace Quantity Comparisons

Specimen	Description	Max. Brace Midspan Displacement (in)	Max. Normalized Brace Axial Force		Max. Brace Elongation (%)
			T	C	
NHSS-B1	Specimen was designed to explore perceived deficiencies of NCBF bolted connections (bolt shear, brace net section, brace block shear) using a shared shear tab.	17.5	1.03	0.43	1.5
NHSS-B2	Specimen was designed to explore perceived deficiencies of NCBF bolted connections (bolt shear & bearing, brace net section & block shear, beam to gusset base metal fracture) using a split shear tab and non-seismically compact brace.	8.3	0.95	0.55	0.40
NHSS-B3	Specimen was designed to explore perceived deficiencies of NCBF bolted connections (bolt shear, brace net section & block shear) using a split shear tab and thinner gusset plate.	17.8	0.90	0.46	0.43

All specimens used an HSS5x5x3/8 brace except NHSS-B2, which used an HSS6x6x1/4 brace. NHSS-B1 was the only test to have brace fracture; the other two had connection failures. NHSS-B1 had the highest brace tensile force (446 kip) of the bolted specimens and was the only specimen whose tensile stress surpassed the expected brace yield strength.

NHSS-B2 had the lowest tensile capacity of the three tests, but the highest compressive force of the tests. Although it had the lowest tensile capacity, it reached the second highest percentage of expected brace yield capacity. This specimen had the lowest experimental slenderness ratio of all the experiments, which supports why it had the highest brace buckling force. NHSS-B2 had the lowest brace OOP displacement at midspan by over 7 in. Once the brace buckled, the hysteretic loops became much wider than the other specimens, dissipating more energy per cycle than the braces with smaller kL/r values. This brace was more slender than the others locally. NHSS-B3 had the highest brace OOP midspan displacement, and was the only specimen to surpass the AISC expected buckling capacity with its experimental buckling value.

6.6.3 Brace Buckled Shape

The brace buckled shape was plotted using Optotrak markers on the top wall of the brace along its length. Figure 6.17 presents the brace buckled shape as it reached each brace performance state (described in Chapter 5), compared to a photo of brace buckling from the test. For reference, the "0" end is the NE corner, and the brace length is the SW corner. The Optotrak camera volumes were unable to capture the full brace length and for these instances, the brace behavior was mirrored from the recorded data and marked in a lighter grey line with no makers.

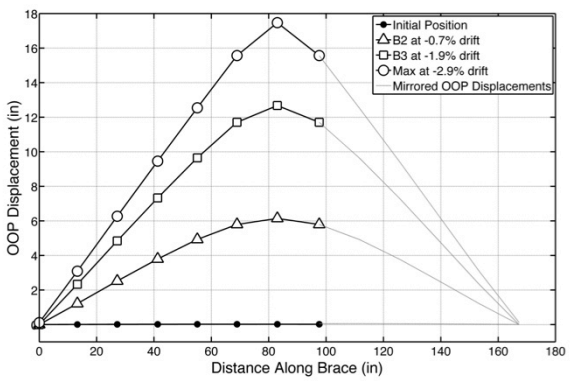

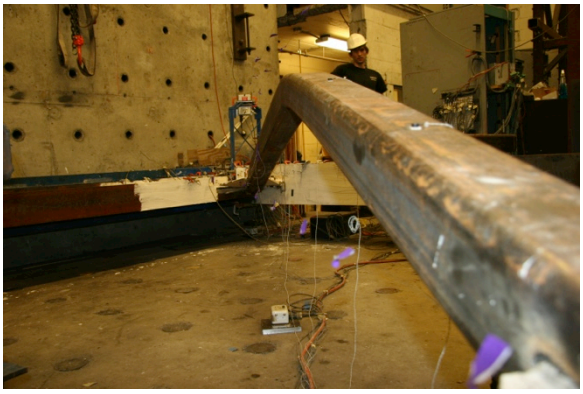

a. NHSS-B1 [photo at max OOP displacement]

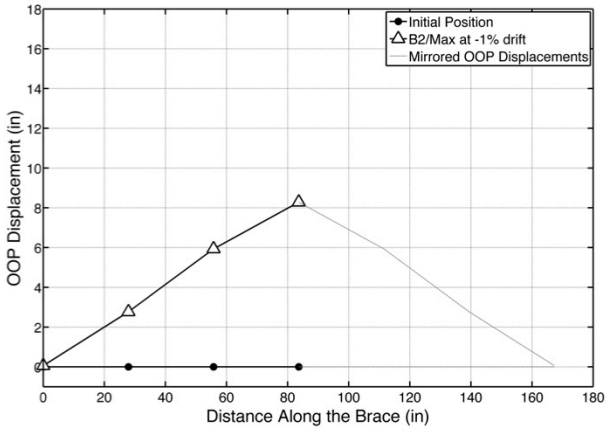

b. NHSS-B2 [photo at max OOP displacement]

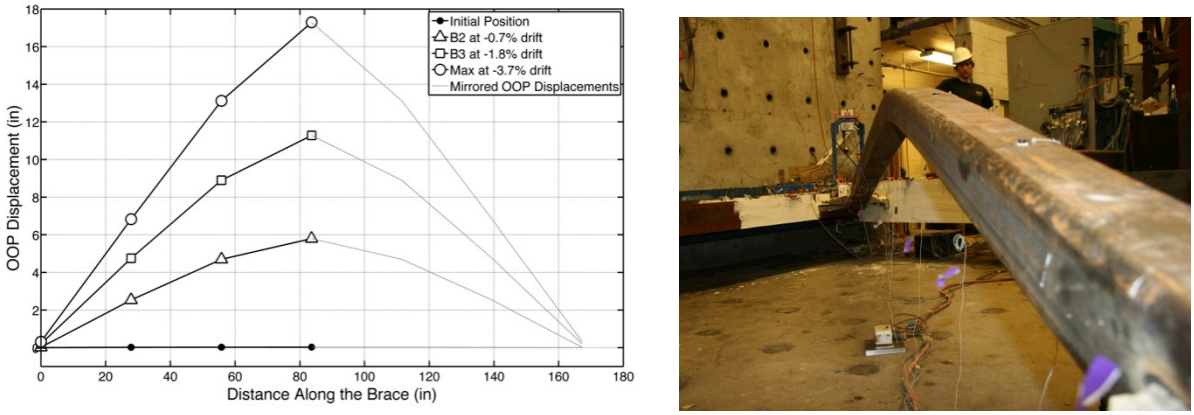

c. NHSS-B3 [photo at max OOP displacement]

Figure 6.17 - Brace Out-of-Plane Buckled Shape for Each Specimen

The maximum OOP displacement of each specimen achieved is listed in Table 6.12. Visual observations match the plots well. It was postulated that since the NCBF specimens had no rotation clearance provided on the gusset plate, that the brace ends might have some restraint causing the brace buckled shape to resemble a "bell" shape rather than a sine curve. It can be seen from the plots in Figure 6.17 that this behavior did not occur. The lack of rotational clearance for the NCBF specimens did not prohibit a curve resembling an ideal pinned end condition to occur. For all specimens, during early cycles when the brace was in stage B1, the brace took on a more gradual curved shape over the entire brace length. As local strain concentrations increased at the plastic hinge region, the brace OOP shape became more triangular, meeting close to a point at brace midspan. For NHSS-B2, the only non-seismically compact brace, this triangular shape occurred at a lower OOP displacement by about 50% (at 8 in.) than the other specimens. At this severe pointed shape, the plastic hinge region displayed cupping and bulging of the brace walls. The severity of this local deformation varied based on the braced frame failure mode. Specimens NHSS-B1, and NHSS-B2 saw tearing at the bottom corners of the brace, which led to brace fracture for NHSS-B1. NHSS-B3 saw local deformation at the brace hinge of slight cupping and bulging, but not close to the extent of the other specimens.

Figure 6.18 compares the buckled shape at similar drift levels for the NCBF specimens. These three specimens had different OOP progressions. NHSS-B2, only reached performance state B2 before the gusset plate connection failed in the NE corner. Figure 6.18a shows NHSS-B2 has a more pointed shape, while NHSS-B1 and NHSS-B3 have curved shapes over the length of the brace. At -0.7% drift, NHSS-B1 and NHSS-B3 had similar brace OOP displacements. However, in NHSS-B3, when the beam to gusset plate welds fractured in both NE and SW corners, the brace OOP displacement increased at a slower rate than NHSS-B1. This rate decrease occurred because the force transferred into the brace was smaller after weld fracture. At approximately the same drift level when NHSS-B1 reached its maximum OOP displacement, shown in Figure 6.18b, NHSS-B1 has buckled OOP (17.5 in.) about 3.5 in. more than NHSS-B3. NHSS-B3 did not reach its maximum OOP displacement (17.8 in.) until -3.7% story drift, due to its connection failures.

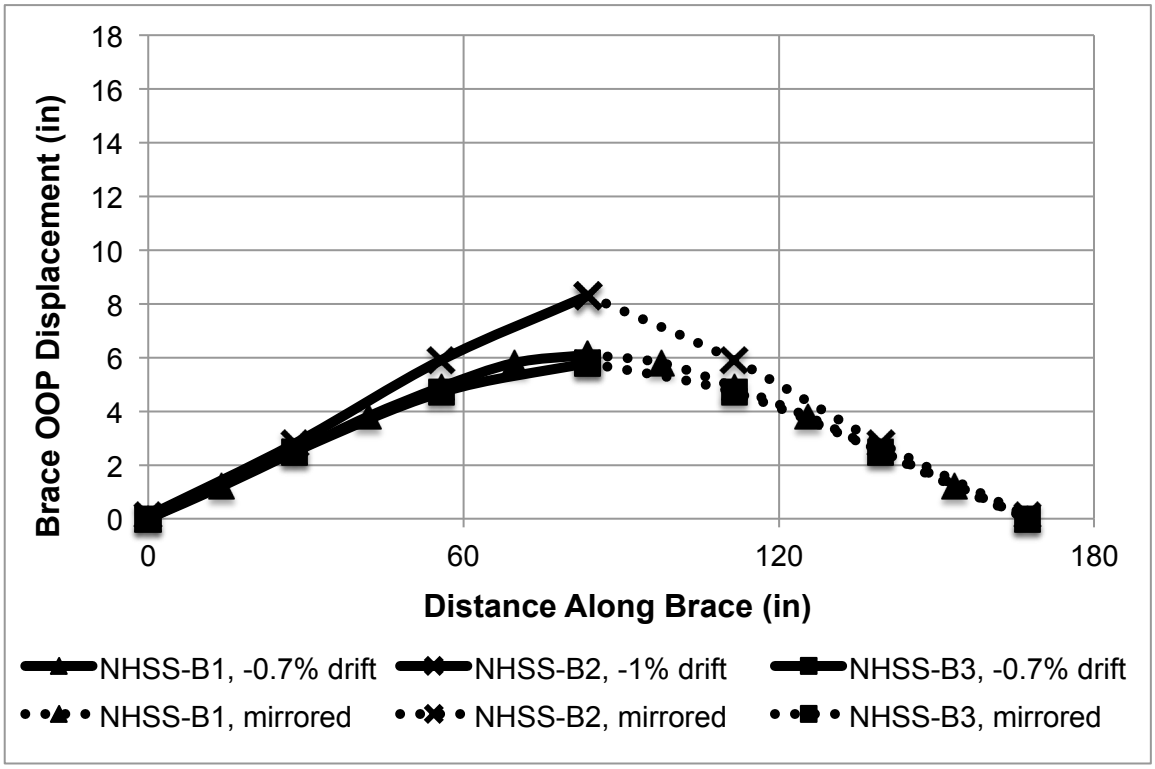

a. NCBF Bolted Specimens at Performance State B2

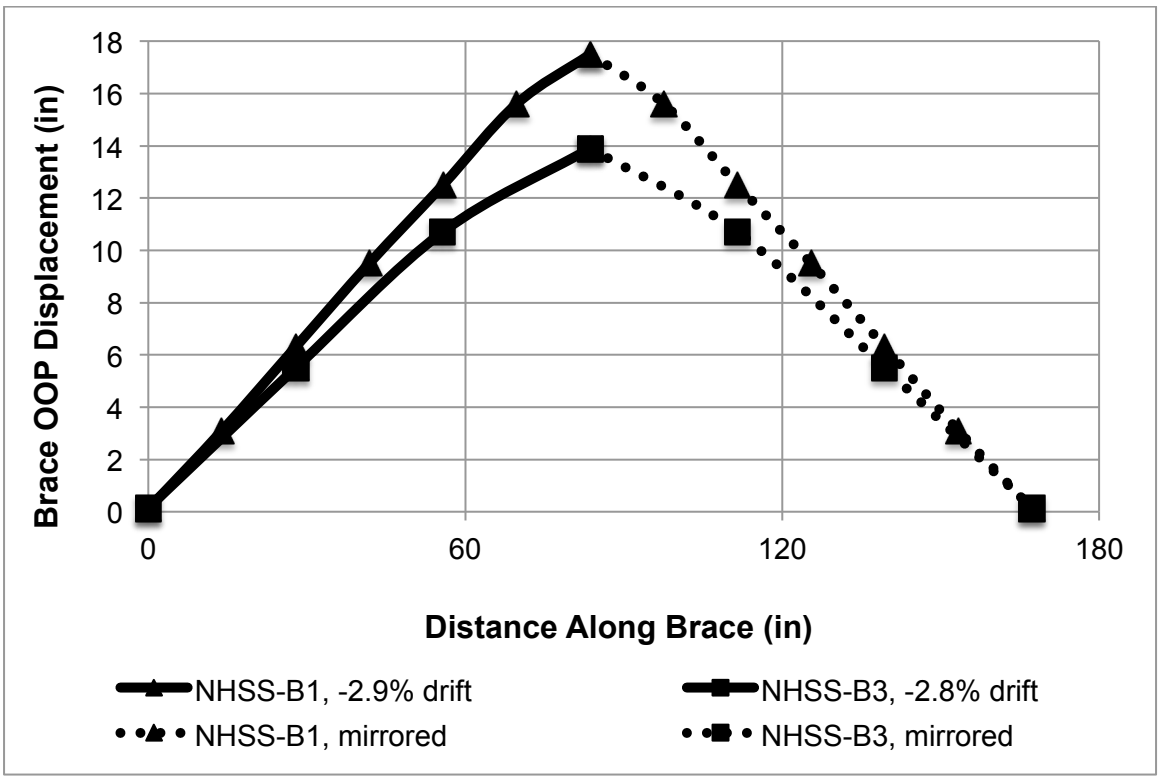

b. NCBF Bolted Specimens at NHSS-B1 Max

Figure 6.18 - Comparison of NCBF Brace Buckled Shapes at B2 and NHSS-B1 Max OOP Displacement

6.6.4 Brace elongation

Brace elongation is defined as the change in length of the brace while stretched in tension. This value is reported as a percentage of the total brace length. Brace elongation is an important behavior to study because when compared to the frame diagonal elongation, it can indicate how much deformation is concentrated in the brace relative to the other components in the system. The brace elongation can also be used in conjunction with the amount of energy dissipated by the brace to draw conclusions about the brace behavior.

The brace elongation was determined through the use of Optotrak sensors placed on one half of the brace length. Again, the camera orientations did now allow the full brace to be visible, and the data for brace elongation from the Optotrak had to be doubled. The data from the LED placed

at the brace midspan, and the LED placed at the NE end of the brace (full brace length) was used to:

1. Calculate original location and exact distance (using Pythagorean theorem) between the NE brace marker and the brace midspan marker. The original distance between the two markers was multiplied by two to approximate the full brace length.
2. Increment through the Optotrak data and record the new positions of the two markers and the difference in their new distance and their original distance to calculate the elongation. The new distance between the two was also multiplied by two to approximate the full brace behavior.
3. Their recorded elongation was divided by the original brace length to present a percentage of the brace length.

The results from these calculations are shown in Figure 6.19 and the maximum elongation values are reported in Table 6.13. All specimens reached different maximum drift ranges and had different failure modes. Table 6.13 and Figure 6.19 show that NHSS-B1 had brace fracture as the failure mode and it had the highest total brace elongation value. The specimens where damage was concentrated in the connections had lower total brace elongation values.

Table 6.13 – Maximum Brace Elongation Values for Each Specimen

Specimen	Total Brace Elongation (%)	Failure Mode
NHSS-B1	1.48	Brace Fracture
NHSS-B2	0.40	Connection Failure
NHSS-B3	0.43	Connection Failure

NHSS-B1 had the highest experimental effective slenderness ratio of the three specimens and also consistently had the highest brace elongation of the three specimens for the entirety of the

curve after 0.5% total drift range. NHSS-B2 had more elongation than NHSS-B3 likely because it was able to hinge and locally deform the brace prior to connection failure and NHSS-B3 could not.

NHSS-B2 and NHSS-B3 had very similar maximum total brace elongation values despite using different brace sections and the fact that NHSS-B3 achieved almost twice the total drift range as NHSS-B2 prior to connection failure. The reason for this behavior is likely due to their failure modes. NHSS-B2 developed a sudden weld fracture almost 50% of its total connection length that fractured within a couple cycles of appearing. NHSS-B3 on the other hand, had weld tearing propagating in both the NE and SW gusset plate to beam connections. As the severity of the tearing increased to fracture in the NE corner at close to 2% total story drift range, the brace elongation leveled out. The SW beam to gusset plate weld fractured in the following within two compression cycles but in that time the brace elongation value did not increase because of the weld tearing.

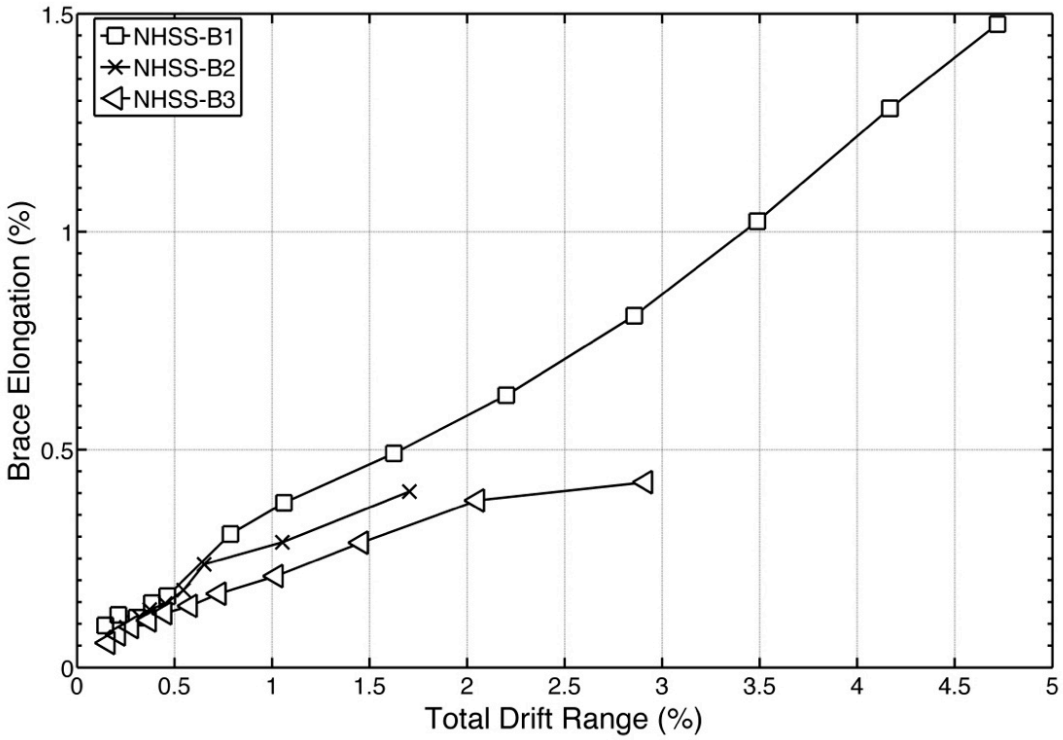

Figure 6.19 - Brace Elongation vs. Total Drift Range for NCBF Specimens

6.7 NW & SE Connection Response

The NW and SE beam to column connections were simple shear tab connection that used (4) – 3/4 in. A490 bolts for all specimens. Two potentiometers were placed on the inside of the north and south flange of each beam to measure displacements and to determine the rotation of the shear tab connection. None of the specimens had a bolt fracture during the main portion of the experiment; however, some tests had slight bolt hole elongation and bolt deformation in these connections. The calculation to find shear tab rotations is shown below in Eq. (6-4) and Figure 6.20, where δ_a and δ_b are the measured values from the potentiometers attached to the beam flanges in the SE and NW shear tab, and L_{rot} is the distance between instruments.

$$\gamma_{shear\ tab} = \frac{(\delta_a - \delta_b)}{L_{rot}} \tag{6-4}$$

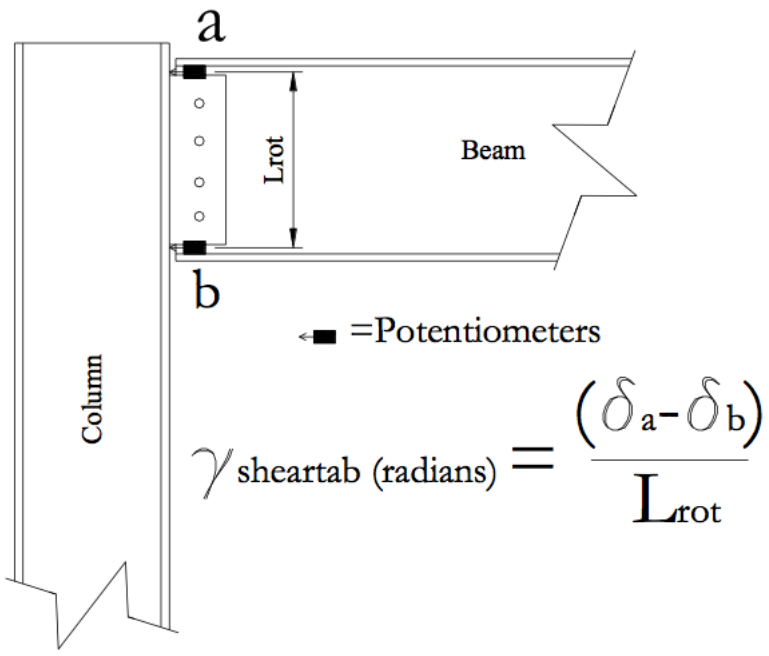

Figure 6.20 - Shear Tab Rotation Calculation [Powell, 2010]

The shear tab rotations are shown separately below for the NW and SE corners in Figure 6.21 and Figure 6.22, respectively. These figures show fairly consistent linear behavior between the shear tab rotations in both bending directions. NHSS-B3 had consistently less rotation for both the SE and NW corners, NHSS-B1 had the highest NW rotations, and NHSS-B2 had the highest SE rotations. The shear tab rotations for all specimens were slightly less (but comparable) than those seen in previous SCBF specimens (Powell, 2010).

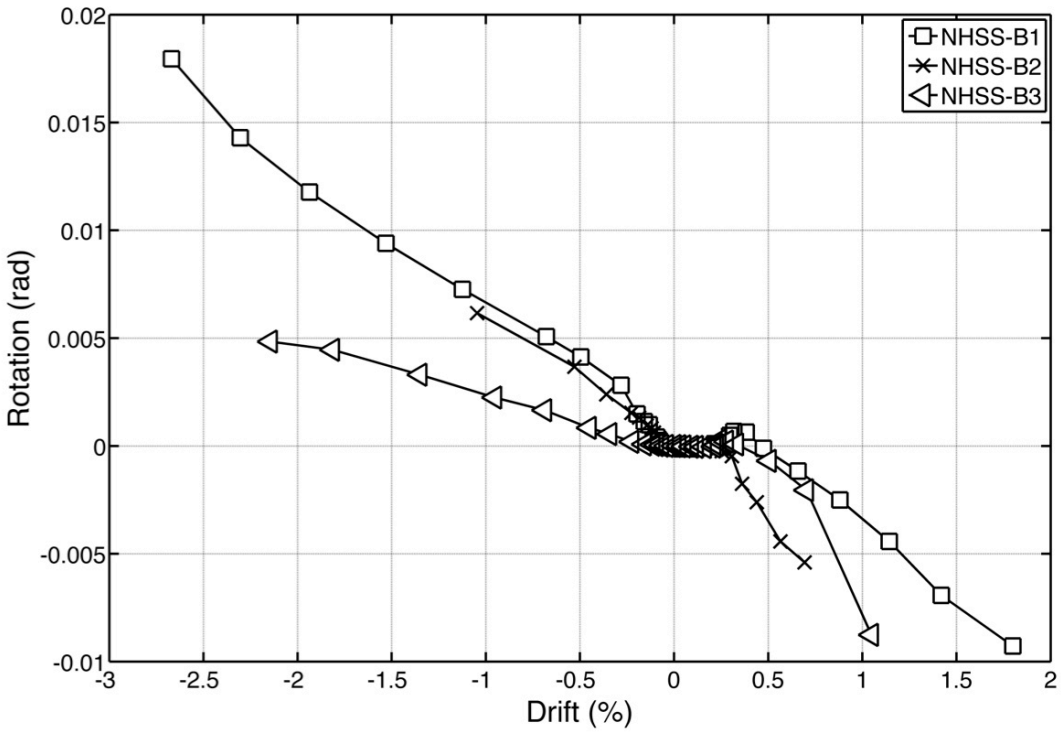

Figure 6.21 - NW Shear Tab Rotations for NCBF Specimens

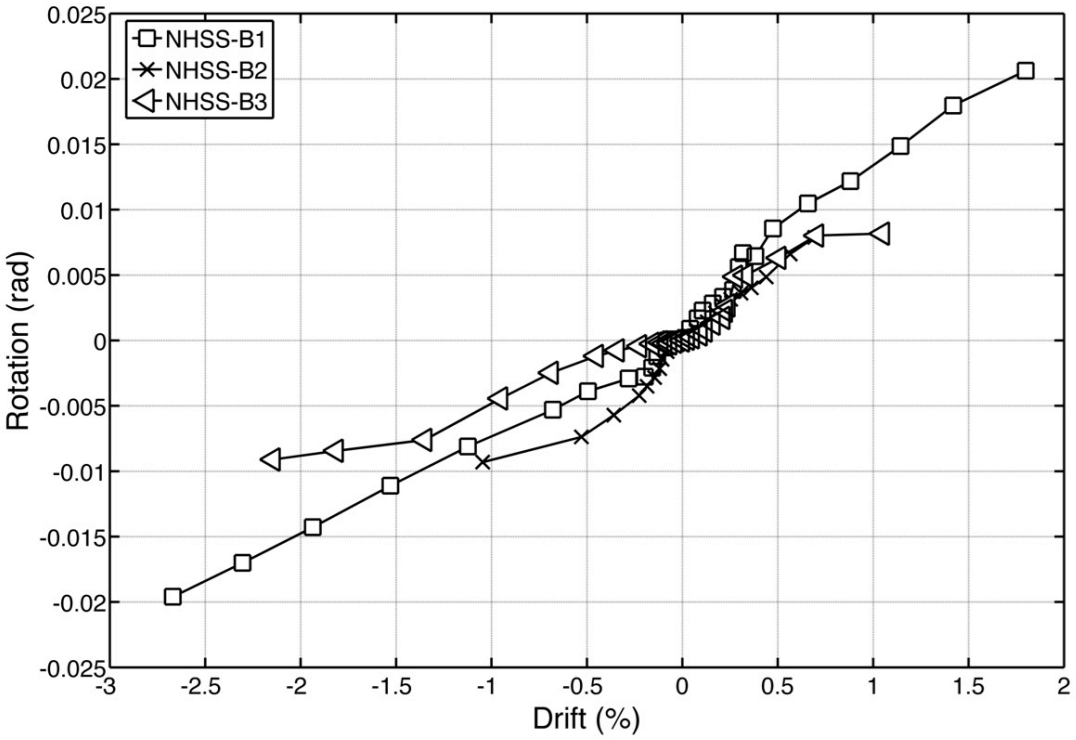

Figure 6.22 - SE Shear Tab Rotations for NCBF Specimens

CHAPTER 7: EVALUATION

The ASCE/SEI Standard 41/13 "Seismic Evaluation and Retrofit of Existing Buildings" (referred to herein as "the Standard") provides a procedure for evaluating and retrofitting existing buildings. This procedure is not mandated but is "intended to serve as a nationally applicable tool for design professionals, code officials, and building owners undertaking the seismic evaluation and retrofit of existing buildings" [4]. It is a tool to help the above listed groups of people better determine when building rehabilitation is needed and how it can be accomplished. The Standard defines target performance levels, considers a variety of earthquake hazards, and provides four different analysis techniques [4]. This chapter highlights excerpts from the Standard, focused on Chapter 9: Steel, related to the evaluation of the three braced frames tested.

The Standard defines a seismic evaluation process as shown in the flow chart in Figure 7.1. The Standard defines a seismic retrofit as "improving the seismic performance of structural and/or nonstructural components of a building by correcting deficiencies identified in a seismic evaluation to a selected Performance Objective," with the retrofit process outlined in Figure 7.2. As seen in these two figures, the Standard has many components within the evaluation and retrofit analysis, and this Chapter focuses only on a small part of the evaluation and retrofit process.

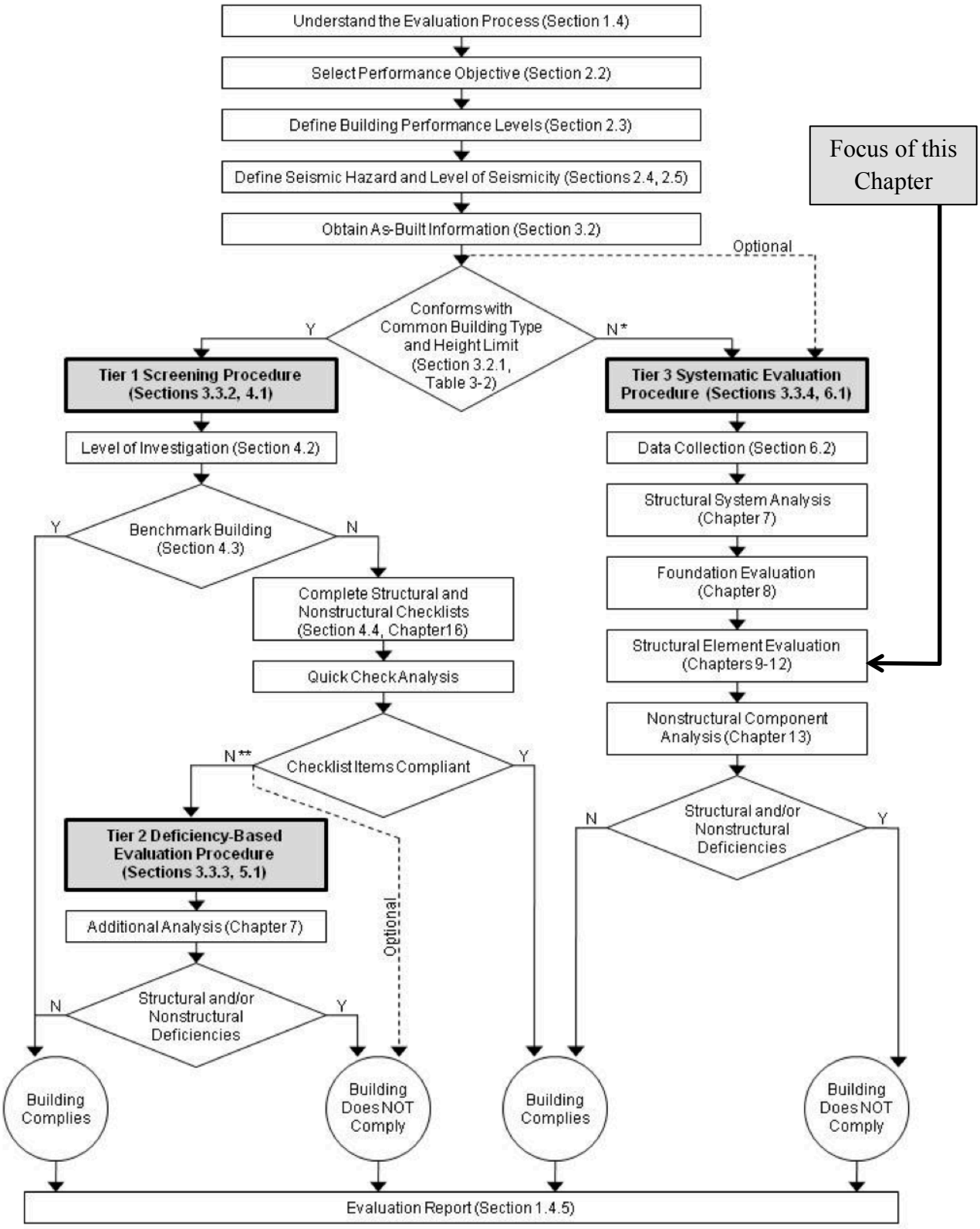

Figure 7.1 - Evaluation Process [ASCE 41/13]

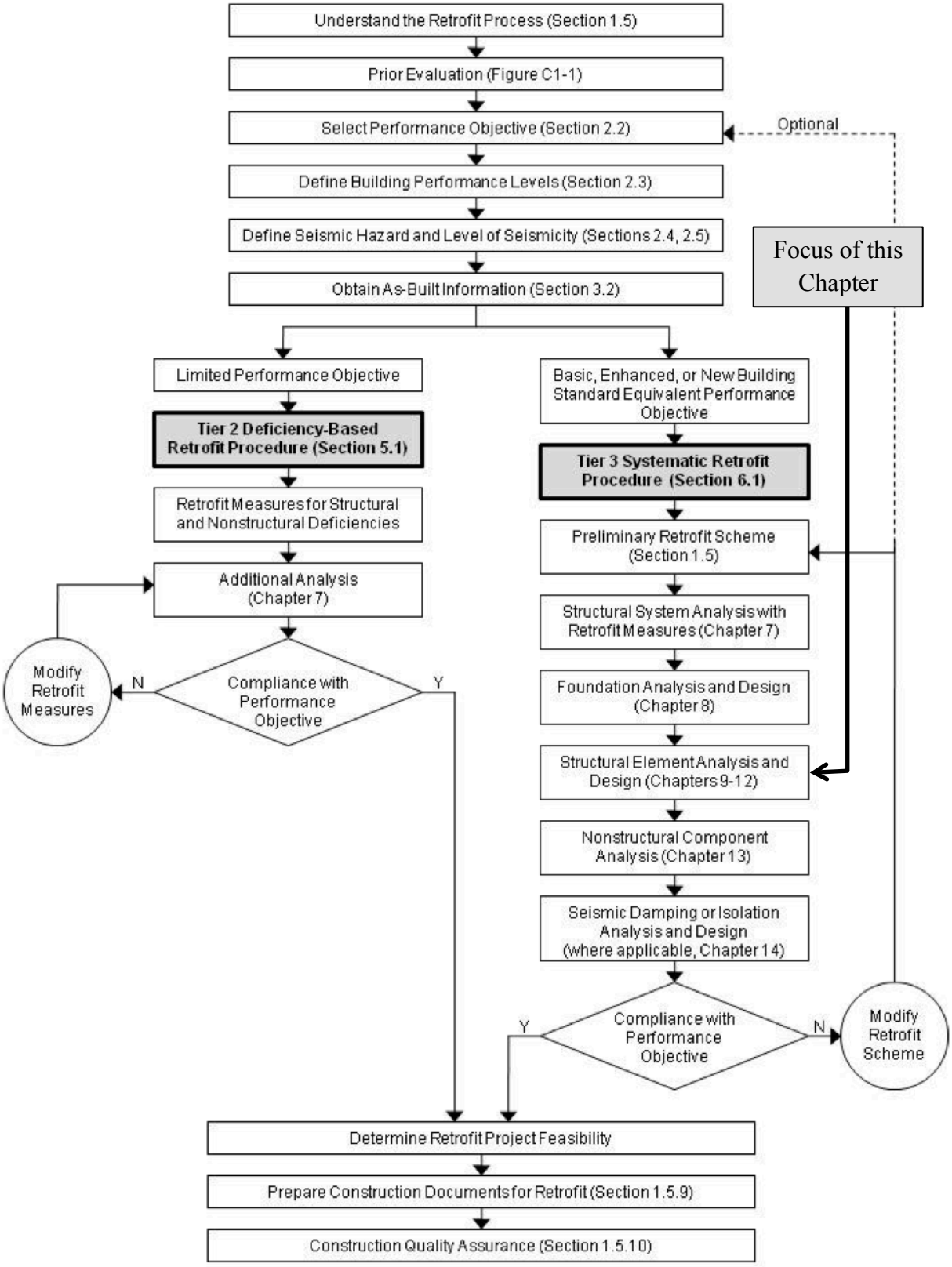

Figure 7.2 - Retrofit Process [ASCE-41/13]

A Performance Objective must be chosen as a goal. The chosen Performance Objective must contain a target Building Performance Level (which includes a combination of a Structural and Nonstructural Performance Level) and an Earthquake Hazard Level. The latter is described in Section 2.4 of the ASCE 41 Standard. The target Building Performance Levels are described in Section 2.3 of the ASCE 41 Standard. Table 7.1 (reproduced from Table C2-2 in ASCE 41) provides a list of overall structural damage that might be observed in a building at each performance level in an earthquake. Table 7.2 (partially reproduced from Table C2-3 in ASCE 41) illustrates damage states specific to lateral load resisting systems for steel concentrically braced frames.

Table 7.1 - Damage Control and Building Performance Levels [modified from Table C2-2 from ASCE 41]

	Target Building Performance Levels			
	Collapse Prevention Level (5-E)	**Life Safety Level (3-C)**	**Immediate Occupancy Level (1-B)**	**Operational Level (1-A)**
Overall Damage Structural	Severe	Moderate	Light	Very Light
	Little residual stiffness and strength to resist lateral loads, but gravity load-bearing columns and walls function. Large permanent drifts. Some exits blocked. Building is near collapse in aftershocks and should not continue to be occupied.	Some residual strength and stiffness left in all stories. Gravity-load-bearing elements function. No OOP failure of walls. Some permanent drift. Damage to partitions. Continued occupancy might not be likely before repair. Building might not be economical to repair.	No permanent drift. Structure substantially retains original strength and stiffness. Continued occupancy likely.	No permanent drift. Structure substantially retains original strength and stiffness. Minor cracking of facades, partitions, and ceilings as well as structural elements. All systems important to normal operation are functional. Continued occupancy and use highly likely.

Table 7.2 - Structural Performance Levels and Illustrative Damage States [modified from Table C2-3 from ASCE 41]

Seismic Force Resisting System	Type	Structural Performance Levels		
		Collapse Prevention Level (S-5)	Life Safety Level (S-3)	Immediate Occupancy Level (S-1)
Steel Braced Frames	Primary and Secondary Elements	Extensive yielding and buckling of braces. Many braces and their connections might fail.	Many braces yield or buckle but do not totally fail. Many connections might fail.	Minor yielding or buckling of braces.
	Drift	Transient drift sufficient to cause extensive nonstructural damage. Extensive permanent drift.	Transient drift sufficient to cause nonstructural damage. Noticeable permanent drift.	Transient drift which causes minor or no nonstructural damage. Negligible permanent drift.

For non-linear modeling of existing buildings, the Standard has developed generalized force-deformation relations for yielding comparisons in common lateral systems. The general force-deformation curve is shown in Figure 7.3. The y-axis showing the force, Q, has been normalized by the expected yield strength of the component, Q_y. For braces, or as proposed here for braced frame systems, Point "A" on the curve is the initial point of the brace response; Point "B" occurs at the deformation when the brace has reached its expected yield load in tension or its expected buckling load in compression; Point "C" occurs at the peak strength of the brace prior to loss in resistance either from brace fracture or connection failure; Points "D" and "E" represent the residual strength values. In braced frames these latter values may be residual moment frame strength after brace or connection failure. The modeling parameters "a", "b", and "c" depend on the deformation capacity of the brace and its connections. The value "a" represents the plastic deformation capacity of the brace either post-yield or post-buckling. The value "b" represents the full plastic deformation capacity of the system at maximum strength. The value "c" is the residual strength ratio of the component.

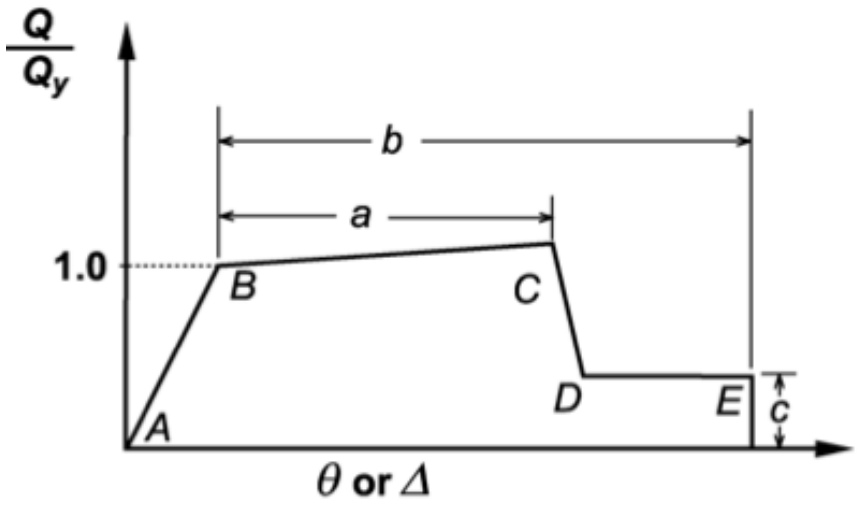

Figure 7.3 - Generalized Force-Deformation Relation for Steel Elements or Components [1]

ASCE 41 has modeling parameters corresponding to components of various systems are tabulated in tables of the Standard. The curves typically are generated for each displacement-controlled component of the system. For example, in a braced frame, there are separate modeling parameters for the brace in compression and the brace in tension and then further modeling parameters based on the brace section used. There are also tabulated values for the acceptance criteria specific to primary and secondary components of the lateral system for the nonlinear analysis methods. A selection of this table has been included in Table 7.3. The parameter Δ_c represents the axial deformation of the brace at the expected buckling load (at Point "B"). Likewise, the parameter Δ_T represents the axial deformation at the expected tensile yield load in the brace. The Standard Commentary clearly states that these values have been developed from experiments on braced frames that have required ductile detailing, and brace slenderness and compactness requirements. NCBFs did not have the same requirements and therefore are unlikely to have the same behavior as SCBFs. The Standard suggests these tabulated values be reduced but used with caution due to the lack of experimental results on NCBFs [4].

Table 7.3 - Modeling Parameters and Acceptance Criteria for Nonlinear Procedures - Structural Steel Components - Axial Actions [modified from Table 9-7 in the Standard]

Component/ Action		Modeling Parameters			Acceptance Criteria				
					Plastic Deformation				
		Plastic Deformation		Residual Strength Ratio	Primary			Secondary	
		a	b	c	IO	LS	CP	LS	CP
Brace in Compression	Slender HSS, Pipes, Tubes	$0.5\Delta_c$	$9\Delta_c$	0.3	$0.5\Delta_c$	$5\Delta_c$	$7\Delta_c$	$7\Delta_c$	$9\Delta_c$
	Stocky HSS, Pipes, Tubes	$1\Delta_c$	$7\Delta_c$	0.5	$0.5\Delta_c$	$4\Delta_c$	$6\Delta_c$	$6\Delta_c$	$7\Delta_c$
Brace in Tension	HSS, Pipes, Tubes	$5\Delta_T$	$11\Delta_T$	0.6	$0.5\Delta_T$	$6\Delta_T$	$8\Delta_T$	$8\Delta_T$	$11\Delta_T$

The parameters for NCBFs have not yet been developed and is an objective of this research project. As there were numerous components in the NCBFs tested that contribute to the deformations of the system, and because NCBF performance may be governed by connection failure rather than brace fracture, the proposed parameters were developed for the entire braced frame system as opposed to just the braces. Figure 7.4 shows the plots for the NCBF specimens tested and the coordinates for points A-E are listed in Table 7.4 though Table 7.5. Following these plots and tables is a description of how they were developed.

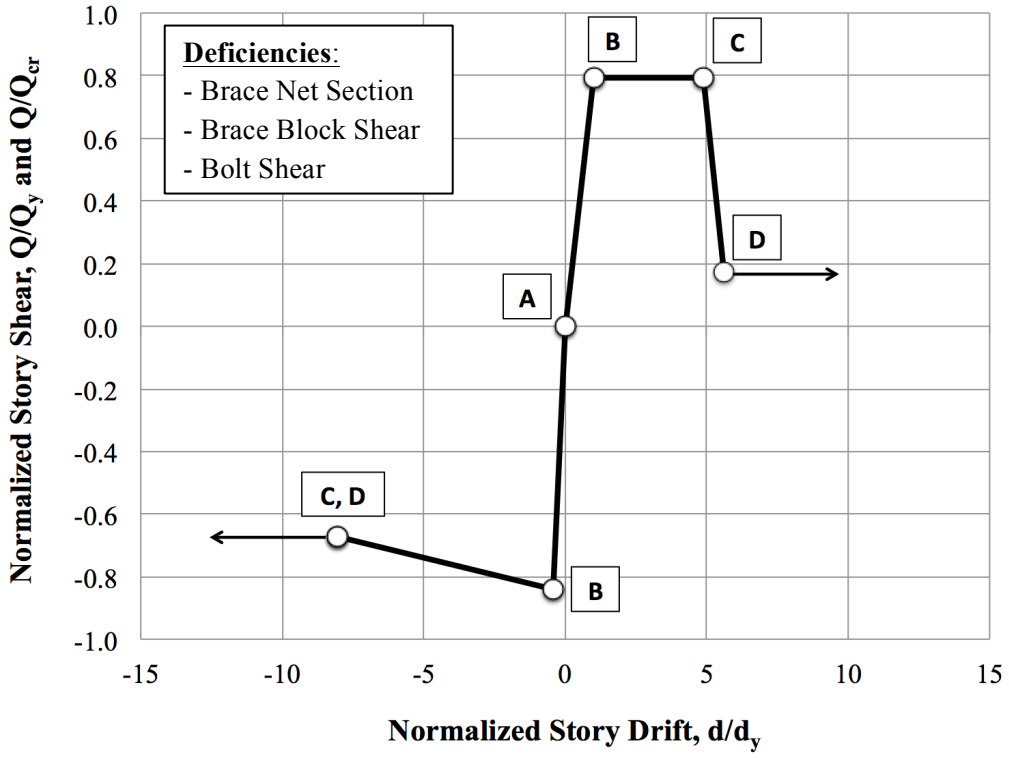

a. NHSS-B1

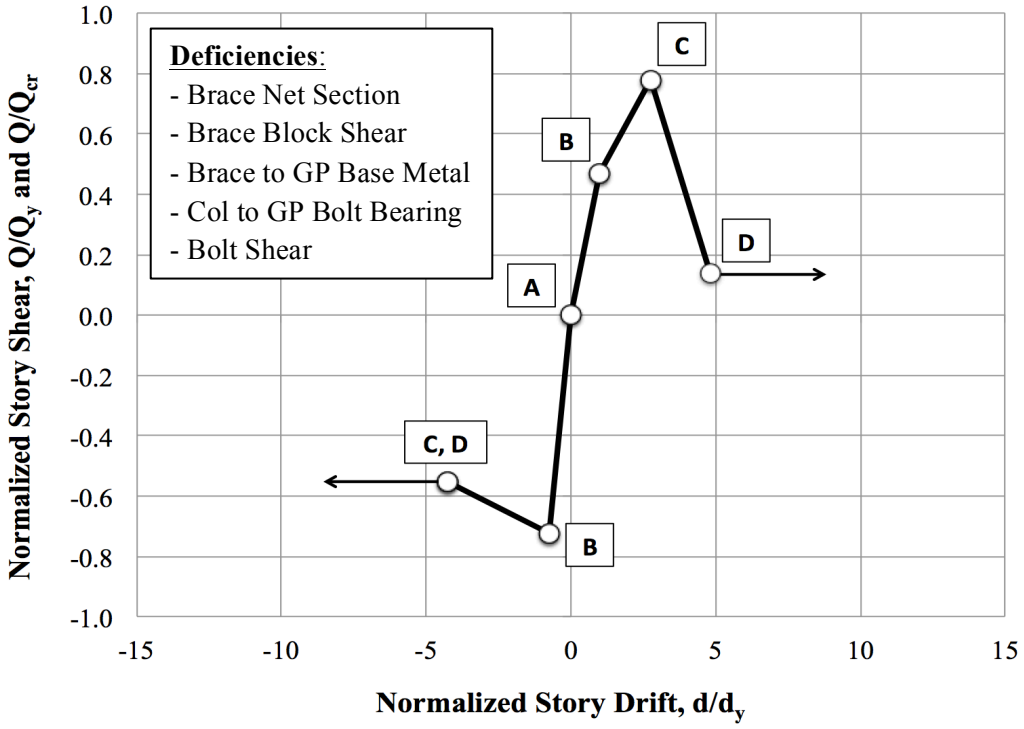

b. NHSS-B2

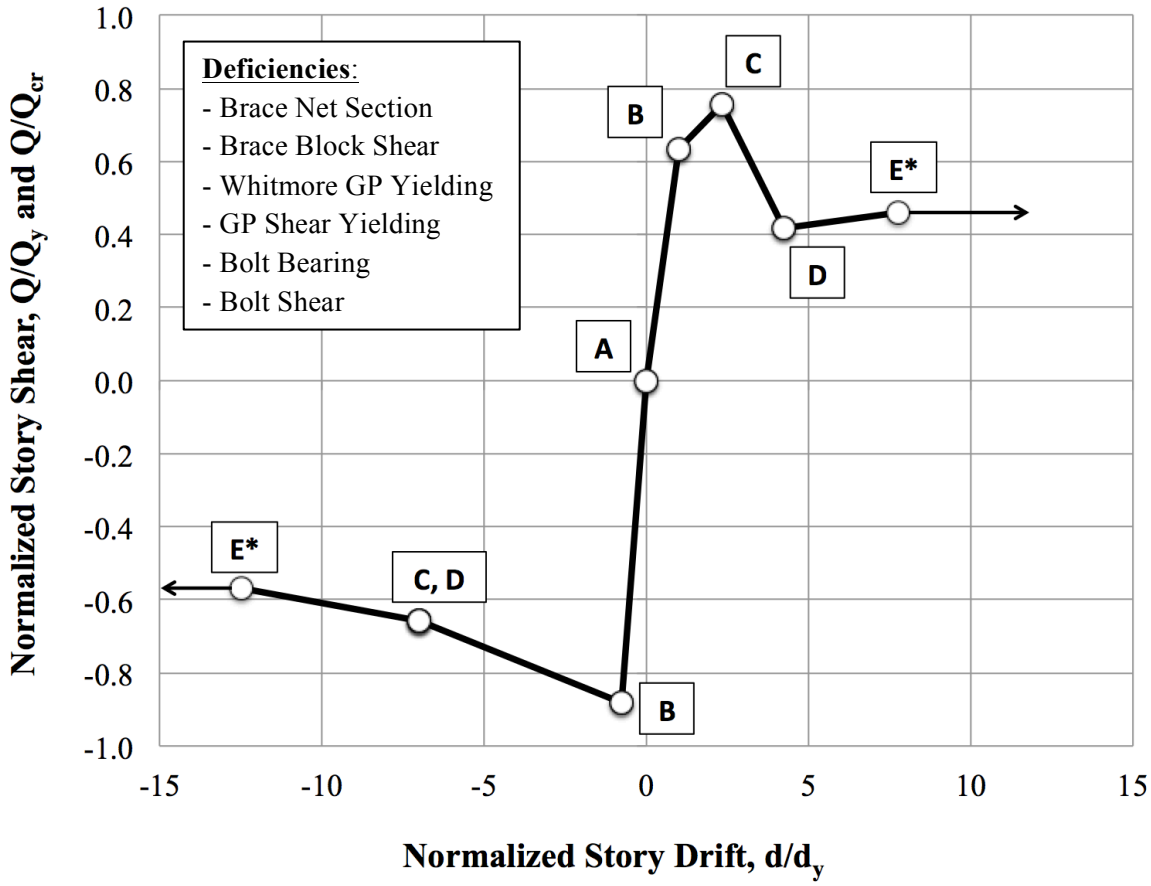

c. NHSS-B3

Figure 7.4 – NCBF Force-Deformation Plots

These plots were created using the hysteretic behavior of the frame prior to brace fracture or connection failure and the behavior post-brace or connection failure. The y-axis is the story shear normalized by the expected brace tensile capacity (for tensile force values) and by the expected brace buckling capacity (for the compressive force values). The x-axis is the story drift normalized by the drift level (%) of the frame when the brace yielded in tension. The coordinates for A-D in tension and A-C in compression were found directly from the hysteretic response of the frame. Because the frames failed in tension, there is no recorded compressive value for point D, and it was taken as the same value as point C. The arrows represent that the specimens did not completely fail at point D or E, but that is where cycles were discontinued. It is important to note that when looking at Table 7.4 and Table 7.5, NHSS-B3 was the only specimen, of the three, that

had post-fracture cycles completed continuously with the full brace frame cycles prior to fracture and is labeled as “E* ”.

Table 7.4 – Tension Modeling Parameters

Specimen	A		B		C		D		E*	
	d	P	d	P	d	P	d	P	d	P
NHSS-B1	0	0	1.0	0.79	4.9	0.80	5.6	0.17	-	-
NHSS-B2	0	0	1.0	0.47	2.7	0.78	4.8	0.14	-	-
NHSS-B3	0	0	1.0	0.63	2.3	0.76	4.3	0.42	7.7	0.46

Table 7.5 - Compression Modeling Parameters

Specimen	A		B		C		D		E*	
	d	P	d	P	d	P	d	P	d	P
NHSS-B1	0	0	-0.43	-0.84	-8.1	-0.67	-8.1	-0.67	-	-
NHSS-B2	0	0	-0.74	-0.72	-4.2	-0.55	-4.2	-0.55	-	-
NHSS-B3	0	0	-0.75	-0.88	-7.0	-0.66	-7.0	-0.66	-12.5	-0.57

The data is also presented for the combined tension and compression response of the frame. To merge the two, the new plots were created with total drift range on the x-axis and the average normalized story shear on the y-axis. Figure 7.5 shows the combined force-deformation curves and Table 7.6 gives the combined force-deformation modeling parameters. NHSS-B1 had the highest force capacity, and the highest deformation parameters. It is important to note that NHSS-B2 used an HSS6x6x1/4 as opposed to an HSS5x5x3/8 like NHSS-B1 and NHSS-B3, which is responsible for some of the differences between force-deformation behaviors. While the normalized tensile capacity of NHSS-B1 remained consistent after yield, its rapid loss of

normalized compressive resistance caused a loss in normalized average story shear between points B and C. A similar negative stiffness was also seen in Specimen NHSS-B3. NHSS-B2 had a positive normalized post-yield stiffness value that offset the normalized compressive loss when averaging the values.

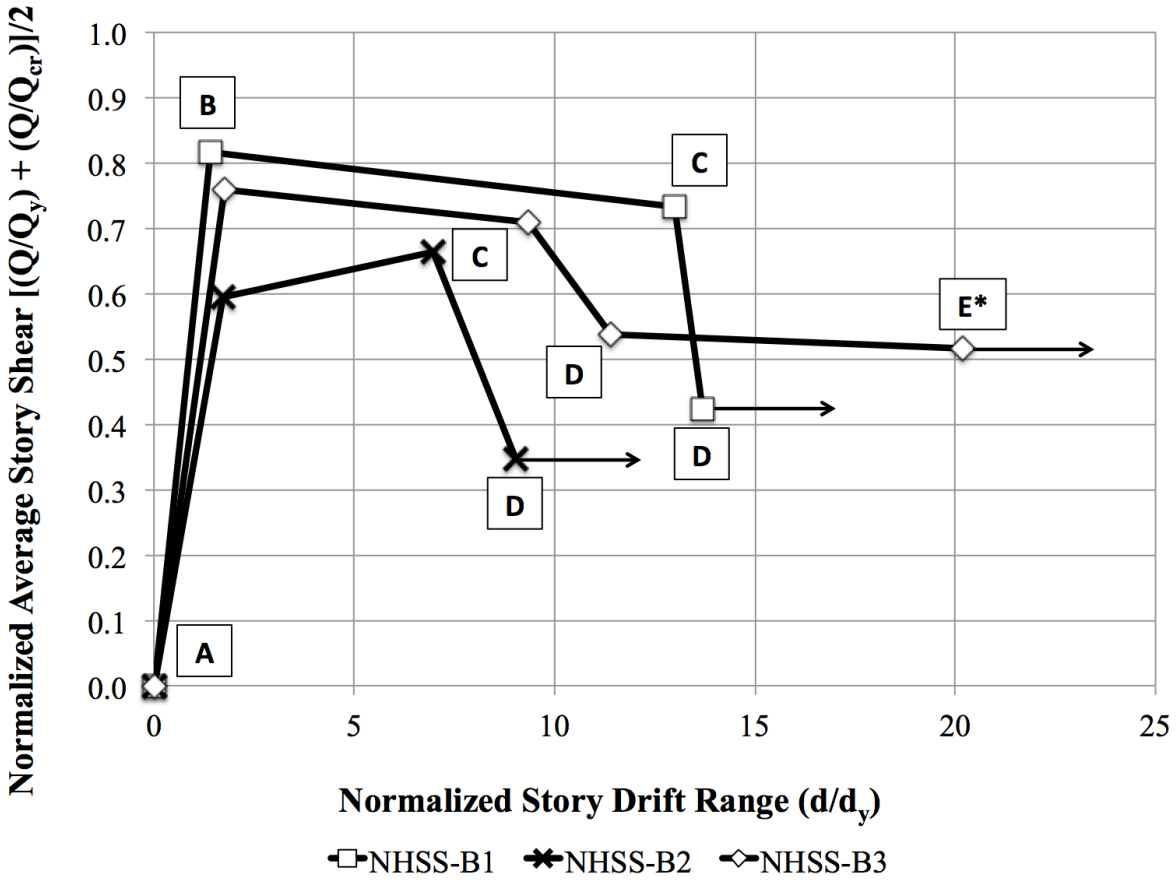

Figure 7.5 - Combined Force-Deformation Curves for NCBF Bolted Specimens

Table 7.6 – Combined Modeling Parameters

Specimen	A		B		C		D		E*		a
	d	P	d	P	d	P	d	P	d	P	
NHSS-B1	0	0	1.4	0.82	13	0.73	13.7	0.42	-	-	12
NHSS-B2	0	0	1.7	0.59	7.0	0.66	9.1	0.35	-	-	5
NHSS-B3	0	0	1.8	0.76	9.4	0.71	11.4	0.54	20.2	0.51	8

The values for the modeling parameters, and the force-deformation relations also make sense following the analysis in Chapter 6. The higher plastic deformation values of NHSS-B1 indicate it was more ductile than the other specimens, supported by also having the highest amount of total energy dissipation and energy dissipation per cycle of the NCBF specimens. Point A is the highest in NHSS-B1, as it also had the highest total drift range of the NCBF specimens. NHSS-B1 was the only specimen to sustain brace fracture; the other two specimens had connection failures. However, the connection failures in NHSS-B3 did not completely disconnect the braced frame system from the framing elements as in NHSS-B2. NHSS-B3 had weld fracture at the beam to gusset plate welds in the NE and SW corner, but the gusset plates were still connected to the columns, and the brace was still in tact. It is likely this remaining connectivity of the system is why NHSS-B3 had the highest residual strength ratio than the other specimens.

These modeling curves can be applicable to specimens with:

- High DCR values (above 1.5) for bolt shear in the gusset plate to column and/or beam to column connections.
- Either split or shared shear plates of 3/4 in. thickness.
- Configurations with no rotational buckling clearance on the gusset plate.

More experiments should be conducted with the above characteristics to further develop the parameters.

CHAPTER 8: SUMMARY & CONCLUSIONS

8.1 Summary of Specimen Performance

Three bolted NCBF specimens were tested to improve understanding of NCBF behavior and identify critical risks within the systems. They are part of a larger research initiative to explore NCBF seismic behavior and identify specific NCBF vulnerabilities. In particular, limited research has been conducted on bolted CBF connections, and the results from these specimens are intended to aid in remedying this lack of experimental data.

NHSS-B1

This specimen used a bolted shared shear tab to connect the beam and gusset plate to the column, and a seismically compact HSS5x5x3/8 brace section. The connection was deficient in brace net section, brace block shear, bolt shear, and bolt bearing; it also had no rotational clearance on the gusset plates, did not use net section reinforcement, and used filler metal for the welds with no minimum toughness requirements. Despite its deficiencies, NHSS-B1 achieved a total drift range of 4.9% with a total resistance of 533 kip, and a ductile failure mode of brace fracture. Bolt hole elongation and bolt deformation was evident in the specimen and likely increased the specimen's drift capacity. There was notable weld tearing in the beam to gusset plate welds, and gusset plate to column shear tab welds.

NHSS-B2

This specimen used the same general geometric configuration as NHSS-B1 except it used a bolted split shear tab to connect the gusset plate and beam to the column. NHSS-B2 also used an HSS6x6x1/4 brace section with a higher local slenderness value than NHSS-B1. Like NHSS-B1, the connection was deficient in brace net section, brace block shear, bolt shear, and bolt bearing; it was also deficient in brace to gusset plate base metal fracture due to the thinner brace wall. NHSS-B2 had no rotational clearance on the gusset plates, did not use net section reinforcement, and used filler metal for the welds with no minimum toughness requirements. This specimen had a much worse performance than NHSS-B1, only achieving a total drift range of 1.8% with a total resistance of 457 kip and a brittle failure mode of weld/bolt fracture at the NE gusset plate

connection. There was limited bolt hole elongation in this connection, much less than seen in NHSS-B1. The weld tear in the NE beam to gusset plate weld appeared suddenly at 40% of the length and fractured within a couple cycles.

NHSS-B3

This specimen also had the same general geometric configuration as NHSS-B1 and NHSS-B2. This specimen used bolted split shear tabs (like NHSS-B2) and a seismically compact HSS5x5x3/8 brace section (like NHSS-B1), but used a thinner gusset plate than the two previous specimens. Like NHSS-B1 and NHSS-B2, the connection was deficient in brace net section, brace block shear, bolt shear, and bolt bearing; it was also deficient in Whitmore gusset plate yielding, gusset plate shear yielding, and bolt bearing in the gusset plate because of its reduced thickness. NHSS-B3 had no rotational clearance on the gusset plates, did not use net section reinforcement, and used filler metal for the welds with no minimum toughness requirements. This specimen had a better performance than NHSS-B2 but not as good as NHSS-B1. It achieved a 3.2% total drift range with a total resistance of 517 kip and a brittle failure mode of beam to gusset plate weld fracture in both NE and SW connections. Returning to a brace with a lower b/t ratio and using a thinner gusset plate allowed almost twice the drift capacity as NHSS-B2.

8.2 Research Conclusions

The following conclusions were drawn from the analysis in this thesis:

1. The bolted NCBF connection with a shared shear tab (NHSS-B1) was able to perform as well as the optimal welded connection (HSS-05) designed with the BDP. Despite NHSS-B1's numerous deficiencies this specimen performed as follows:
    - *Force-drift capacity:* NHSS-B1 had a higher total force range and reached the same drift level as HSS-05. Bolt hole elongation and bolt deformation likely contributed to this specimen's performance.
    - *Failure mode:* Like HSS-05, specimen NHSS-B1 achieved ductile brace fracture.
    - *Energy Dissipation Capacity:* NHSS-B1 dissipated more energy by about 1000 kip-in than HSS-05 at the same final total drift range.

2. Two of the NCBF specimens, NHSS-B2 and NHSS-B3, had brittle fracture at low drift levels due to insufficient capacity of the beam to gusset plate welds and opposing eccentricities from using a split shear tab configuration.

3. Bolt shear failure was not evident in any of the specimens (except NHSS-B2 post-weld fracture), despite having highly deficient bolt configurations. The NCBF specimens had the highest DCR values for the bolt shear limit state at 1.9 (NHSS-B1 and NHSS-B3) and 1.6 (NHSS-B2). There was observed bolt hole elongation and bolt deformation from their high bolt bearing DCR values in all NCBF specimens to varying degrees. These performances suggest that ductility can be achieved with older bolted NCBFs with proper balance of bolt shear strength and bolt bearing deficiencies. Bolt hole elongation clearly increased the inelastic deformation capacity while delaying other undesirable failure modes, such as bolt shear and weld fracture.

4. Designing the beam to gusset plate interface weld using the AISC resistance factors and the UFM is not sufficient to resist weld fracture. Instead there appears to be evidence in favor of designing the weld for at least the expected capacity of the gusset plate. NHSS-B1 had the lowest DCR value from the BDP at 1.1 and had 50% weld tearing, while NHSS-B2 and NHSS-B3 had weld fracture with DCR values at 1.5 and 1.4, respectively.

5. The use of filler weld metals that do not have minimum toughness requirements do not allow ductile weld tearing and were found to limit the drift capacity of the systems.

6. The use of a shared shear tab configuration as opposed to a split shear tab configuration showed an increase in the drift capacity, total force range, energy dissipation, elastic stiffness, and ductility of the NCBF specimens. The shared shear tab configuration also allowed for a desirable ductile failure mode of brace fracture and was able to relieve stress on the beam to gusset plate weld by more evenly distributing forces in the connection.

8.3 Recommendations for Future Research

As seen in this research, bolted connections have the potential to perform as well as welded connections within CBF configurations, and should be the focus of continued research such as:

- Further research on bolted shared shear tabs. For example: a bolted shared shear tab with a highly deficient beam to gusset plate weld (from gusset plate demands) to explore the extent to which a shared shear tab can protect that interface weld.

- The development of balance factors for bolted SCBF configurations to allow the use of the BDP for modern bolted connections.

- Bolts as retrofit options for deficient welded shear tab NCBF configurations.

- Multi-story NCBF (and SCBF) bolted connections.

- Other bolted configurations such as bolted endplates and mega-gusset plates.

REFERENCES

1. AISC "Steel Construction Manual," 14th Edition, American Institute of Steel Construction, Chicago, Illinois, 2011.

2. AISC "Seismic Provisions for Structural Steel Buildings," American Institute of Steel Construction, Chicago, Illinois, 2010.

3. ASCE "Standard ASCE/SEI 7-10 Minimum Design Loads for Buildings and Other Structures," American Society of Civil Engineers, Reston, VA, 2010.

4. ASCE "Standard ASCE/SEI 41-13 Seismic Evaluation and Retrofit of Existing Buildings," Public Comment Draft, American Society of Civil Engineers, 2013.

5. Aslani, F., Goel, S., "Experimental and Analytical Study of the Inelastic Behavior of Double Angle Bracing Members Under Severe Cyclic Loading," Research Report UMCE 89-5, Department of Civil Engineering, University of Michigan, Ann Arbor, Michigan, February, 1989.

6. ATC 24, "Guidelines for Cyclic Seismic Testing of Components of Steel Structures," Applied Technology Council, 1992.

7. Bjorhovde, R. and Chakrabarti, S.K., "Tests of Full-size Gusset plate Connections." *Journal of Structural Engineering*, American Society of Civil Engineers, 111(3), 667-115, 1985.

8. Cives Steel Company, "The Uniform Force Method," Retrieved from: http://www.cives.com/sites/default/files/papers/UFM.pdf.

9. Clark. K.A., "Experimental Performance of Multi-Story X-Brace Systems," Department of Civil Engineering, University of Washington, Seattle, Washington, December 2009.

10. Fastenal, "Fastenal Engineering & Design Support," Retrieved from: https://www.fastenal.com/content/feds/pdf/Article%20-%20Bolted%20Joint%20Design.pdf , 2009.

11. Georgia Institute of Technology, Retrieved from: https://nees.org/data/download/NEES-2006-0202/Documentation/Progress%20Reports/progress_sept-98/sld012.htm, 2006.

12. Herman, D.J., “Further Improvements on and Understanding of Special Concentrically Brace Frame Systems,” Department of Civil Engineering, University of Washington, Seattle, Washington, 2007.

13. Hsiao et al., “Seismic Vulnerability of Older Braced Frames”, unpublished 2011.

14. Jain, A.K., Goel, S.C., Hanson, R.D, "Hysteresis Behavior of Bracing Members and Seismic Response of Braced Frames with Different Proportions," Research Report UMEE 78R3, Department of Civil Engineering, University of Michigan, Ann Arbor, Michigan, July, 1978.

15. Johnson, S.M., “Improved Seismic Performance of Special Concentrically Brace Frames,” Department of Civil Engineering, University of Washington, Seattle, WA, June 2005.

16. Kotulka, B.A., “Analysis for a Design Guide on Gusset Plates used in Special Concentrically Brace Frames,” Department of Civil Engineering, University of Washington, Seattle, Washington, 2007.

17. Malakout, M., “Bolted Connections”, Presentation for CEE 451 Design of Metal Structures, University of Washington, Seattle, WA, 2011.

18. Popov E., and Takhirov, S., “Bolted large seismic steel beam-to-column connections Part 1: experimental study,” Engineering Structures 24, 1523-1534, 2002.

19. Powell, J.A., “Evaluation of Special Concentrically Braced Frames for Improved Seismic Performance and Constructability,” Department of Civil Engineering, University of Washington, Seattle, WA, 2010.

20. Quimby, T. B., “A Beginner’s Guide to the Steel Construction Manual, 13th ed.,” Retrieved from: http://www.bgstructuralengineering.com/BGSCM13/BGSCM003/BGSCM00306.htm, 2008.

21. Rai D.C., and Goel S.C., “Seismic evaluation and upgrading of chevron braced frames,” Journal of Constructional Steel Research 59, 971-994, 2003.

22. Roeder et al., “Seismic Performance of SCBF Braced Frame Gusset Plate Connections,” *4th International Conference on Earthquake Engineering*, Taipei, Taiwan, Paper No. 80, October 2006.

23. Roeder, C.W., Lumpkin, E.J., Lehman, D.E., “A balanced design procedure for special concentrically braced frame connections,” Journal of Constructional Steel Research, 67, 1760-1772, 2011.

24. SAC Steel Project, "Protocol for Fabrication, Inspection, Testing and Documentation of Beam-Column Connection Tests and Other Experiments," Report No. SAC/BD-97/02, SAC Joint Venture, October 1997.

25. Sen, A.D., Sloat, D., Pan, L., Roeder, C.W., Lehman, D.E., and Berman, J.W., “Evaluation of the Seismic Performance of Two-Story Concentrically Braced Frames with Weak Beams,” *5th International Conference on Advances in Experimental Structural Engineering*, Taipei, Taiwan, 2013.

26. Sen, A.D., Pan, L., Sloat, D., Roeder, C.W., Lehman, D.E., Berman, J.W., Tsai, K.C., Li, C.H., and Wu, A.C., “Numerical and experimental assessment of chevron braced frames with weak beams,” *Proceedings of the 10th National Conference in Earthquake Engineering*, Earthquake Engineering Research Institute, Anchorage, AK, 2014.

27. Shaback, B., Brown, T., "Behaviour of square hollow structural steel braces with end connections under reversed cyclic axial loading," Canadian Journal of Civil Engineering, v 30, n 4, p 745-753, August, 2003.

28. Shivashankar, G.S., Vijayarangan, S., “A Numerical Approach on Load Sharing Analysis and Optimization of Bolted Joint Efficiency,” Academic Open Internet Journal, V.15, 2005.

29. Sloat (2014)

30. The European Steel Design Education Programme, “Lecture 11.4.4: Analysis of Connections: Resistance to Moment by Combined Tension and Compression,” Retrieved from: http://www.haiyangshiyou.com/esdep/master/wg11/l0440.htm, on 2014.

31. Thornton, W.A., and Lini, C., “The Whitmore Section,” Modern Steel Construction, 2011.

32. Tremblay R., "Inelastic seismic response of steel bracing members," Journal of Constructional Steel Research, 58, 665-701, 2002.

33. Whitmore, R.E., "Experimental Investigation of Stresses in Gusset Plates," Bulletin No. 16, Engineering Experiment Station, University of Tennessee, 1952.

APPENDIX A: DRAWINGS

A.1 NHSS-B1

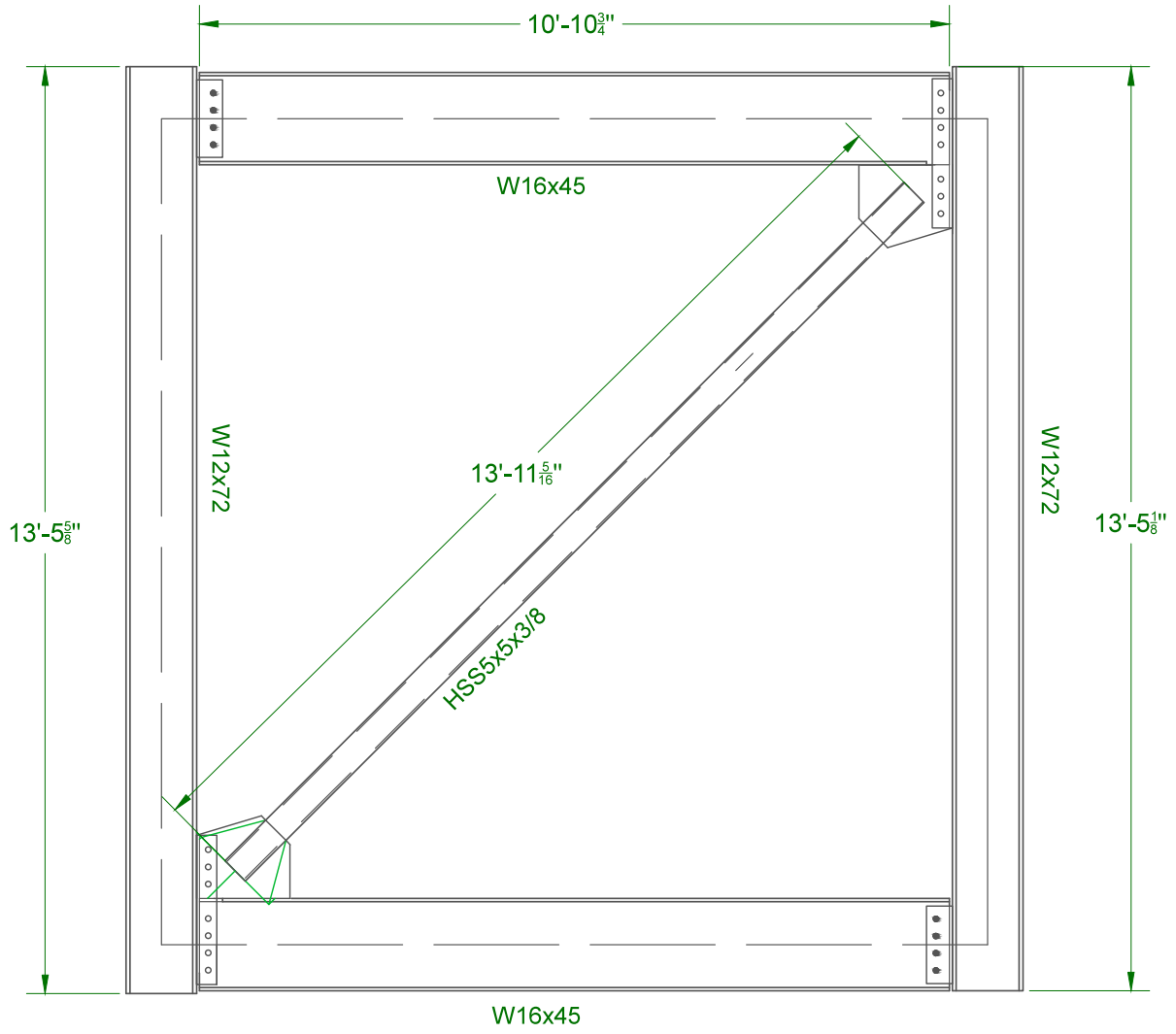

Figure A.1 - NHSS-B1 Full Frame Drawing

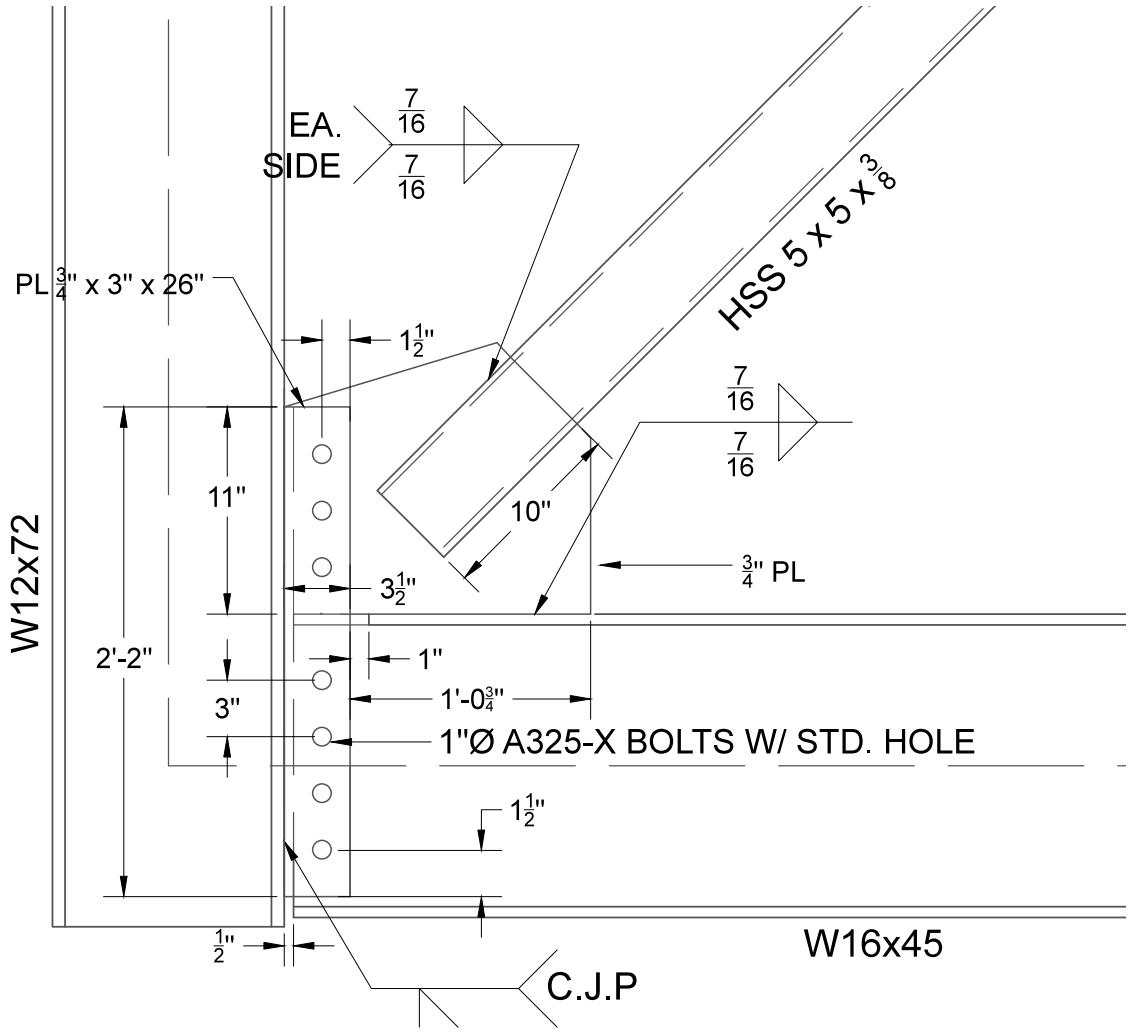

Figure A.2 - NHSS-B1 Connection Drawing

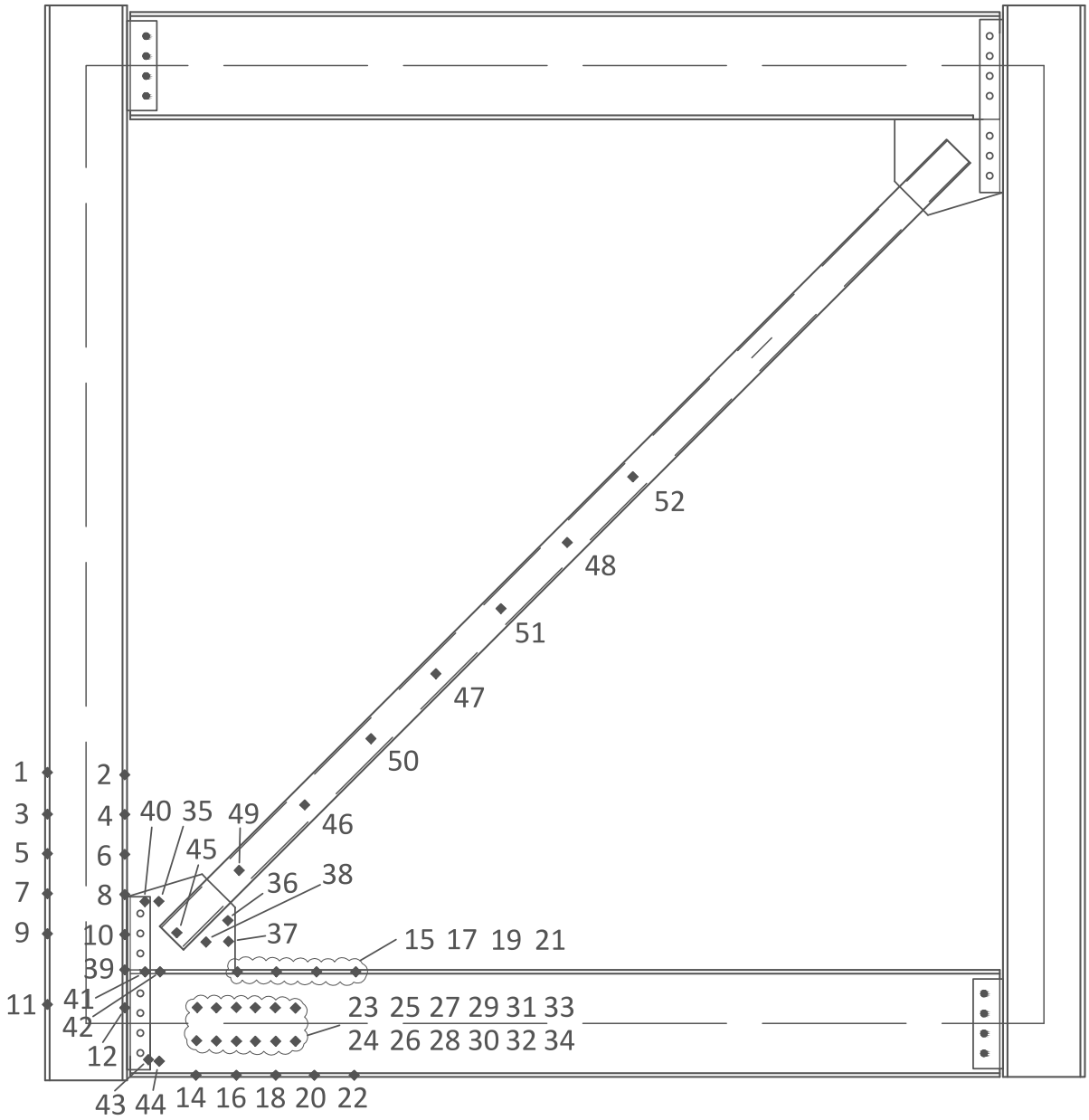

Figure A.3 - NHSS-B1 LED Optotrak Layout

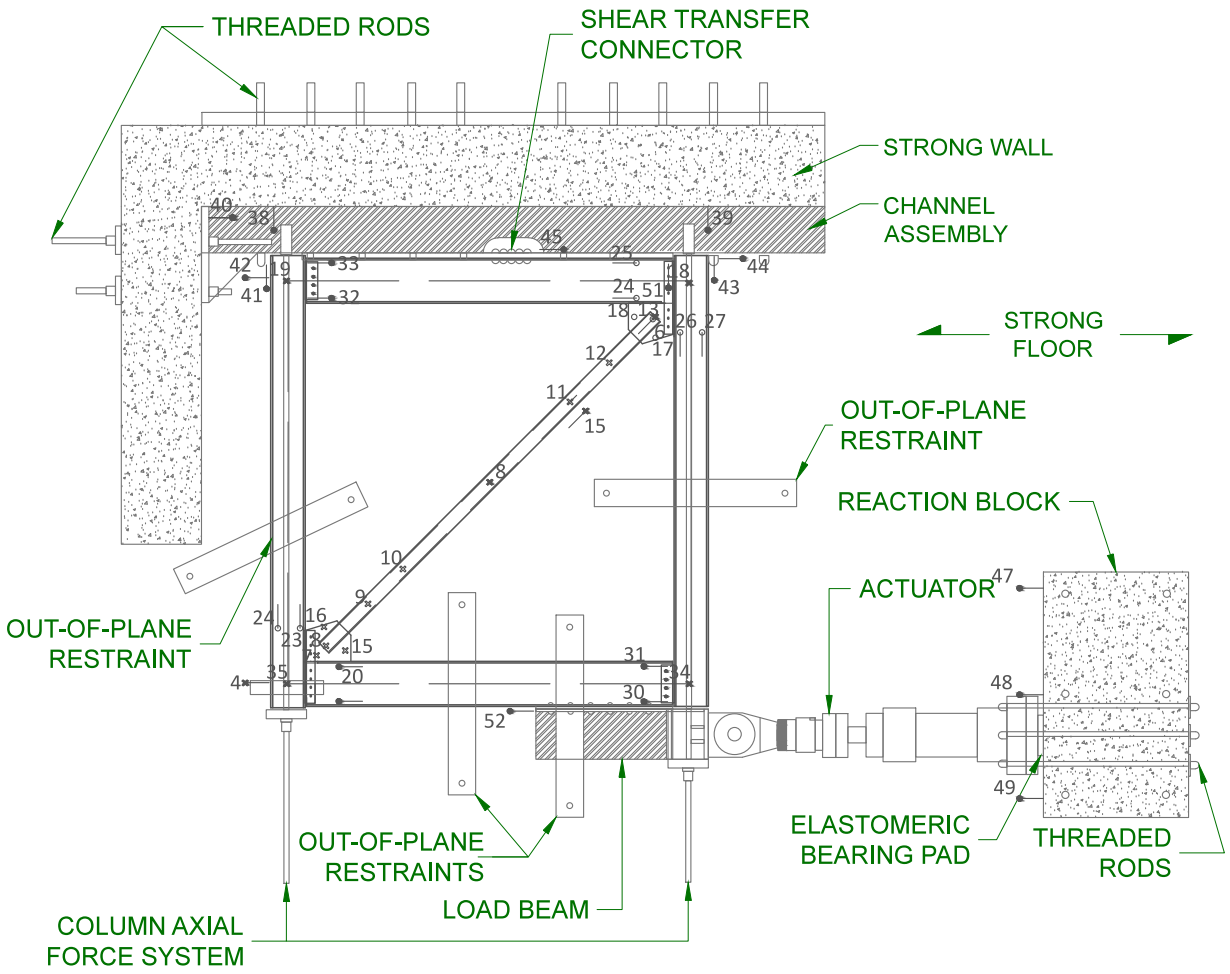

Figure A.4 - NHSS-B1 Potentiometer Layout

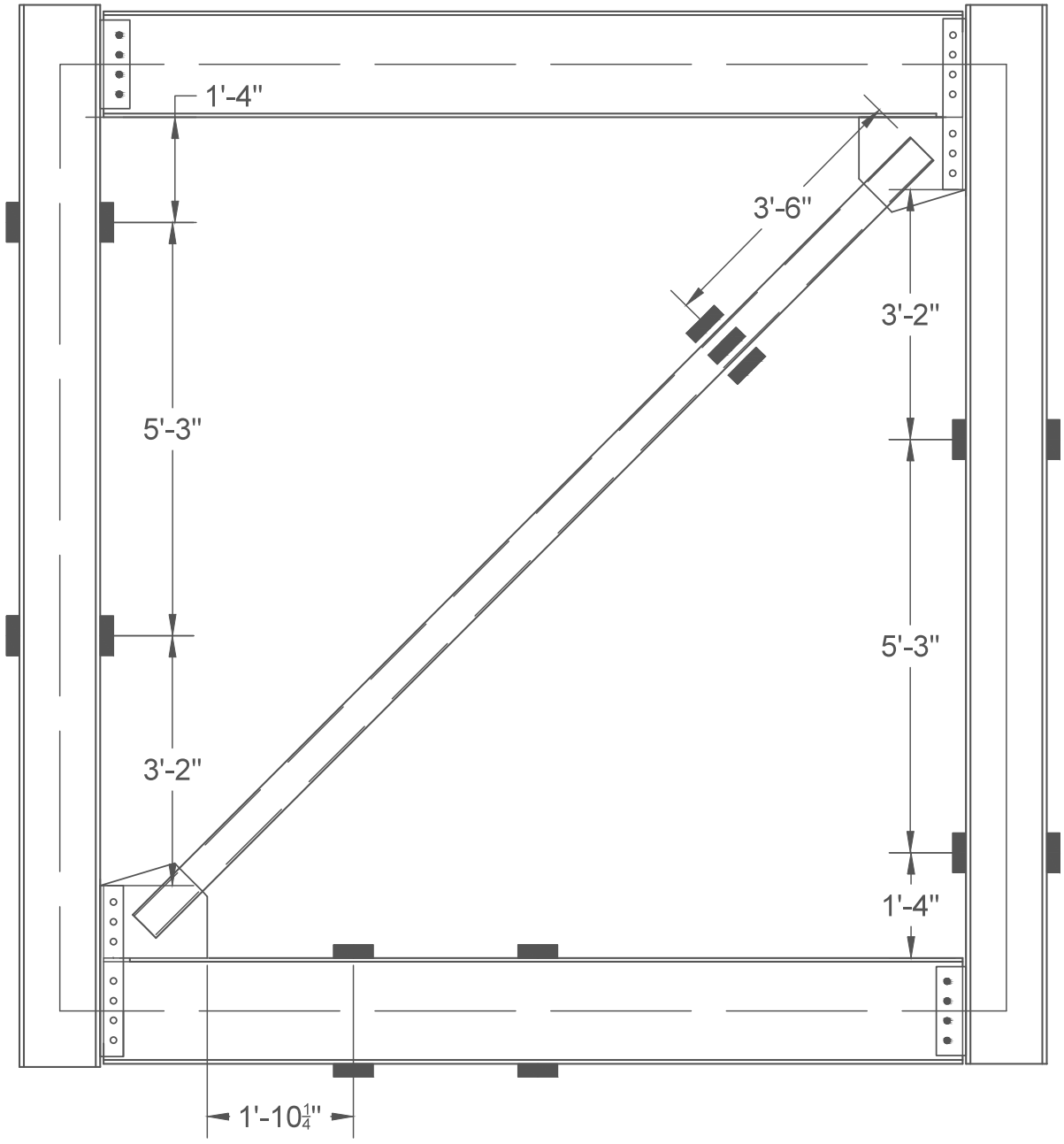

Figure A.5 - NHSS-B1 Strain Gauge Layout

A.2 NHSS-B2

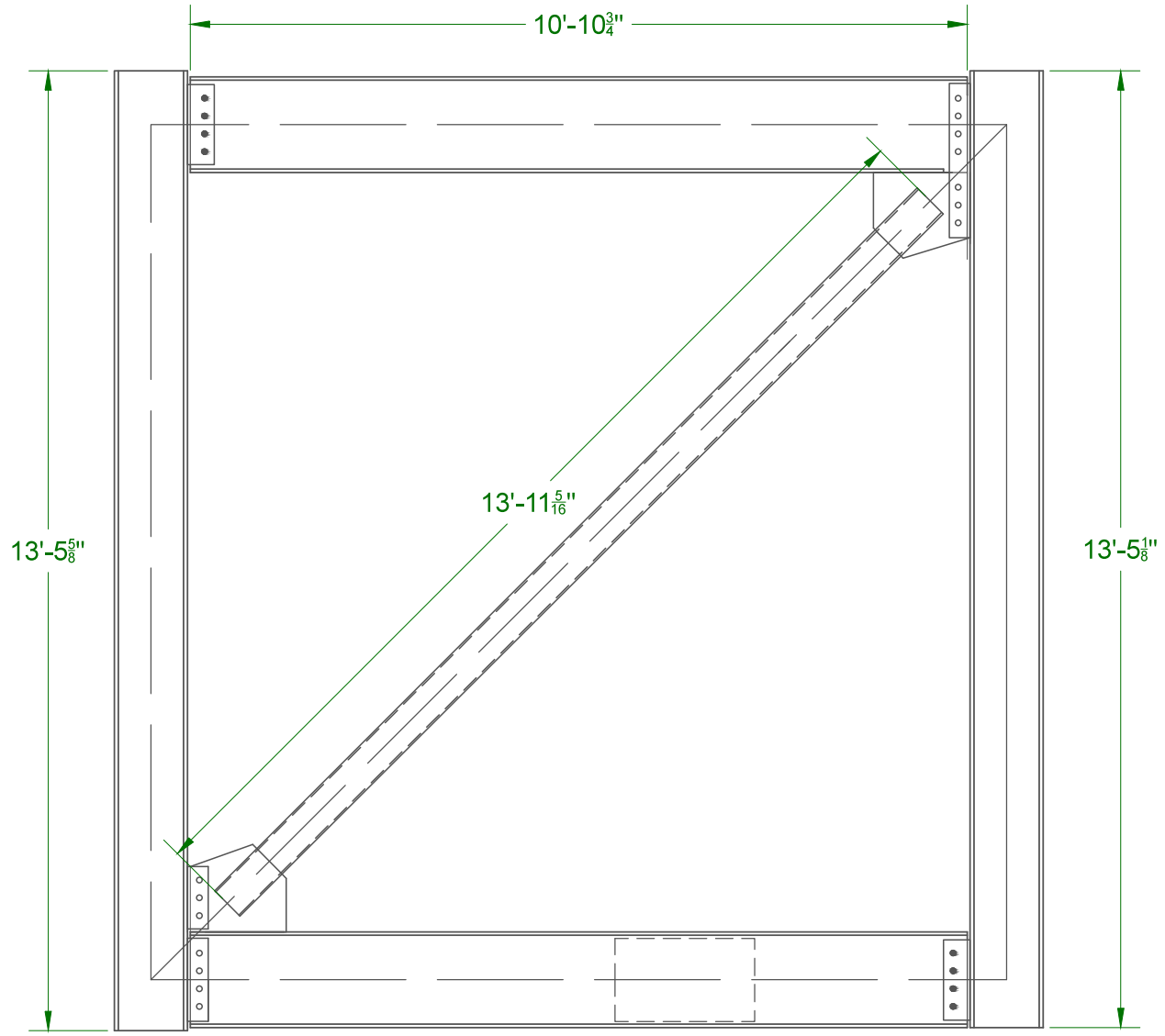

Figure A.6 - NHSS-B2 Full Frame Drawing

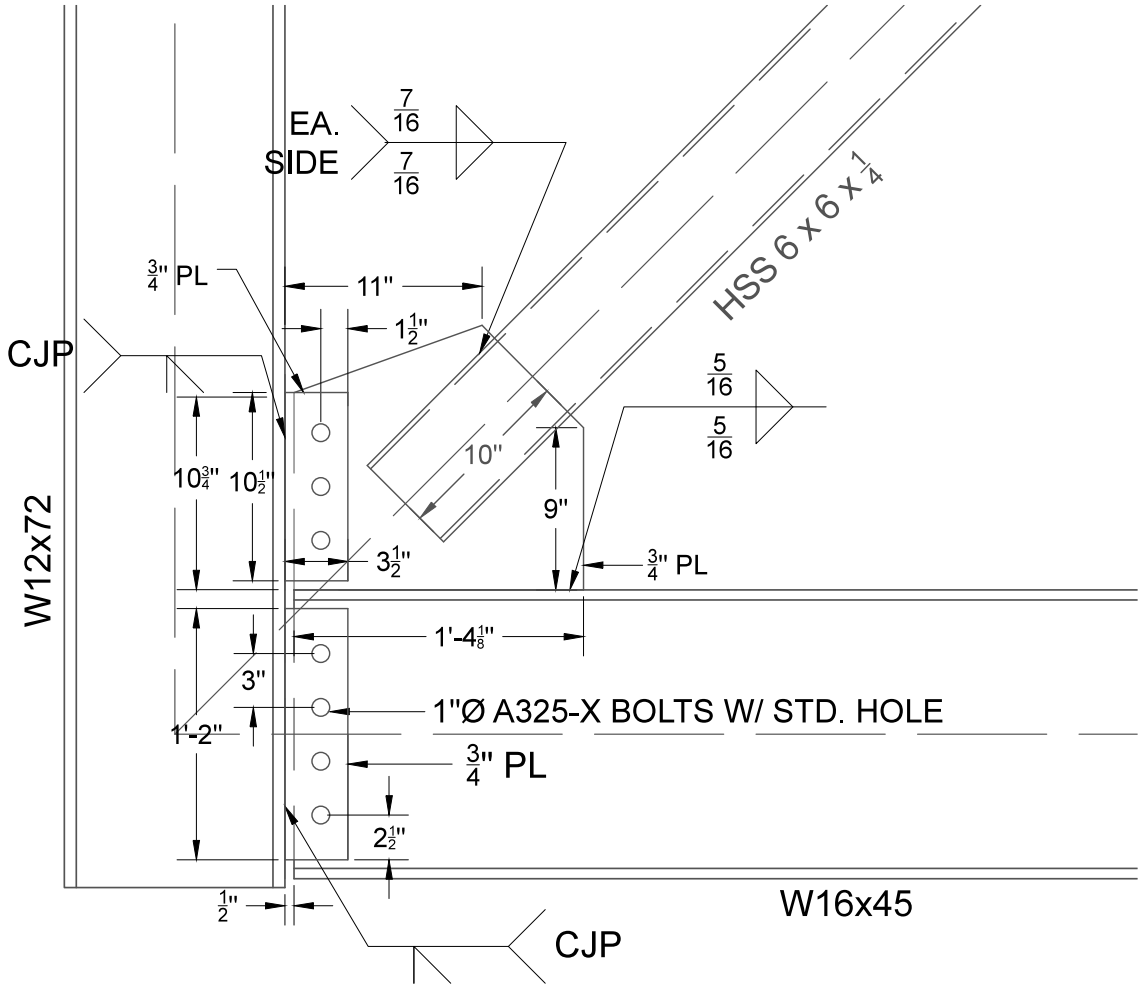

NE & SW GUSSET CONNECTION DETAILS

Figure A.7 - NHSS-B2 Connection Drawing

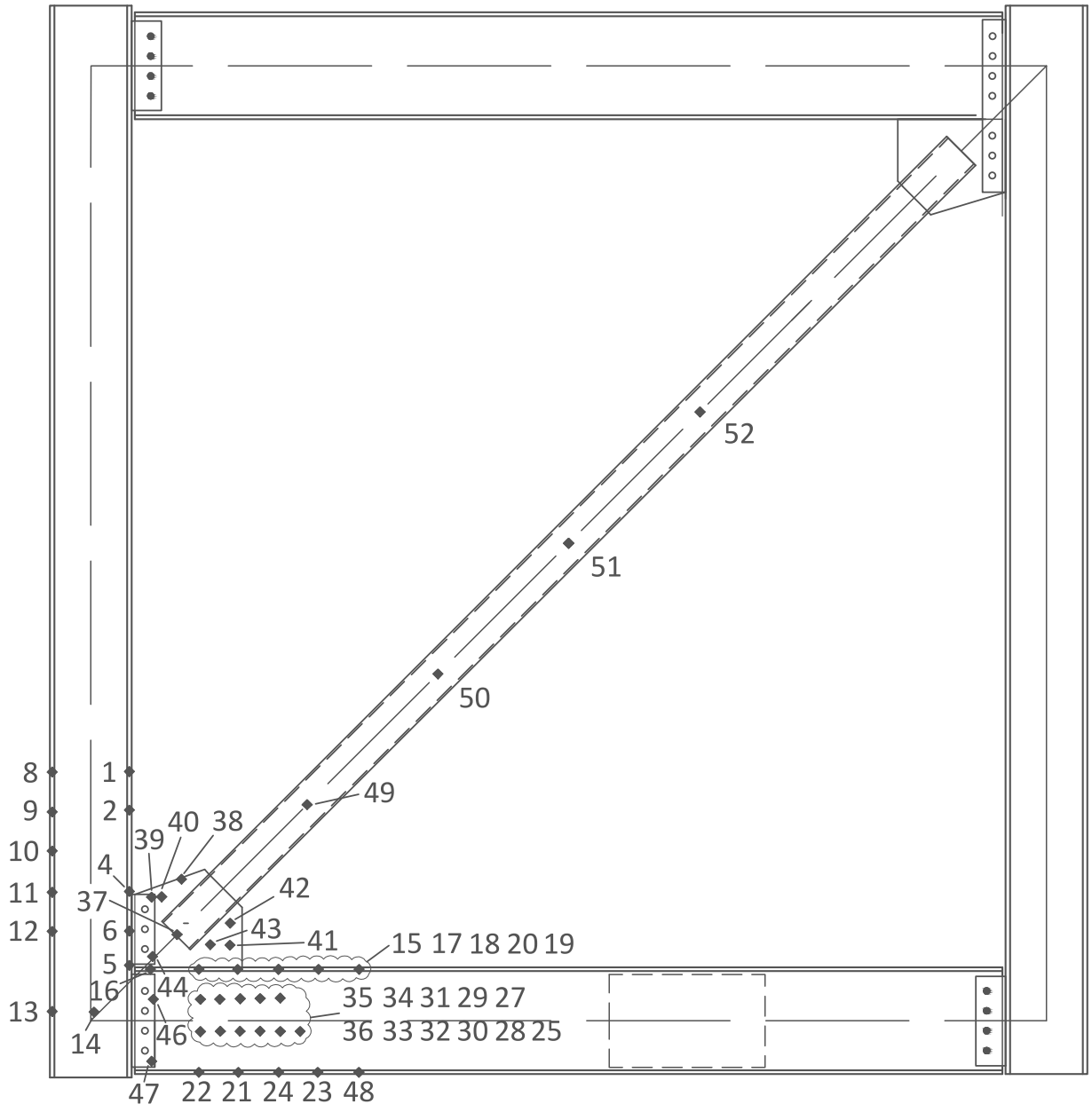

Figure A.8 - NHSS-B2 LED Optotrak Layout

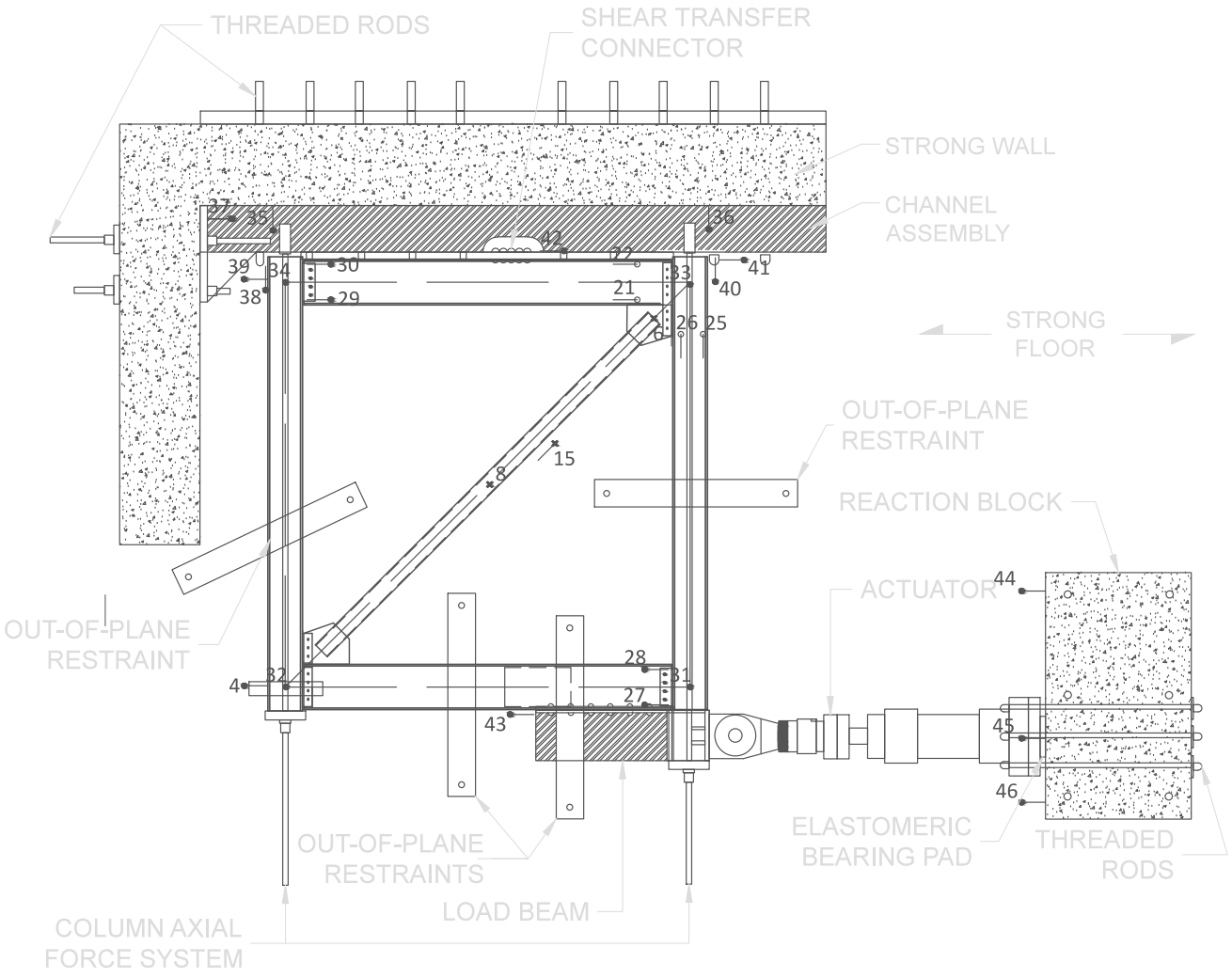

Figure A.9 - NHSS-B2 Potentiometer Layout

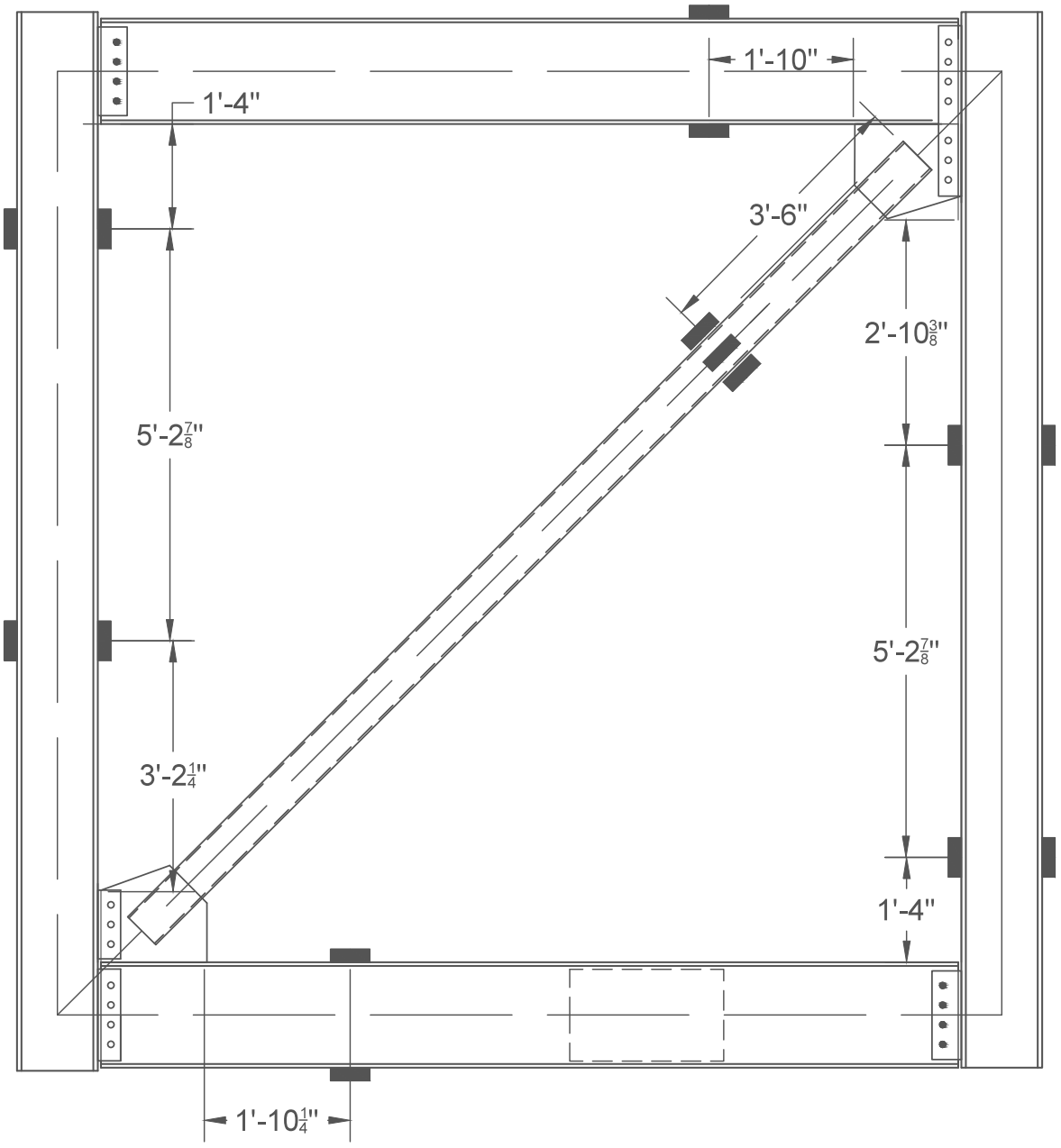

Figure A.10 - NHSS-B2 Strain Gauge Layout

A.3 NHSS-B3

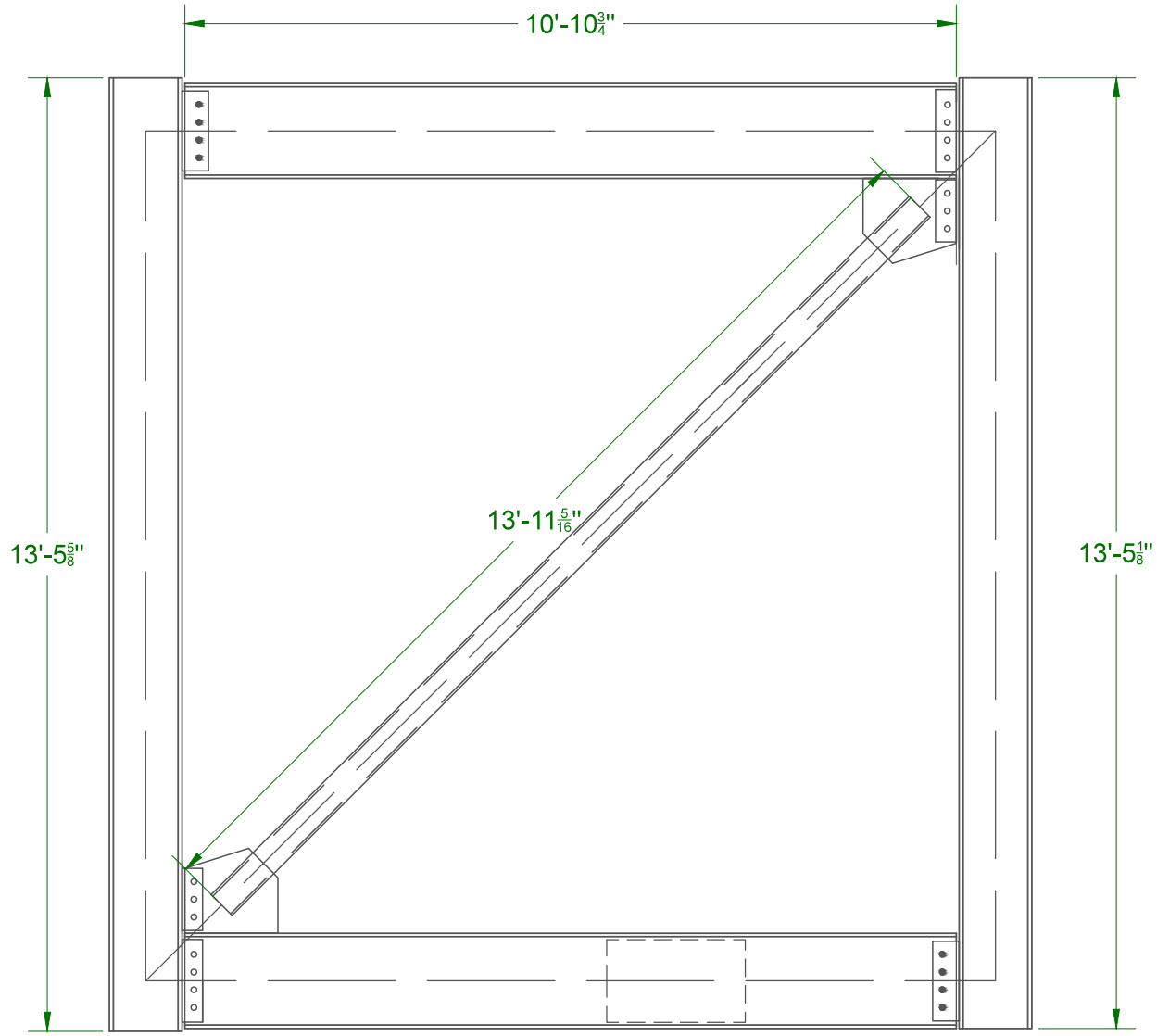

Figure A.11 - NHSS-B3 Full Frame Drawing

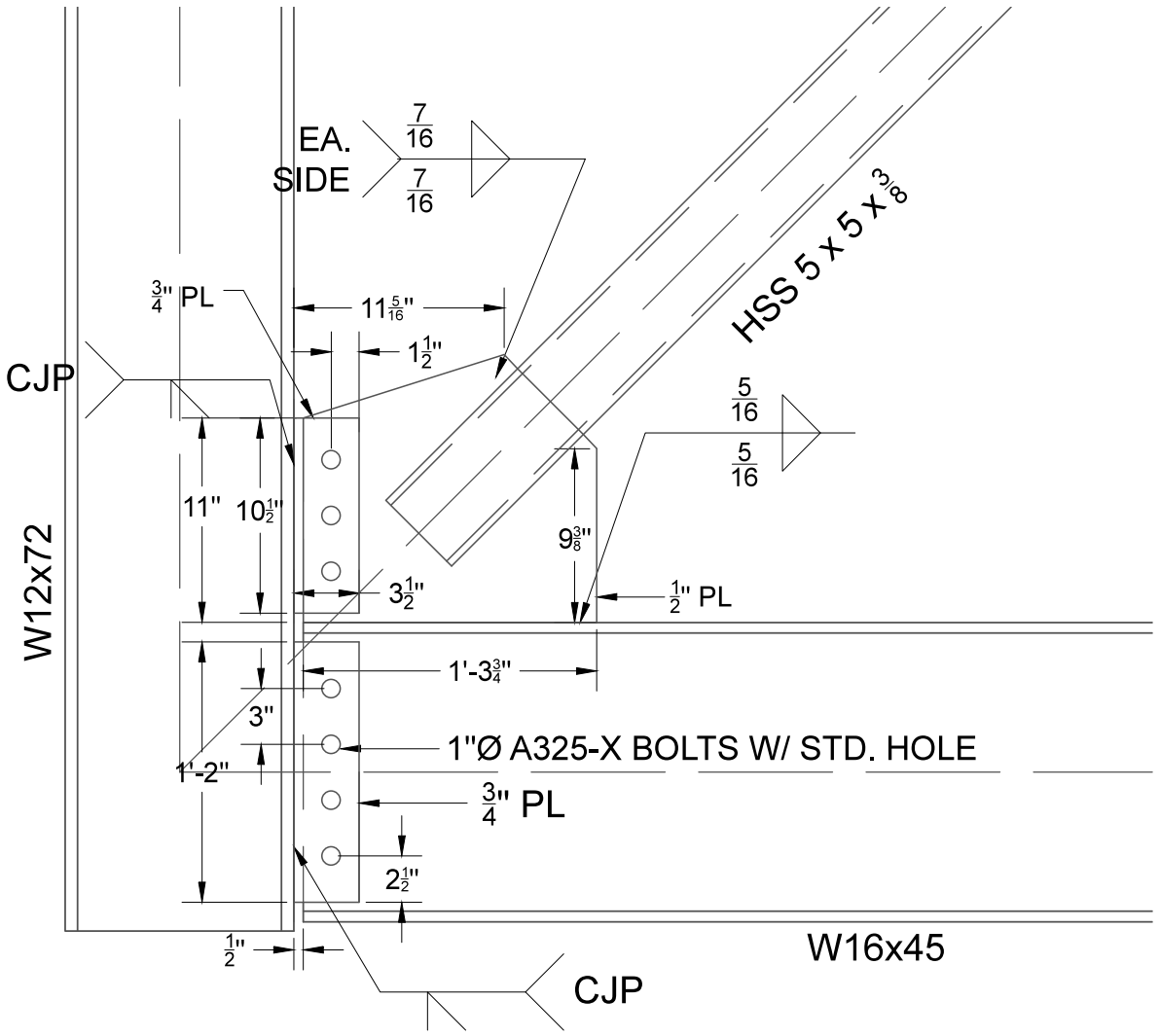

NE & SW GUSSET CONNECTION DETAILS

Figure A.12 - NHSS-B3 Connection Drawing

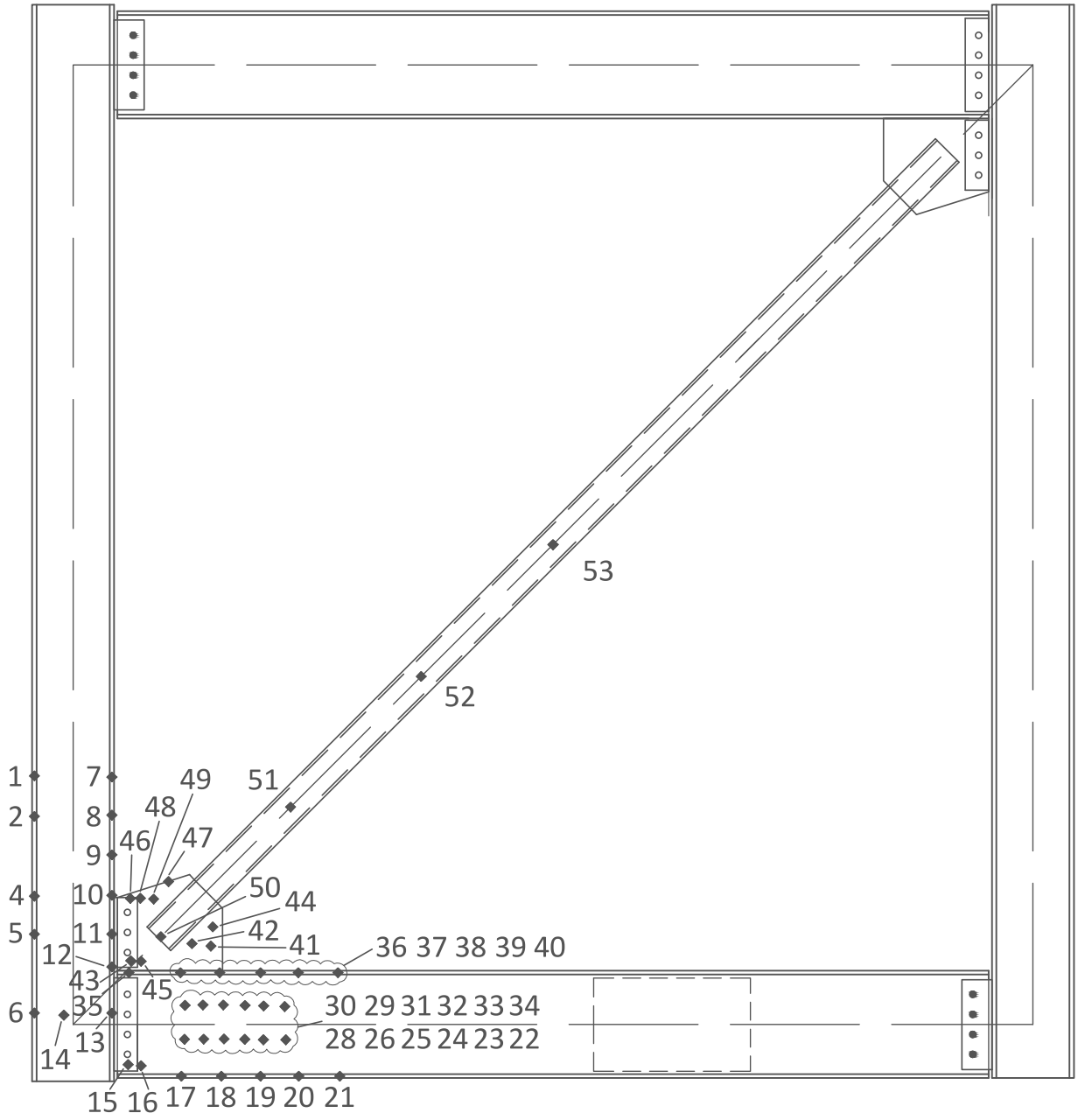

Figure A.13 - NHSS-B3 LED Optotrak Layout

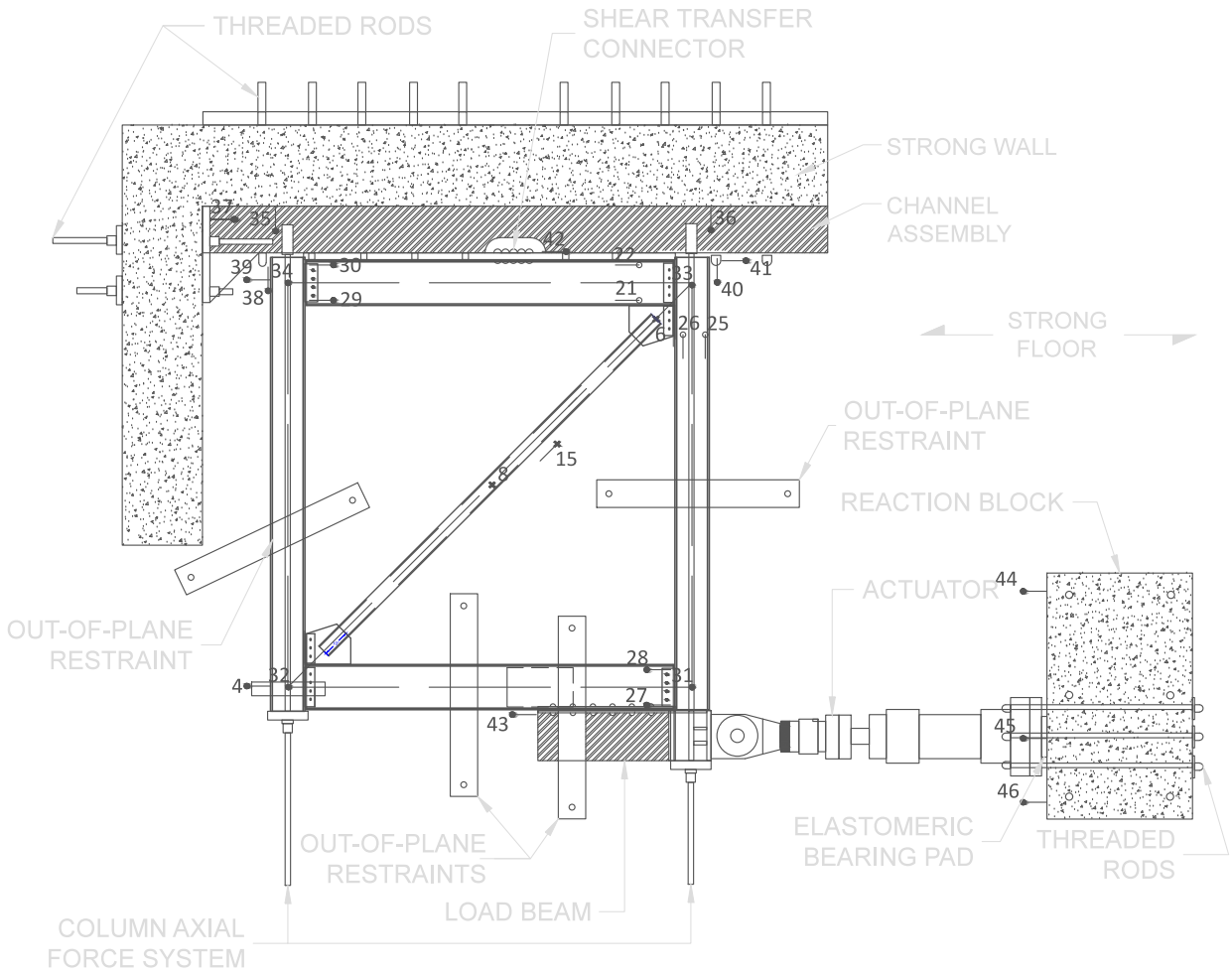

Figure A.14 - NHSS-B3 Potentiometer Layout

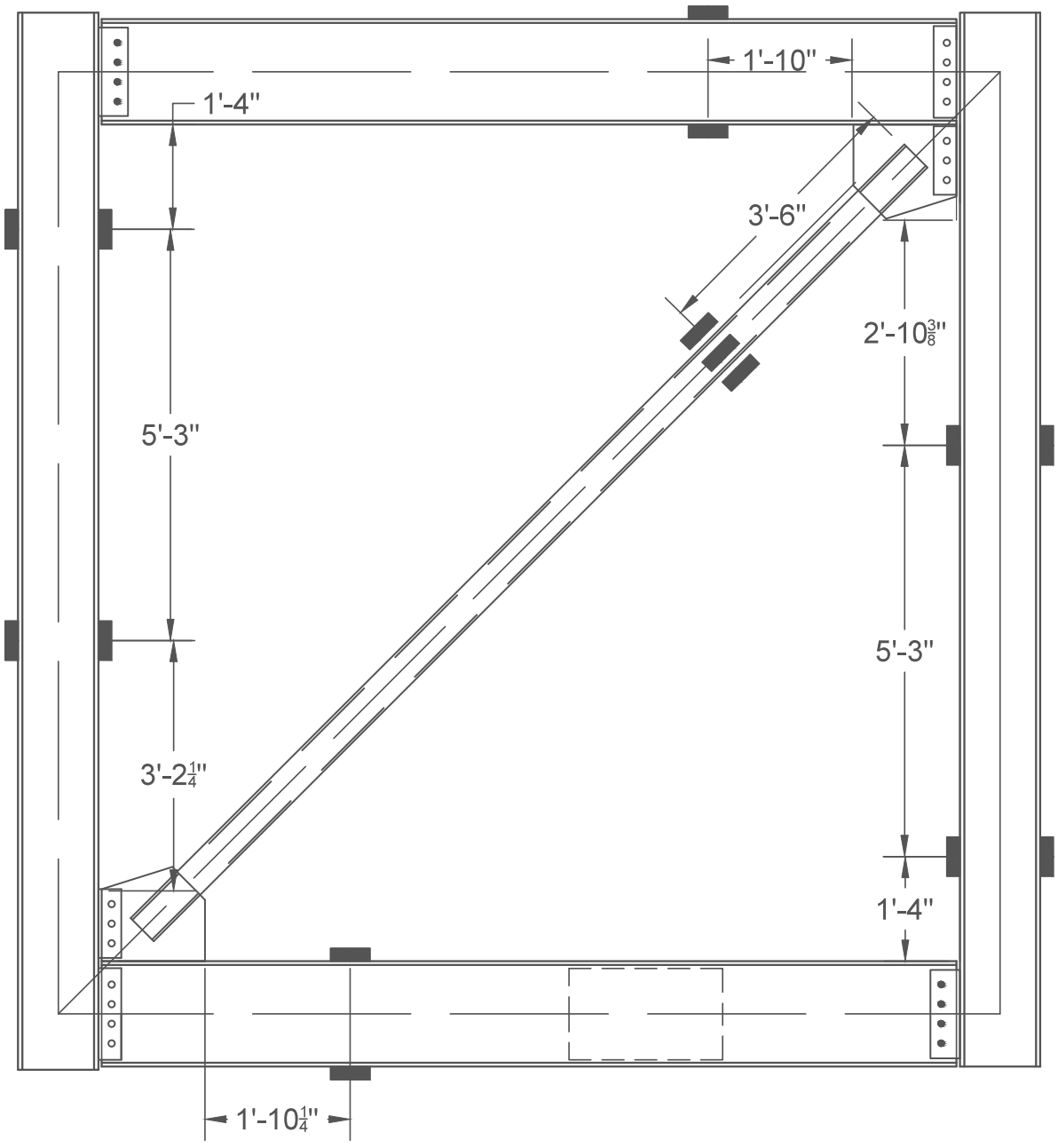

Figure A.15 - NHSS-B3 Strain Gauge Layout

APPENDIX B: LOAD HISTORIES

Table B.1 - NHSS-B1 Load History

CYCLE	LOAD (kip)
1	-39.3 35
2	-39.3 39.3
3	-72 76.5
4	-73.5 76.4
5	-103.5 106.5
6	-106 106.4
7	 130.5
8	-132.2 132
9	-155.3 144.9
10	-145.5 143.3
11	-167 158.1
12	-166.4 156.6
13	 164.2
14	-190.3 163.3
15	-201 164.9
16	-207.4 162.1
17	-238 158.5

CYCLE	LOAD (kip)
18	-239.3 154.5
19	-269.3 153.5
20	 150.1
21	-314 152.7
22	-299 149.8
23	-337 152
24	-317 149
25	-350 151
26	-325 147
27	-354 150
28	-324 145
29	-352 143
30	-323 135
31	-353 129
32	-331

Table B.2 - NHSS-B2 Load History

CYCLE	LOAD (kip)
1	-33.3 36.5
2	-33.6 36.4
3	-66.4 68.3
4	-67.5 68.2
5	-96.3 97.2
6	-99.2 96.8
7	-124.1 122.5
8	-126.9 121.3
9	-150 142.7
10	-152.1 141.5
11	-171.9 154.3
12	-170.5 152.2
13	-186.5 159.5
14	-186 157.1
15	-201.3 162.3
16	-202.4 159
17	-231.4 160.3
18	-231.7 156.7

CYCLE	LOAD (kip)
19	-251.6 155.3
20	-249.5 152.7
21	-281.6 120.7
22 END	-278.6 -98.6

Table B. 3 - NHSS-B3 Load History

CYCLE	LOAD (kip)
1	-35.7 40
2	-36.5 39.7
3	-72.5 76
4	-72.7 75.5
5	-103.7 109.1
6	-107.2 109.8
7	-135 139.7
8	-136.7 140.2
9	-163.7 161.7
10	-163.2 157.3
11	-184.8 171.2
12	-186.7 169.2
13	-207.7 166.5
14	-211.8 164.3
15	-229.2 161.5
16	-231 157.5
17	-261 156
18	-256 153.5

CYCLE	LOAD (kip)
19	-284 152.6
20	-276 151.6
21	-316 152.4
22	-304 147
23	-334 139
24	-191 127
25	-209 129
26	-166.7 114
27	-185 116
28	-180 114
29	-192 113.5
30	187 114
31	-198 113.8
32	-189 113
33	-202 113
34	-193 112
35	-204 112
36	-198 109

APPENDIX C: CALCULATIONS

Calculations are attached following this page in the form of hand calculations.

Input Variables:

HSS 5×5×3/8: $A_g = 6.18 in^2$, $L_{br} = 167.3 in$, $r = 1.87 in$, $R_Y = 1.4$, $R_t = 1.3$; $t_{br} = 0.349"$ (design thickness), $h_{br} = 5"$, $F_{Ybr} = 50 ksi$, $F_{ubr} = 62 ksi$ → Gr. C/A500

Gusset Plate: $F_{YP} = 50 ksi$, $F_{up} = 65 ksi$, $k_p = 0.65$ [corner], $L_1 = 0.5"$, $L_2 = 6.80"$, $L_3 = -1.50"$ → for Whitmore; $t_p = 0.75"$, $L_c = 10"$ [splice length]

W16×45: $h_{bm} = 16.1"$, $L_{cb} = 11.75"$ [top] ← controls, $15.75"$ [bottom] [coped flange gives diff lengths], $t_{wb} = 0.345"$, $b_{wb} = 0.70"$

W12×72: $h_c = 12.3"$, $L_{cc} = 26"$

BOLTS: 1" ϕ A325, $F_{nv} = 54 ksi$ [threads not excluded]

WELDS: $F_{exx} = 70 ksi$

ASSUMPTIONS: NO ϕ factors used because we want to predict actual capacities & demands.

use the uniform force method to allocate forces and find demands

FOR bolts... assume horiz & vert. component from UFM at centroid of bolt group but acting at face of COLUMN. c_x = dist from col. face to bolt group centroid. Assume RESULTANT 45° force to find "C." use "C" for bearing & bolt shear.

References

Brace Tensile Capacity: $P_{nt} = R_y F_y A_g$
$= (1.4)(50\,ksi)(6.18\,in^2) = \boxed{433k = P_{nt}}$ — manual D2-1 / F2.3 seismic provisions

Brace Compressive Capacity: $P_{nc} = 1.14 F_{cr} A_g$ — F2.3 seismic provisions

$$KL/r = \frac{(1.0)(167.3in)}{1.87in} = 89.5$$

$$4.71\sqrt{E/F_y} = 4.71\sqrt{29000ksi/50ksi} = 113.4$$

$\frac{KL}{r} < 4.71\sqrt{E/F_y}$ use: $F_{cr} = [0.658^{F_y/F_e}]F_y$ — Manual E3-2

$$F_e = \frac{\pi^2 E}{(KL/r)^2} = \frac{\pi^2(29000ksi)}{(89.5)^2} = 35.7\,ksi$$ — E3-4

$$F_{cr} = [0.658^{(R_yF_y/35.7)}]R_yF_y$$

$= 30.8\,ksi$

not including 1.1 factor as suggested in seismic provisions. → $\boxed{P_{nc} = 1.14(30.8ksi)(6.18in^2) = 217\,kip}$ — E3-1

Whitmore: width, $b_w = h_{br} + 2\tan(30)L_c$
$= 5" + 2\tan(30)(10")$ — p.9-4 Manual

$= 16.5"$

inertia, $I_w = 1/12(b_w)(t_p^3) = (1/12)(16.5")(3/4")^3$

$= 0.58in^4$

area, $A_w = b_w t_p = (16.5")(0.75") = 12.4in^2$

radius of gyration, $r_w = \sqrt{I_w/A_w} = \sqrt{(0.58in^4)/(12.4in^2)}$

$= 0.22in$

length, $L_p = \frac{L_1 + L_2 + L_3}{3} = \frac{0.5" + 6.8" - 1.5"}{3}$

$= 1.93"$

References

Euler GP buckling: $\frac{KL}{r} = \frac{(0.65)(1.93")}{0.22"} = 5.7$

$4.71\sqrt{E/F_{YP}} = 113.4$

$\frac{KL}{r} < 4.71\sqrt{E/F_{YP}}$, use $F_{cr} = [0.658^{F_{YP}/F_e}]F_{YP}$ — E3-2 Manual

$F_e = \frac{\pi^2 E}{(KL/r)^2} = \frac{\pi^2(29000ksi)}{(5.7)^2} = 8809\,ksi$

$F_{cr} = [0.658^{(50ksi/8809ksi)}](50ksi)$

$= 49.9\,ksi$

Brace to GP connection:

Net section properties: $\bar{x} = \frac{B^2 + 2BH}{4(B+H)} = \frac{(5")^2 + 2(5")(5")}{4(5" + 5")} = 1.875"$ — Table D3.1 #6

$U = 1 - \bar{x}/L_c = 1 - 1.875"/10" = 0.8125"$

$A_{nb} = A_{gb} - t_p t_{br} N_s = 6.18in^2 - (3/4")(0.349")(2)$ (2 = #slots)

$= 5.66in^2$

$A_{eb} = A_{nb}U = (5.66in^2)(0.8125)$ — D3-1

$= 4.6in^2$

Brace Block Shear:

Gross Shear Area: $A_{gvb} = 4[(10")(0.349")] = 14in^2$
Net Tension Area: $A_{ntb} = 0in^2$
Net Shear Area: $A_{nvb} = A_{gvb} - 0in^2 = 14in^2$

GP Block Shear:

Gross Shear Area, $A_{gvp} = 2(10")(0.75") = 15in^2$
Net Shear Area, $A_{nvp} = A_{gvp} - 0in^2 = 15in^2$
Net Tension Area, $A_{ntp} = (5")(0.75") = 3.75in^2$

Loading Uniformity, $U_{bs} = 1.0$ — J4-5 Manual

References

in brace section of steel Manual

UFM to allocate forces:

$e_b = 16.1"/2 = 8.05"$ $\alpha = 8.4"$

$e_c = 12.3"/2 = 6.15"$ $\beta = 5.5"$

$r = \sqrt{(\alpha + e_c)^2 + (\beta + e_b)^2} = \sqrt{(8.4" + 6.15")^2 + (5.5" + 8.05")^2} = 19.9"$

$V_c = \frac{\beta}{r} \cdot P = \left(\frac{5.5"}{19.9"}\right)(433k) = 119.7k$

$H_c = \frac{e_c}{r} \cdot P = \left(\frac{6.15"}{19.9"}\right)(433k) = 133.8k$

$V_b = \frac{e_b}{r} \cdot P = \left(\frac{8.05"}{19.9"}\right)(433k) = 175.2k$

$H_b = \frac{\alpha}{r} \cdot P = \left(\frac{8.4"}{19.9"}\right)(433k) = 182.8k$

GP to B weld designed for $182.8k$ & $175.2k$

$P_{GP} = \sqrt{(182.8k)^2 + (175.2k)^2} = 253.2k$

Bolts in shared shear tab for $119.7k$ & $133.8k$ [from GP]

combine forces

& $R_b - V_b$ & A_b & $(H - H_b)$ [from B to C]

0 0 $= P\cos 45$

$P_{VERT} = 119.7k + 175.2k = 295k$

$P_{HORIZ} = 133.8k + [H - H_b] = 257k$

$P_{BOLTS} = \sqrt{295k^2 + 257k^2} = 391k$

BOLTS IN GP to COL for V_c & H_c $\rightarrow \sqrt{119.7k^2 + 133.8k^2} = 180k$

Beam to COL for V_B & $H - H_b$ $\rightarrow \sqrt{175.2k^2 + 124k^2} = 215k$

DESIGN CHECKS:

References

Brace Net Section Fracture: $\phi R_t F_u A_c = \phi(1.3)(62ksi)(4.6in^2)$ — D2-2 Manual

$= \phi(370.8k)$

Brace Block Shear: $\phi[0.6F_uA_{nv} + U_{bs}F_uA_{nt}] \leq \phi[0.6F_yA_{gv} + U_{bs}F_uA_{nt}]$ — J4-5 Manual

$\phi[0.6(62ksi)(14in^2)+(1)(62ksi)(0)] \leq \phi[0.6(50ksi)(14in^2)+(1)(62ksi)(0)]$

$\phi[520.8k] \leq \phi[\underline{420k}]$ (R_t)

Plate Block Shear: $\phi[0.6(65ksi)(15in^2)+(1)(65ksi)(3.75in^2)] \leq \phi[0.6(50ksi)(15in^2)+(1)(65ksi)(3.75in^2)]$ — J4-5 Manual

$\phi[828.8k] \leq \phi[\underline{693.8k}]$

Whitmore GP Yielding: $\phi F_yA_G = \phi[F_{yp}b_wt_p + F_{yb}b_wt_{bm}]$ — J4-1 Manual

(b_w = width in GP; b_w = width in beam web)

$= \phi[(50ksi)(15.1")(3/4") + (50ksi)(0.7")(0.345")]$

$= \phi[578.3k]$

Whitmore Fracture: $\phi F_uA_e = \phi[F_{up}b_wt_p + F_{ub}b_wt_p]$ — J4-2 Manual

$= \phi[(65ksi)(15.1")(3/4") + (65ksi)(0.7")(0.345")]$

$= \phi[751.8k]$

GP Buckling: $\phi F_{cr}A_G = \phi F_{cr}b_wt_p = \phi(49.9ksi)(15.1")(0.75")$ — E3-1

$= \phi[565.1k]$

Brace to GP weld fracture: $\phi[0.6F_{exx}(1+0.5\sin^{1.5}\theta)A_{we}]N_w$ — J2-4 / J2-5

$= \phi[0.6(70ksi)(1)(\sqrt{2}/2)(7/16)(10")]4$

$= \phi[520k]$

Brace to GP base metal fracture: $\phi[F_{nBM}A_{BM}N_w] = \phi[0.6F_uA_{nv}N_w]$ — J2-2 / J4-4

$= \phi[0.6(62ksi)(10")(0.349")(4)] = \phi[519.3k]$

References

Gusset Plate Shear Yielding: $\phi[0.6F_yA_{gv}]$ — J4-3

$= \phi[0.6(50ksi)(3/4")(11.75")]$

$= \phi[264.4kip]$

BEAM to GP WELD FRACTURE: $\phi[0.6F_{exx}(1+0.5\sin^{1.5}\theta)A_{we}N_w]$

$= \phi[0.6(70ksi)(1+0.5\sin^{1.5}(45°))(\sqrt{2}/2)(\frac{7}{16})(11.75")(2)]$

$= \phi[396.1k]$

COLUMN to BEAM & GP BOLT SHEAR: $\phi[F_{nv}A_bN_b]$ see p.7 — J3-1

$= \phi[(54ksi)(\pi(0.5")^2)(6.65)]$

$= \phi[282.0k]$

COLUMN to GP BOLT BEARING: $\phi[1.2L_ct_pF_u] \leq \phi[2.4dt_pF_u]$ — J3-6a
(deformation at service a concern)

$\phi[1.2(1.41")(0.75")(65ksi)] \leq \phi[2.4(1")(0.75")(65ksi)]$

$\phi[82.5k \cdot 7bolts] \leq \phi[117k \cdot 7bolts]$

$= \phi[577.5k]$

COLUMN TO BEAM BOLT BEARING: $t_p = 0.345in$ (4bolts) $\rightarrow \phi[151.8k]$

BLOCK SHEAR COLUMN TO GP & BEAM IN PLATE: $\phi[U_{bs}F_uA_{nt} + 0.6F_uA_{nv}] \leq \phi[0.6F_yA_{gv} + U_{bs}F_uA_{nt}]$

$U_{bs} = 1$, uniform

LINE: $\phi[(1)(65ksi)(0) + 0.6(65ksi)(13.9in^2)] \leq \phi[0.6(50ksi)(19.5in^2) + (1)(65ksi)(0)]$

$= \phi[542.1k] \leq \phi[585k]$

"C": $\phi[(1)(65ksi)(11\ in^2) + 0.6(65ksi)(1.5in^2)] \leq \phi[0.6(50ksi)(2.25in^2) + (1)(65ksi)(11\ in^2)]$

$= \phi[773.5k] \leq \phi[782.5k]$

"L": $\phi[(1)(65ksi)(1.1in^2) + 0.6(65ksi)(12.4ksi)] \leq \phi[0.6(50ksi)(17.6in^2) + (1)(65ksi)(1.1in^2)]$

$= \phi[555.1k] \leq \phi[599.5k]$

BLOCK SHEAR COLUMN TO GP & BEAM

- in PLATE : all vertical

$A_{gv} = (0.75")(26") = 19.5 in^2$
$A_{nv} = (0.75")(26" - 7(1"/16")) = 13.9 in^2$
$A_{nt} = 0 in^2$

*can't have block shear in GP without also in beam web
*can't travel vertically through beam to GP because of beam flange

- in PLATE: HORIZONTAL "C" OR "L" shape

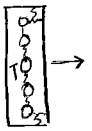

"C" : $A_{gv} = (3/4")(1.5")2 = 2.25 in^2$
$A_{nv} = (3/4")(1")2 = 1.5 in^2$
$A_{nt} = (3/4")(21" - 6(1"/16")) = 11 in^2$

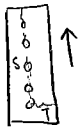

"L" : $A_{gv} = (3/4")(23.5") = 17.6 in^2$
$A_{nv} = (3/4")(23.5" - 6.5(1"/16")) = 12.4 in^2$
$A_{nt} = (3/4")(1.5") = 1.1 in^2$

USING TABLE 7-6

~~$e_x = 1.05"$ 2.7" GP to C , 4.07" BM to C~~
$S = 3"$
bolts = 7
~~C = 0.65 interpolation between $e_x = 0$ & $e_x = 2$~~

SAME AS NCBF8 : C (B to C) = 2.54

C (GP to C) = 1.95

DEMAND TO CAPACITY RATIOS:

BRACE NET SECTION: 433K/371K = 1.2

BRACE BLOCK SHEAR: 433K/420K = 1.1

GP BLOCK SHEAR: 433K/694K = 0.62

WHITMORE GP YIELDING: 433K/578K = 0.75

WHITMORE GP FRACTURE: 433K/752K = 0.58

GP BUCKLING: 217K/565K = 0.38

BRACE TO GP WELD FRACTURE: 433K/520K = 0.83

BRACE TO GP BASE METAL FRACTURE: 433K/519K = 0.83

GP SHEAR YIELDING: 182K/264K = 0.69

BEAM TO GP WELD FRACTURE: 253K/396K = 0.64

COLUMN TO BEAM BOLT SHEAR: 1.56

COLUMN TO GP BOLT BEARING: 1.29

BLOCKSHEAR COLUMN TO GP: BEAM: LINE: 391K/542K = 0.72

COLUMN TO GP BOLT SHEAR: 2.52

COLUMN TO BEAM BOLT BEARING: 1.73

New Input Variables:

HSS6x6x1/4: $A_g = 5.24in^2$ $h_{br} = 6"$
$L_{br} = 167.3in$
$r = 2.34in$
$t_{br} = 0.233in$

Brace Tensile Capacity: $P_{nt} = R_y F_y A_g = (1.4)(50ksi)(5.24in^2) = 367k$

Brace Compressive Capacity: $P_{nc} = 1.14 F_{cr} A_g$

$$\frac{KL}{r} = \frac{(1)(167.3")}{2.34"} = 74.7 < 4.71\sqrt{E/F_y}$$

$$F_e = \frac{\pi^2 E}{(KL/r)^2} = \frac{\pi^2(29000ksi)}{(74.7)^2} = 51.3ksi$$

$$F_{cr} = [0.658^{R_y F_y / F_e}] R_y F_y$$
$$= [0.658^{R_y F_y / 51.3}] R_y F_y = 39.5ksi$$

$$P_{nc} = 1.14(39.5ksi)(5.24in^2) = 236k$$

Whitmore: $b_w = 6" + 2\tan 30(10") = 17.5"$

$I_w = (1/12)(17.5")(3/4")^3 = 0.62in^4$

$A_w = (17.5")(0.75") = 13.1in^2$

$r_w = \sqrt{(0.62in^4)/(13.1in^2)} = 0.22in$

$L_p = \frac{0" + 6.79" - 2"}{3} = 1.6"$

euler buckling GP: $KL/r = (0.65)(1.6")/0.22" = 4.73 < 4.71\sqrt{E/F_y}$

$F_e = \pi^2 E/(KL/r)^2 = 12793ksi$

$F_{cr} = [0.658^{F_y/F_e}] F_y = 49.9ksi$

Brace to GP connection:

NET SECTION: $\bar{x} = \frac{(6")^2 + 2(6")(6")}{4(6" + 6")} = 2.25"$

$U = 1 - \bar{x}/L_c = 1 - 2.25"/10" = 0.775"$

$A_{nb} = 5.24in^2 - (0.75")(0.233")(2) = 4.89in^2$

$A_{cb} = UA_{nb} = 3.79in^2$

Brace Block Shear: $A_{gvb} = 4(10")(0.233") = 9.32in^2$
$A_{ntb} = 0$
$A_{nvb} = 9.32in^2$

GP Block Shear: $A_{gvp} = 15in^2$ $A_{nvp} = 15in^2$ → see NCBF4
$A_{ntp} = (6")(0.75") = 4.5in^2$

$U_{bs} = 1.0$

UFM to ALLOCATE FORCES:

$e_b = 8.05"$ $\alpha = 8.6"$ $r = 20.2"$
$e_c = 6.15"$ $\beta = 5.75"$

$V_c = 105k$ $V_b = 147k$

$H_c = 112k$ $H_b = 156k$

GP to BEAM Weld DESIGNED FOR V_b & H_b → $\sqrt{147^2 + 156^2} = 215k$

BOLTS IN GP to COLUMN FOR V_c & H_c → $\sqrt{105^2 + 112^2} = 154k$

IN BEAM to COLUMN FOR VB & $H - H_b$ → $\sqrt{147^2 + 104^2} = 180k$

Table 7-6

GP to C: $s = 3"$ (45°)
$N = 3$
$e_x = 2"$
$C = 2.23$

B to C: $s = 3"$ (45°)
$N = 4$
$e_x = 2"$
$C = 3.26$

DESIGN CHECKS:

BRACE NET SECTION: $\phi R_t F_u A_c = \phi(1.3)(62ksi)(3.79in^2) = \phi(305k)$

BRACE BLOCK SHEAR: $\phi[0.6(62ksi)(9.32in^2)+(1)(62ksi)(0)] \leq \phi[0.6(50ksi)(9.32")+(1)(62ksi)(0)]$

$\phi[280k]$

PLATE BLOCKSHEAR: $\phi[0.6(65ksi)(15in^2)+(1)(65ksi)(4.5in^2)] \leq \phi[0.6(50ksi)(15in^2)+(1)(65ksi)(4.5in^2)]$

$\phi[743k]$

WHITMORE GP YIELDING: $\phi[(50ksi)(15.6")(0.75")+(50ksi)(1.2")(0.345")]$

$\phi[606k]$

WHITMORE GP FRACTURE: $\phi[(65ksi)(15.6")(0.75")+(65ksi)(1.2")(0.345")]$

$=\phi[794k]$

GP BUCKLING: $\phi(49.9ksi)(15.6")(0.75") = \phi[584k]$

BRACE TO GP WELD FRACTURE: $\phi[0.6(70ksi)(1)(\sqrt{2}/2)(7/16")(10")(4")] = \phi[520k]$

BRACE TO GP BASE METAL FRACTURE: $\phi[0.6(62ksi)(10")(0.233")(4)] = \phi[347k]$

GP SHEAR YIELDING: $\phi[0.6(50ksi)(3/4")(16")] = \phi[360k]$

BEAM TO GP WELD FRACTURE: $\phi[0.6(70ksi)(1+0.5\sin^{1.5}(45))(\sqrt{2}/2)(5/16")(16")(2)]$

$=\phi[385k]$

COLUMN TO GP BOLT SHEAR: $\phi[(54ksi)(\pi(0.5")^2)(2.23)] = \phi[94.6k]$

COLUMN TO BEAM BOLT SHEAR: $\phi[(54ksi)(\pi(0.5")^2)(3.20)] = \phi[138.3k]$

COLUMN TO GP BOLT BEARING:

in GP: $\phi[82.5k \cdot 2.23 bolts] = \phi[184k]$

in BEAM: $\phi[1.2(1.41")(0.345")(65ksi)] \leq \phi[2.4(1")(0.345")(65ksi)]$

$\phi[124k]$

BLOCK SHEAR: * still has to move as a unit, cant have block shear in GP only
* can't have vertical line because of beam flange
* won't GOVERN

DCR'S:

BRACE NET SECTION: 367K/305K = 1.2

BRACE BLOCK SHEAR: 367K/280K = 1.3

GP BLOCK SHEAR: 367K/743K = 0.49

WHITMORE GP YIELDING: 367K/606K = 0.61

WHITMORE GP FRACTURE: 367K/794K = 0.46

GP BUCKLING: 236K/584K = 0.40

BRACE TO GP WELD FRACTURE: 367K/520K = 0.71

BRACE TO GP BASE METAL FRACTURE: 367K/347K = 1.1

GP SHEAR YIELDING: 215K/360K = 0.60

BEAM TO GP WELD FRACTURE: 215K/385K = 0.56

COLUMN TO GP BOLT SHEAR: 154K/94.6K = 1.63

COLUMN TO BEAM BOLT SHEAR: 180K/138.3K = 1.30

COLUMN TO GP BOLT BEARING: 154K/184K = 0.84

COLUMN TO BEAM BOLT BEARING: 180K/124K = 1.45

NCBF8 Input Variables: [return to HSS5x5x3/8]

Gusset Plate: $t_p = 0.5"$
$L_1 = 0.49"$
$L_2 = 6.79"$ $\longrightarrow L_p = 1.93"$
$L_3 = -1.49"$

Same calcs as NCBF4: $P_{nt} = 433k$ $A_{gvb} = 14in^2$
$P_{nc} = 217k$ $A_{ntb} = 0in^2$
$F_{cr(GP)} = 49.9ksi$ $A_{nvb} = 14in^2$
$U_{(brtoGP)} = 0.8125$ $U_{bs} = 1.0$

Brace to GP connection:

Net Section: $A_{nb} = A_{gb} - t_p t_{br} N_s = 6.18in^2 - (1/2")(0.349")(2)$
$= 5.83in^2$

$A_{eb} = A_{nb} U = (5.83in^2)(0.8125) = 4.74in^2$

GP Block Shear: $A_{gvp} = 2(10")(0.5") = 10in^2$

$A_{nvp} = A_{gvp} - 0in^2 = 10in^2$

$A_{ntp} = (5")(1/2") = 2.5in^2$

UFM: $e_b = 8.05"$ $\alpha = 8.4"$ $r = 20.1"$
$e_c = 6.15"$ $\beta = 5.75"$

$V_c = (\beta/r)P = (5.75"/20.1")(433k) = 124k$

$H_c = (e_c/r)P = 133k$

$V_b = (e_b/r)P = 174k$

$H_b = (\alpha/r)P = 181k$

UFM:

GP to Beam Weld Designed for V_b : $H_b \rightarrow \sqrt{(174k^2)+(181k)^2} = 251k$

BOLTS IN GP to COLUMN for V_c : $H_c \rightarrow \sqrt{(124k)^2+(133k)^2} = 182k$

BOLTS IN Beam to column for V_B : $H-H_b \rightarrow \sqrt{(174k)^2+(306k-181k)^2} = 214k$

DESIGN CHECKS:

Brace Net Section Fracture: $\phi R_t F_u A_c = \phi(1.3)(62ksi)(4.74in^2) = \phi(382k)$

Brace Block Shear (NCBF4): $\phi(420k)$

Plate Block Shear: $\phi[0.6(65ksi)(10in^2)+(1)(65ksi)(2.5in^2)] \leq \phi[0.6(50ksi)(10in^2)+(1)(65ksi)(2.5in^2)]$

$\phi[553k] \leq \phi[463k]$

Whitmore GP Yielding: $\phi F_y A_G = \phi[F_{yp} b_w t_p + F_{yb} b_w t_{bm}]$

$= \phi[(50ksi)(15.1")('1/2") + 12.1k] = \phi[390k]$

WHITMORE FRACTURE: $\phi F_u A_c = \phi[F_{up} b_w t_p + F_{ub} b_w t_p]$

$= \phi[(65ksi)(15.1")('1/2") + 15.7k] = \phi[506k]$

Brace to GP base metal fracture: $\phi[519.3k]$ (NCBF4)

Gusset Plate Shear Yielding: $\phi[0.6 F_y A_{gv}] = \phi[0.6(50ksi)('1/2")(15.75")]$

$= \phi[236k]$

Beam to GP Weld fracture: $\phi[0.6 F_{exx}(1+0.5\sin^{1.5}\theta) A_{we} N_w]$

$= \phi[0.6(70ksi)(1+0.5\sin^{1.5}(45))(\sqrt{2}/2)(5/16)(15.75")(2)]$

$= \phi[379k]$

COL to GP Bolt Shear: $\phi[94.6k]$ COL to Beam : $\phi[138.3k]$

COL to GP Bolt Bearing: $\phi[1.2 L_c t_p F_u] \leq \phi[2.4 d_b t_p F_u]$

$= \phi[1.2(1.41")('1/2")(65ksi)] \leq \phi[2.4(1")('1/2")(65ksi)]$

$= \phi[55k \cdot N_b] \leq \phi[78k \cdot N_b]$ (FOR GP) $= \phi[124k]$ (FOR BM)

to Bm → to GP $= \phi[55k \cdot 2.23] = \phi[123k]$

*BLOCK SHEAR SEE NCBF6 GP BUCKLING: $\phi F_{cr} b_w t_p = \phi(49.9ksi)(15.1")(.12") = \phi[377k]$

Demand to Capacity Ratios:

Brace Net Section: 433k/382k = 1.1

Brace Block Shear: 1.1

GP Block Shear: 433k/463k = 0.94

Whitmore GP Yielding: 433k/390k = 1.1

Whitmore GP Fracture: 433k/506k = 0.86

GP Buckling: 217k/377k = 0.58

Brace to GP Weld Fracture: 433k/520k = 0.83

Brace to GP base metal fracture: 0.83

GP Shear Yielding: 251k/236k = 1.1

Beam to GP weld fracture: 251k/379k = 0.66

Column to GP bolt shear: 182k/94.6k = 1.92

Column to BM bolt shear: 214k/138.3k = 1.55

Column to GP bolt bearing: 182k/123k = 1.48

Column to BM bolt Bearing: 214k/124k = 1.73

Fabshield® 21B

AWS A5.20: E71T-11

WELDING POSITIONS:

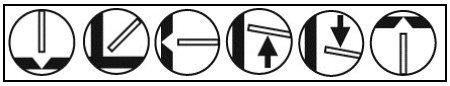

FEATURES:	BENEFITS:
• Excellent operator appeal	• Increases productivity
• Versatile	• Ideal for a variety of applications
• Self-shielded	• Suitable for welding outdoors
• Excellent bead appearance	• Helps to ensure weld integrity, reduces re-work
• Excellent slag removal	• Makes clean-up easy and quick

APPLICATIONS:

- General fabrication
- Pre-fab construction
- Short assembly welds
- Machine parts
- Non-alloyed and fine grain steels
- Rail car repairs
- Light structurals [under 3/4" (19.1mm) thick]
- Tanks

SLAG SYSTEM: Fast freezing, basic/fluoride type, flux-cored wire

SHIELDING GAS: None required

TYPE OF CURRENT: Direct Current Electrode Negative (DCEN)

STANDARD DIAMETERS: 0.030" (0.8 mm), 0.035" (0.9 mm), 0.045" (1.2 mm), 1/16" (1.6 mm), 0.068 (1.7 mm), 5/64" (2.0 mm)

RE-DRYING: Not recommended

STORAGE: Product should be stored in a dry, enclosed environment, and in its original intact packaging

TYPICAL WELD METAL CHEMISTRY* (Chem Pad):

Weld Metal Analysis	Fabshield 21B	AWS Spec
Carbon (C)	0.28	0.30
Manganese (Mn)	0.34	1.75
Silicon (Si)	0.15	0.60
Phosphorus (P)	0.008	0.03
Sulphur (S)	0.003	0.03
Aluminum (Al)	1.72	1.80

Note: AWS specification single values are maximums.

TYPICAL MECHANICAL PROPERTIES* [Aged 48 Hrs. @200°F (93°C)]:

Mechanical Tests	Fabshield 21B	AWS Spec
Tensile Strength	91,000 psi (627 MPa)	70,000-95,000 psi (490-670 MPa)
Yield Strength	62,000 psi (427 MPa)	58,000 psi (390 MPa) Minimum
Elongation % in 2" (50mm)	22%	20% Minimum

TYPICAL CHARPY V-NOTCH IMPACT VALUES*: Not applicable

Fabshield® 21B

Diameter Inches	(mm)	Weld Position	Amps	Volts	Wire-Feed Speed in/min	(m/min)	Deposition Rate lbs/hr	(kg/hr)	Contact Tip to Work Distance Inches	(mm)
0.030	(0.8)	All Position	25	14	55	(1.4)	0.3	(0.1)	1/2	(13)
0.030	(0.8)	All Position	125	16	225	(5.7)	3.8	(1.7)	1/2	(13)
0.035	(0.9)	All Position	55	17	75	(1.9)	1.8	(0.8)	1/2	(13)
0.035	(0.9)	All Position	80	19	110	(2.8)	2.1	(0.9)	1/2	(13)
0.035	(0.9)	All Position	120	20	160	(4.1)	2.5	(1.2)	1/2	(13)
0.045	(1.2)	All Position	115	15	105	(2.7)	1.4	(0.6)	1/2	(13)
0.045	(1.2)	All Position	130	16	125	(3.2)	1.8	(0.8)	1/2	(13)
0.045	(1.2)	All Position	160	17	170	(4.3)	2.8	(1.3)	1/2	(13)
0.045	(1.2)	All Position	200	18	195	(5.0)	3.5	(1.6)	1/2	(13)
1/16	(1.6)	All Position	160	17	70	(1.8)	2.1	(1.0)	3/4	(19)
1/16	(1.6)	All Position	190	18	100	(2.5)	3.2	(1.5)	3/4	(19)
1/16	(1.6)	Flat & Horizontal	210	19	110	(2.8)	3.4	(1.6)	3/4	(19)
1/16	(1.6)	Flat & Horizontal	260	20	145	(3.7)	4.8	(2.2)	3/4	(19)
0.068	(1.7)	All Position	145	22	159	(4.0)	1.9	(0.9)	3/4	(19)
0.068	(1.7)	All Position	155	18	60	(1.5)	2.3	(1.1)	3/4	(19)
0.068	(1.7)	All Position	185	17	70	(1.8)	2.7	(1.2)	3/4	(19)
0.068	(1.7)	All Position	240	18	100	(2.5)	4.2	(1.9)	3/4	(19)
0.068	(1.7)	Flat & Horizontal	255	21	111	(2.8)	5.2	(2.3)	3/4	(19)
0.068	(1.7)	Flat & Horizontal	315	18	49	(1.2)	7.4	(3.4)	3/4	(19)
5/64	(2.0)	All Position	185	16	55	(1.4)	2.6	(1.2)	1	(25)
5/64	(2.0)	All Position	190	18	60	(1.5)	2.8	(1.3)	1	(25)
5/64	(2.0)	All Position	220	19	70	(1.8)	3.5	(1.6)	1	(25)
5/64	(2.0)	Flat & Horizontal	265	21	90	(2.3)	4.7	(2.1)	1	(25)
5/64	(2.0)	Flat & Horizontal	315	22	124	(3.1)	7.1	(3.2)	1	(25)

- **Maintaining a proper welding procedure - including pre-heat and interpass temperatures - may be critical depending on the type and thickness of steel being welded.**
- **All position includes:** Flat, Horizontal, Vertical Up, Vertical Down, and Overhead.

STANDARD DIAMETERS AND PACKAGES: For a complete list of diameters and packaging, please contact Hobart Brothers at (800) 424-1543, or (937) 332-5188 for International Customer Service.

Diameter Inches	(mm)	2-lb. (0.9kg) Spool	10-lb. (4.5kg) Spool	33-lb. (15kg) Spool
0.030	(0.8)	S222106-019	S222106-022	—
0.035	(0.9)	S222108-019	S222108-022	S222108-029
0.045	(1.2)	—	S222112-022	S222112-029
1/16	(1.6)	—	S222119-022	S222119-029
0.068	(1.7)	—	—	S222123-029
5/64	(2.0)	—	—	S222125-029

CONFORMANCES AND APPROVALS:
- **AWS A5.20,** E71T-11
- **AWS A5.20M,** E491T-11
- **ASME SFA 5.20,** E71T-11
- **ABS,** E71T-11
- **CWB,** E491T-11-H8

CAUTION:
Consumers should be thoroughly familiar with the safety precautions on the warning label posted in each shipment and in the American National Standard Z49.1, "Safety in Welding and Cutting," published by the American Welding Society, 550 NW LeJune Road, Miami, FL 33126; OSHA Safety and Health Standards 29 CFR 1910 is available from the U.S. Department of Labor, Washington, D.C. 20210

Material Safety Data Sheets on any Hobart Brothers Company product may be obtained from Hobart Customer Service or at www.hobartbrothers.com.

Because Hobart Brothers Company is constantly improving products, Hobart reserves the right to change design and/or specifications without notice.